Integrated Applications of Analytical, Empirical, and Reservoir Simulation Methods to Accurately Determine Original Oil In Place and Estimated Ultimate Recovery of a Mature Field

by
Muhammad Ramos Suryanta Lubis

A thesis submitted to the Department of Petroleum Engineering,
Cullen College of Engineering
in partial fulfillment of the requirements for the degree of

MASTER OF SCIENCE

in Petroleum Engineering

Chair of Committee: Dr. Ganesh C. Thakur

Committee Member: Dr. Syed M. Farouq Ali

Committee Member: Dr. Kyung Jae Lee

University of Houston
May 2020

DEDICATION/EPIGRAPH

To my wife Rieski A. Dewi, both of my sons Muhammad Hanif A. Lubis, Muhammad Hafizh A. Lubis and my newborn baby daughter Aisha N. Lubis. I am grateful for their patience and unconditional support for me throughout the entire M.S. program.

ACKNOWLEDGMENTS

First of all, I would like to express my sincere gratitude to my committee chair Dr. Ganesh C. Thakur for his patience, guidance and support provided to me throughout the course of this research. In addition, I would like to thank Dr. Syed M. Farouq Ali and Dr. Kyung Jae Lee for their availability in serving as my committee members and their support in reviewing this research work.

A mention of my gratitude goes to Dr. Sumantra Chatterjee for providing the geomodel used in this research and his guidance on its proper use. I also would like to acknowledge the support received from University of Houston – Energy Industry Partnership (EIP) post-doctoral researchers - Dr. Peila Chen, Dr. Sayantan Ghosh, and Dr. Zeinab Zargar - for their advice and availability to discuss various aspects of this project/research. Also, to my friend in UH-EIP Anand Selveindran (a Ph.D. candidate), for his help and knowledge sharing about reservoir simulation.

Last but not least, I appreciate the support and permission from UH-EIP to publish this research work. However, any future publications of this work as journal, conference or any other means will only be made after receiving their written approval. I am indebted to our industry partner (a national oil company based in India) that provided the necessary data required for this research. The geological, production/injection, and other engineering data provided by our partner is highly appreciated.

ABSTRACT

This thesis is a field data-driven research that focuses on the evaluation of a mature oil field in South Asia (LK-4). The investigation started with the evaluations of a variety of available surface and subsurface data. It is essential to quality check the geology, petrophysics, and production data in the existing geomodel before using it towards reservoir simulation. Significant efforts were devoted to estimate Original Oil in Place (OOIP) and Estimated Ultimate Recovery (EUR) by using various methods. Classical production diagnostic plots and material balance analysis were performed to understand the reservoir performance.

The currently applied water injection was briefly evaluated to understand its benefit in improving field performance. Reservoir simulation studies were conducted to calibrate the reservoir properties with available production data. The main focuses of the simulation studies were to improve water production match in the field, to assist the determination of Oil-Water Contact (OWC), and to represent the behavior of the active producers better. Sensitivity studies were performed to understand the effect of various subsurface uncertainties to OOIP determination and history matching. Future production scenarios were developed based on different development strategies to increase production.

Application of Rate Transient Analysis and Transient PI, in addition to other methods, successfully assisted in minimizing the OOIP range. Field EUR values were estimated based on calibrated simulation models, analytical methods, and empirical methods. Future development opportunities such as workovers, changes in operating procedures, and new drilling locations were identified.

TABLE OF CONTENTS

LIST OF TABLES

LIST OF FIGURES

NOMENCLATURE

OOIP = Original Oil In Place (MMSTB)

EUR = Estimated Ultimate Recovery (MMSTB)

SBHP = Shut-in Bottom Hole Pressure (psi)

FBHP = Flowing Bottom Hole Pressure (psi)

N_p = Cumulative oil production (MMSTB)

V = Dykstra-Parsons Permeability variation

d = Decline rate (%/yr)

M = Mobility ratio

$q_{current}$ = Last oil rate, reported on August 2019 (STB/D)

q_{limit} = Economic oil rate (STB/D)

R_s = Solution gas-oil ratio (SCF/STB)

S_{oi} = Initial oil saturation

S_{or} = Residual oil saturation

S_{wc} = Connate water saturation

k_{rw} = Water relative permeability

k_{ro} = Oil relative permeability

q_o = Oil production rate (STB/D)

q_w = Water production rate (STB/D)

B_o = Oil formation volume factor (RBbl/STB)

PI = Productivity Index (STB/D/psi)

OIL = Oil India Limited

CHAPTER I. INTRODUCTION

Currently, a vast majority of the world oil production comes from mature fields. Increasing oil recovery from such resources is a major concern for oil companies and governments alike. In addition, the rate of replacement from produced reserves by new discoveries has been declining steadily in the last few decades. Therefore, increasing recovery factors from mature fields under primary and secondary production will be critical to meet the growing energy demand in the upcoming years *(Manrique, E., Thomas, E., Ravikiran, R., et al., 2010).*

Improved Oil Recovery (IOR) methods encompass Enhanced Oil Recovery (EOR) methods as well as new drilling and well technologies. It also includes intelligent reservoir management and control, advanced reservoir monitoring, and the application of different enhancements of primary/secondary recovery processes *(Surguchev, L. M., Eduardo., Alvarado, V., 2005)*. Depending on the characteristics of the reservoir being developed, a fit-for-purpose IOR has been widely applied in the oil field to increase oil production, particularly as the field becomes mature. Ultimately, additional effort is required to sweep the remaining oil out of the formation.

This research is focused on the evaluation of a mature oil field in Southern Asia, operated by a national oil company, Oil India Limited (OIL). This reservoir currently undergoes secondary recovery via water injection. As a field data-driven research, the investigation was started with the evaluation of available subsurface and surface data (such as well logging, core analysis, formation test, production rate, injection rate, pressure, and PVT test results). These were done to enable understanding of the field's geology, petrophysics, and reservoir characteristics. Efforts were concentrated on Original Oil in

Place (OOIP) calculation, evaluation of drive mechanisms, and estimation of remaining oil (S_o) using classical reservoir engineering methods and reservoir simulation. Production diagnostic plots using well data were generated to gain a qualitative understanding of the holistic reservoir performance and to assist in identifying IOR or infill drilling opportunities.

To conclude the research loop, evaluation of workovers, modification of operating conditions, and determination of future drilling prospects were performed to identify opportunities to increase oil production. I conducted this part of the research by utilizing the Petrel platform (Eclipse E-100®) and CMG suites (Imex®, Builder® and, Result®) black oil simulators. The reservoir simulation study objectives were to match production history data and to develop several production scenarios based on different development cases.

Another industry standard application such as IPM-MBAL® was used to conduct material balance analysis. Kappa Engineering software (Topaze®) was utilized for Rate Transient Analysis (RTA).

I.1 Thesis Structure

This thesis is divided into six chapters. The first chapter includes an introduction/ background about the research. Chapter II focuses on field introduction, reservoir fluid characterization, and rock physics. Chapter III is dedicated to analyzing production and injection data through analytical, empirical plots, and material balance analyses. Chapter IV provides details about the development of the reservoir simulation models, history matches, sensitivity studies, and production forecasts. The main focus of chapter IV is to obtain a better history matched model. Chapter V presents additional methods used in this

research, which had not been used in the previous studies. Lastly, chapter VI summarizes the conclusions, recommendations, and future work/recommendations.

I.2 Scope and Objectives

This study is built upon real field data obtained from a reservoir located in South Asia (LK-4). Production data, injection data, PVT analysis, well test, drilling and completion, logging, and core analysis data were obtained to perform this study. The most recent study presented high uncertainties of OOIP in this reservoir. Therefore, it becomes one of the main objectives of this study. Additionally, this research was attempted to quantify the Estimated Ultimate Recovery (EUR) of the LK-4 reservoir. It also proposes future development projects to increase EUR.

Summary of thesis objectives that are covered in the manuscript are listed below:

1. Perform reservoir and fluid characterization based on PVT and core data.
2. OOIP estimation based on a variety of empirical, analytical, and simulation methods.
3. Material balance study to understand drive mechanism, investigate aquifer properties, and OOIP determination.
4. Assess and evaluate the reservoir performance using empirical data, decline curve analysis, rate transient analysis, and variety of other classical reservoir engineering diagnostic plots.
5. Develop calibrated (history matched) reservoir models using Petrel (Eclipse-100) and conclude with CMG-Imex black oil simulator.
6. Assess possible future development scenarios to improve oil production from this field by using the calibrated simulation model to create future prediction scenarios.

I.3 Field Reserve and Reservoir Management

A reservoir's life begins with exploration, which leads to discovery and reservoir delineation, followed by field development through primary, secondary, and tertiary recovery stages, and finally abandonment. Estimating in-place volume (OOIP) associated with each well and group of wells, followed by final estimation of total reservoir in-place volume, is the foundation of any reservoir management practice *(Ismadi, D., Kabir, C. S and Hasan, R., 2011)*. It is a consequential question that arises during the exploration, production, and even in the late time when the decision to abandon the field is made.

The uncertainty range of OOIP can be minimized as more information becomes available, and as the field becomes mature. Despite the amount of available data and maturity of the reservoir, it is not possible to quantify the exact value of OOIP in a given reservoir. At the current state, the recent evaluation indicates high uncertainty in OOIP in the LK-4 reservoir.

Reliable and accurate OOIP and EUR values are vital aspects of any company's decision-making process. These quantities allow the operator to value the asset and producing life effectively. OOIP and EUR are key components in deciding field development strategies and business decisions. Reserve estimation is an ongoing process throughout the life cycle of the field. In most countries, an annual review and report on reserve estimation is a part of regulatory practices. Such regulations highlight the importance of performing this task with reasonable accuracy.

During the stage of field production, the application of reservoir management with the involvement of a multidisciplinary team is crucial. Integrated data and joint interpretation done by reservoir engineers and geologists helped to deduce and understand

the complexities of the reservoirs being studied (*Thakur, G. C., 1991*). This work utilizes interdisciplinary field surface and subsurface data to produce comprehensive reservoir descriptions, production history matches, and prediction models.

I.4 Research Workflow

The principal function of reservoir engineers is to define and evaluate a reservoir system. Reservoir definitions include determination of the areal extent, thickness, inclination, producing limit, and geological environment within the reservoir system. Reservoir evaluation involves the determination of the physical properties of each discrete reservoir and its fluids, the variation of the physical properties throughout the system, and the location of in-homogeneities that may affect the flow (*Essley, P. L., 1964*). Figure I-1 describes the entire process of the research work.

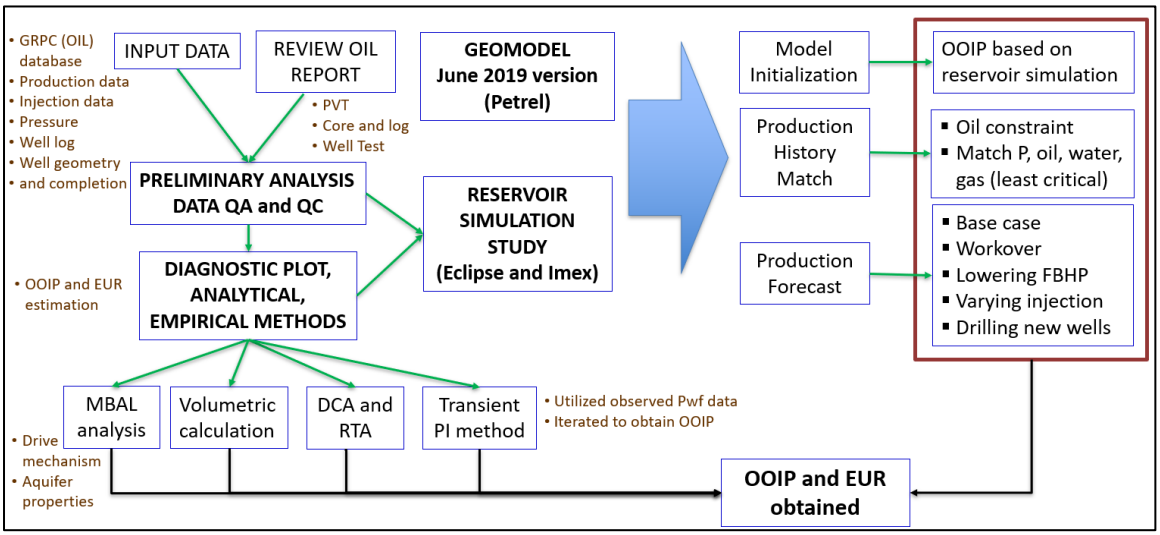

Figure I-1. Research workflow

The process started with examining/quality checking all reported data, well test results, well logs, and laboratory reports to ensure that accurate information was fed into the workflow to yield accurate interpretations. Production and injection data from the

Microsoft access GRPC (OIL database) was imported into excel spreadsheets for plotting and trend observations. The variety of reservoir engineering classical production plots were made and used to understand the holistic reservoir performance. Both pressure (SBHP and FBHP) and production-injection data were formatted to suit Petrel and CMG input requirements and loaded for reservoir simulation purposes.

Possibilities of unintended and minor errors in the PVT, core, and well test reports were not ruled out, even though the reports were prepared reviewed and quality checked by the service company. When empirical/published correlations are available for a certain type of data, a second verification is done as a means of additional quality checks of the reported interpretation. Based on these datasets, preliminary information for relative permeability, capillary pressure, and probable initial conditions of the pre-exploited reservoir were used for the reservoir simulations.

Well information such as geometry, total depth, completion depth, and change of completion depth vs. time were also quality checked and compared with the GRPC data. As an example of a change in completions depths with time, in well NHK-505, the operator plugged the deeper perforations due to higher water production and then re-perforated at a shallower depth to reduce the water production rate. These changes in production profile and perforation depth information in GRPC were carried out into the simulation model.

To minimize the range of OOIP in the LK-4 reservoir, four different empirical and analytical methods - volumetric, material balance analysis, rate transient analysis, and transient productivity index-were utilized. The application of a variety of methods had increased my confidence on the OOIP estimation result.

EUR estimation was one of the primary goals of this research. Base case/baseline EUR estimation was based on currently active well performance and utilized production plots such as Arps Decline Curve Analysis (DCA), q vs. cumulative production (N_p), and Water Oil Ratio (WOR) vs. N_p. Another way to obtain the EUR is based on calibrated reservoir simulation models. These models use a baseline production forecast scenario, where current operating conditions are maintained, and simulation is run for 20 years to compute the EUR.

The final step in the workflow was the calibration of reservoir models through the history match of production data. Significant efforts were devoted to improving the quality of the water production history match. Based on the previous study conducted in 2019, water production was underestimated by more than 20%. It also indicated a mismatch in cumulative water production. Matching water production played a key role in avoiding overestimation of the generated oil production forecast.

The geomodel utilized in this process is a preliminary model. It was released and reviewed during June-July 2019. Later, it was aided by the latest available 3D seismic interpretation from the operator. Finally, different future production scenarios were assessed using the calibrated history matched model to identify future opportunities to increase oil production.

CHAPTER II. FIELD BACKGROUND

This chapter describes field information, geology, petrophysics, and fluid properties. It summarizes the state of historical and current LK-4 production. This chapter also discusses the geomodel properties that were used as initial values for the history match discussed in chapter IV. Information from this chapter assists in understanding the LK-4 reservoir characteristics based on all available measured data sets.

II.1 Introduction

Hydrocarbons were first discovered in the LK-4 structure in 1986. The field was developed with only vertical and deviated wells until August 2019. Starting November 2009, two producers (NHK-473 and NHK-487) were converted to injectors. Injection in NHK-473 was active for almost eight years before it was stopped in June 2017. Since appraisal and field development from 1986 to recently (August 2019), a total of 15 wells had been drilled.

As of August 2019, the total field production rate was 272.3 STB/D, with four production wells and one injection well (NHK-487). Two wells that produced the highest oil rate are NHK-505 and NHK-580, with production rates of 17.6 STB/D and 232.1 STB/D, respectively. NHK-422 and NHK-469 produce at lower oil rate of 11.3 STB/D each. The current Gas Oil Ratio (GOR) of those production wells are relatively high (>3000 SCF/STB), which indicates that the current injection strategy is not yet optimum. However, injection optimization and waterflooding pattern evaluation are not within the scope of this study.

Figure II-1 shows the production and injection profile from this reservoir from 1986 to August 2019. The increase in the oil flow rate in 2018 was attributed to well NHK-505

production increase. The most recent oil production rate shows a slightly declining trend. As of August 2019, the total cumulative fluids produced are 13.546 MMSTB, 13.502 MMSTB, and 19.075 MMSCF of oil, water, and gas, respectively.

The operator reported OOIP is 39.94 MMSTB (6.35 $MMSm^3$), therefore the current estimated oil recovery ≈ 33.9%. Initial GOR (R_{si}) from PVT data ranges from 804 SCF/STB to 939 SCF/STB. Estimated R_{si} = 890 SCF/STB based on initial field production data. The current fieldwide average GOR is very high compared to its R_{si}. Note that the operator also confirmed a 30% inaccuracy in gas measurements, so there are significant uncertainties in the gas data. Implementation of integrated and sound reservoir management is required to improve field performance.

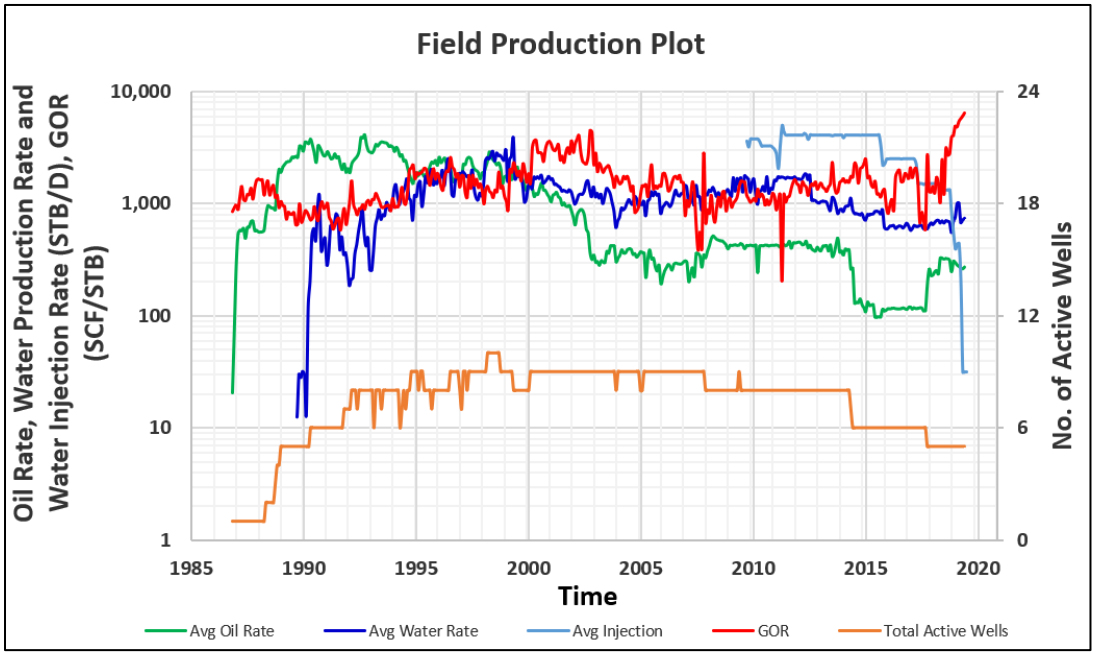

Figure II-1. Field production and injection plot

Figure II-2 shows well by well summary using the most recent well data or the last data point before the well was shut-in. The hollow black circles represent inactive wells and solid black circles indicate active wells. Solid red circles indicate high GOR wells (>5000 SCF/STB), while the solid blue circles indicate high water-cut wells (>85%).

Injection wells are marked with triangles, where the hollow black triangles represent inactive injectors, and solid black triangles represent active injectors.

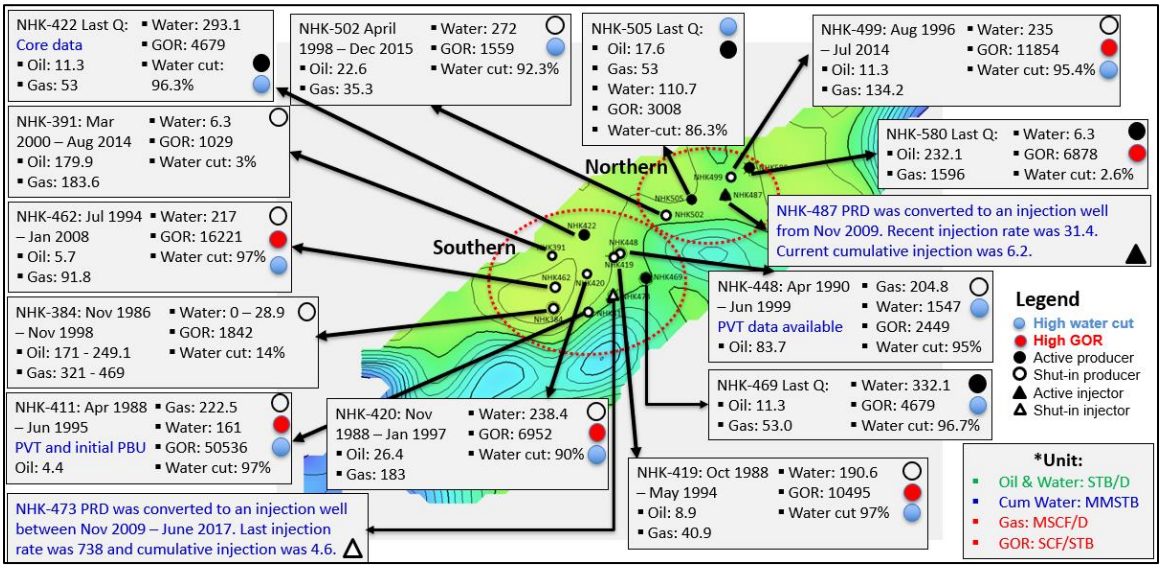

Figure II-2. Highlight of well by well production/injection summary

Upon review of field pressure-production, it was concluded that the drive mechanism of the LK-4 field is a strong aquifer. This was also confirmed by the previous waterflood management study in the LK-4 reservoir reported by *Zhu (2019)*. Figure II-3 shows fieldwide water cut from 1986 to August 2019. Initially, the LK-4's water cut is low, and it increased dramatically from 1992 to 2002. The most recent water cut average fieldwide in this reservoir is 70% (well to well variation from 2.6 to 97%).

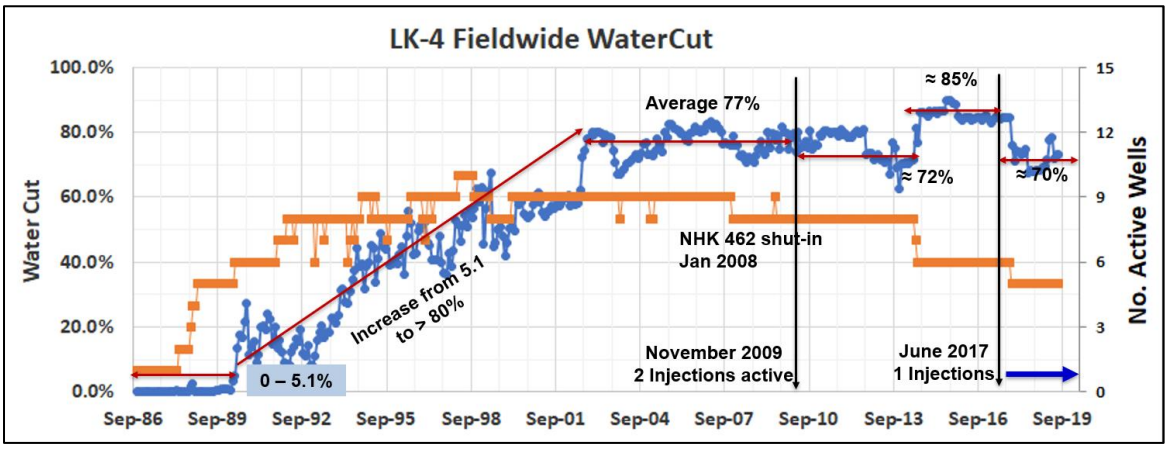

Figure II-3. Fieldwide water cut

The field has high porosity values (average porosity from core data is 19.9%; average from static geomodel is 13.6%; average from calibrated reservoir simulation is 13.9%). Porosity was increased in the region around NHK-469 as the original populated value from the geomodel was very low, causing a rapid pressure drops. The reservoir has a favorable permeability, with the geomodel having an overall average permeability of 53.5 mD.

Based on NHK-422 core data, average permeability from four available samples is 105 mD. PVT report showed that the produced oil has low viscosity (0.46 – 0.56 cP) in the range of the observed reservoir pressure conditions. Conventional core analysis report indicated average relative permeability endpoints of 0.11 and 0.59 for k_{rw} and k_{ro}, respectively. Estimated water viscosity (μ_w) at reservoir conditions is 0.38 cP. Based on these characteristics, the mobility ratio (M) can be calculated as

$$M = \frac{k_{rw}\mu_o}{k_{ro}\mu_w} \tag{2-1}$$

where, M = mobility ratio, k_{ro} = oil relative permeability, k_{rw} = water relative permeability, μ_o = oil viscosity and μ_w = water viscosity. Therefore, mobility ratio based on this measurement is as shown below

$$M = \frac{0.11 \cdot 0.51}{0.59 \cdot 0.35} = 0.27.$$

This value indicates a good mobility ratio (MR ≤ 1.0), which shows that this reservoir is a favorable waterflood candidate.

II.2 Geology and Petrophysics

There are two main producing reservoirs, which are Barail 4th (LK-4) and Barail 5th (LK-5) Sands in the LK area. The reservoirs are separated vertically by an impermeable barrier. Recent 3D seismic interpretation indicates that this reservoir could possibly be separated into two different regions- northern and southern. LK-4 structure is a faulted anticline with a major axis of the structure trending NE-SW. Table II-1 provides a summary of rock and fluid properties of the LK-4 reservoir.

Table II-1. LK-4 Reservoir and fluid properties

LK-4 Reservoir and Fluid Properties	
Field Name	Greater Jorajan - Assam
Block	NHK-384
Formation	Langkasi Barail 4th (LK-4)
Lithology	Sandstone
Gross thickness, ft	110 (33.5 m) to 186 (56.7 m)
Average net pay, ft	88 (27 m) to 147 (45 m)
Initial average reservoir pressure, psi	3786 - 3950
Porosity, % ▪ Core (four samples), NHK-422 ▪ Geomodel, entire reservoir	Average (min-max): 19.9 (19.3 - 21.1) 13.6 (4 - 26.3)
Permeability, mD ▪ Well Test (NHK 411, shaly sand) ▪ Core (k_h), NHK-422 ▪ Core (k_v), NHK-422 ▪ Geomodel, entire reservoir	Average (range min-max): 9.6 (considered low value) 105 (37.5 – 470) 60 (27 – 170) 53.5 (5 – 480)
Average S_{wi}, fraction ▪ Core, NHK-422 ▪ Geomodel, entire reservoir ▪ History matched model, entire reservoir	Average (range min to max): 0.32 (0.215 to 0.413) 0.36 (0.1 to 0.62) 0.3
Primary drive	Strong water influx
Current GOR (from well to well), SCF/STB	3,000 to 6,900
Current water cut (from well to well), %	2.6 to 97
No. of currently active wells	4 producers and 1 injector

Based on the interpreted fieldwide fluid contacts and bottom hole pressure data, the nature of the possible faults is non-sealing, and therefore, most fault blocks are in pressure communication. The non-sealing nature of faults is indicated by small variabilities in the Shut In Bottom Hole Pressures (SBHP). However, the faults could contribute to depth and reservoir thickness variations from one well location to another.

The focus of this study is the Barail 4 sandstone (LK-4 reservoir). Hence all production and injection wells in this study were limited to wells that penetrated this reservoir only. The operator reported that the LK-4 reservoir OOIP is 39.9 MMSTB (6.35 $MMSm^3$). The LK-4 formation is oil-bearing with no initial gas cap (slightly undersaturated reservoir) and a strong bottom water drive. Net pay thickness of the oil zone in the Barail 4^{th} sand reservoir likely ranges between 88 ft and 147 ft (27 m and 45 m).

II.3 Geomodel Properties

This section presents the static geomodel that was used in the reservoir simulation study. This geomodel is one of the preliminary ones that were built during June - July 2019, utilizing well logs and core data (i.e., in the absence of 3D seismic data that arrived later).

The model was built upon a methodical geologic modeling workflow, such as determination of reservoir top and base from Gamma Ray (GR) and Spontaneous Potential (SP) logs, well correlations, and petrophysical analyses. These operations were performed to determine water saturation, porosity, and permeability at the well level. Subsequently, these properties were upscaled to the intersecting grids (with the wells) and finally propagated into the entire geologic grid.

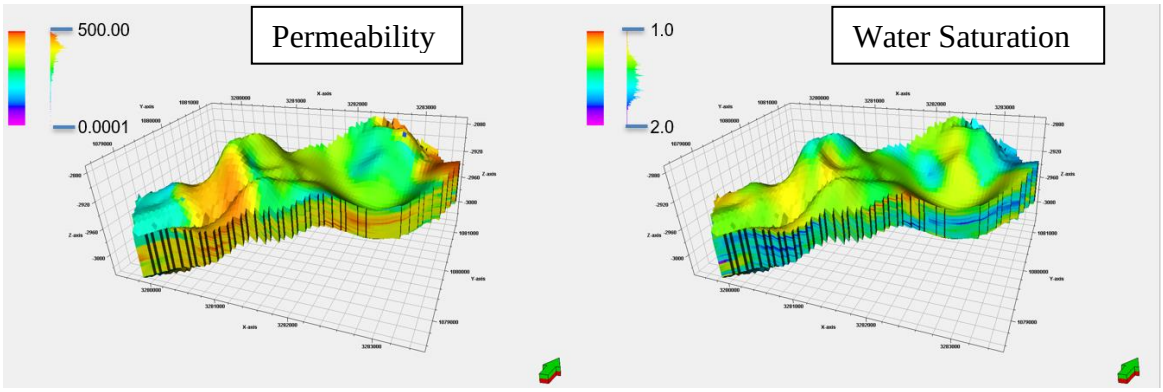

Figure II-4. Permeability and S_w distribution in static geomodel (*Chatterjee, S., 2019*)

Figures II-4 and II-5 show the permeability, porosity, and water saturation distribution in the static geomodel from *Chatterjee, S., 2019*. The average permeability in the geomodel is 53.5 mD, average porosity in the geomodel is 13.6%, and average water saturation in the model is 36%.

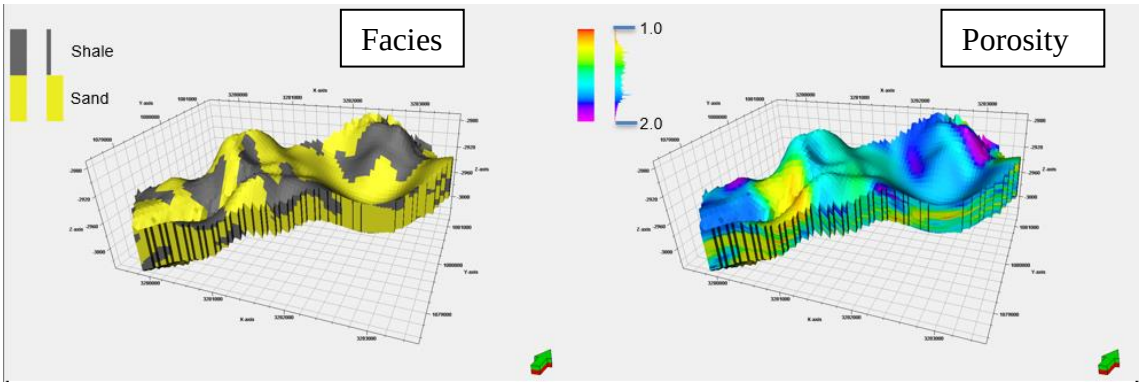

Figure II-5. Permeability and porosity distribution in the static geomodel (*Chatterjee, S., 2019*)

The LK-4 geomodel includes facies (shale and sands) provided by OIL, where 79% of the grid cells were sands while the remaining 21% were shale. Based on the evaluation of the log data, it was concluded that the operator used a shale baseline to determine the facies group.

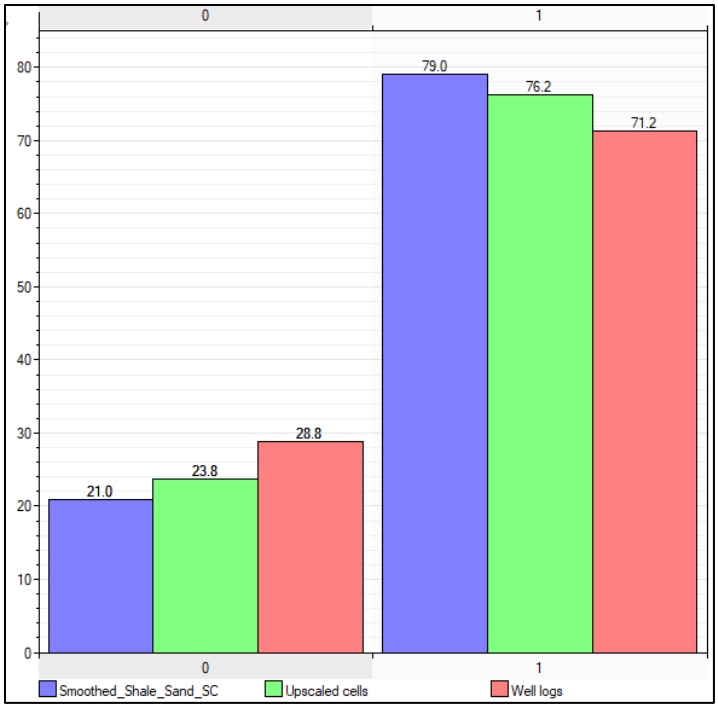

Figure II-6. Shale and sand statistics (*Chatterjee, S., 2019*)

The facies percentages within the well logs, grid cells (upscaled) at the wells, and the geostatistically modeled grid are shown in Figure II-6. OOIPs based on volumetric calculations and those based on reservoir simulations were performed only on the clean sands.

The initial reservoir simulation was run without any changes in the geomodel. The history match performed using this model was considered the base case initial (as-is) history match. This was the starting point before any modifications were made to fully calibrate the reservoir properties with production data.

II.3.1 Oil-Water and Gas-Oil Contacts

The operator provided a map (Figure II-7), showing the oil-water and gas-oil contacts. The map focuses on the area of interest of the LK-4 reservoir. Based on the map, they interpreted that gas-oil contact (shown by the red lines) between 9545 ft - 9551 ft

(2910 m - 2912 m), and the oil-water contact (shown blue lines) between 9709 ft - 9774 ft (2960 - 2980 m).

In the simulation study, 2912 m (9551 ft) was chosen for gas-oil contact, while the water-oil contact is one of the parameters that was analyzed in the simulation to obtain an improved water production history match. Independent OWC determination based on well log data agrees with the final history match model within ± 10 ft accuracy.

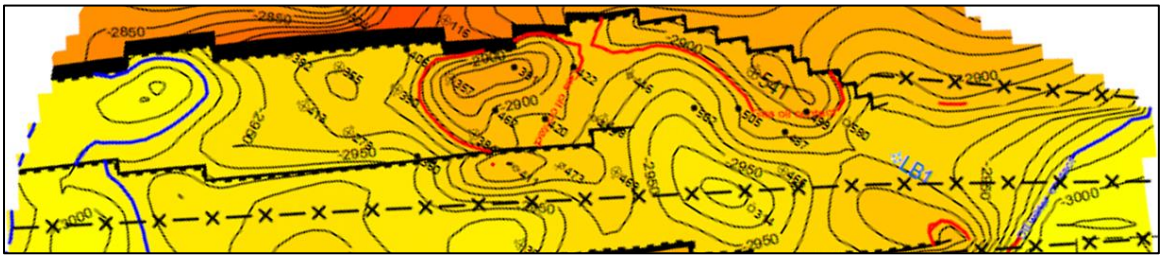

Figure II-7. Map for GOC and OWC

II.4 Laboratory Data Review and Well Test Results

PVT report, conventional core analysis, and well test data were obtained from the operator. This section explains and summarizes the key information available in the report.

II.4.1 Relative Permeability

These relative permeability curves come from Well NHK-422. It was the only available core sample for this reservoir. In total, there are four samples from different depths where the average porosity is 19.9%, and weighted average permeabilities are 105 mD and 60 mD in the horizontal and vertical directions, respectively. Liquid permeability and water sensitivity tests on these samples exhibited a decrease in permeability values to almost zero upon exposure of the core in distilled water instead of brine. This phenomenon could be an indication of the presence of smectites/montmorillonites clay around the depth of interest in this well.

Due to the permeability blockage/breakdown of the samples, only six successful relative permeability measurements were obtained, with two samples for k_{ro} and k_{rw} and four samples for k_{ro} and k_{rg}. Figures II-8 and II-9 show the water-oil and gas-oil relative permeability curves based on the permeability measurements.

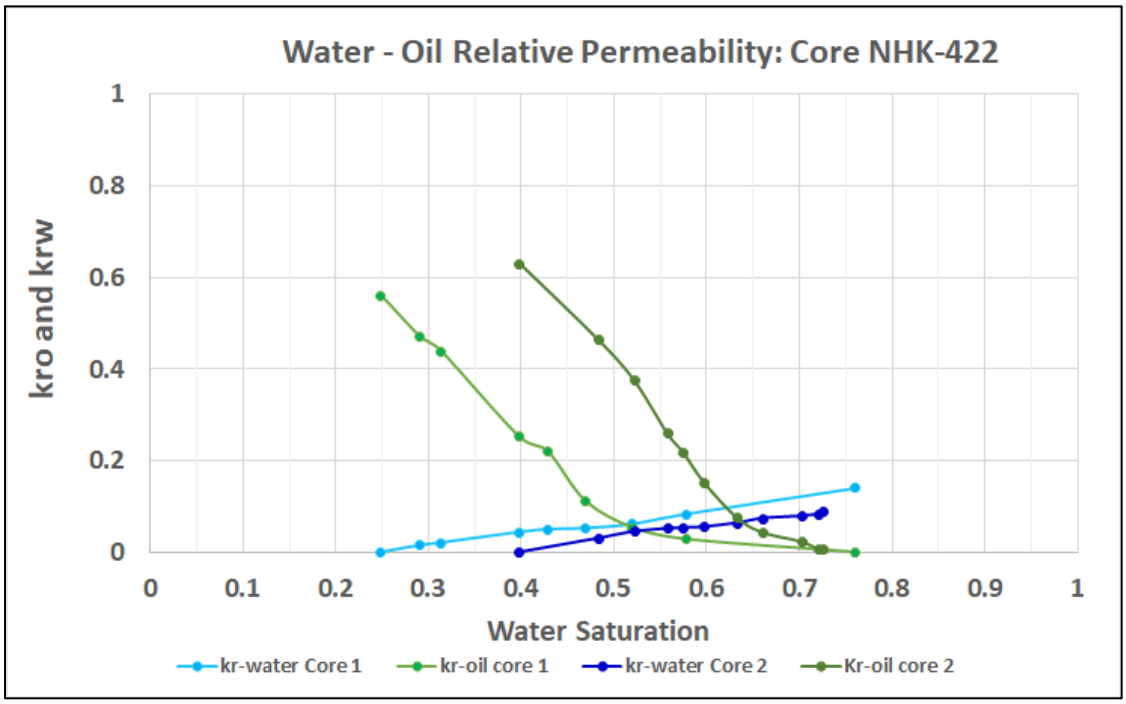

Figure II-8. Water – Oil relative permeability data

From the conventional core analysis report (NHK-422), the following information was summarized:

1. K_{ro} drops quite rapidly, while k_{rw} builds up rather slowly with an increase in S_w.
2. Indicative of formations with moderate to high water sensitivity/wettability.
3. S_{or} from 23.6 to 27% and S_{wi} from 24.9 to 39.8%.

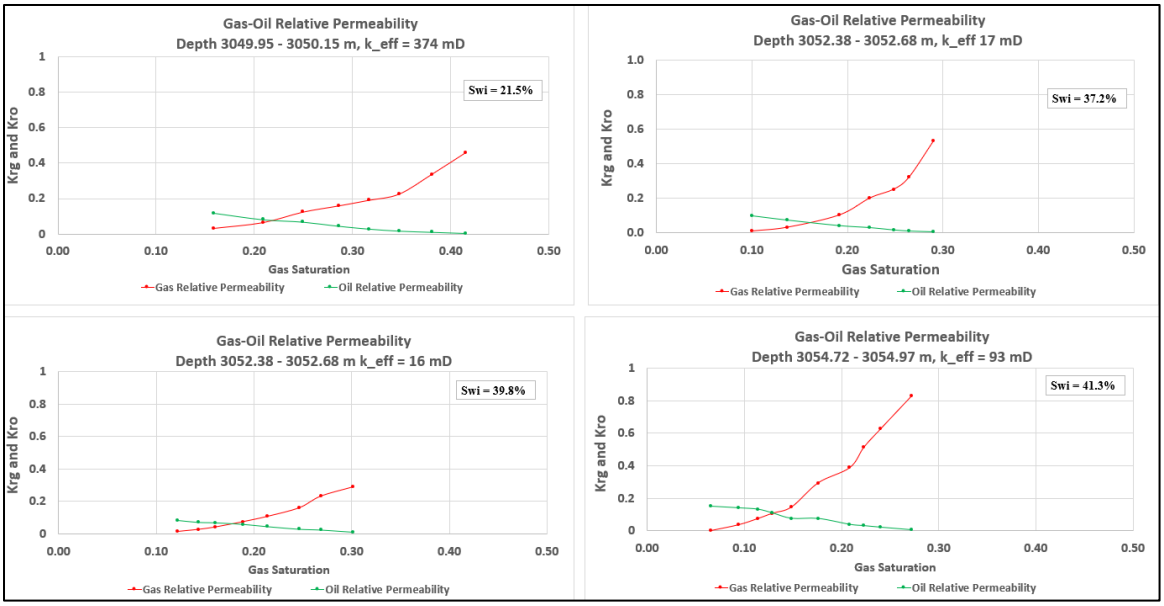

Figure II-9. Gas – Oil relative permeability data

Based on conventional core analysis report (NHK-422) report, the following information were obtained:

1. Critical gas saturation (S_{gc} from 6.5 to 9.5%).
2. K_{rg} characteristic to gas builds up quite rapidly upon reaching the critical gas saturation.

Usually, due to the difficulties and costs involved in measuring relative permeability values, empirical correlations were often used to estimate the values. Given that only two sets of relative permeability measurements are available, another relative permeability curve was generated by using the capillary curve data from core obtained from a depth of 3051 m (10007 ft). The pore size distribution index (λ) empirically can be determined from given P_c data using Corey-Brooks correlation

$$LogP_c = LogP_e - \frac{1}{\lambda} LogS_w^* \quad (2\text{-}2)$$

where: $S_w^* = \left(\frac{S_w - S_{wi}}{1 - S_{wi}}\right)$. (2-3)

The λ value is critical in calculating relative permeability because the actual number represents how uniform the pore size is in the sample/reservoir. A low value of λ (e.g., 2) indicates a wide range of pore sizes, while a high value represents a rock with a more uniform pore size distribution. This value is considered a general value and is thought to represent a wide range of pore sizes. A λ value of 2 is often used when nothing else is known about the reservoir.

Given that capillary pressure data were available for this core depth, I used it to determine the pore size distribution index. A log-log plot of the capillary pressure vs. the normalized water saturation should result in a straight line with a slope of –1/ λ and an intercept of P_e as shown in Figure II-10. This method of determining λ from experimental data is preferable because the value obtained can be backed up with measured data.

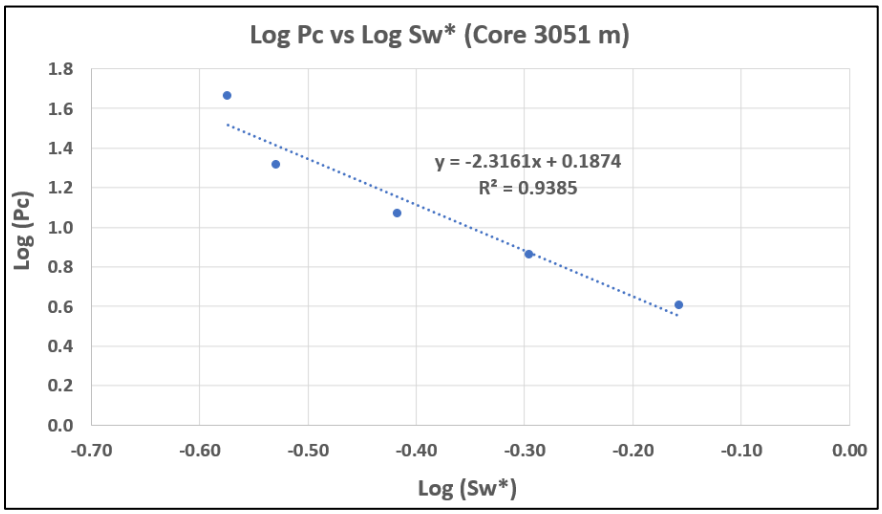

Figure II-10. Log P_c vs. Log S_w* to obtain λ

From the chart, -1/λ= -1.528, thus the pore size distribution index (λ) = 0.65

$$k_r^o = 1.31 - 2.62\,S_{wi} - 1.1\,(S_{wi})^2 \qquad (2\text{-}4)$$

$$k_{rw} = (S_w^*)^{\frac{2+3\lambda}{\lambda}} \qquad (2\text{-}5)$$

$$k_{rn} = k_r^o \left(\frac{S_m - S_w}{S_m - S_{wi}}\right)^2 \left(1 - (S_w^*)^{\frac{2+3\lambda}{\lambda}}\right). \qquad (2\text{-}6)$$

Where,

- k_{rw} = Wetting phase relative permeability
- k_{rn} = Non-wetting phase relative permeability
- k_r^o = Non-wetting phase relative permeability at irreducible wetting phase saturation
- S_w^* = Normalized wetting phase saturation
- λ = Pore size distribution index
- $S_m = 1 - S_{or}$ (1 – residual non-wetting phase saturation)
- S_w = Water saturation
- S_{wi} = Initial water saturation
- P_c = Capillary pressure
- P_e = Minimum threshold pressure

Table II-2. Determination of pore size distribution index @S_{wi} = 32.8%

Determination of Pore Size Distribution Index, Swi = 32.8%				
Sw	Normalized Sw (Sw*)	Pc	Log Sw*	Log Pc
76.4%	64.9%	4	-0.18801	0.60206
61.5%	42.7%	7.2	-0.36981	0.85733
51.9%	28.4%	11.7	-0.54693	1.06819
45.1%	18.3%	20.5	-0.73852	1.31175
42.8%	14.8%	46	-0.82873	1.66276

Water-oil relative permeabilities presented in the NHK-422 core analysis report suggest that S_{or} may vary from 23.6% to 27%. Therefore, by using this correlation, a relative permeability curve using core (obtained from a depth of 3051 m/10007 ft) can be constructed as shown in Table II-3 and Figure II-11:

Table II-3. Relative permeability curve for core sample @ 3051 m

Sw	Krw	Krn (Kro) - Lower Sor	Krn (Kro) - Higher Sor	Krn (Kro) - Average Sor
76.4%	0.113	0.000	0.013	0.003
61.5%	0.016	0.046	0.016	0.030
51.9%	0.003	0.133	0.088	0.111
45.1%	0.001	0.221	0.175	0.199
42.8%	0.0003	0.256	0.210	0.234
32.8%	0.000	0.435	0.403	0.420

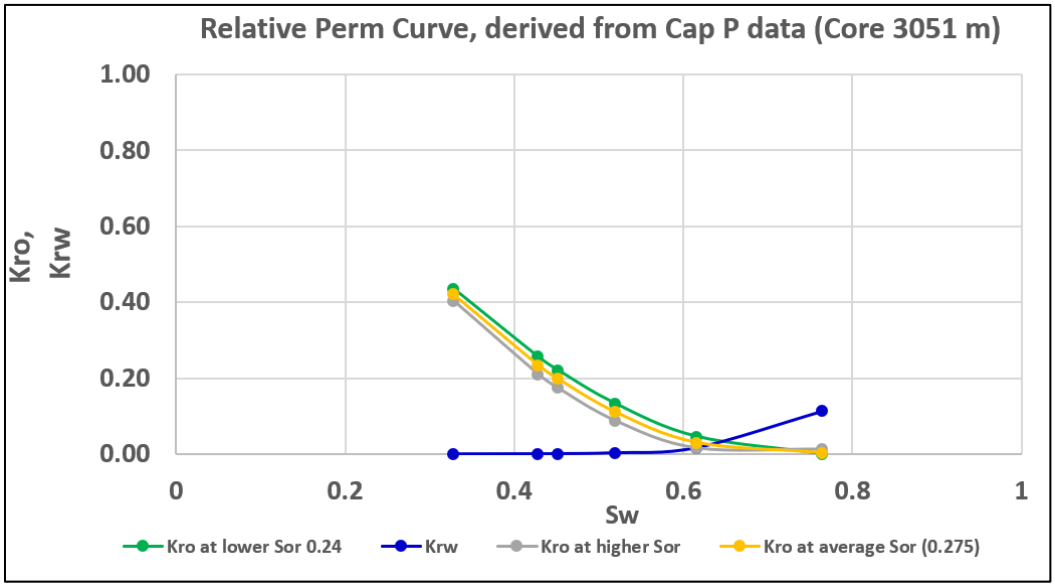

Figure II-11. Relative permeability curves derived from capillary pressure data

All available relative permeability measurements and relative permeability values derived from the capillary pressure correlation was honored and used as an initial rock-physics input in the reservoir simulation model. However, after the history matching process, this input data was slightly tuned, and only one representative value of $k_{rw} – k_{ro}$ was used. In the final history match model, k_{ro} at S_{wi} is 0.9 and k_{rw} at S_{or} is 0.14. This end-point modification is important to get a reasonable history match.

II.4.2 PVT Data and Production GOR

PVT data was obtained from two wells, which are NHK-411 and NHK-448. Table II-4 provides a summary of the fluid properties obtained from the PVT analysis report.

Table II-4. PVT Data

Fluid/Rock Properties	NHK 411	NHK 448
Bubble-point pressure	3500 - 3650 psi	3550 - 3680 psi
Oil compressibility	9.76×10^{-6} /psi	N/A
Water compressibility	3.5×10^{-6} /psi	N/A
Effective rock compressibility	3.69×10^{-6} /psi	N/A
Total reservoir compressibility	11.58×10^{-6} /psi	N/A
Reservoir temperature	182 ^{o}F	186 ^{o}F
Oil viscosity	0.56 cP	0.46 cP
B_o @ $P_{bubble\text{-}point}$	1.4 RB/STB	1.44 RB/STB
API gravity	30.1	31.6
Specific gravity	0.7281	0.7113
R_{so}*	804 – 848 SCF/STB	939 SCF/STB

*R_{so} value based on NHK-411 PVT report, ranges from 804 to 848 SCF/STB. Based on material balance analysis, 804 SCF/STB is too low and yields negative gas calculation. Material balance analysis suggested that R_{so} cannot be lower than 810 SCF/STB.

In addition to the values from the PVT report, the GOR parameter was estimated using *Standing (1947)* correlation because the reported GOR has a wide range. The calculation is explained in the following solution GOR (R_s) sub-section. This was considered as a secondary check because the reported value came from a reputable service company and was verified by the operator.

II.4.2.1 Bubble Point Pressure

Bubble point pressure (P_{bp}) could be inferred graphically by plotting B_o, μ_o, and R_s with pressure. Figures II-12 and II-13 show the plots for this data set. P_{bp} could be interpreted from the point where the B_o is the highest, μ_o is the lowest, and R_s is flat. I

considered that more accurate P_{bp} is based on the R_s, and B_o values, which converged to be 3500 to 3680 psi. In the case of Well NHK-411, there was an inaccuracy in the reported viscosity value. Thus, based on this well, only R_s and B_o values were used to determine P_{bp}. In this study, 3676 psi was selected as the bubble point pressure.

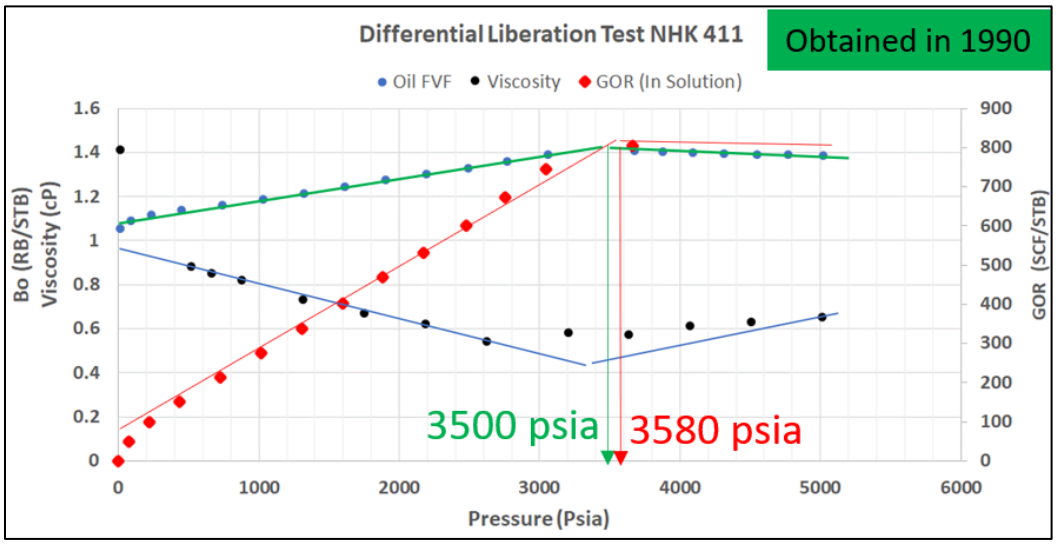

Figure II-12. Differential liberation test results on NHK-411

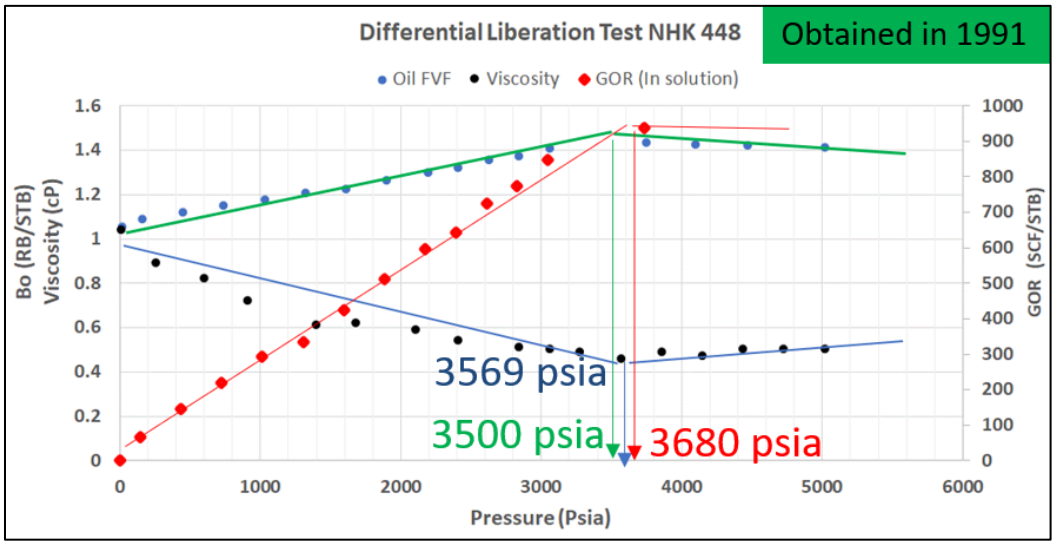

Figure II-13. Differential liberation test results on NHK-448

II.4.2.2 Solution Gas Ratio (R_s)

Solution gas ratios from the available PVT reports given for NHK-411 and NHK-448 are in the range of 804 to 939 SCF/STB. Using the Standing correlation chart

with the equation by Beggs (Equation 2-7 and 2-8), a secondary check was performed on this reported value:

$$R_{so} = \gamma_g \,.\left(\frac{P}{18\,.\,10^{Y_g}}\right)^{1.204} \tag{2-7}$$

$$Y_g = 0.00091\,.\,T - 0.0125\,.\,(API^0) \tag{2-8}$$

where: T is temperature in deg F and P is pressure in psi.

Equations 2-7 and 2-8 are applicable for the following range of values:

$130 < P_b$ (psi) < 7000

100 < T (^{o}F) < 258

20 < GOR (SCF/STB) < 1425

16.5 < (^{o}API) < 63.8

$0.59 < \gamma_g < 0.95$

$1.024 < B_o$ (RBbl/STB) < 2.05

$$Y_g = 0.00091\,.\,181.4 - 0.0125\,.\,(30.9) = -0.22118$$

$$R_{so} = 0.7113.\left(\frac{3865}{18\,.\,10^{-0.22118}}\right)^{1.204} = 843 \text{ SCF/STB}$$

There was good agreement between the lab result and the correlation. The estimation yielded a middle point between the two measurements. Therefore, this information could be readily used to represent an average value in the fluid model input for reservoir simulation. In addition to that, initial gas in the solution can also be determined by using production data, as shown in Figure II-14 (890 SCF/STB). In the simulation

model, options were available to adjust Rs_i values based on this R_{si} range (from 804 to 939 SCF/STB) during initialization; and this helped to match initial pressure and gas production.

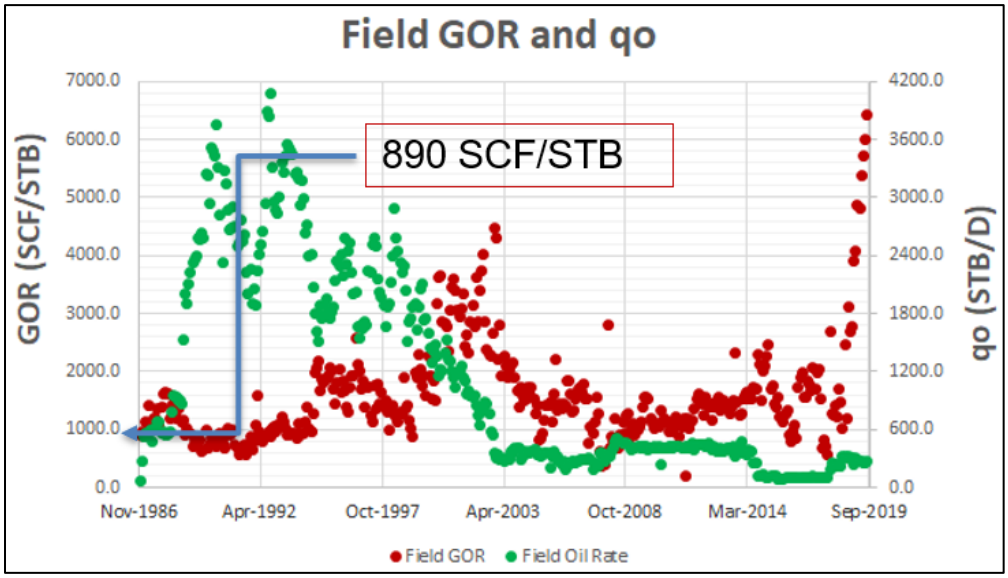

Figure II-14. R_{si} based on field production data

II.4.3 Core Data Review

A conventional core analysis report was provided for NHK-422 rock sample. The summary of the reservoir parameters obtained from these cores are summarized in Table II-5.

Table II-5. Permeability and porosity from core

Core sample	Depth Range (m)		Depth Range (ft)		Permeability (mD)		Porosity	K_v/K_h
	From	To	From	To	Horizontal	Vertical	%	
1	3054.7	3055.0	10022.0	10022.9	61.6	46.7	19.4	0.76
					57.3	27.3		0.48
2	3052.4	3052.7	10014.4	10015.4	90.3	43.8	20.0	0.49
					42.3			
3	3051.1	3051.4	10010.3	10011.1	64.8	37	19.3	0.57
					37.5			
4	3050.0	3050.2	10006.4	10007.1	470.3	170.1	21.1	0.36
WEIGHTED AVERAGE					105	60	19.9	0.53

The plot of permeability vs. porosity yields a reasonable positive relationship with a high R^2 value. It would be good to have more data points to increase the confidence level. Unfortunately, this is the only available core data. For the geomodel, permeability derived from porosity around this well was obtained using Equation 2-9

$$Permeability\ (Y) = 2.10^{-7} e^{1.0064\ .\ Porosity\ (X)}. \qquad (2\text{-}9)$$

In addition to this, porosity log data (density porosity and neutron porosity) that was available in most of LK-4 wells were utilized in constraining and distributing the permeability values in the geomodel.

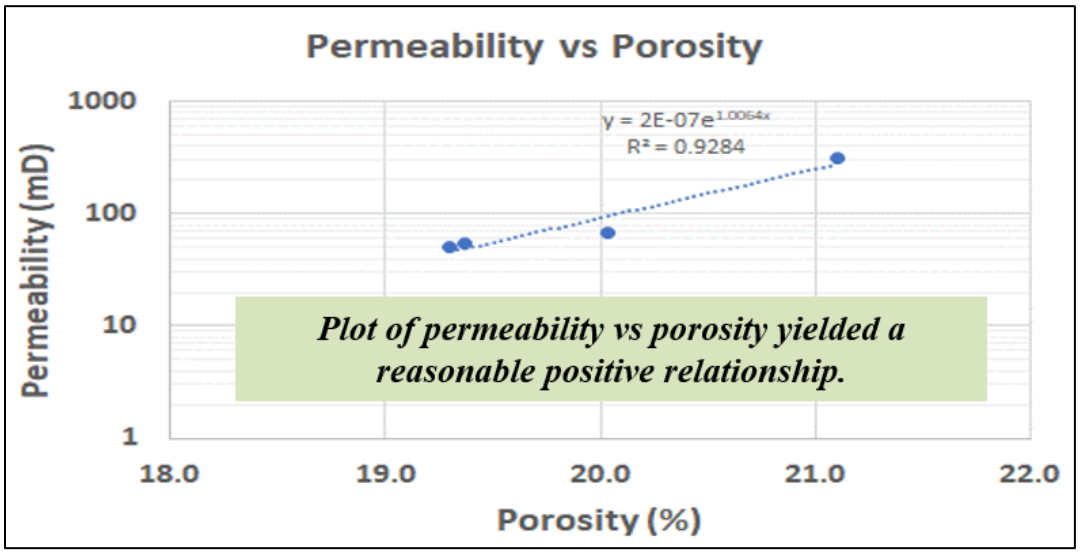

Figure II-15. Permeability vs. porosity correlation

The Dykstra-Parsons coefficient based on core data was calculated to evaluate the reservoir permeability variation. The concept of the permeability variation was introduced by Dykstra and Parsons in 1950; hence it is called Dykstra-Parsons coefficient (V). This V coefficient may be used to describe the degree of heterogeneity within the reservoir. The values range between 0 (system with completely uniform permeability) to 1 (extremely heterogeneous system). To obtain the value of permeability variation V, permeability

dataset was sorted from minimum to maximum and displayed on a chart of log probability scale, as shown in Figure II-16.

Dykstra-Parsons coefficient was computed using Equation 2-10

$$V = \frac{k_{P50} - k_{P84.1}}{k_{P50}} \tag{2-10}$$

$$V = \frac{68-37}{68} = 0.46\ ,$$

where k_{p50} is the permeability at 50% probability (mean), and $k_{p84.1}$ is the permeability at 84.1% probability. Figure II-16 shows that a V value of 0.46 was obtained from NHK-422 core data. This is an indication of a relatively uniform reservoir permeability distribution. This translates to a good candidate for waterflooding because its permeability distribution is favorable for the vertical sweep efficiency.

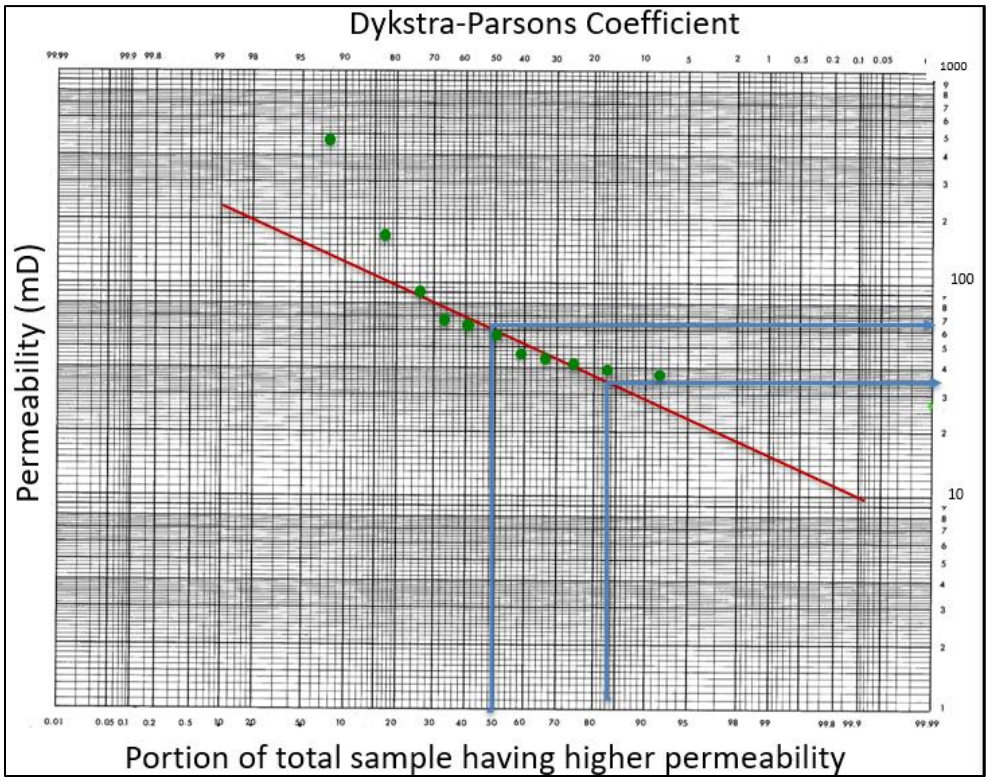

Figure II-16. Determination of Dykstra-Parsons coefficient

II.4.4 Capillary Pressure (P_c)

Air-brine capillary P were only determined on a few core plugs, with moderate permeabilities. Key information obtained from capillary pressure curves are as follows:

- Threshold P_c required to force air into a 100% brine saturated core is in the range of 1 – 2.7 psi, which is equivalent to 0.33 – 0.9 psi at reservoir pressure.
- 100% water-saturated column above FWL would be in the range of 3.1 – 8.3 ft due to capillary rise.
- From capillary curve, S_{wirr} is from 35 – 42%. Irreducible/connate water saturation from the available core was in the range of 21.5 – 42 %.

The available capillary pressure data was plotted in Figure II-17 and one set of measurement that show fluctuations was ignored.

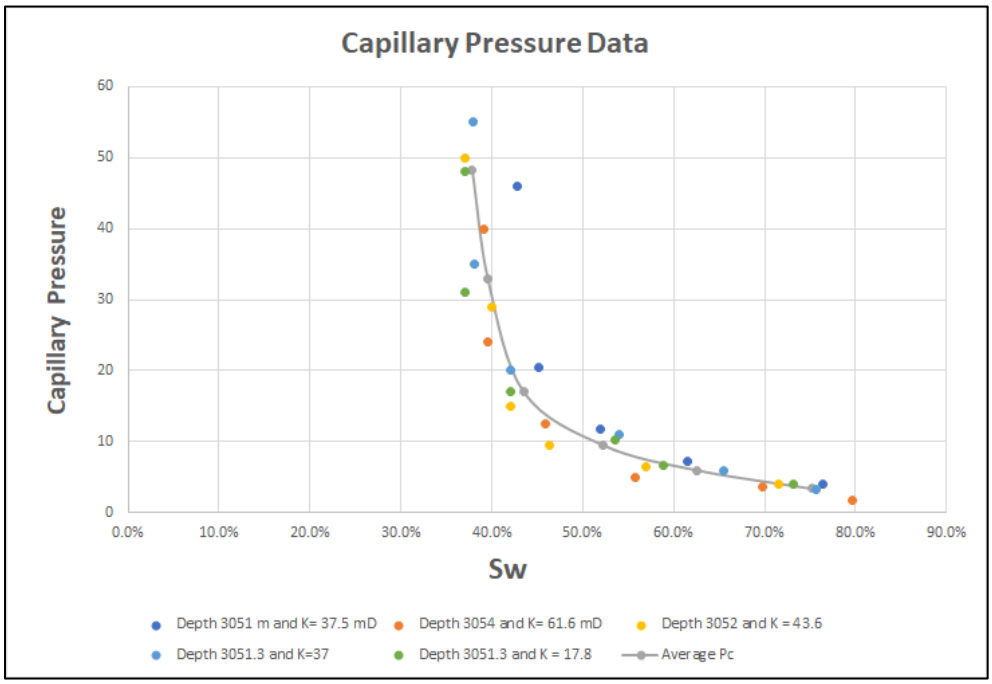

Figure II-17. Capillary pressure curve (in psi) from laboratory measurement

This information from laboratory measurements could not be directly used for reservoir simulation. Laboratory measured values were reconverted to reservoir conditions using a correlation *(Crain, 2010)* shown in Equation 2-11

$$P_{c\_res} = P_{c\_lab} \cdot \frac{(\sigma_{ow} \cdot cos\theta_{ow})}{(\sigma_{gw} \cdot cos\theta_{gw})}. \quad (2\text{-}11)$$

By utilizing typical air-brine conversion to oil-water $\sigma_{ow} = 24$ dynes/cm ; $\sigma_{gw} = 72$ dynes/cm ; θ_{ow} = 30 deg and θ_{ow} = 0 deg. Correlation between P_c in the lab and P_c at reservoir conditions were obtained using Equation 2-12

$$P_{c\_res} = 0.289 \cdot P_{c\_lab}. \quad (2\text{-}12)$$

Initial P_c input at reservoir condition is shown in Table II-6

Table II-6. Conversion from laboratory to reservoir conditions

P_c Lab (Psi)	S_w	P_c reservoir (Psi)
3.38	0.75	0.98
6	0.63	1.73
9.48	0.52	2.74
17	0.44	4.91
33	0.40	9.53
48.25	0.38	13.93
Not available	0.30	24.96*

**Extrapolated based on available data to S_{wi} 0.3*

Figure II-18 shows the capillary pressure curves from these measurements. In the reservoir simulation study, the capillary pressure effect was evaluated as part of the sensitivity study. Selecting a best representative capillary pressure value helped the effort to improve the water production match.

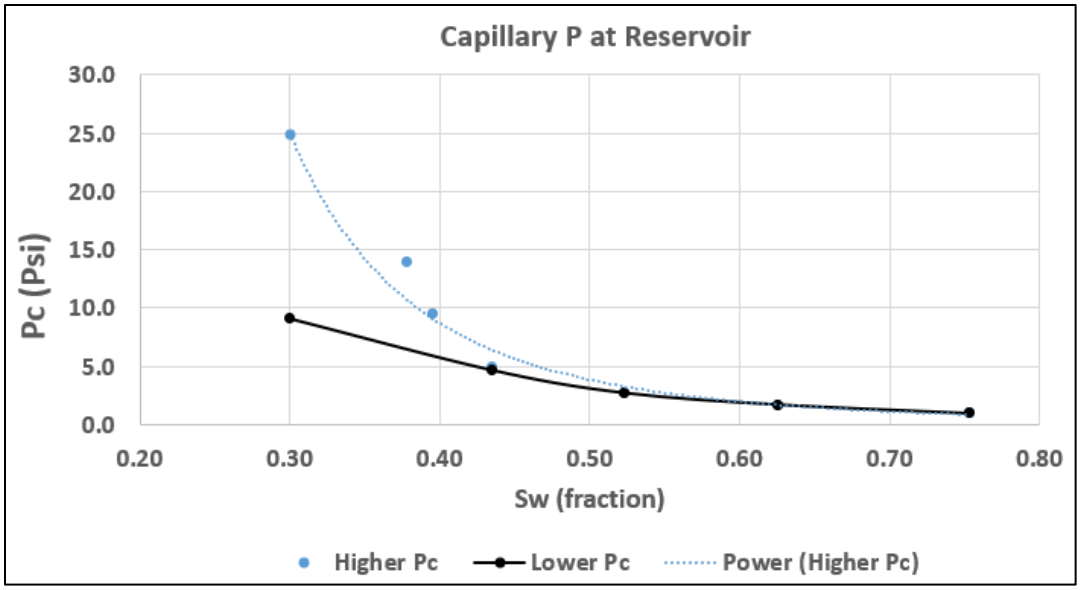

Figure II-18. Capillary pressure curves at reservoir conditions

II.4.5 Well Tests

Pressure build-up data is available from well NHK-411. From this well test data, key reservoir parameter for the drainage radius of this well was obtained and summarized as follows:

- Average reservoir pressure: 3786 to 3829 psi
- Effective permeability to oil: 9.6 mD. This interpreted permeability is not representative of the overall reservoir permeability. This value is lower because the pay-zone in this well is mostly shaly sand.
- Skin Factor: 6.7

CHAPTER III. EMPIRICAL and ANALYTICAL METHODS

This chapter discusses field performance analysis by using analytical and empirical methods. These methods mainly utilize different classical and proven Reservoir Engineering (RE) plots. These diagnostic plots are simple yet compelling techniques that help in understanding the reservoir process and field performance. Classical plots such as q vs. time, q vs. N_p, and WOR vs. N_p were used in this analysis. EUR can be estimated from these plots; these plots may also provide an indication of whether there is production improvement during the injection period/waterflooding (*Thakur, G. C., 1991*).

In addition to discussing classical plots, the IPM MBAL tool was used to perform material balance analysis. Performing all of these processes are very important not only to understand the field performance but also to guide the reservoir simulation study.

III. 1 Production Plots

Figure III-1 shows the fieldwide production rate, cumulative oil, and active wells. Generally, the oil rate increases when more wells are active. Normalized rate per well demonstrates that infill drilling yields incremental oil.

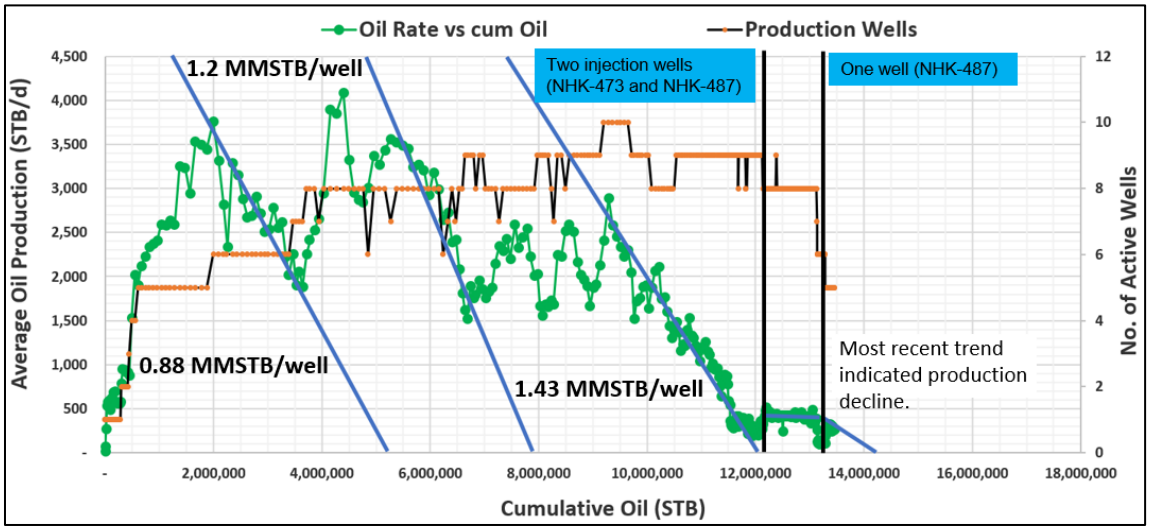

Figure III-1. Production (q) and no. of active wells vs. cumulative oil (N_p)

The implementation of two injectors (NHK-473 and NHK-487) maintained the oil production rate. It implies that injection implementation yields additional oil recovery from 12.2 MMBO to around 13.3 MMBO.

At the later time, the southern injector (NHK-473) was stopped, and the injection rate in NHK-487 was decreased. Arguably, this could attribute to the decrease in the oil production rate in the last few years. Based on the extrapolation of this plot, EUR is estimated to be around 14.1 MMBO. The operator-reported OOIP at LK-4 sand is ≈ 39.9 MMBO. Therefore, the ultimate recovery factor with the current reservoir management strategy will be 35.3%.

III. 2 Water Oil Ratio vs. Cumulative Oil

Water-oil ratio (WOR) forecasting is a method to evaluate the trend of future water production, which can further be used for oil production forecasting and EUR determination. Water-oil ratio forecasting is an empirical analysis method, so there is no formal model. This plot is typically semi-log, where the water-oil ratio is the Y-axis, and cumulative oil production is X-axis. Equation 3-1 defines the water-oil ratio

$$WOR = \frac{q_w}{q_o} \tag{3-1}$$

where q_w is water flowrate, and q_o is oil flowrate.

To create the forecast, a linear trend is placed on the water-oil ratio semi-log plot. Additionally, a maximum water-oil ratio cutoff is usually applied to truncate the forecast. Since this field has a strong water drive and applied water injection, this WOR forecasting method will be beneficial. One primary assumption in this method is similar to the decline

curve analysis, where the trend created with the WOR plot should be considered under constant operating conditions.

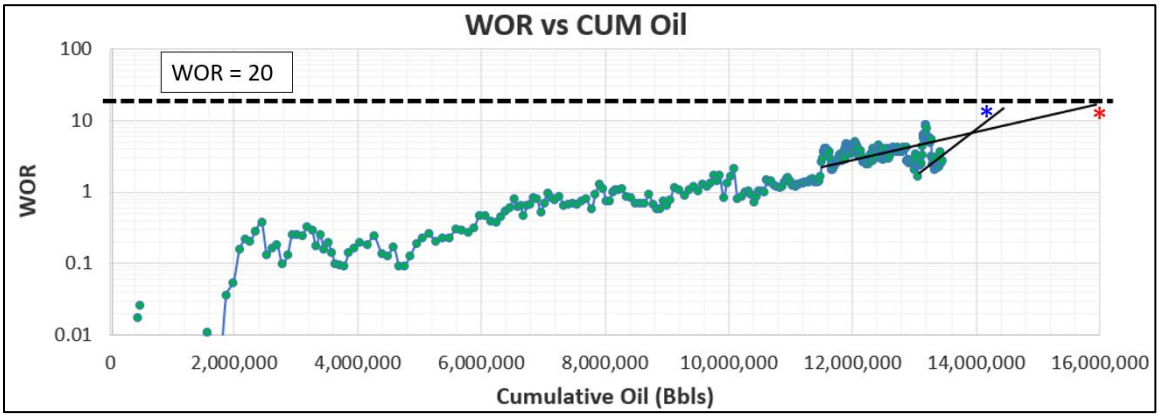

Figure III-2. Water Oil Ratio vs. Np

Reading from Figure III-2 and supposing that 95% water-cut is the economic limit, at least two possible trends can be extrapolated from the last data point. One possibility based on the last data trend suggests that the field can yield oil EUR between 14 – 14.4 MMBO*. Another possible interpretation based on a longer historical trend, and better reservoir management, the field can potentially yield a EUR of up to 16 MMBO*.

III. 3 Decline Curve Analysis

Identification of flow regime change is vital in selecting the best forecasting model to be used at any stage in a production analysis (*Sharma, A., and Lee, J. W., 2016*). As a minimum requirement for an empirical decline curve analysis, a reservoir has to exhibit Boundary Dominated Flow (BDF). A method to determine the onset of BDF is to plot the oil flow rate vs. Material Balance Time (MBT) on a log-log scale. *Raghavan, R., Palacio, J. C., and Blasingame, T. A. (1993*) introduced MBT as shown by Equation 3-2

$$t_{MB} = \frac{1}{q(t)} \int_0^t q(t)\, dt = \frac{Q(t)}{q(t)}. \qquad (3\text{-}2)$$

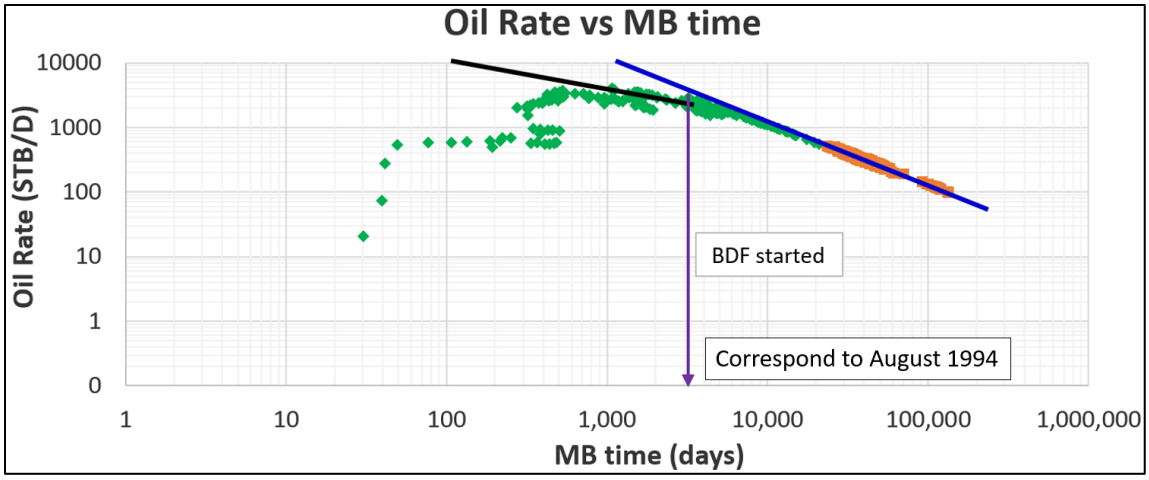

Figure III-3. Determining the onset of BDF (fieldwide)

The initial data point shows that the flow is in the transient regime, as indicated by -1/2 slope (black line in Figure III-3). On the other hand, BDF is marked by a unit slope, as shown by the blue line in the same Figure. The onset of BDF starts at MB time corresponds to August 1994. Therefore, decline curve analysis should be evaluated using data after August 1994. This study utilized the exponential decline equation, as shown in Equation 3-3. This equation was used to quantify two possible different decline curves that this field exhibited.

$$q_t = q_o . e^{-d.t} \tag{3-3}$$

where: q_t = Flowrate at the end of evaluation time (terminal rate)

q_o = Flowrate at time zero (STB/D)

d = Decline rate (%/yr)

t = Time (year).

Figure III-4 shows observation from a fieldwide perspective, field decline rate before the injection was 29.2%/year. From December 2002 to October 2009, period (depending on data filtering), a rather flat trendline or low declines were observed. At a later time when the injection started in the field, fieldwide decline was 18.3%/ year. The

most recent decline trend was 17.8%/year. As more data becomes available, this number could be verified in the future.

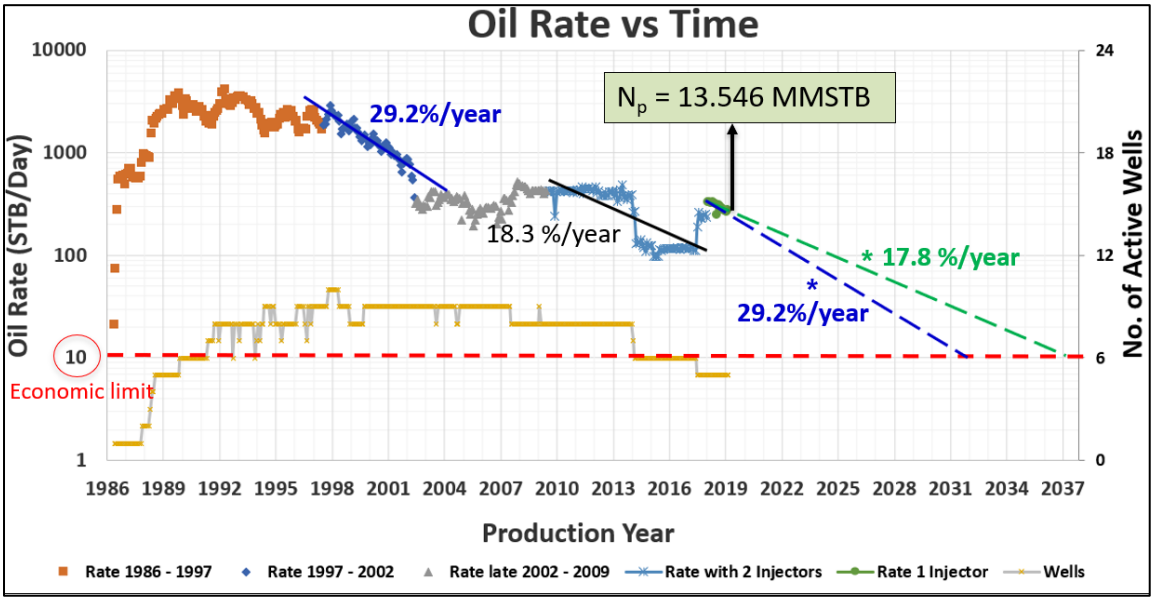

Figure III-4. Field decline curve analysis

According to the historical production profile, the fieldwide declines were 29.2%/year, 18.3%/year, and 17.8%/year. Utilizing two past decline trends, i.e., 29.2%/year (high value) and 17.8%/year (low value and most recent), EUR was calculated using Equation 3-4

$$EUR = N_p + \frac{q_{current} - q_{limit}}{d} \Delta t \quad (3\text{-}4)$$

where:

N_p is cumulative oil (MMSTB) and d = Decline rate (%/year)

$q_{current}$ is the flowrate (last rate as of August 2019), and the economic limit was assumed to be 10 STB/D.

Cumulative oil (N_p) as of August 2019 is 13.546 MMSTB; the EUR based on this value will be ranging from 13.93 to 14.14 MMSTB. Detailed EUR calculations for this scenario is shown in Table III-1:

Table III-1. EUR calculation for the higher and lower decline rates

Higher Decline (Assume 29.2%/year)		
q (t), STB/D	**t (year)**	**Cum (STB)**
272.3	0	99457.6
203.3	1	74271.8
151.9	2	55463.8
113.4	3	41418.6
84.7	4	30930.1
63.2	5	23097.7
47.2	6	17248.6
35.3	7	12880.7
26.3	8	9618.9
19.7	9	7183.1
14.7	10	5364.1
11	11	4005.8
10	11.3	3669.8
GRAND TOTAL		384,611

Lower Decline (Assume 17.8%/year)		
q (t), STB/D	**t (year)**	**Cum (STB)**
272.3	0	99457.6
227.9	1	83240.3
190.7	2	69667.3
159.6	3	58307.5
133.6	4	48800.0
111.8	5	40842.8
93.6	6	34183.1
78.3	7	28609.3
65.6	8	23944.3
54.9	9	20040.0
45.9	10	16772.3
38.4	11	14037.5
32.2	12	11748.6
26.9	13	9832.9
22.5	14	8229.5
18.9	15	6887.7
15.8	16	5764.6
13.2	17	4824.6
10.0	18.59	3635.4
GRAND TOTAL		588,825

Depending on the fitting window and data filtering, it is commonly understood that DCA can be subjective. Hence a secondary check was done using Kappa-Topaze with a slightly different data grouping. Instead of combining all wells into one field analysis, wells were grouped into the southern and the northern sectors. If this result is relatively close to the fieldwide estimation, the fieldwide interpreted decline rate will be a reasonably representative number.

Figure III-5 and Figure III-6 show the decline rates for the northern well group. The northern group consists of NHK-487, NHK-499, NHK-502, NHK-505, and NHK-580. In this well group, the decline rate before the injection is 28.4%.

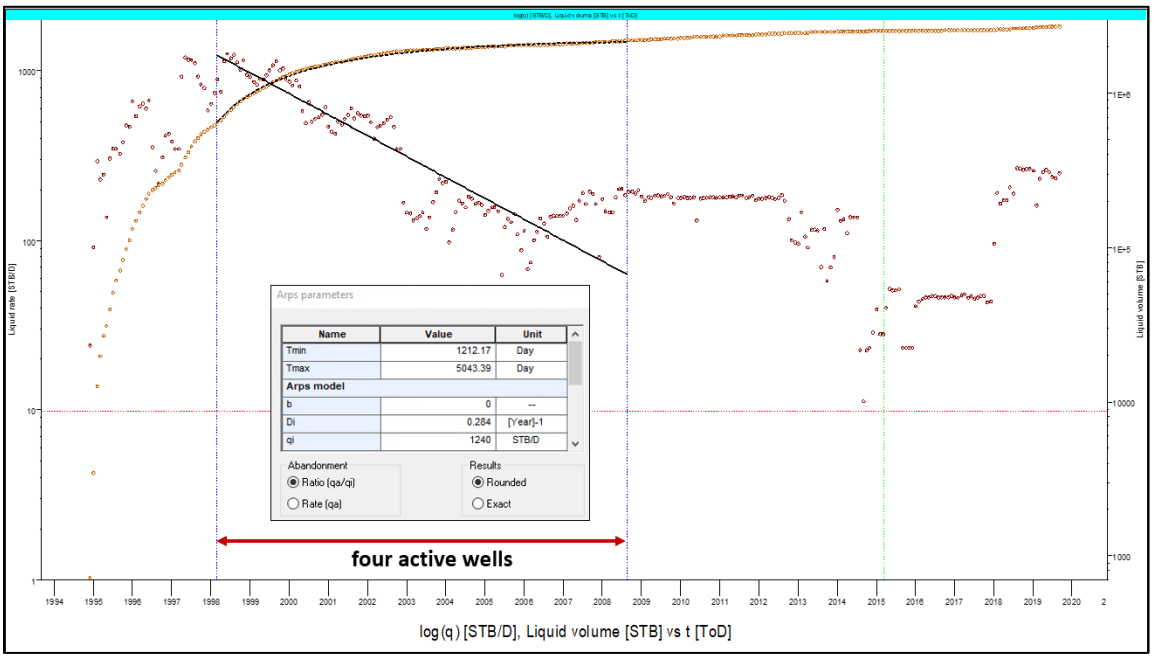

Figure III-5. Decline curve analysis for the five northern wells before injection

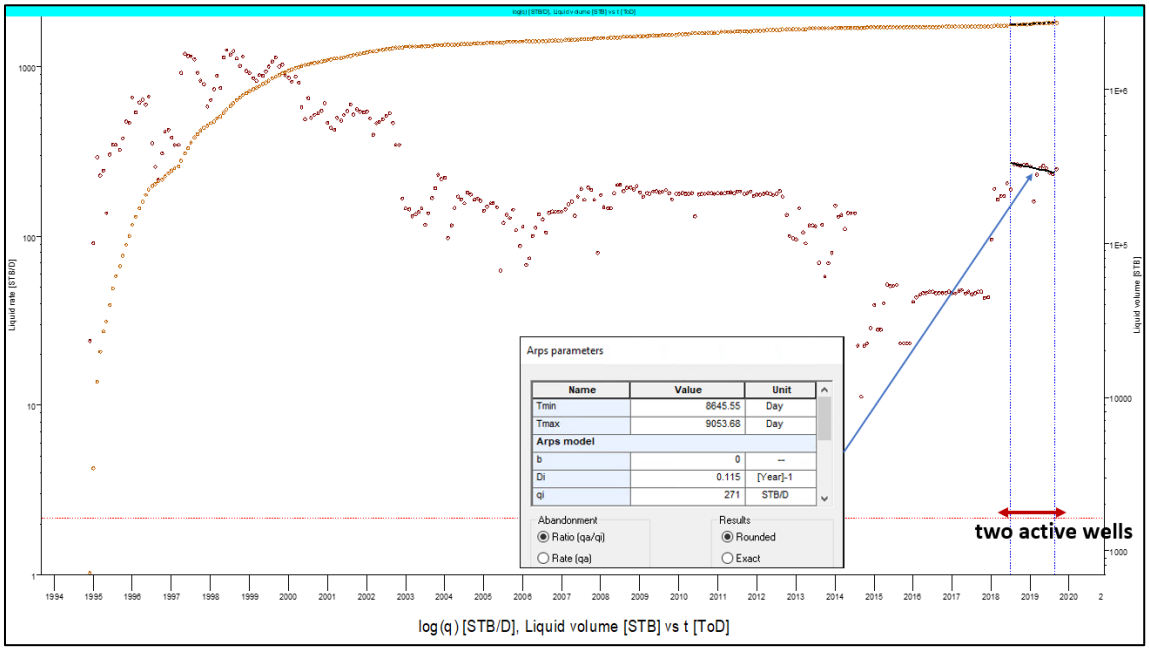

Figure III-6. Decline curve analysis for the five northern wells after injection

After injection, as shown by Figure III-6, the decline rate is 11.5%/year. The trendline for pre-injection events is quite convincing. For the post-injection event, further confirmation of the trend is required upon additional data availability.

Figure III-7 and Figure III-8 show the southern well group. The southern well group consists of NHK-384, NHK-391, NHK-411, NHK-419, NHK-420, NHK-422, NHK-448, NHK-462, NHK-469, and NHK-473. In this group, the decline rate before injection event was 24.5%, while the decline rate after injection was 14.7%/year.

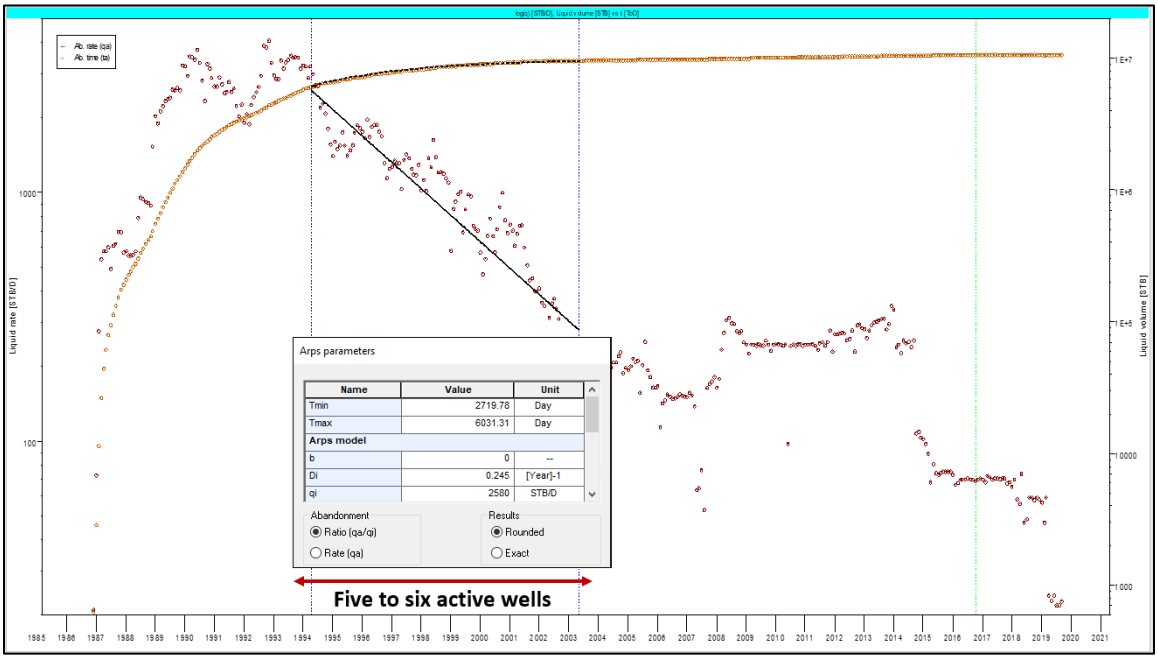

Figure III-7. Decline curve analysis for the ten southern wells before injection

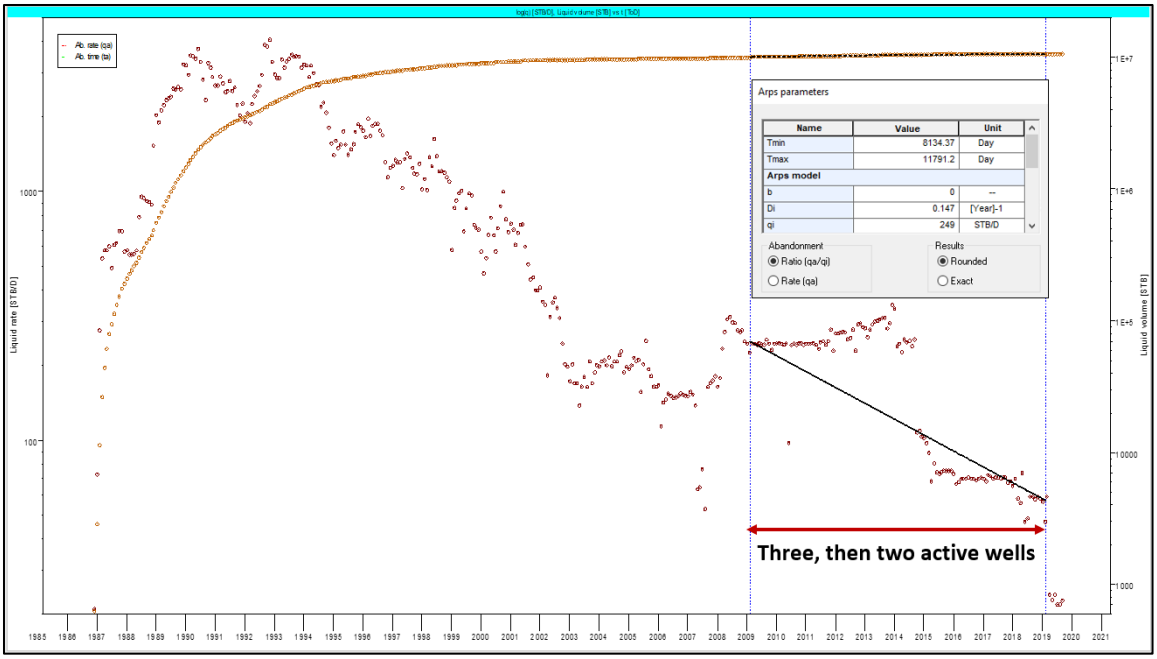

Figure III-8. Decline curve analysis for the ten southern wells after injection

Figure III-8 shows a decline curve analysis for ten wells in the southern sector. Unlike a well-defined trend for the northern well group, the post-injection decline trend for the southern well group is 14.7%/year. This trend is somewhat arbitrary and is not a solid line, due to a step-change in the total rate. This observation was correct even when the period of decline curve analysis split into three-well and two-well timeframe.

III. 4 Material Balance Analysis

Material balance analysis is one of the fundamental petroleum engineering techniques that can be used to aid the understanding of a reservoir and its connecting aquifer. The material balance equations considered tank-type behavior at any given datum depth. Based on this assumption, the reservoir was considered to have the same pressure and fluid properties at any location in the reservoir. As soon as production started, the reservoir depleted because production caused reservoir pressure to drop from its initial pressure (p_i) to an average reservoir pressure ($\bar{p}$).

I used commercial software (MBAL from Petroleum Expert) to perform the material balance analysis. I treated the LK-4 reservoir as one tank, and a fieldwide evaluation based on pressure and production data was performed. Equations 3-5 and 3-6 summarize the general material balance equation for oil

$$Oil\ Expansion + Gas\ Cap\ Expansion + Water\ Expansion + Formation\ Contraction + Water\ Influx + Water\ Injection + Gas\ Injection = Oil\ \&\ Dissolved\ Gas\ Production + Free\ Gas\ Production + Water\ Production \quad (3\text{-}5)$$

and, mathematically written as follow

$$N(B_t - B_{ti}) + N\ m\ B_{ti}\frac{(B_g - B_{gi})}{B_{gi}} + (N\ B_{ti} + N\ m\ B_{ti})\ \frac{c_w\ S_w}{1-S_w}\Delta p + \ c_f\ \Delta p\frac{(N\ B_{ti} + N\ m\ B_{ti})}{1-S_w} + W_e + W_I\ B_{wI} + G_I\ B_{gI} = N_p\ B_t + N_p\ (R_p - R_{soi})\ B_g + W_P\ B_w. \quad (3\text{-}6)$$

The equation above means that as the pressure in the reservoir falls, the oil, gas, and water must be allowed to expand. This expansion volume, together with a reduction in pore volume and any fluid injection, must be equal to the total fluid production. These volumes should be expressed in reservoir barrels so that the mass is conserved in the system.

Available SBHP, production data, PVT, core data, and well test analysis were the primary properties that became the main inputs in MBAL. Figure III-9 shows all the available pressure data points and selected pressure as input. The smooth decline pressure data were chosen to avoid issues in MBAL regression. Material balance analysis was done from the first production (November 1986) to the time before injection started. This primary depletion period was considered long enough (23 years) for use in the material balance study.

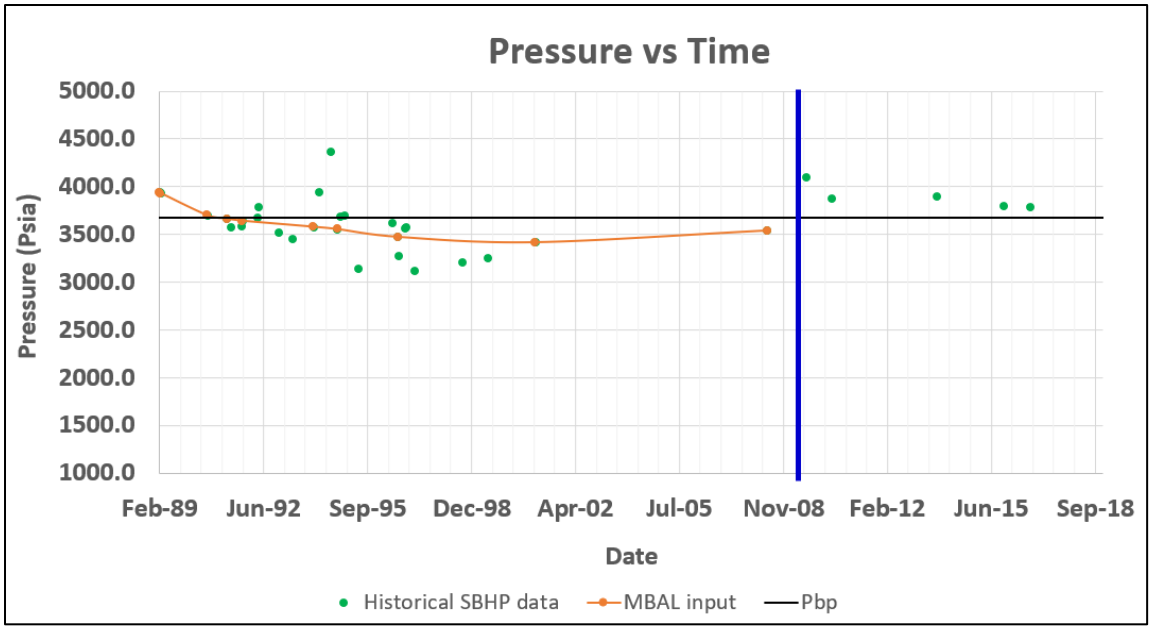

Figure III-9. Selected pressure data in MBAL input

The key objectives of material balance analysis were to understand the reservoir drive mechanisms, to estimate the OOIP, and to investigate the aquifer properties. Table III-2 summarizes the input parameters used in the MBAL simulation.

Table III-2. Input parameters in MBAL

Parameter	**Values**
Temperature, ^{o}F	184
Initial pressure, psi	3950
Porosity, %	19.9
Connate water saturation	0.3
GOR, SCF/STB	843
Gas gravity	0.7113
Oil gravity, ^{o}API	31.6

The MBAL used two methods to obtain the best match. First is an analytical method. Figure III-10 shows the tank pressure vs. N_p plot between the measured data and the model. The match was considered reasonably accurate.

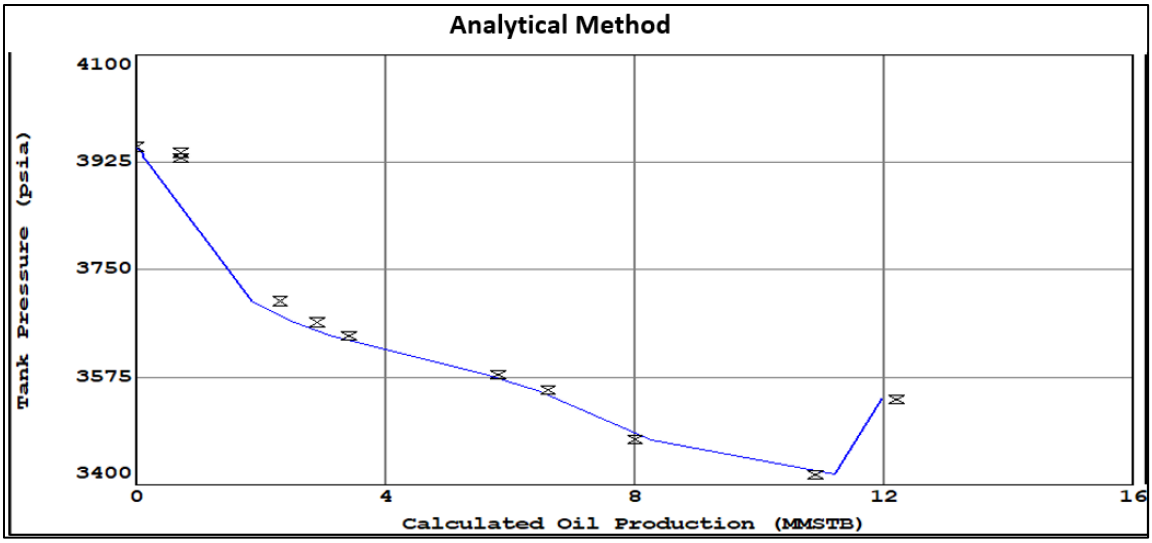

Figure III-10. MBAL analytical method (tank pressure vs. Np)

Figure III-11 shows the drive mechanism plot from this MBAL simulation. Reading the drive mechanism plot confirms that the LK-4 reservoir's primary drive mechanism is dominated by water influx with some minor contributions from fluid expansion and weak PV compressibility. Based on this method, OOIP was estimated to be 43.1 MMSTB (6.85 $MMSm^3$), and the aquifer size was estimated to be 39,072 $MMft^3$. PV ratio between aquifer water volume to reservoir oil volume is 113.

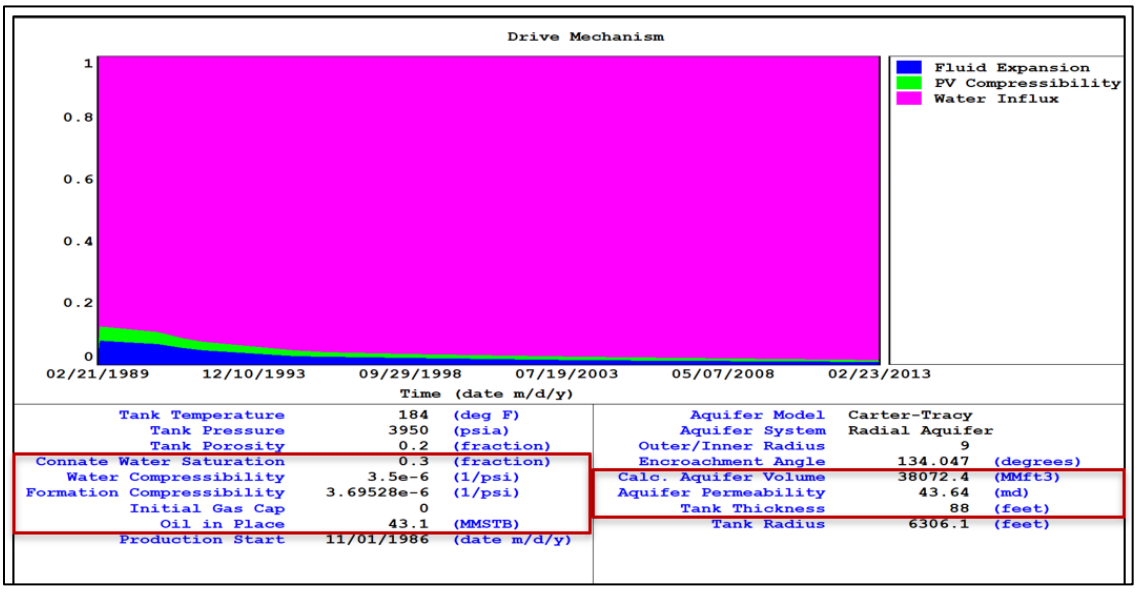

Figure III-11. MBAL drive mechanism plot

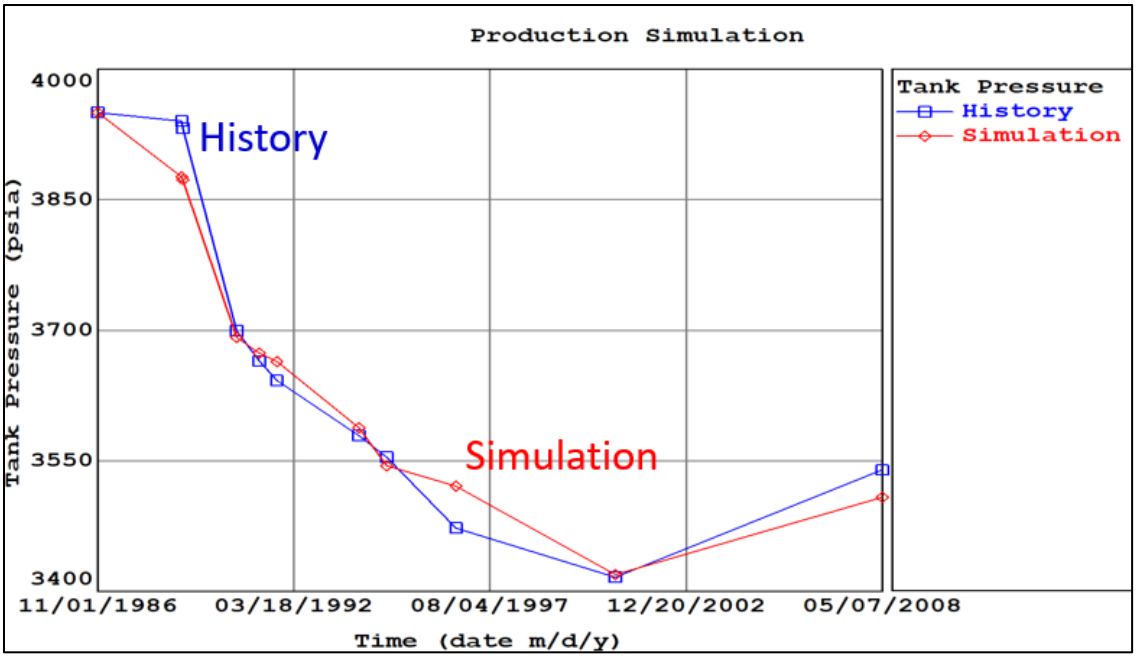

Figure III-12. MBAL pressure match plot

Figure III-12 shows the match between pressure data with modeled pressure as a function of time. The good pressure match indicated that the chosen parameter values in the analytical methods were reasonably good. Figure III-13 shows Havlena – Odeh straight-line method to estimate OOIP. Based on this method, the best straight-line fit of the points yielded an OOIP of 43.2 MMSTB (6.87 $MMSm^3$).

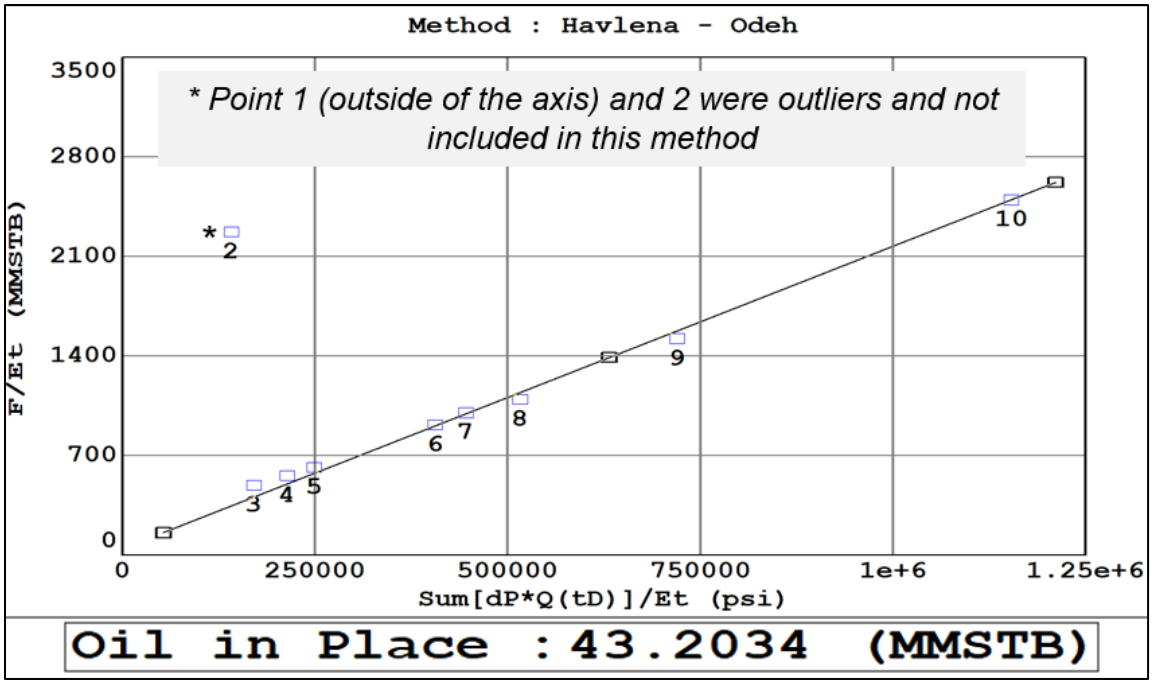

Figure III-13. MBAL graphical method (Havlena – Odeh)

Table III-3 shows the summary of the MBAL with the best match.

Table III-3. MBAL output results

Parameter	Values
Initial gas cap (m) ratio	0
Water compressibility (1/psi)	3.5×10^{-6}
Aquifer model	Carter Tracy
Aquifer permeability, mD	43.6
Tank thickness, ft	88
Outer/inner radius ratio	9
Rock compressibility 1/psi	3.69×10^{-6}

CHAPTER IV. RESERVOIR SIMULATION

Reservoir simulators are used widely to study reservoir performance and to determine methods for enhancing the ultimate recovery from the reservoir. When it is used correctly with sound engineering judgment, simulation can solve problems that cannot be solved otherwise. Simulation can also provide meaningful insight for the field development plan. Simulation is the only way to describe the multiphase flow in a heterogeneous reservoir quantitatively. In the simulation, the user could specify a production schedule that can be manipulated not only by the properties of the reservoir but also by the operational constraints, market demand/economy constraints, investment strategies, government regulations, etc. All of these possible developments or operational scenarios can be studied in 'what-if' fashion using reservoir simulation. Hence the impact of surface and subsurface uncertainty can be evaluated adequately.

Reservoir simulation is a material balance calculation that is performed by discretizing the reservoir into certain grid sizes as specified by the user. For the material balance calculations at the grid cell level, the key assumption is the principle of mass conservation and Darcy's law applied in the system.

The development of various simulation tools with enhanced capability is supported strongly by the vast improvement in computer technology. Throughout this study, the Eclipse-100 black oil simulator within the Petrel Reservoir Engineering platform was used extensively. Eclipse 100 is a fully implicit, three-phase, three-dimensional, general-purpose black oil simulator. As of now, Eclipse is one of the most widely used simulators and has become a standard in black oil simulation. It can model almost any reservoir description; it is reliable, accurate, and easy to use. In addition, it also allows for effective

collaboration between reservoir engineers and geoscientists as the Petrel platform integrates geological and mapping packages into one software. The later part of this simulation study (production forecast) was carried out using CMG suites (Builder, Imex, and Result) due to Petrel's and Eclipse's license expiration issues.

IV.1 Model Input and Constraints

As mentioned in the previous section, there are three types of data supplied to the research team, i.e., production data, well logging/formation evaluation data, laboratory test data, and seismic data (during later part of the research). Essential information that became the input into the reservoir model is as follows:

1. Preliminary geomodel that was built and fine-tuned around June – July 2019 (*Chatterjee, S., 2019*).
2. All wells that are either producers or injectors in the LK-4 reservoir only.
3. Well logs / formation evaluation data.
4. The LK-4 reservoir has been producing since November 1986. Continuous measurements of oil rates, water rates, and gas rates are available for each well. SBHP and FBHP are only available at a particular time.
5. Injection started in November 2007 with two injectors (NHK-473 and NHK-487). Starting in June 2017, only one injector is active (NHK-487).
6. 3D seismic data was obtained by our team in December 2019; this was used to guide the placement of aquifers in the model.

The history match runs were performed using the oil rate as the constraint for the production history. The final history match section provided complete input data and properties used in the simulation.

IV.2 Model Description

The LK-4 reservoir model consists of approximately 203,000 grid cells. The number of grid cells is 83 x 57 x 43 in I, J, and K directions, respectively. The model consists of 43 geological layers with an average thickness of about 2 m (7.6 ft). The average dimensions of the grid cells are 163.9 ft x 163.9 ft x 7.6 ft (50 m x 50 m x 2 m). Figure IV-1 shows the shape of the reservoir body.

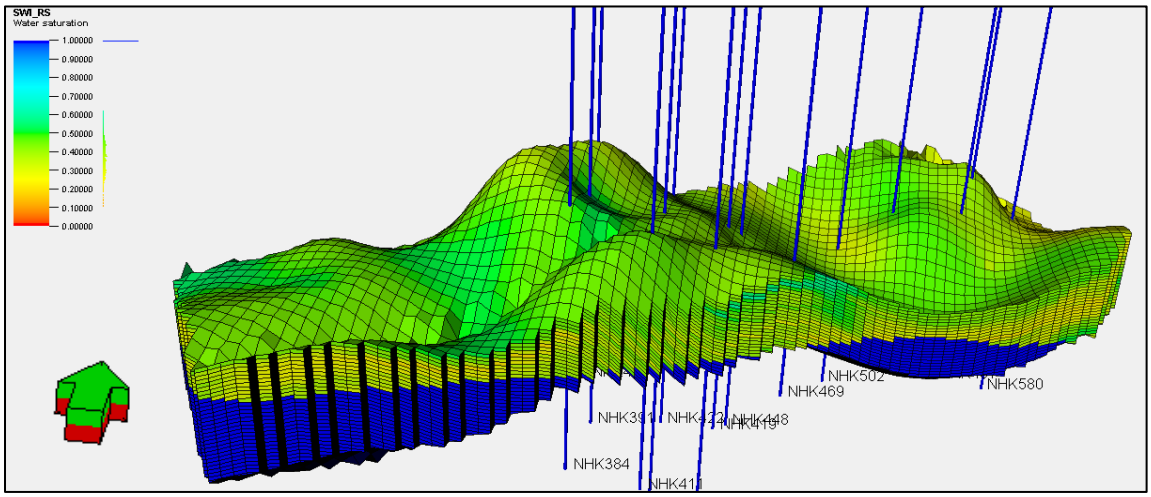

Figure IV-1. LK-4 reservoir model

The LK-4 reservoir model was built as a black oil model that includes a substantial aquifer from the bottom and the edge of the field. Over the years, as production progressed, the number of wells in the field grew to fifteen. Initially, all of them were producing wells. At a later time (November 2009), two producers (NHK-473 and NHK-487) were converted into injectors. Starting in June 2017, only one injector (NHK-487) was utilized in the field. As explained in Chapter II, Oil-Water Contact (OWC) was one of the critical uncertainties

that could be ranging between 2960 and 2980 m (9709 – 9774 ft) SSTVD. Gas-Oil Contact (GOC) was determined by OIL at 2912 m (9551 ft) SSTVD.

IV.3 Model Initialization and Volume Calculations

Initialization is a process that defines the initial state of the model before actual history matching. The initialization process is required to obtain pressure and phase saturation at the start date of the simulation. The initial state of the model can be defined by either equilibration, enumeration, or a restart run.

In this study, equilibration was used to initialize the model before the history match. Restart runs were used as a starting point of all future production forecasts after history matching was completed. The enumeration method was not appropriate for this study because it requires knowledge of water saturation, capillary pressure, and pressure distribution accurately throughout the reservoir at a specific time. If this condition is not met, inconsistencies in the pressures and saturations will make the model unstable.

The initialization process requires field properties such as initial pressure conditions, relative permeability curves, rock compaction function, PVT data, and fluid contacts as initialization inputs. The initial pressure and saturation set-up were based on a saturation function using rock physics functions process. Fluid contacts, datum depth, and pressure need to be pre-determined in the fluid model dialog box. The final history match section presented the parameters used to get the best fieldwide history match in Petrel. These reservoir and fluid properties were imported to CMG for history match benchmarking, and prediction runs.

The volume calculation process under Petrel volumetric calculation workflow can accurately calculate the volumes in a 3D grid (bulk, pore, and fluid). Sensitivity analysis

can help in determining areas where efforts in reservoir evaluation should be allotted. It is imperative to validate the OOIP reported by the simulator through initialization with OOIP that was obtained from the static volumetric calculations.

In the initialization process, OOIP from simulation can be obtained and compared with the volumetric OOIP. The disparity between the calculated OOIP values using these methods is not unexpected. However, it should be within a ±10% range. Figures IV-2 and IV-3 show a comparison between volumetric and simulation initialization. The OOIP in the sands can be obtained directly from volumetric calculations using Petrel. However, reservoir simulation using either Eclipse or CMG-Imex does not discriminate between sand and shale. Therefore, the OOIP output using simulation was multiplied with 0.79 (i.e., sand proportion from Petrel) to obtain a proper comparison between the volumetric and simulation OOIPs. These 79% sand and 21% shale facies are explained in the geomodel section.

```
                                        ================================================
                                        :              FIELD TOTALS                    :
                                        :         PAV =       261.57  BARSA            :
                                        :         PORV=    794089847.   RM3             :
                                        :(PRESSURE IS WEIGHTED BY HYDROCARBON PORE VOLUME:
                                        : PORE VOLUMES ARE TAKEN AT REFERENCE CONDITIONS):
                     :--------------- OIL    SM3  ---------------:-- WAT    SM3  -:--------------- GAS    SM3  ---------------:
                     :     LIQUID         VAPOUR         TOTAL   :       TOTAL    :       FREE      DISSOLVED         TOTAL   :
-------------------------:-----------------------------------------:----------------:-----------------------------------------:
CURRENTLY IN PLACE       :      7715079.                  7715079.:     769566092. :    173682934.   1114473510.    1288156444.:
-------------------------:-----------------------------------------:----------------:-----------------------------------------:
OUTFLOW THROUGH WELLS    :                                2150726.:        369141. :                              445636628.:
ANALYTIC AQUIFER INFLUX  :                                       :       3781965. :                                       :
WELL  MATERIAL BAL. ERROR:                                   -0.:            0. :                                    -10.:
FIELD MATERIAL BAL. ERROR:                                  520.:         -1386. :                                 107350.:
-------------------------:-----------------------------------------:----------------:-----------------------------------------:
ORIGINALLY IN PLACE      :      9866325.                  9866325.:     766151882. :    305958645.   1427941767.    1733900411.:
=========================================================================================================================================
```

Figure IV-2. OOIP output from the history match model

Detailed results

Zones	Segments/Regions	Facies	Boundaries	HC intervals	Contact regions	STOIIP (in oil)[sm3]	GIIP (in oil)[sm3]
Barail_4th_Bigger_Lankashi_2 - Barail_5th_Bigger_Lankashi	Segment 1	Shale	Langkasi_Area_SC_YZ	Oil interval	No Contact regions	1303334	188983373
Barail_4th_Bigger_Lankashi_2 - Barail_5th_Bigger_Lankashi	Segment 1	Shale	Langkasi_Area_SC_YZ	Gas interval	No Contact regions	0	0
Barail_4th_Bigger_Lankashi_2 - Barail_5th_Bigger_Lankashi	Segment 1	Sand	Langkasi_Area_SC_YZ	Oil interval	No Contact regions	7425244	1076660381
Barail_4th_Bigger_Lankashi_2 - Barail_5th_Bigger_Lankashi	Segment 1	Sand	Langkasi_Area_SC_YZ	Gas interval	No Contact regions	0	0

Figure IV-3. OOIP from the volumetric calculation

Table IV-1. OOIP from the volumetric and the reservoir simulation in the sand

OOIP Calculation Methods	Volume
Volumetric, with OWC 9735 ft (2968 m)	46.7 MMSTB (7.43 $MMSm^3$)
Reservoir Simulation	49.1 to 50.4 MMSTB (7.8 to 8.02 $MMSm^3$)

IV.4 History Matching

History matching, by nature, is an ill-posed inverse problem. History matching is a subjective and labor-intensive process, as it involves individual adjustments of static reservoir parameters for each run (*Kabir, C. S., Chien, M. C. H., and Landa, J. L., 2003*). In reality, the quality of the history match is primarily driven by the experience of the engineers and the available budget for high-quality surveillance data acquisition.

Nevertheless, history matching is one of the most crucial aspects of completing a reservoir model. The properties in the reservoir model have to be calibrated to match the observed production data. History matching plays a fundamental role in ensuring reliable future forecasts and reliable evaluation of different future development scenarios. It is understood that petroleum reservoirs are a very complex system. Building the correct reservoir model is challenging. There are significant difficulties involved in describing the system accurately in terms of how the fluid moves, and what the possible external support mechanisms are.

Depending on the level of knowledge, available production data, and complexity of a reservoir, this activity is often a very time-consuming process (*Odinukwe, J. C., 2010*). Changes were made on the geological and reservoir properties, especially for those attributes with higher uncertainty in matching historical production data. Some of these

properties are permeability in the reservoir, relative permeability curves, aquifer strength, k_v/k_h ratio, and other parameters with scarce data points.

One of the objectives of this work is to improve the current state of calibrated history matching model on the LK-4 reservoir. As explained in the earlier section, the simulation study was carried out both by using Schlumberger's simulation software platform Petrel, using Eclipse black oil (E-100) and CMG-Imex as the calculation engine. The history match was done based on trial and error by modifying some reservoir properties, endpoint relative permeability scaling, capillary pressure curve modeling, and including the aquifer support into the system. The previous analytical and empirical study proved to be helpful in providing insight into this process.

Modifying several parameters in the model, such as by permeability, k_v/k_h, and OWC, are required to get the best history match. It is also necessary to adjust the relative permeability curve end-point scaling as one best representative curve for the entire reservoir. To mimic the strong water drive in this reservoir, I had to provide external support by adding a bottom aquifer using PV multiplier and edge aquifer support using the Carter Tracy model.

The time range for the history match is from November 1986 to August 2019. As mentioned in the earlier section, the development strategy used for the production history match mode was oil rate constraint. This strategy is commonly used during history matching. The main reason is because oil is the primary commodity, and the accuracy of reported oil production is very high. Therefore, the history match model has to match oil perfectly. In this reservoir simulation study, using both Petrel-Eclipse and CMG-Imex, a

total of over 400 different cases had been tested and simulated to obtain the current best results.

IV.4.1 Baseline (AS IS) History Match

A baseline history match case was created and tested before doing any global, regional, or local modification in the model. Initially, the simulation case was executed without aquifer support using initial properties in the static geomodel, as described earlier in Chapter II. The objective was to get an understanding of how the system responds to the given extraction rates throughout the historical production time.

The reservoir is depleted very fast without aquifer support. It reaches very low pressure in mid-2002, as shown by the purple line in the pressure vs. time chart in Figure IV-6 (section sensitivity on bottom aquifer support). This case is not correctly describing the LK-4 reservoir because the field is still up and running until now. This exercise provided additional evidence that there is external energy support for the LK-4 reservoir. Figures IV-4 and IV-5 show base (as is) history match result with the inclusion of a bottom edge aquifer with pore volume multiplier of 100.

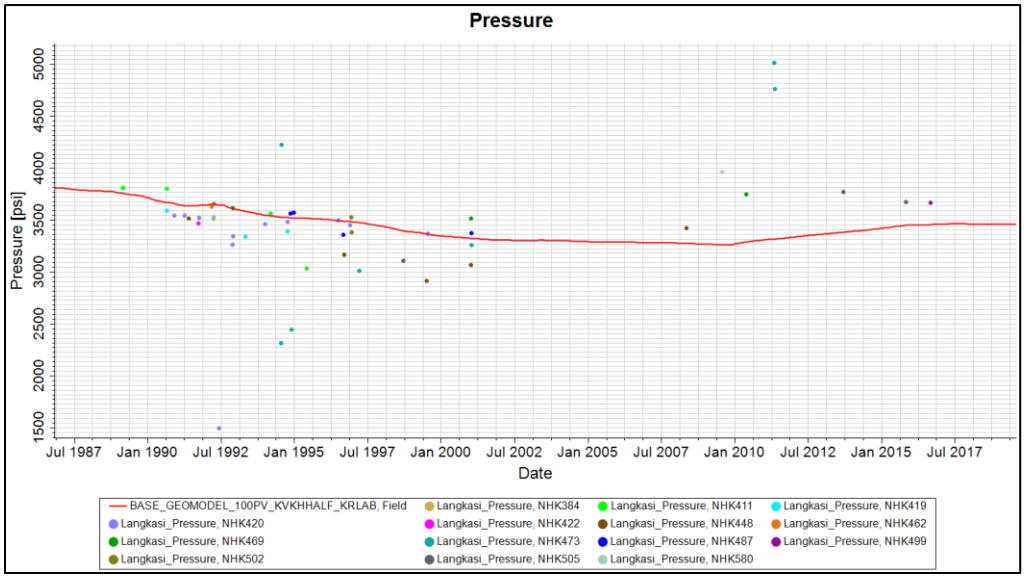

Figure IV-4. Simulated and measured P for base history match result

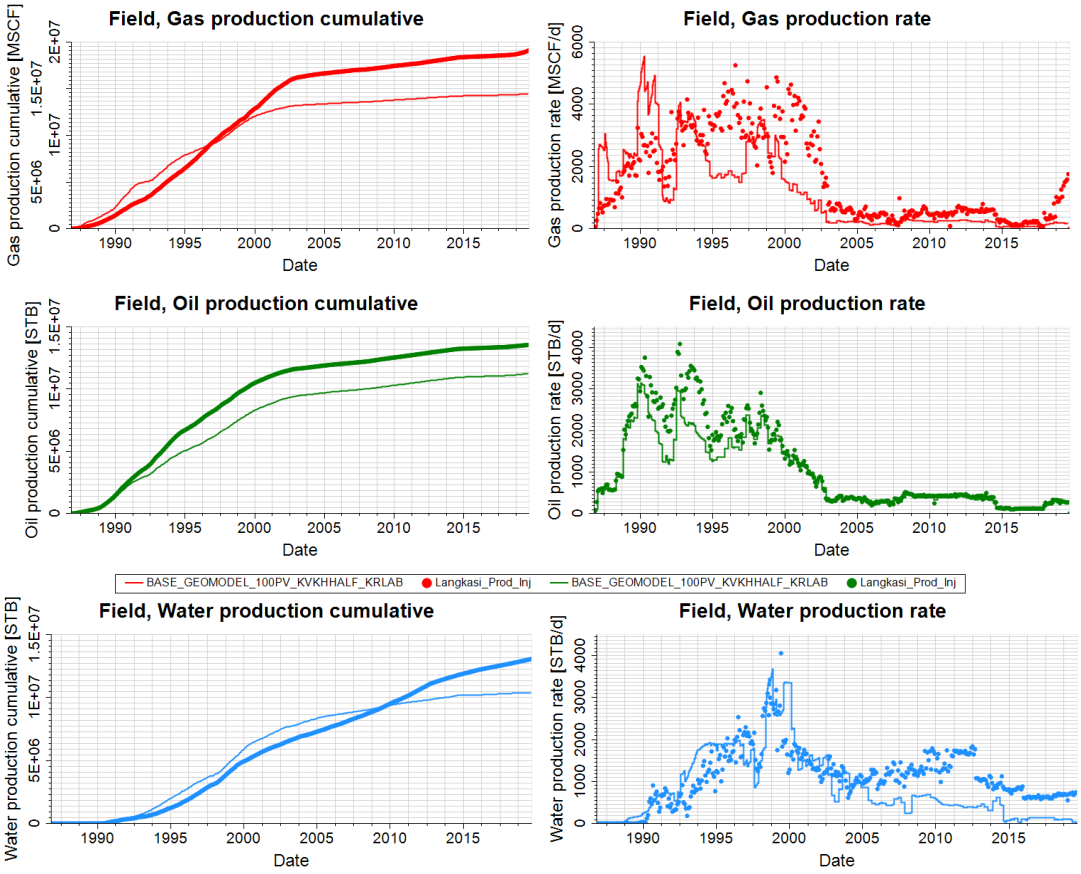

Figure IV-5. Baseline history match result

Table IV-2. Comparison between simulation and field data for the base case

Property	Simulation	Field data	Error
Oil rate (BOPD)	266.4	272.33	2.1%
Water rate (BWPD)	53.6	742.14	92.8%
Gas rate (MSCF/D)	193.5	1582.4	87.8%
Cumulative oil production (MMSTB)	11.296	13.546	16.6%
Cumulative water production (MMSTB)	10.437	13.502	22.7%
Cumulative gas production (MMSCF)	14.523	19.075	23.9%

Without any changes in the model properties, there are significant errors between simulated and observed data. The process of history match is mainly for calibration of reservoir properties to match the production data reasonably. This comparison was made

at the end of history data (August 2019), focusing on both production rate and cumulative production. Based on all the categories, water and gas show the most significant error, while cumulative oil was 16.6% lower, which was not acceptable.

This comparison was not too bad for a baseline history match result. One of the reasons was because this scenario used optimum oil-water contact (2968 m / 9735 ft), that yields a better water production match. As far as the gas production is concerned, the operator confirmed that there is a considerable error in gas measurements (± 30%). Therefore, the gas production match was not considered critical in the history match process.

Some difficulties were encountered for cells that have very low permeability (0.002 mD). It became necessary to filter and put a lower limit (5 mD) for the active cells to avoid unnecessary computation error. The following sections present a sequential sensitivity study using the baseline parameters to provide more clarity and continuity in explaining and describing the history matching process.

IV.4.2 Sensitivity Studies

Subsurface data acquisition is substantially expensive due to the high costs of drilling, coring, logging, and direct reservoir fluid sampling. This situation is a challenge for establishing representative rock-fluid properties. Additionally, this situation is not ideal for representing the entire reservoir because these data are available in relatively few locations. However, properties such as permeability, porosity, and relative permeability vary throughout the reservoir. Therefore, reservoir properties corresponding to each grid block in the simulator are subject to estimation (*Watson, A. T., 1989*).

Before proceeding to a detailed modification of the geomodel grid properties, it is essential to do sensitivity studies. Sensitivity studies were done to examine and to understand how a change in a particular parameter will impact the output profile, such as pressure, oil rate, water rate, and gas rate. Even though the geomodel was made with the best available data and used the most appropriate geostatistical method to distribute the property throughout the 3D framework, there is always some uncertainty inherent in each method and each distributed property.

The value of doing a sensitivity study is not only to understand how each parameter would impact the history match but also to provide insights on future surveillance plans. In all the sensitivity studies, the main set up is varying one parameter and keeping other parameters at their baseline values. Therefore, the effect of lowering or increasing a parameter can be clearly understood.

IV.4.2.1 Bottom Aquifer Support Sensitivity

This scenario compares the model without aquifer support and with varying aquifer strengths. Baseline value properties were directly from the geomodel. The sensitivity results were obtained and presented in the subsequent figures. This study intended to obtain a range of possible PV multipliers that result in a good pressure match. Based on this sensitivity study, the range of PV multipliers for bottom aquifer ranges between 50 and 250.

PV 100 results in the best pressure profile match as shown in Figure IV-6, while No PV and PV 10 result in the lowest pressure profile (worst pressure match). Assigning low PV (PV10) or no bottom support (no PV) will not be accurately describing the pressure behavior in the system.

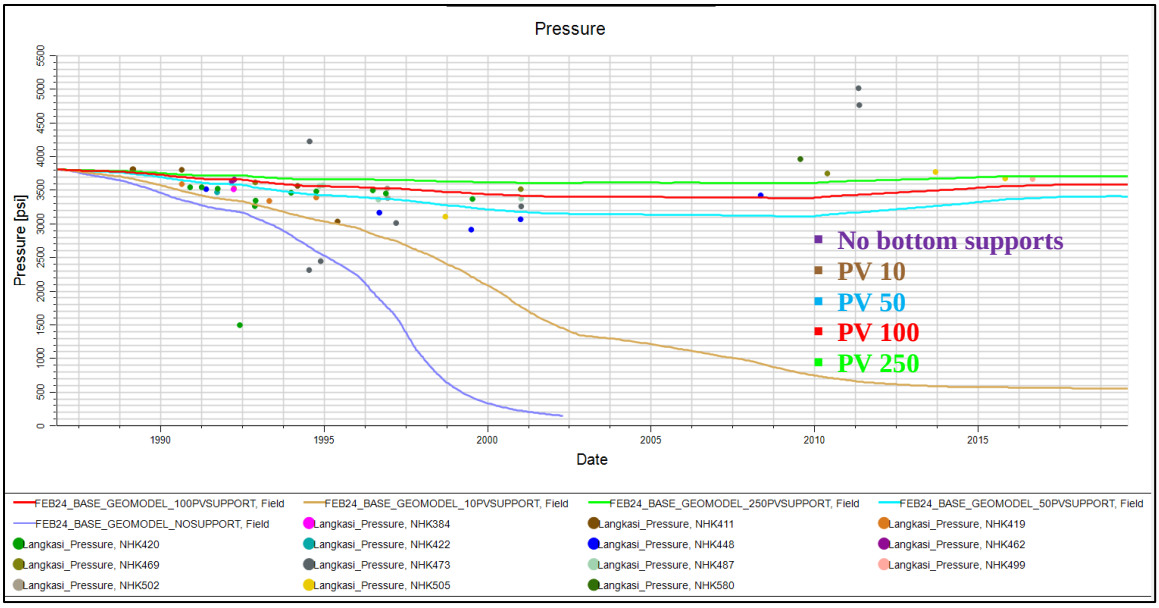

Figure IV-6. Pressure response to different bottom aquifer PV multiplier

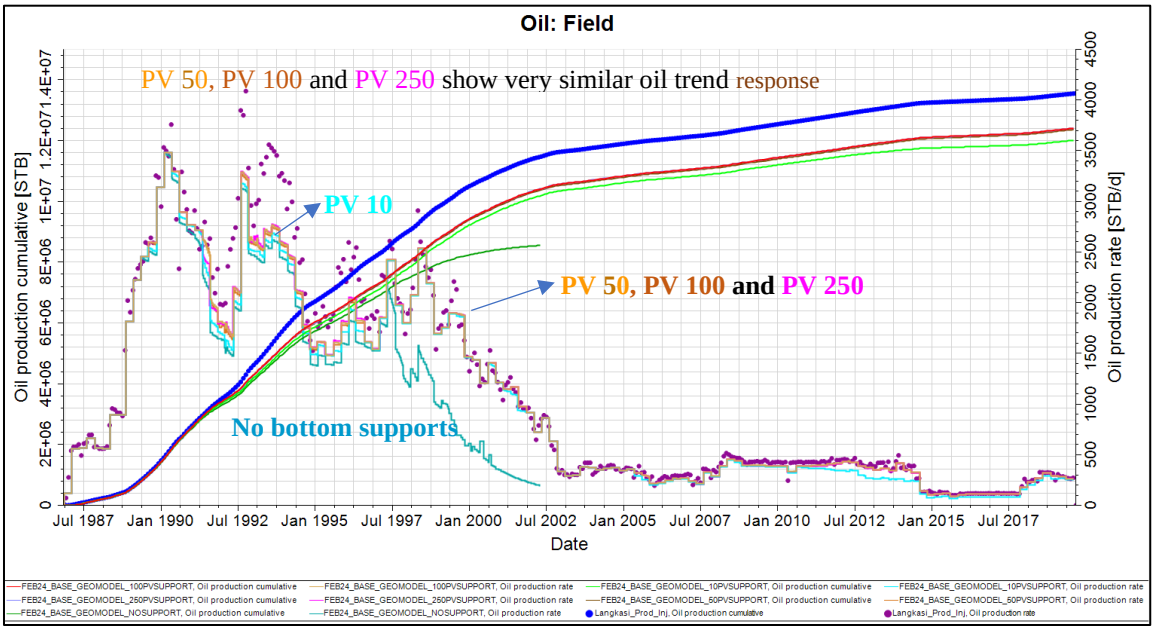

Figure IV-7. Fieldwide oil rate and cumulative oil production with variations of bottom PV

Figure IV-7 shows that oil production profile is very similar for PV higher than 50. In the case of water production rate, as shown in Figure IV-8, PV 100 and PV 250 cases show a very similar water production profile. PV 10 shows the highest water production.

The same observations are noticed from the gas production rate profile shown in Figure IV-9.

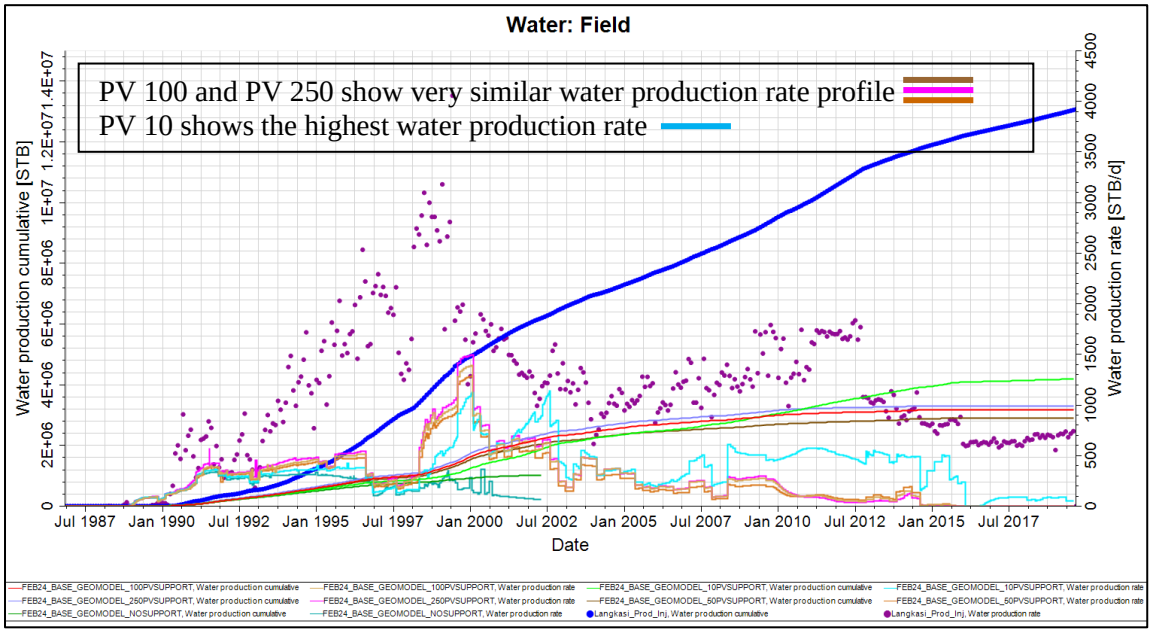

Figure IV-8. Fieldwide water rate and cumulative water production with variations of bottom PV

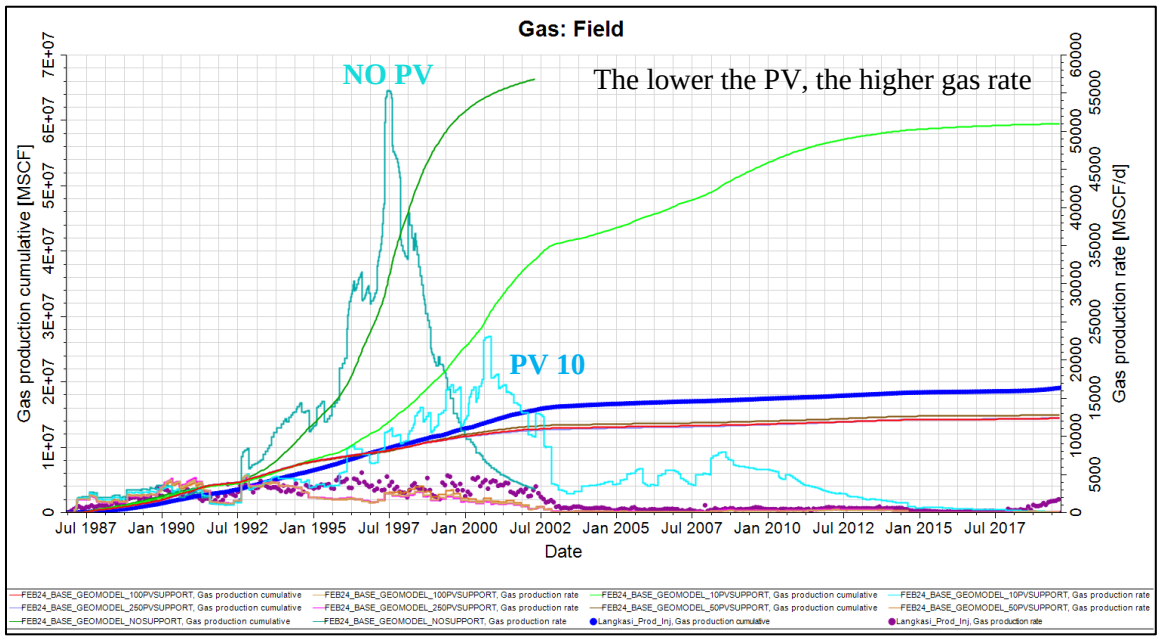

Figure IV-9. Fieldwide gas rate and cumulative gas production with variations of bottom PV

PV 100 results in the best pressure profile match as shown in earlier Figure IV-6, while No PV and PV 10 result in the lowest pressure profile (worst pressure match). Figure

IV-10 shows the production rate comparisons between simulated and observed data based on the PV-100 case.

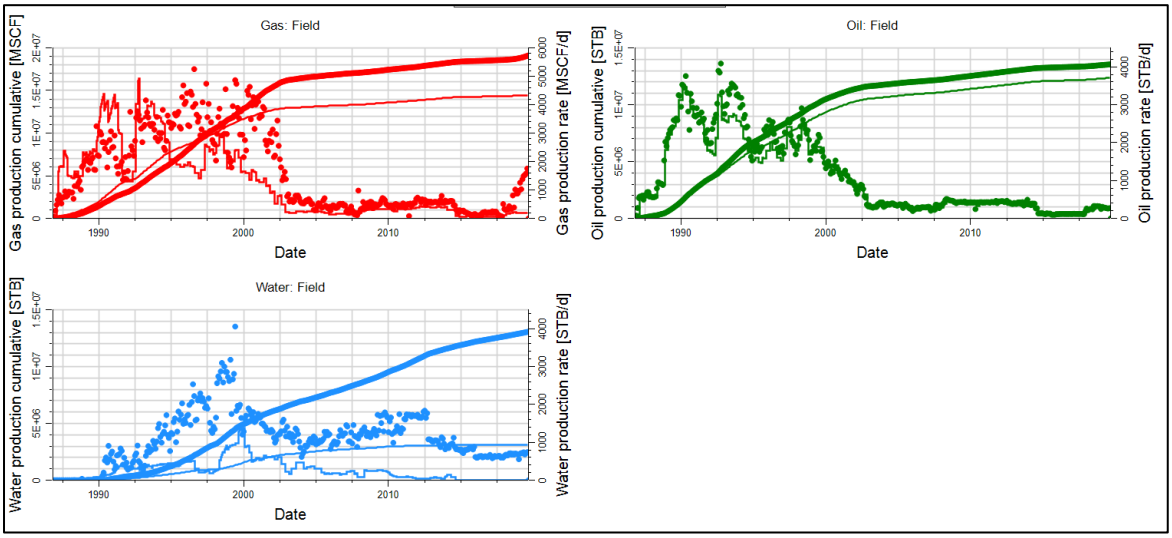

Figure IV-10. Fieldwide oil, gas, and waterflow rate and cumulative

IV.4.2.2 K_v/K_h Ratio Sensitivity

Horizontal permeability controls the flow in a direction perpendicular to gravity. By contrast, vertical permeability controls flow in the direction of the gravitational field. Permeability measurements are conducted in the laboratory or inferred from pressure transient tests conducted in the field. In many cases, vertical permeability is not measured and must be assumed. A rule of thumb is to assume vertical permeability to be approximately one half to one-tenth of horizontal permeability (*Fanchi, R. J., 2010*). These are reasonable assumptions and very often used when there is no data to the contrary.

It is preferable from a technical point of view to make direct measurements of all relevant reservoir data. Sometimes it is necessary to use a rule of thumb or data from an analogous formation to estimate a particular variable. The sensitivity of the history matching result in changes to the input variable should be clearly understood.

One of the main reasons for lower permeability in the vertical direction compared to the horizontal direction is the alignment of rock grains during deposition. These differences can be an order of magnitude or more. Therefore, the k_v/k_h ratio used in the simulation study should be less than 1.

The only available core data values are from NHK-422, which was described earlier in Chapter II. Based on those measurements, the range of k_v/k_h for this well is 0.36 to 0.76, and the average is 0.53. This section presents the results on the variability of k_v/k_h ratio and its impact on pressure and production performance.

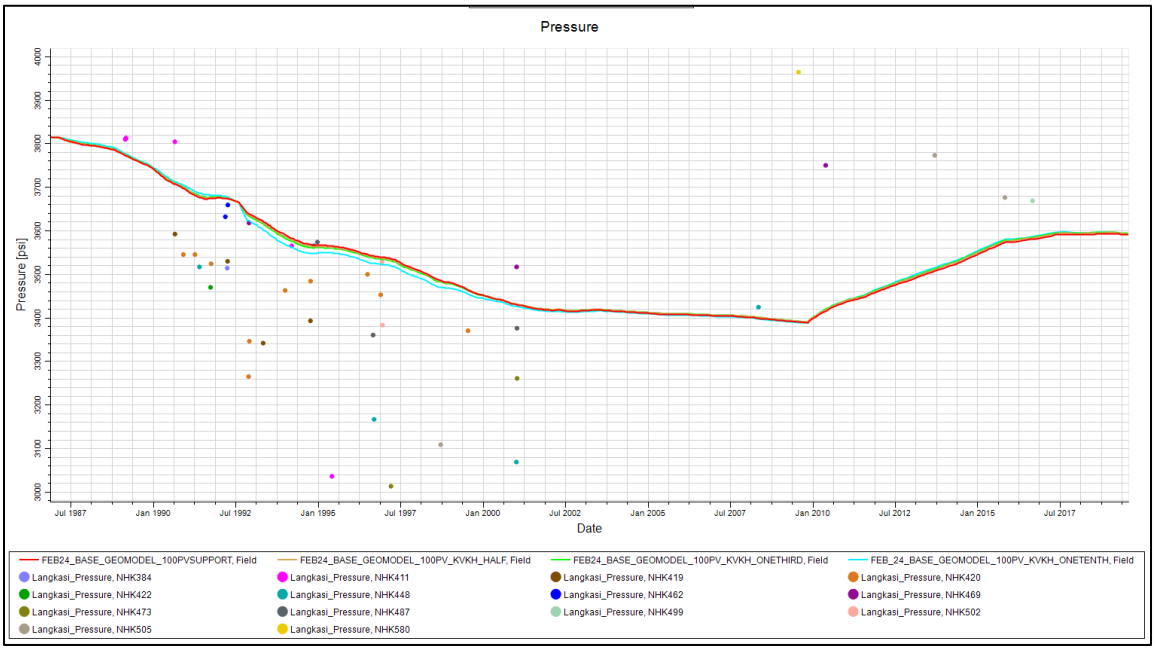

Figure IV-11. Pressure response with k_v/k_h variations

As far as the pressure profiles are concerned, k_v/k_h does have a minimal impact on the slope of declining and increasing pressure, as can be seen in Figure IV-11. Generally, there is not much difference in pressure response in each of these cases.

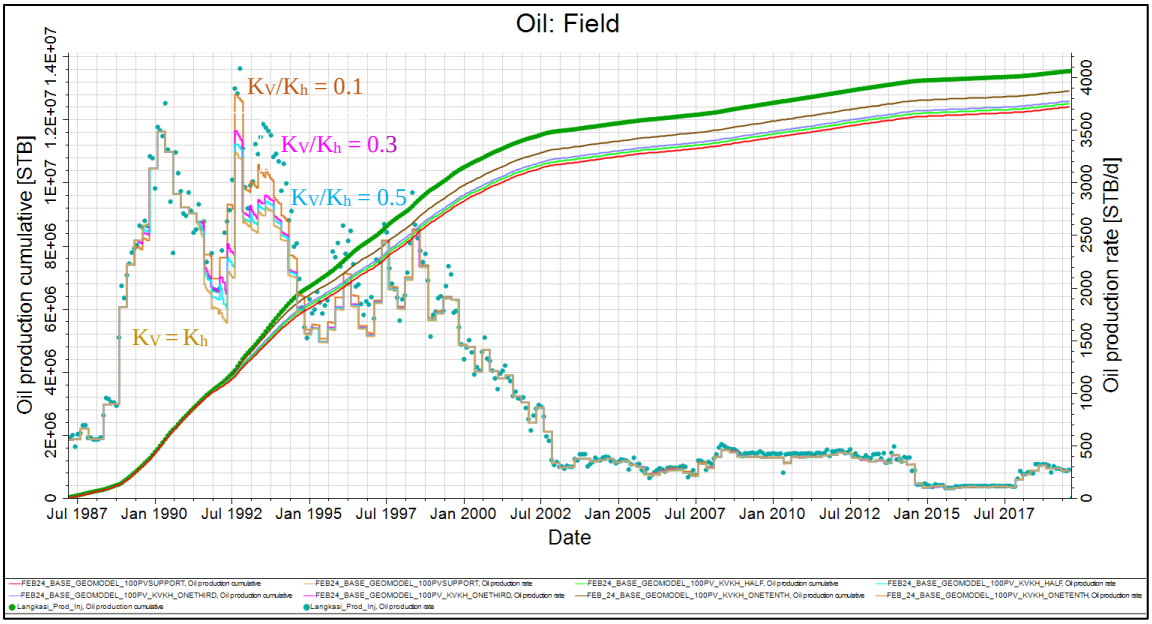

Figure IV-12. Fieldwide oil rate and cumulative oil production with variations of k_v/k_h

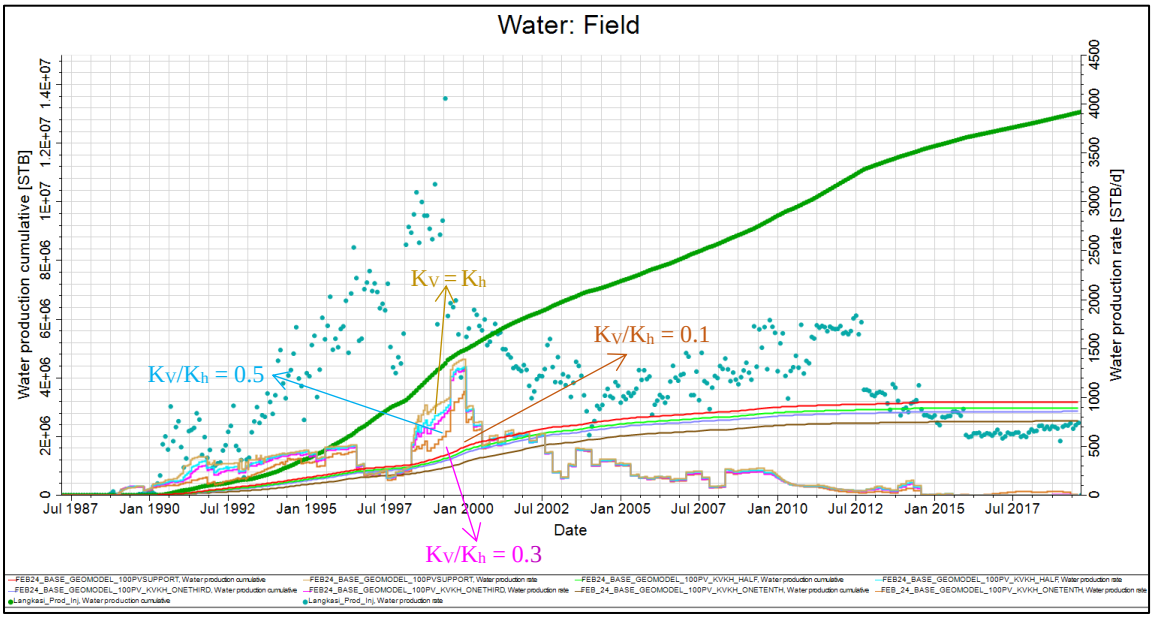

Figure IV-13. Fieldwide water rate and cumulative water production with variations of k_v/k_h

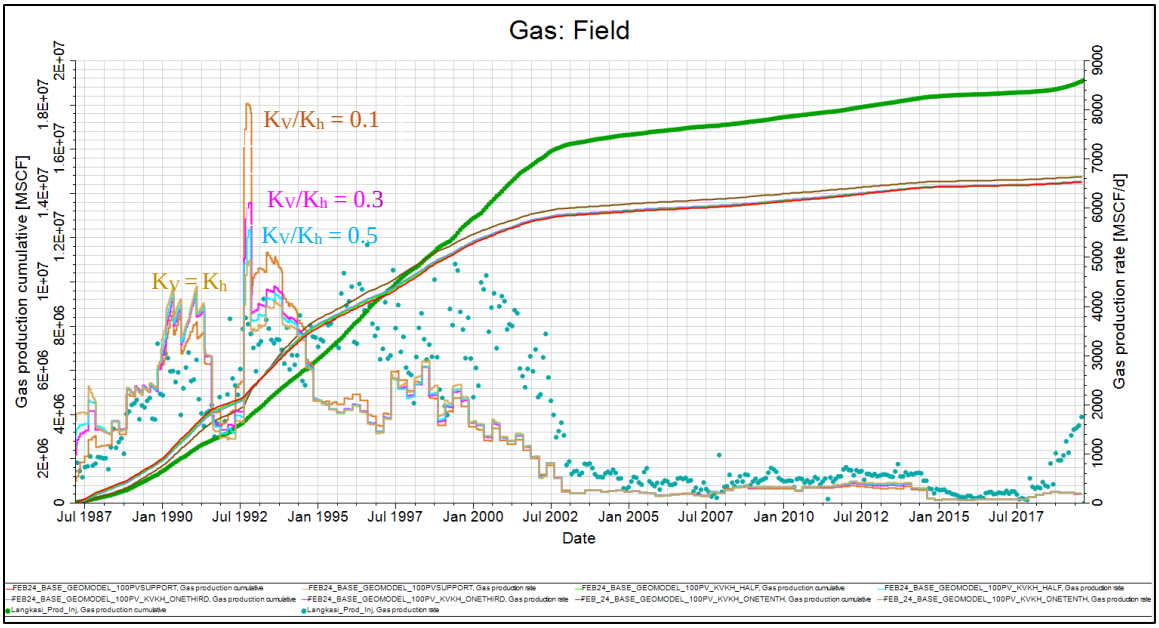

Figure IV-14. Fieldwide gas rate and cumulative gas production with variations of k_v/k_h

Figures IV-12 to IV-14 show the impact of k_v/k_h to oil, water, and gas production profiles. The highest oil production was observed in the lowest k_v/k_h ratio, and the highest water production was observed in $k_v = k_h$ case. Gas production follows the trend of oil production proportionally.

IV.4.2.3 Relative Permeability Sensitivity

Relative permeability is one of the essential parameters in history matching. This parameter can help in increasing or decreasing the fieldwide fluid flowrate systematically. In addition, the timing and magnitude of water breakthrough are controlled by this parameter. The laboratory measurement data were used as the baseline in this evaluation, and variations were made around it. In this sensitivity study, attempts were made to understand the overall impact of:

1. Changing the endpoint of water and oil permeability.
2. Changing the starting point of water and oil permeability.

3. Changing the curvature of water and oil permeability.

IV. 4.2.3.A Relative Permeability Endpoint Sensitivity

These cases were formulated by adjusting the endpoint relative permeabilities based on the laboratory reported values, followed by a case where the value is doubled and another case where it is halved. Table IV-3 shows the input summary of these cases.

Table IV-3. Relative permeability input

S_{gcr}	0.065	S_{orw}	0.34			S_{wmin}	0.32		
Corey gas	2	S_{org}	0.32			S_{wcr}	0.323		
K_{rg} @ S_{wmin}	1	Corey O/W	2			Corey water	3		
K_{rg} @ S_{org}	1	Corey O/G	2			K_{rw} @ S_{orw}	0.12	0.24	0.06
		K_{ro} @S_{omax}	0.49	0.98	0.245	K_{rw} @S= 1	1		

Figure IV-15 shows the relative permeability inputs and how they are different from one set up to another. Figure IV-16 shows the pressure profile for each of the case and compares each other. As far as pressure in the system is concerned, there is minimal impact on the pressure profile as a result of variation in the relative permeability endpoint.

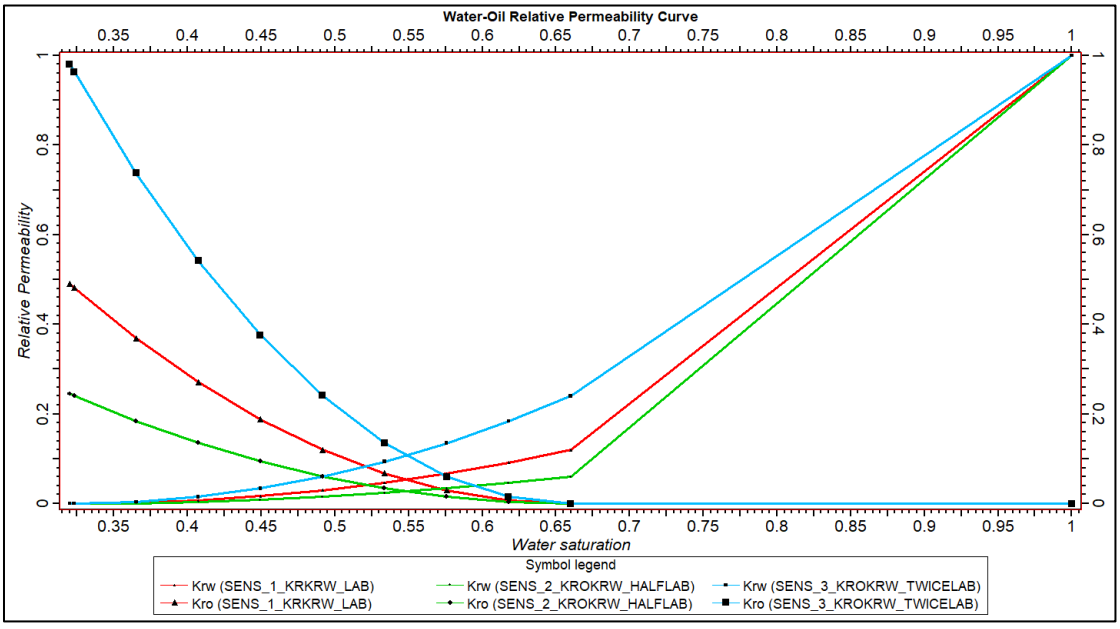

Figure IV-15. Relative permeability input for endpoint effect

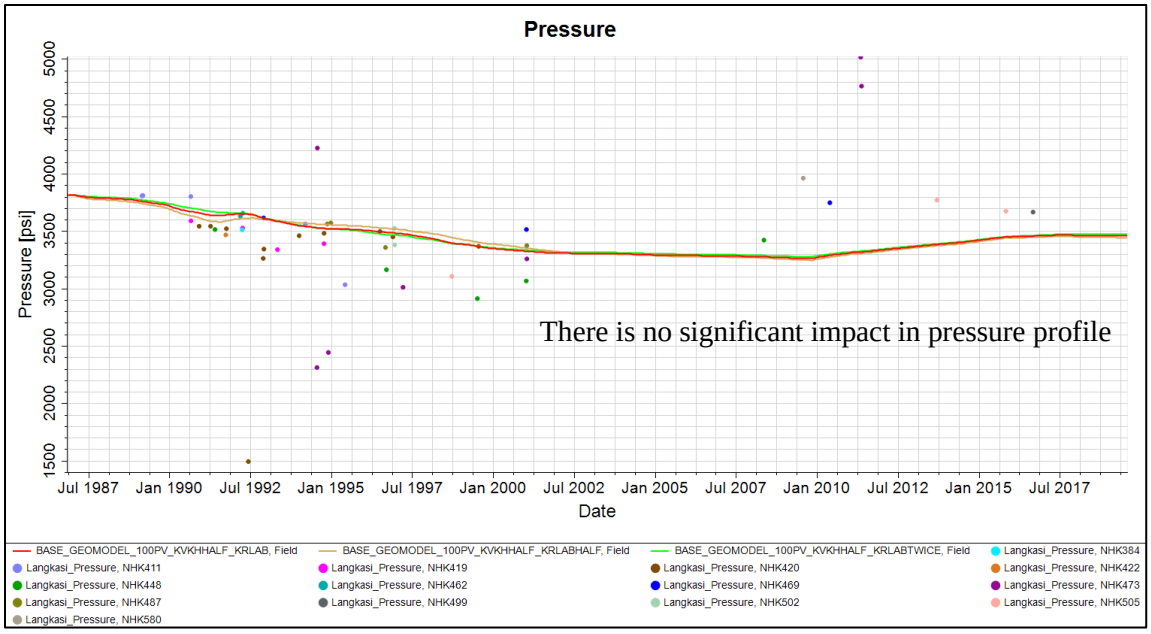

Figure IV-16. Pressure response with various relative permeability endpoints

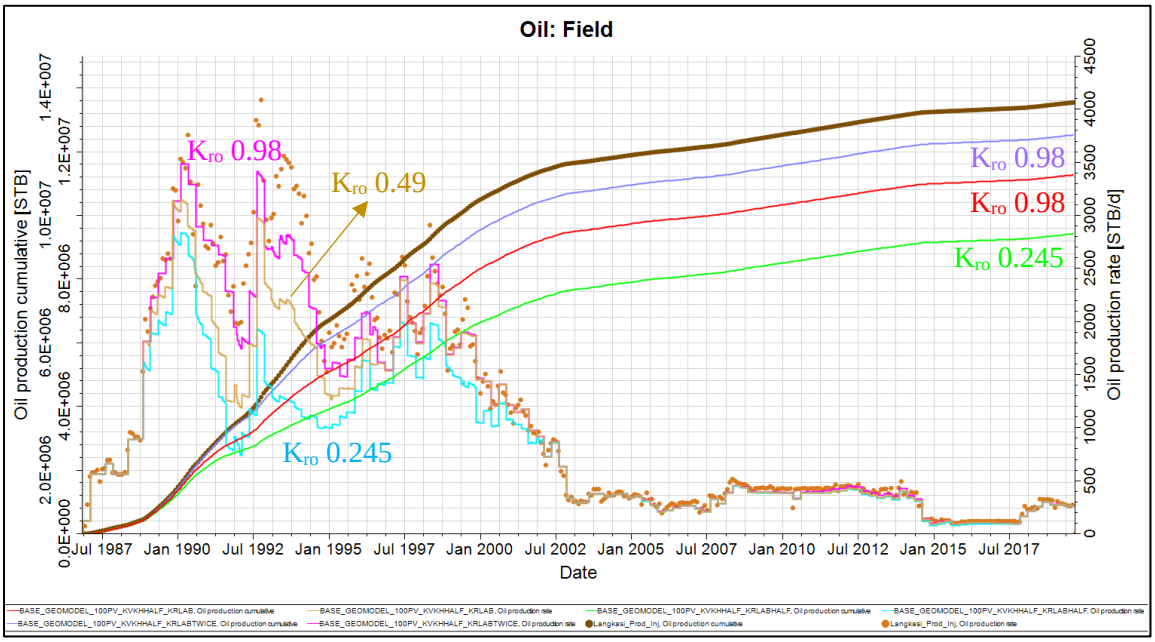

Figure IV-17. Oil production profile with various relative permeability endpoints

Figure IV-17 and Figure IV-18 show the oil and water fieldwide profiles and how they change as a response to varying permeability endpoints. When the endpoint of oil relative permeability increased, oil flowrate increased as a response. Similarly, for water rate, it will increase when the endpoint of water relative permeability increases. The

magnitude of an increase in the oil flow rate between each case is more apparent compared to the increase in the water flow rate. This observation caused by the baseline k_{ro} value, which is much higher than k_{rw} (four times higher).

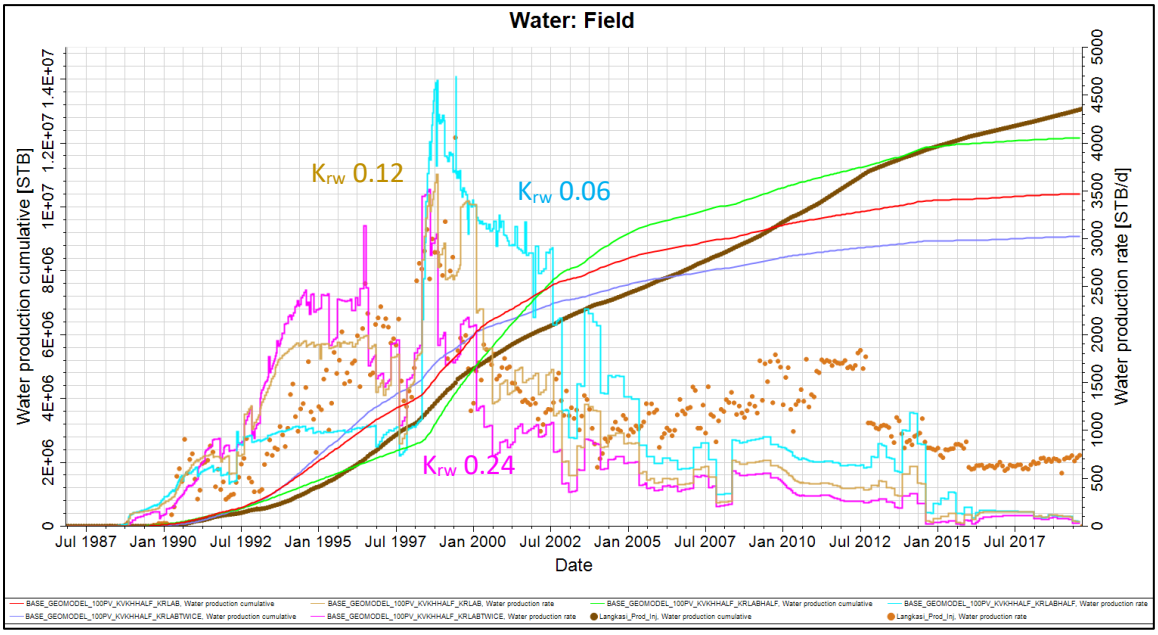

Figure IV-18. Water production profile with various relative permeability endpoint

The oil rate is directly proportional to the increase of k_{ro} endpoint. It can be seen clearly from both oil rates and cumulative oil charts. On the water flow rate, the opposite effect is observed because the initial k_{rw} value is much lower than the measured k_{ro}. Therefore, when 0.5 and 2 multiplication factors were applied to an endpoint, the effect of the k_{rw} was masked by the effect of oil relative permeability (as the baseline laboratory measurement value is four times higher).

To validate this observation, when only k_{rw} endpoint is increased while k_{ro} is not varied, an increase in the water rate is observed. This method was used as a way to improve the water production rate in the final history match. Last but not least, this modification does not have much impact on the gas rate, as shown in Figure IV-19, because gas relative permeability property was not varied.

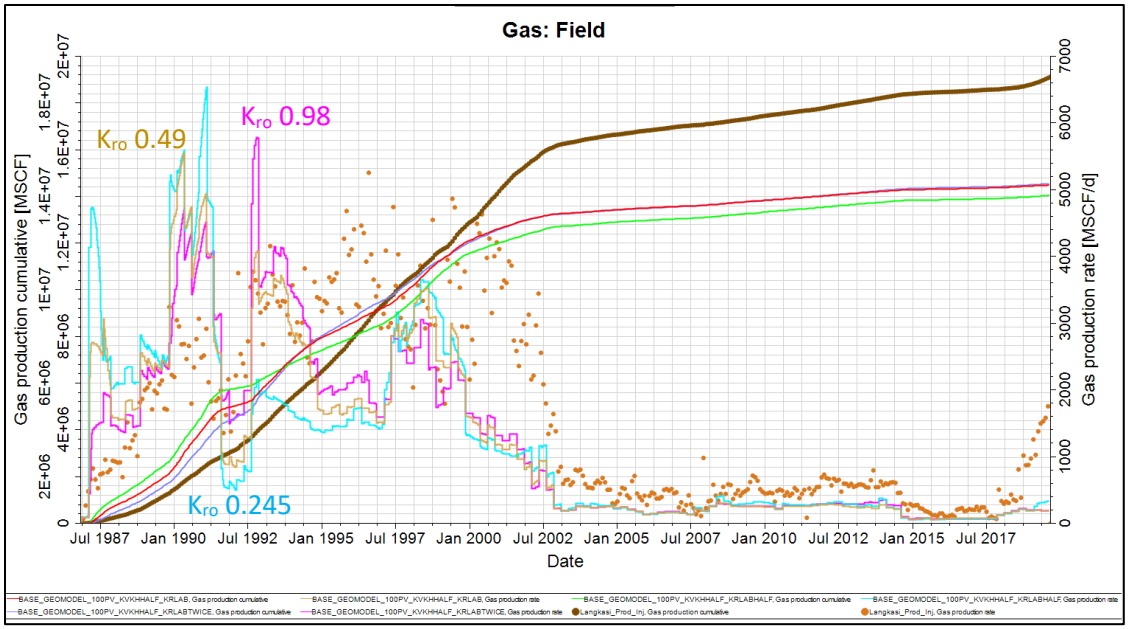

Figure IV-19. Gas production profile with various relative permeability endpoint

IV.4.2.3.B Starting point of Water and Oil Relative Permeability Sensitivity

This sensitivity study was meant to examine the effect of initial water saturation (S_{wi}) to the production profile. Three cases with significant difference S_{wi} were made, which are 0.21, 0.3, and 0.39. Pressure response shown in Figure IV-20 indicated that higher S_{wi} would have steeper pressure decline.

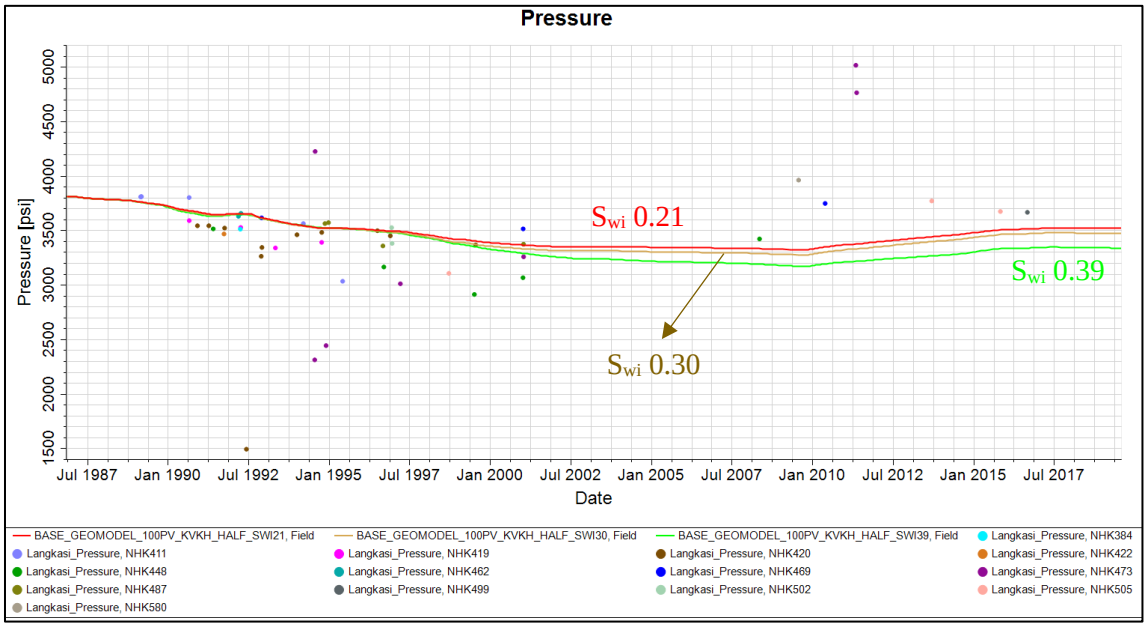

Figure IV-20 Pressure response with variations in S_{wi}

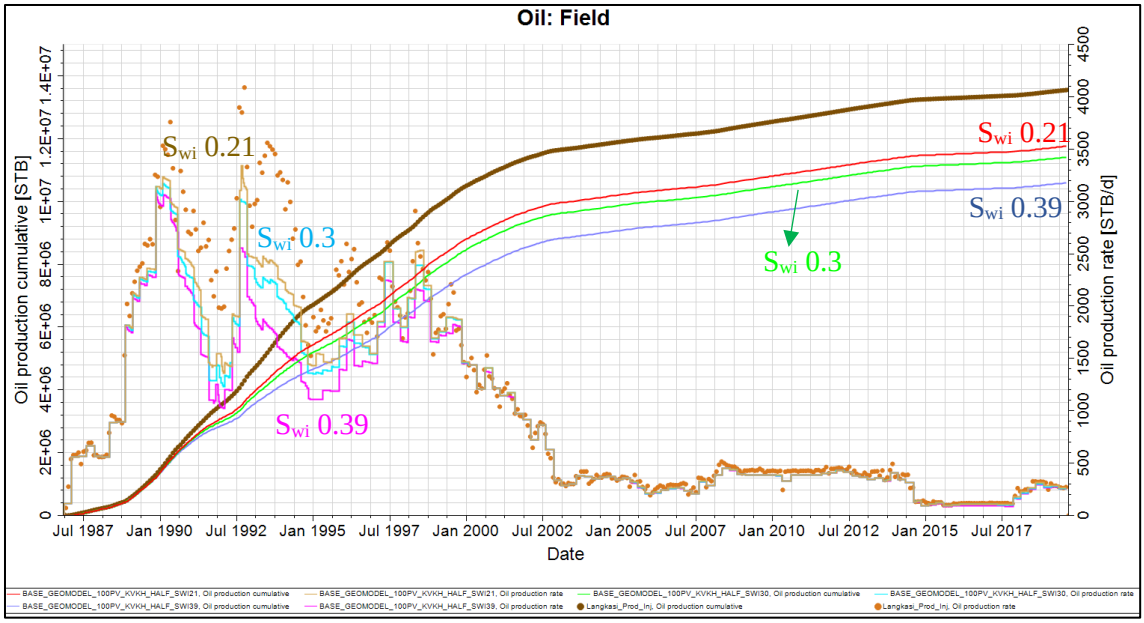

Figure IV-21. Fieldwide oil rate and cumulative oil production with S_{wi} variations

Figure IV-21 shows that the oil production rate and cumulative production proportionally decrease as the S_{wi} increase. The higher S_{wi} lesser the initial oil saturation, which causes the profile to be the lowest. On the other hand, Figure IV-22 shows that water production is following the S_{wi} trend. As S_{wi} becomes higher, water production also increases. The gas production profile is directly corresponding to the oil production profile, as shown in Figure IV-23.

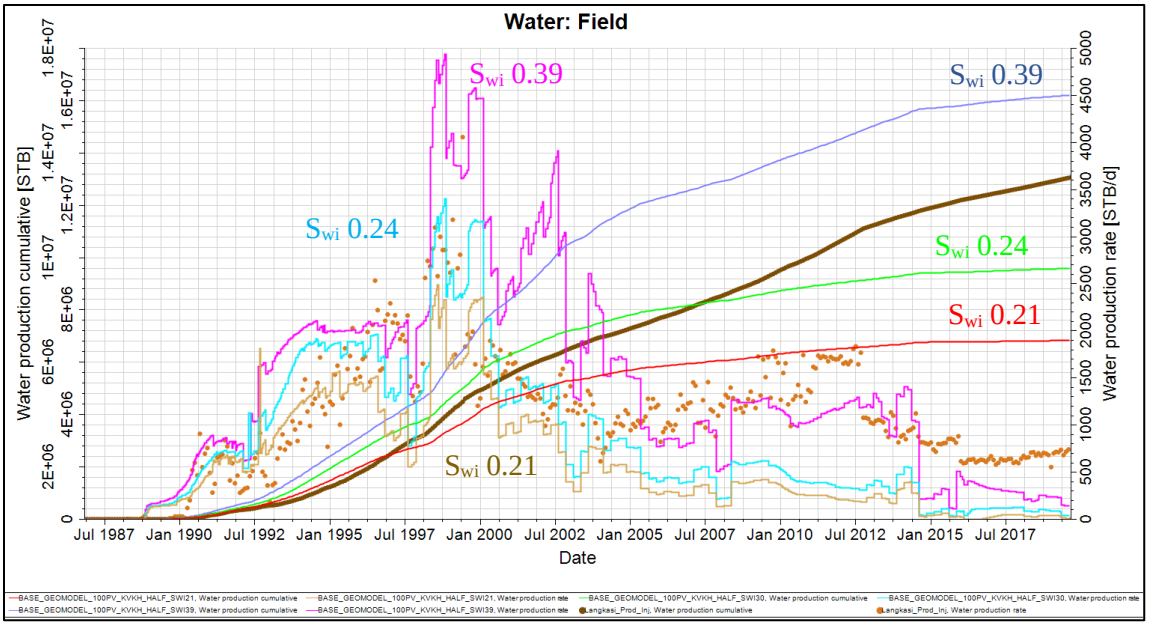

Figure IV-22. Fieldwide water rate and cumulative water production with S_{wi} variations

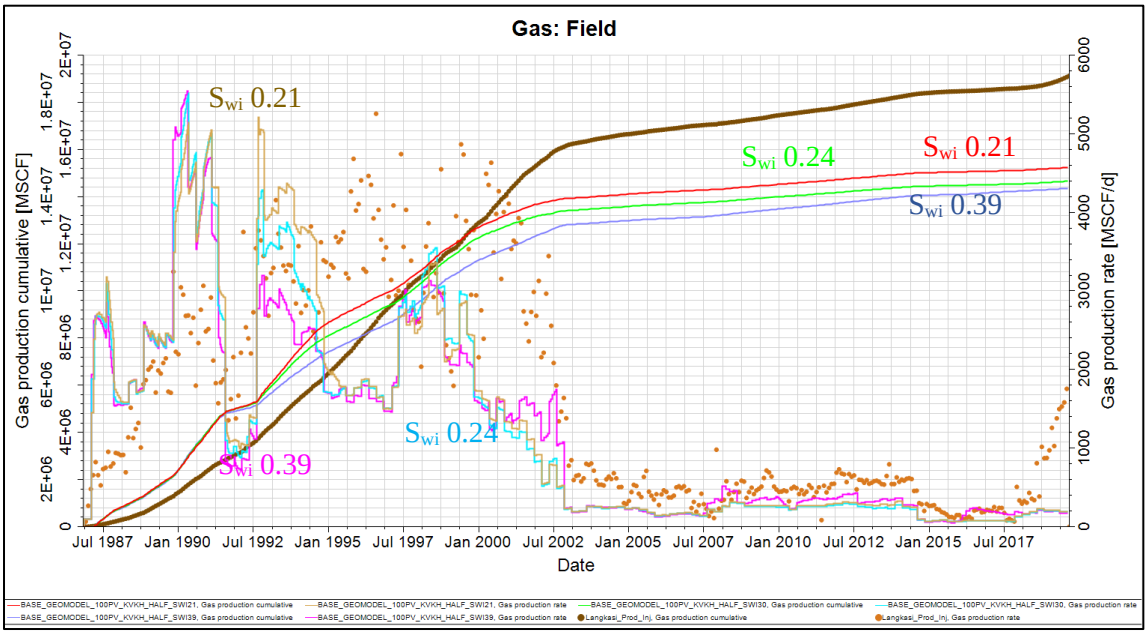

Figure IV-23. Fieldwide gas rate and cumulative gas production with S_{wi} variations

The best history match was obtained using S_{wi} value of 0.3. When S_{wi} value of 0.215 was used, a good history match for the water production could not be obtained. When S_{wi} value of 0.413 was used, there were difficulties in matching the amount of produced

oil in the field. Therefore, S_{wi} of 0.3 was considered as the most appropriate water saturation value.

IV.2.3.C The Curvature of Water and Oil Relative Permeability Sensitivity

For this evaluation, the highest endpoint (k_{ro} = 0.98 and k_{rw} = 0.24) was chosen. The aim was to observe the effect of permeability curvature on the flowrate of each phase. Figure IV-24 and Figure IV-25 show these inputs.

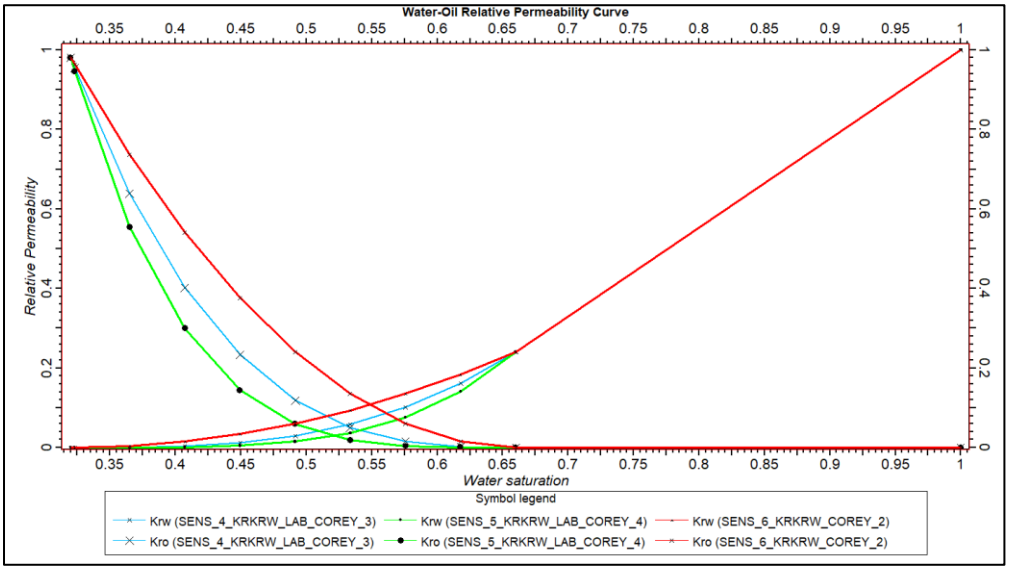

Figure IV-24. K_{ro}-k_{rw} for varying Corey coefficients

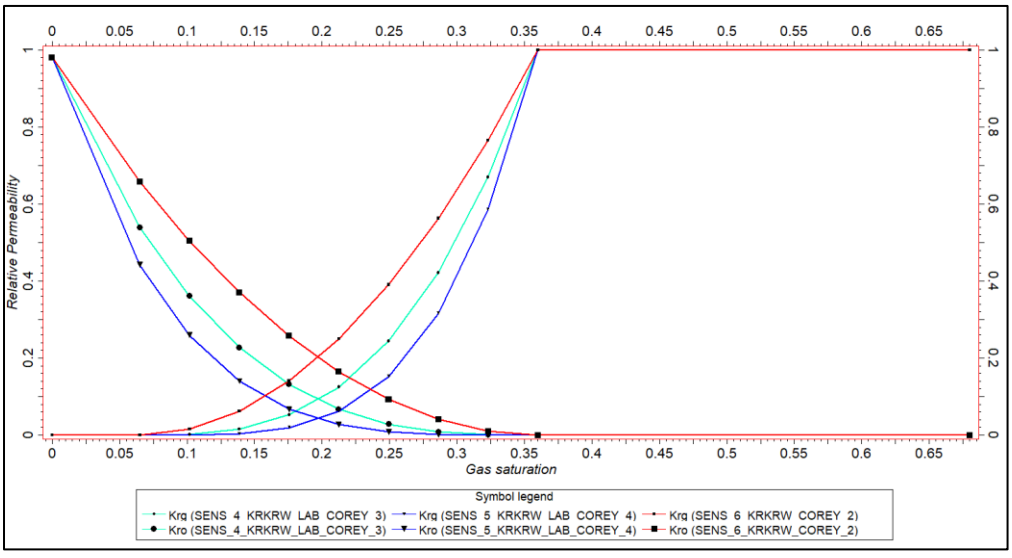

Figure IV-25. K_{ro}-k_{rg} for varying Corey coefficients

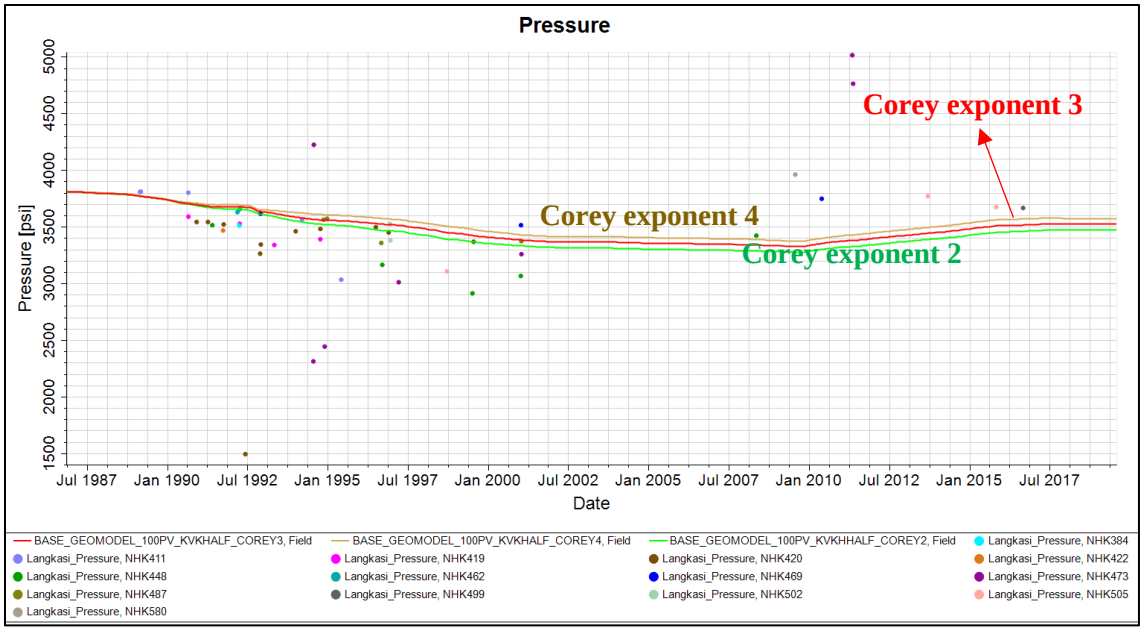

Figure IV-26. Pressure response with various permeability curve curvatures

Figure IV-26 shows the effect of Corey exponent to pressure response. As the Corey exponent decreases, pressure decline is sharper. This observation can be explained by looking at the production rate profiles of oil, water, and gas shown in Figures IV-27, IV-28, and IV-29, respectively. This variation causes a systemic increase or decrease in the overall profile.

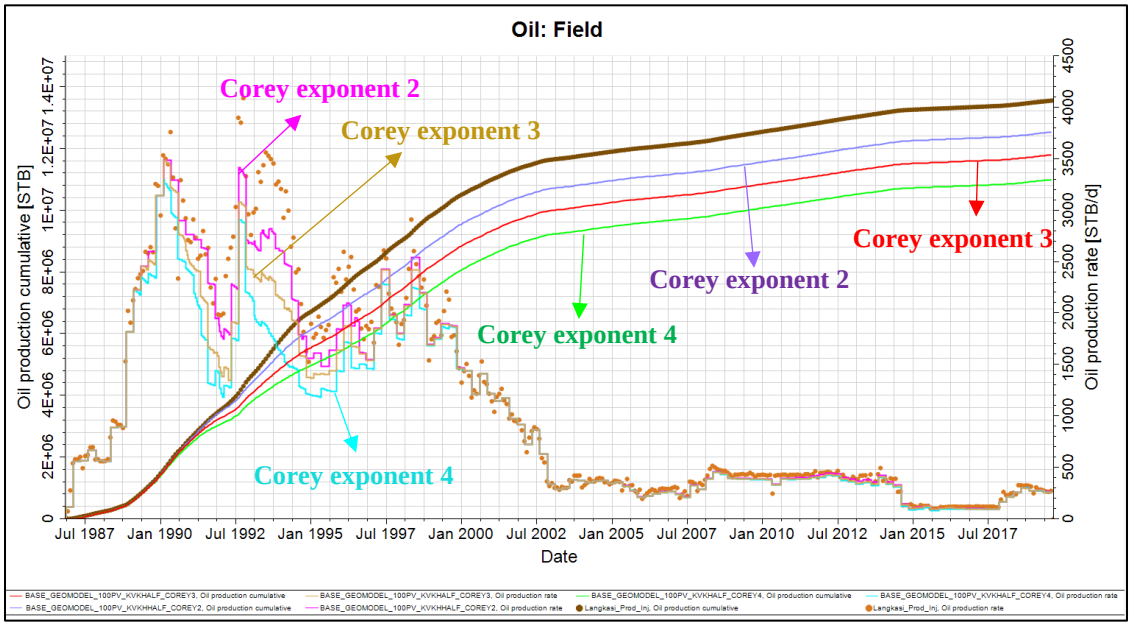

Figure IV-27. Oil production profiles with various permeability curve curvatures

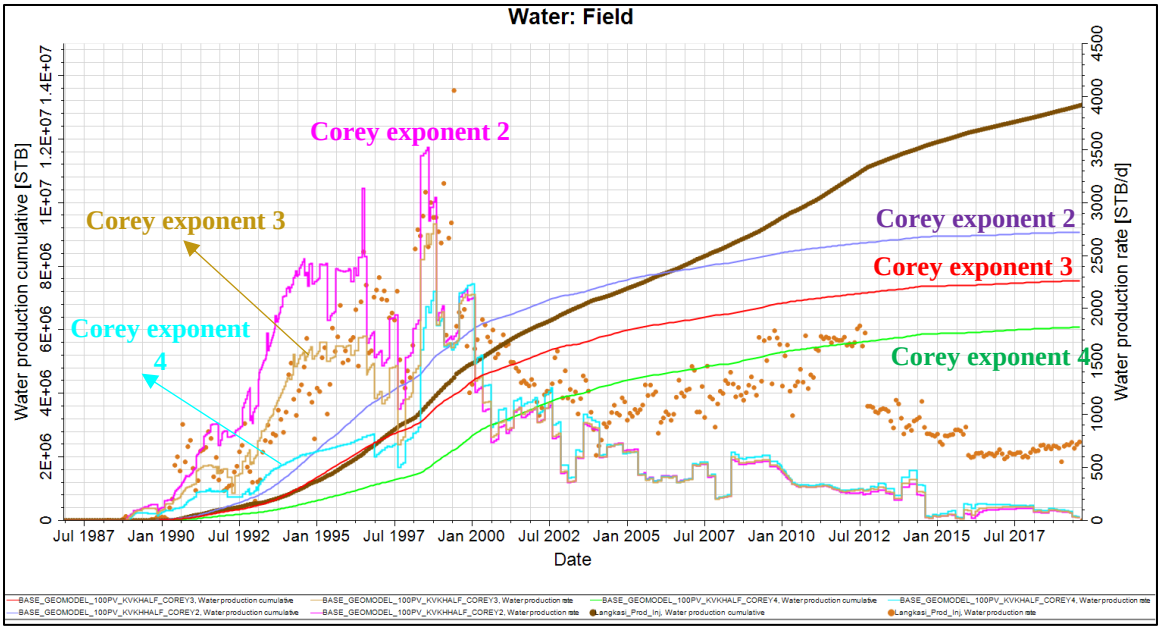

Figure IV-28. Water production profiles with various permeability curve curvatures

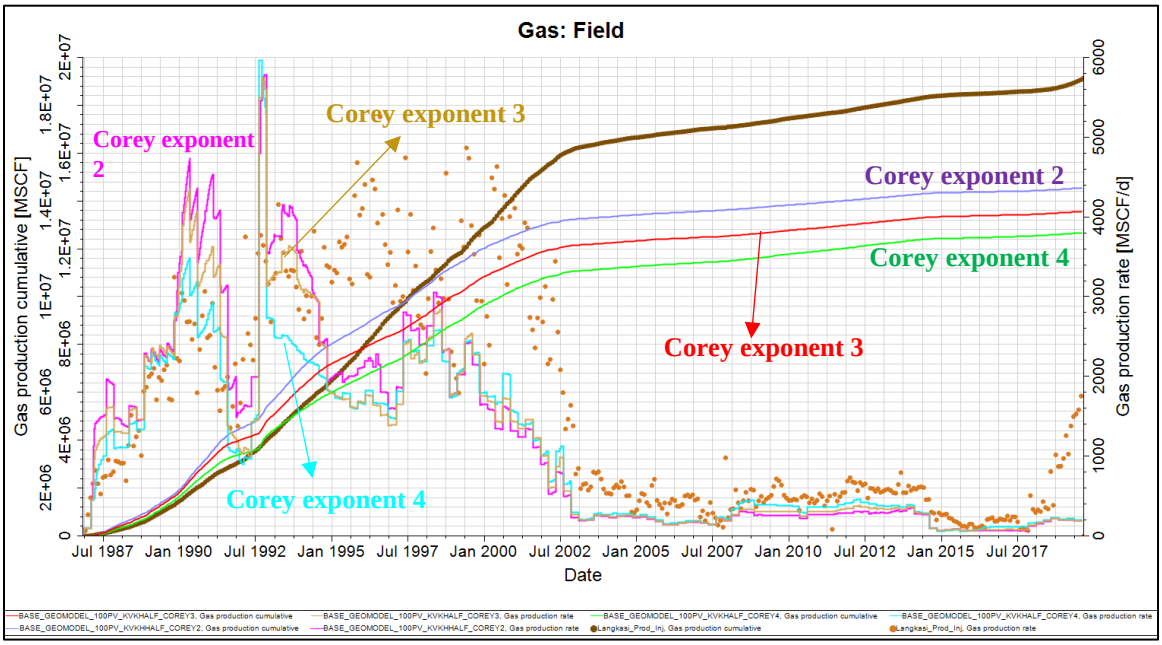

Figure IV-29.Gas production profiles with various permeability curve curvatures

IV.4 Capillary Pressure Curve Sensitivity

Based on all the sensitivity cases so far, one common observation is that the model produced much less water compare to the actual field production. Applying capillary pressure in the rock physics input could help to increase the overall water production. This

section explores the impact of different capillary pressures on the water production profile. Figure IV-30 shows the capillary pressure curves tested in this sensitivity study.

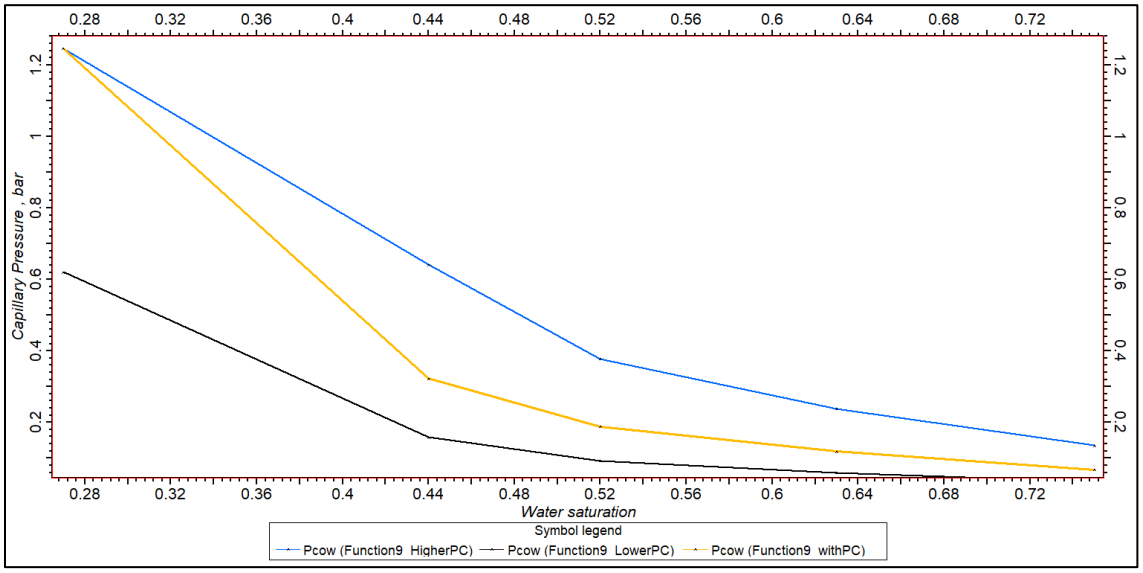

Figure IV-30. Capillary pressure curves

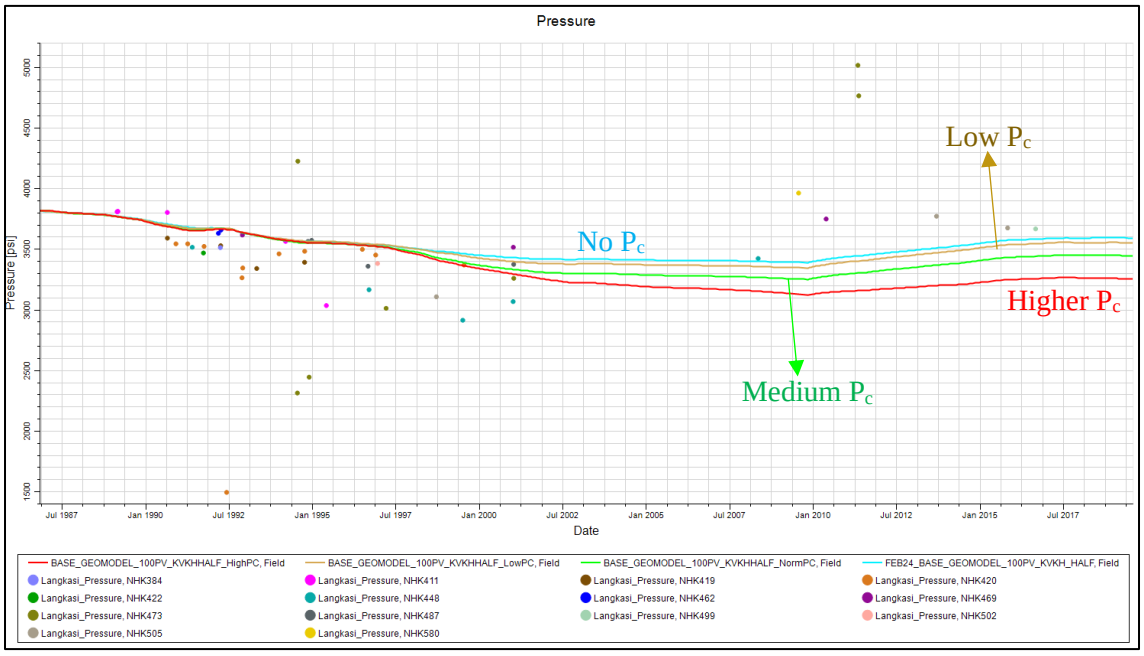

Figure IV-31. Capillary pressure effect on reservoir pressure

Figure IV-31 shows the highest-pressure decline in the higher P_c case. This behavior is caused by the massive amounts of water extraction from the reservoir. Even

though this case has the lowest oil and gas production, the amount of water production is much higher compared to the amount of oil + gas production in other cases.

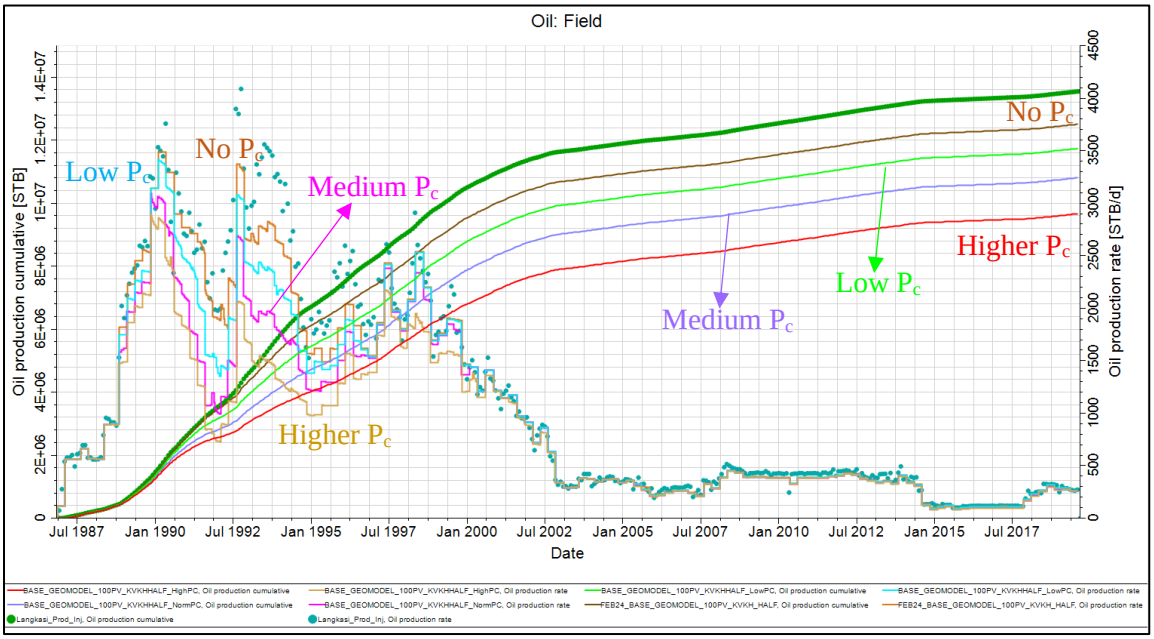

Figure IV-32. Fieldwide oil rate and cumulative oil production with various capillary pressures

Figure IV-32 shows the comparison between no P_c, low P_c, medium P_c, and higher P_c to oil production profile. It can be concluded that oil volume decreases once capillary pressure is included and become even lower as P_c increases. Capillary pressure creates a transition zone between OWC to the hydrocarbon column. The higher the P_c, the longer the transition zone. Therefore, it will restrict the movement of oil from the particular grid cells to the wellbore.

Figures IV-33 and IV-34 show the production profiles for water and gas as the P_c is varied. P_c increases the water volume, so higher P_c yields the highest water production rate and cumulative water production. P_c impacts the gas production rate in the same way it impacts the water production rate. However, the effect is not as pronounced as in the case of water production rate.

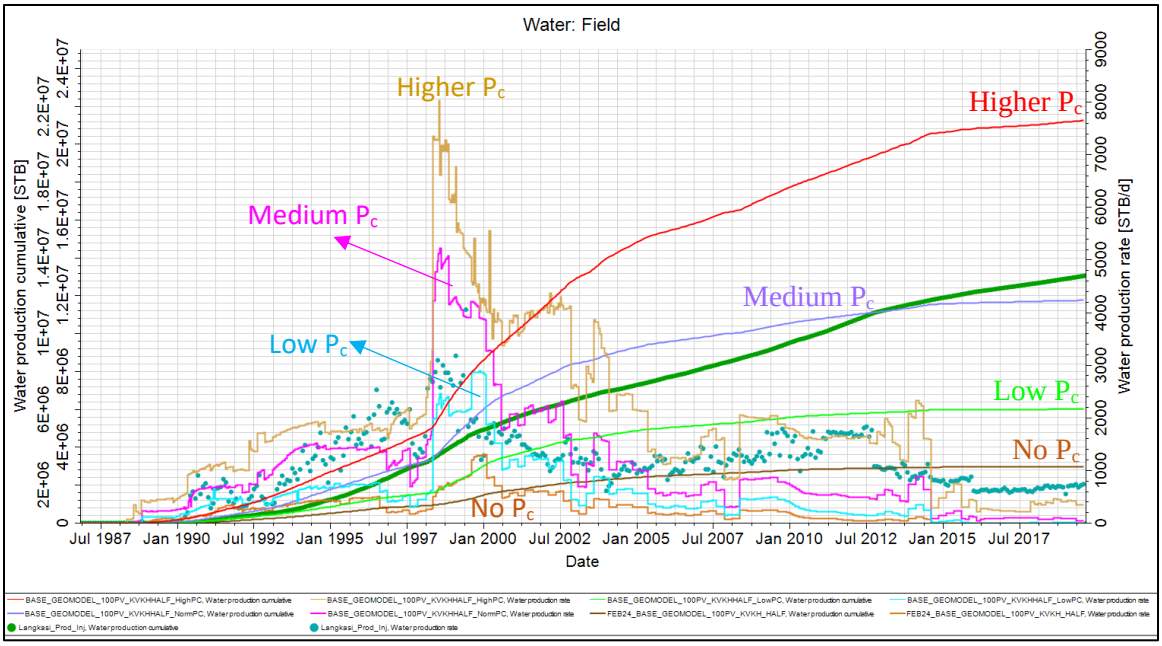

Figure IV-33. Fieldwide water rate and cumulative water production with various capillary pressures

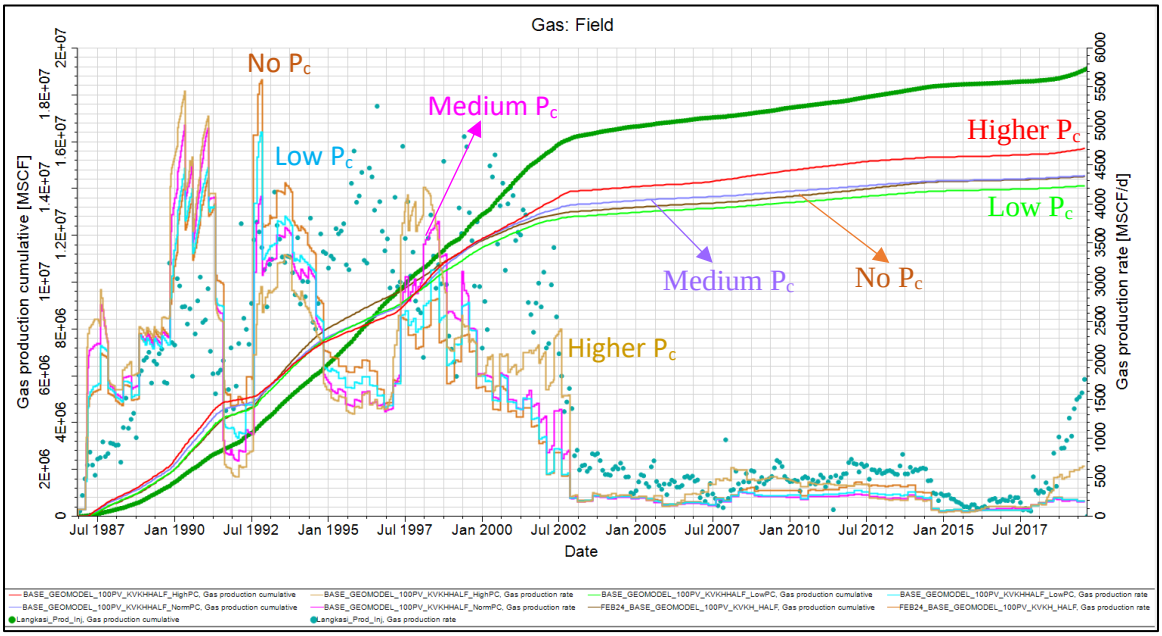

Figure IV-34. Fieldwide gas rate and cumulative gas production with various capillary pressure

IV.5 Oil-Water Contact (OWC) Sensitivity

As mentioned earlier, this section addresses the impact of OWC on the history match. A model with the deepest OWC will produce less water and more oil, and vice

versa. Obtaining optimum OWC aided the effort to improve the water production match. Four different cases were prepared, which are OWC 9709 ft (2960 m), 9735 ft (2968 m), 9758 ft (2975 m), and 9774 ft (2980 m).

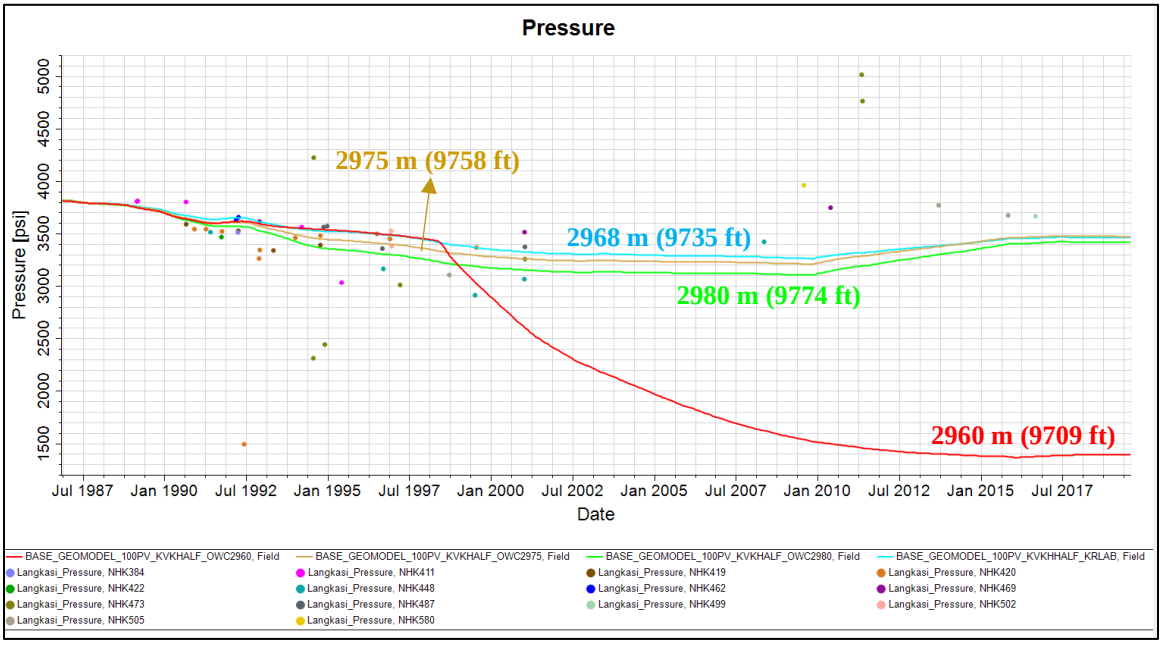

Figure IV-35. Fieldwide reservoir pressure variations of OWC

Figure IV-35 shows the effect of OWC on reservoir pressure. Too shallow 9709 ft (2960 m) OWC causes fast pressure depletion. The shallowest OWC results in the least hydrocarbon column. For the other three cases, the variation between each case is not significant. The least pressure declines between these three cases are observed at OWC of 9735 ft (2968 m), while the highest-pressure declines are observed at OWC of 9774 ft (2980 m).

Figure IV-36 shows the impact of OWC on the fieldwide oil production profile. As expected, shallower the OWC, the lower the oil production rate will become because of the reduction in the oil zone. The reverse effect can be observed in Figure IV-37 and Figure

IV-38 for the water production profile. Shallower OWC will result in an increase in water production.

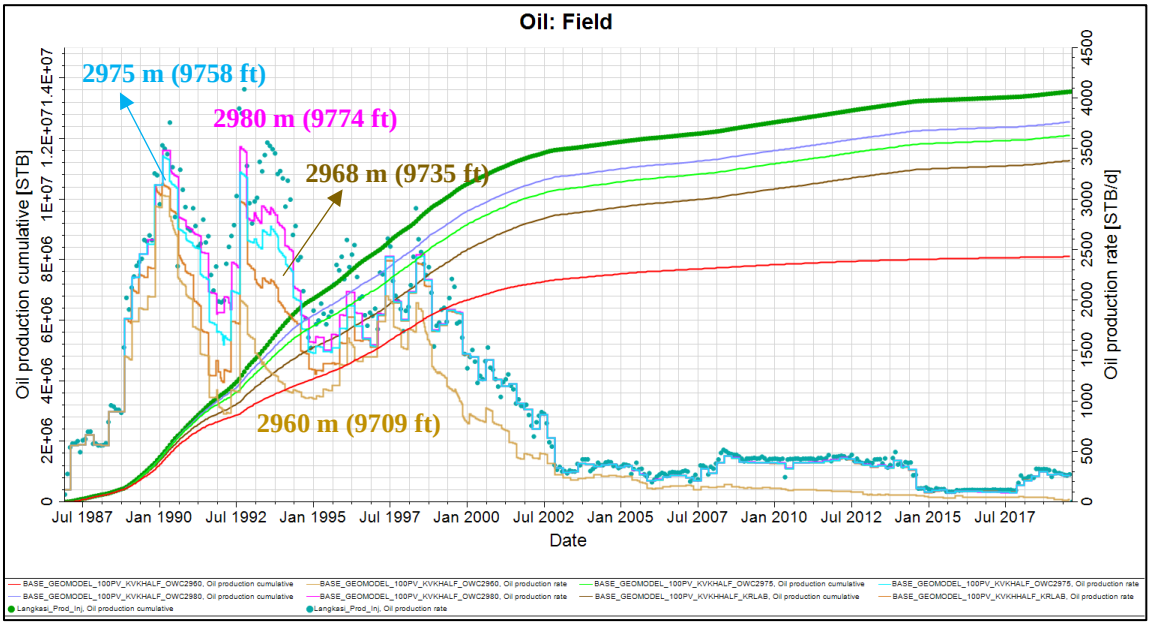

Figure IV-36. Fieldwide oil rate and cumulative with OWC variations

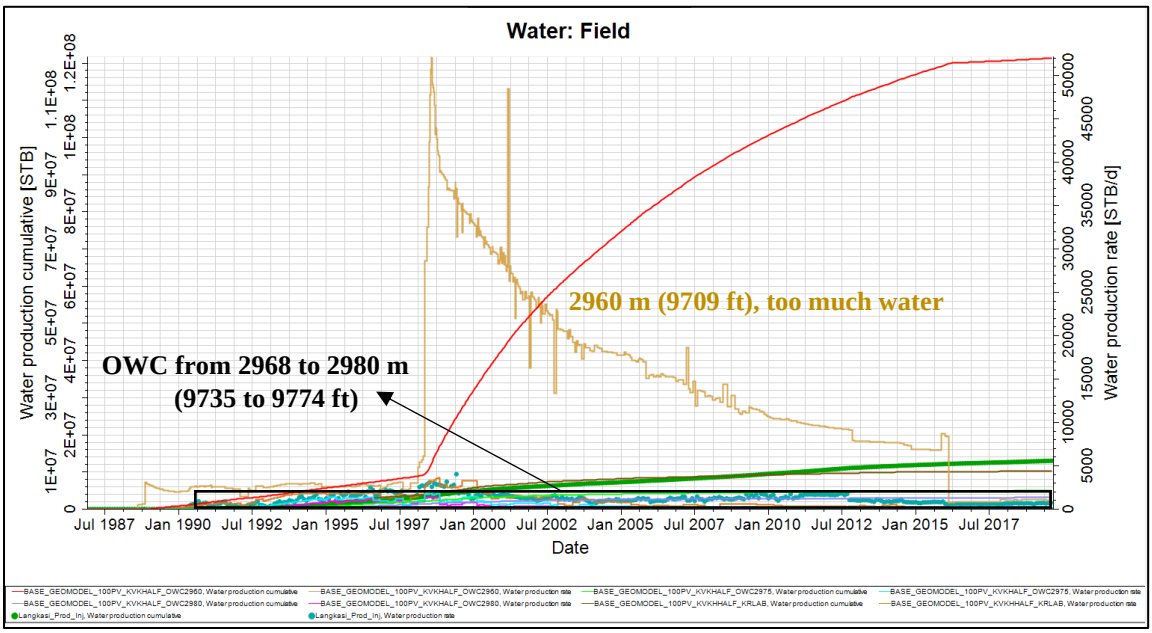

Figure IV-37. Fieldwide water rate and cumulative water production with OWC variations

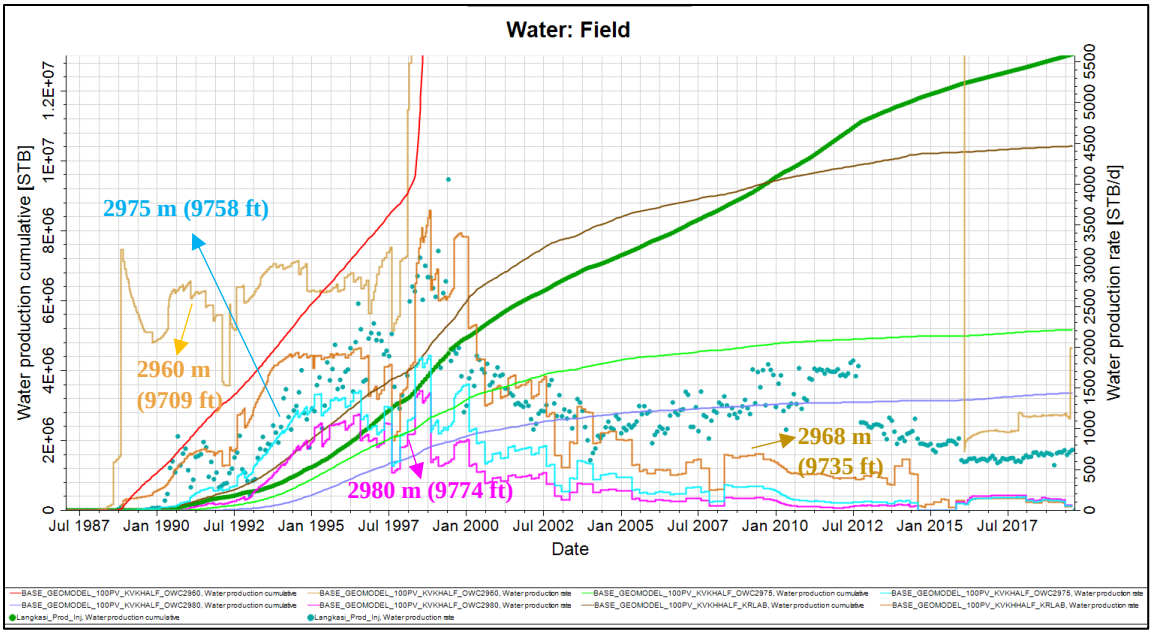

Figure IV-38. Fieldwide water rate and cumulative water production with OWC variations (zoom-in)

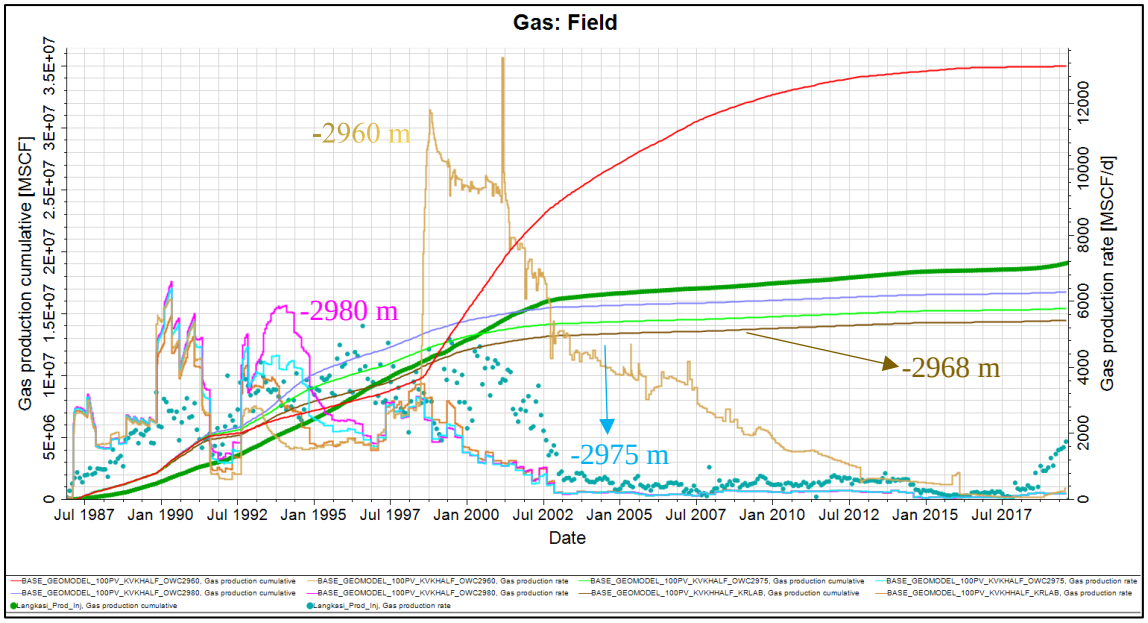

Figure IV-39. Fieldwide gas rate and cumulative with various OWC

Figure IV-39 shows the gas production profile for each different OWC depth. Gas production profile behaves similarly with the observed oil flow rate, except for the OWC depth 9709 ft (2960 m). As shown in the pressure profile, this case had pressure depleted very quickly and go much lower below P_{bp}. This sharp pressure drop creates excessive gas

liberation in the reservoir and eventually contributes to a significant increase in gas production.

IV.6 Permeability Sensitivity

In the LK-4 reservoir, permeability is one of the critical uncertainties. The main reason is the scarceness of data, where for the entire field, I have one set of permeability measurements from the core in NHK-422. In addition to that, another source of permeability data is from the Pressure Build-Up (PBU) test of NHK-411. However, this well test is not representative of this productive reservoir because based on the well log data, the pay-zone in this well is shaly sand.

Another reason for the difficulty in pinpointing the accurate permeability (k) range is that the two main permeability estimates (coming from well tests) come from the southern LK-4 reservoir. Different permeabilities in the active cells were interpreted based on the correlation with density porosity and neutron porosity logs. This correlation was used to propagate permeability property throughout the model. For the simulations, the lowest permeability in the net reservoir was set to be 5 mD. Figure IV-40 shows the pressure comparison between minimum permeability 5 mD, original geomodel permeability, and enhanced permeabilities by factors of 2, 4, and 8.

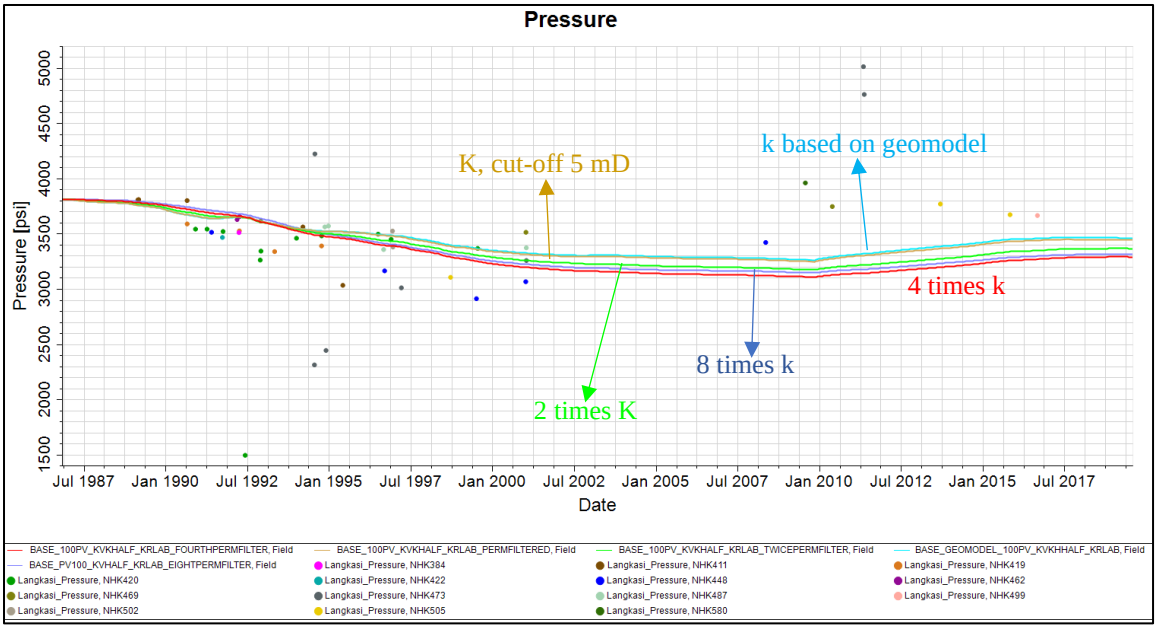

Figure IV-40. Pressure profile based on permeability (k) variations

Pressure profile in Figure IV-40 shows that as permeability increases, pressure decline is sharper than in the case with lower permeability. This observation is demonstrated with a comparison between permeability with 5 mD cut-off and permeability based on geomodel with the cases where permeabilities are enhanced. The shapes of these profiles are as such because higher permeability delivers higher oil, water, and gas production rates. However, there is not much difference in the oil production rate between 4- and 8-times permeability; hence, the pressure profile in the case of 8 times permeability is not significantly different.

The 4-times permeability case shows lower pressure compare to the 8-times permeability case. This is because permeability enhancement causes two effects, lower pressure declines, and production increase. Between cases 4 to 8-times permeability, the increase is by a factor of 2; however, the oil extracted is not by a factor of 2 because it is limited by oil rate constraint. Hence, the effect of increasing production is not as dominant as the effect of lowering pressure decline. As a result, the pressure profile in 8-times

permeability is slightly higher than 4-times permeability. Based on this result, if no other variable changes, the optimum multiplier from the base static geomodel is between 4 to 8 times permeability.

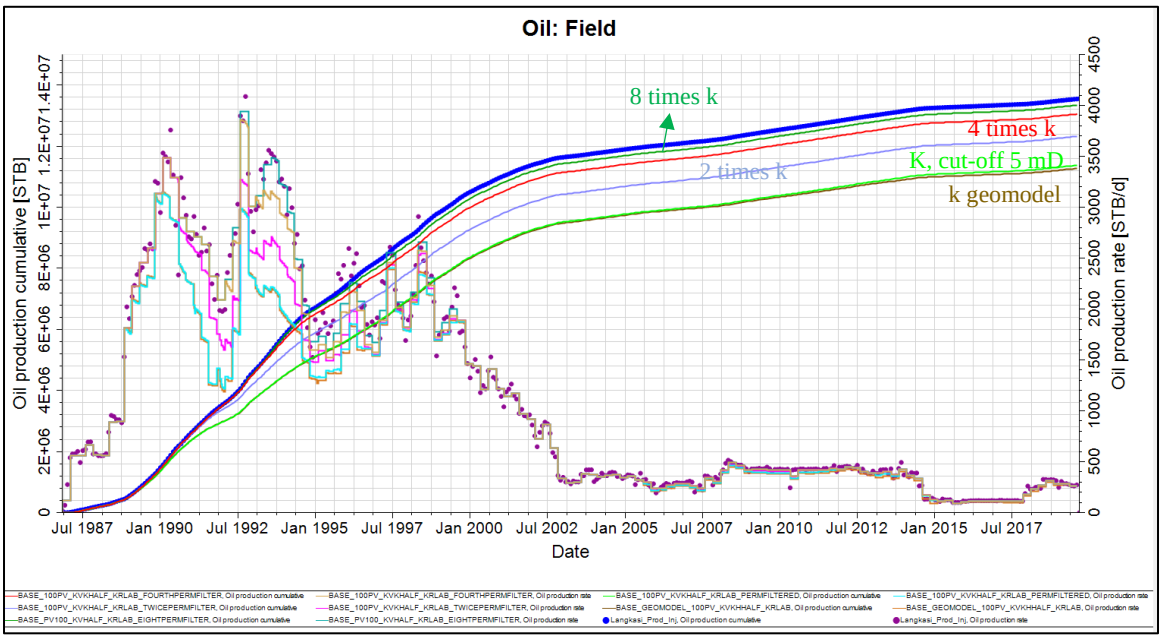

Figure IV-41. Oil production profiles based on permeability variations

Figure IV-42 and Figure IV-43 show the water production and gas production profile for these five different cases. Observations from these figures support a previous explanation about the shape of pressure decline in these cases. The water and gas production profiles show that the case with 4X permeability yields the highest cumulative production. One possible explanation is because this case shows the lowest reservoir pressure compared to the other cases. Lower pressure could create more gas liberation and water encroachment into the reservoir.

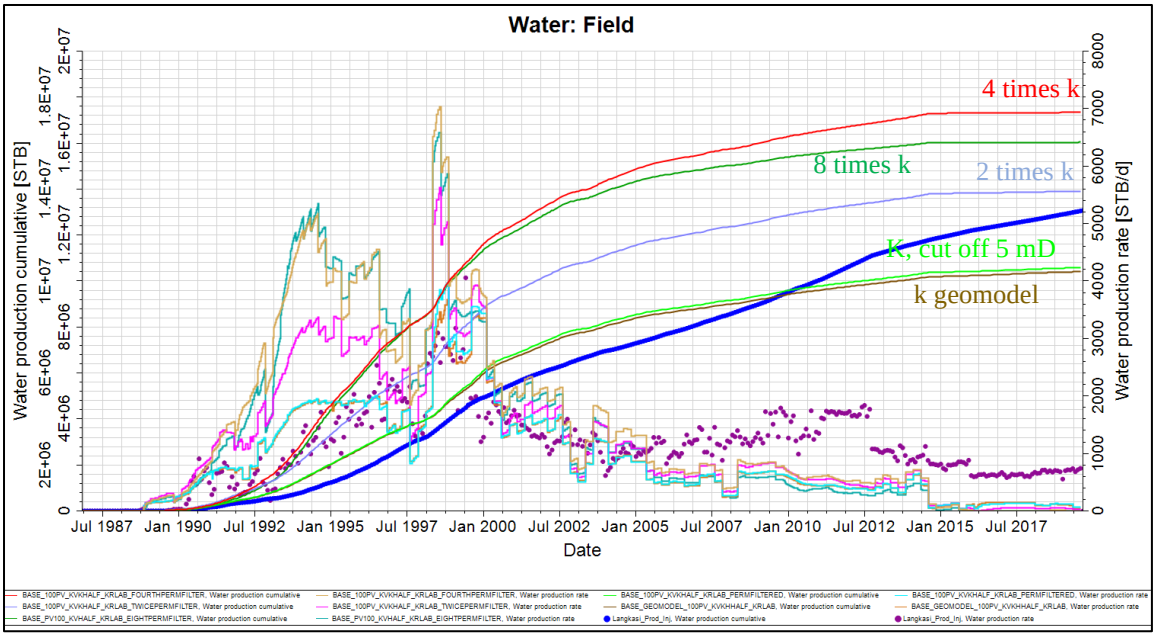

Figure IV-42. Water production profiles based on permeability variations

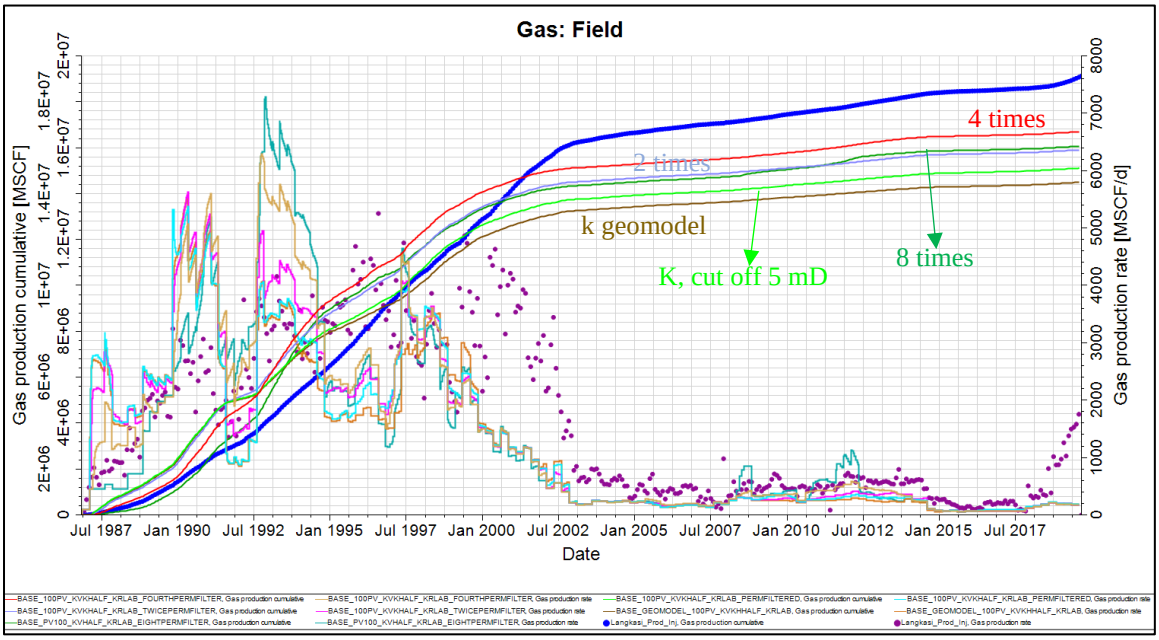

Figure IV-43. Gas production profiles based on permeability variations

IV.7 Porosity Sensitivity

Unlike permeability, where the primary data is from one core and one well test only, there are more available primary data sources for porosity. In addition to the core data set, density porosity and neutron porosity logs are available for most of LK-4 wells.

Therefore, the model has a more accurate porosity distribution. Therefore, any porosity modification in the model will require stronger justification. The reason is not only more abundant data availability but also potential changes in the in-place reservoir fluid volume upon changing porosity. Nevertheless, it is still essential to have a good sense and understand how porosity variations impact the history match profile.

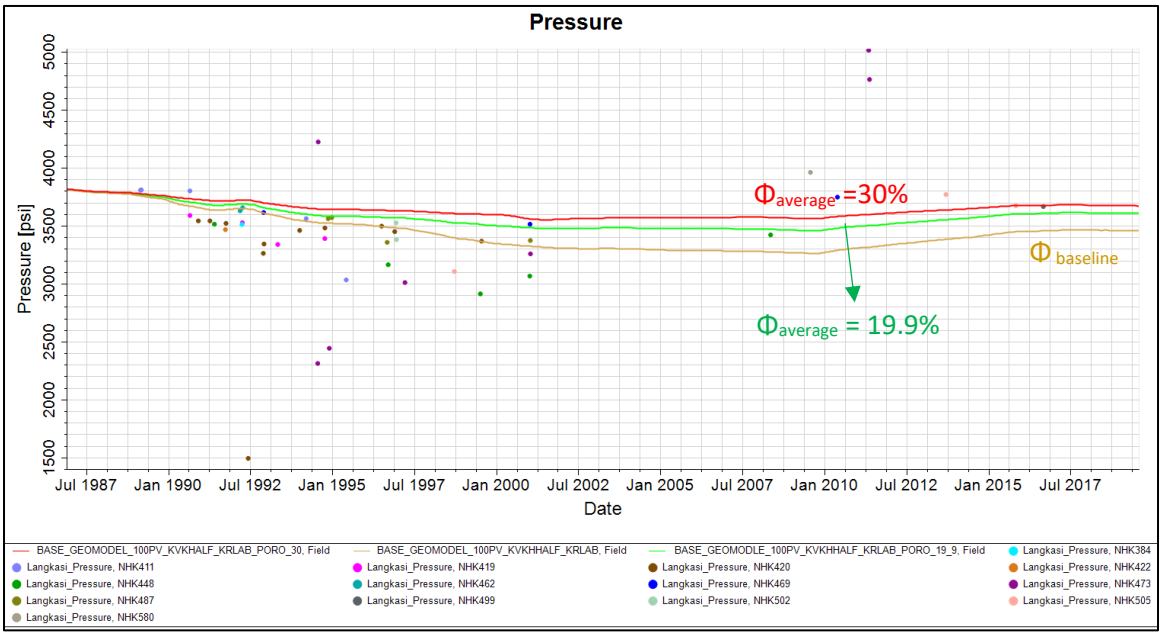

Figure IV-44. Pressure profiles based on porosity variations

Figure IV-44 shows the pressure profiles based on porosity variations. The higher porosity, the less pressure will decline. Higher porosity has more void space to be filled by the fluid, which causes the system to maintain its pressure longer than a system with lower porosity. Consistent with this observation, the highest oil flow rate and cumulative oil production are observed in the highest porosity case, as shown in Figure IV-45.

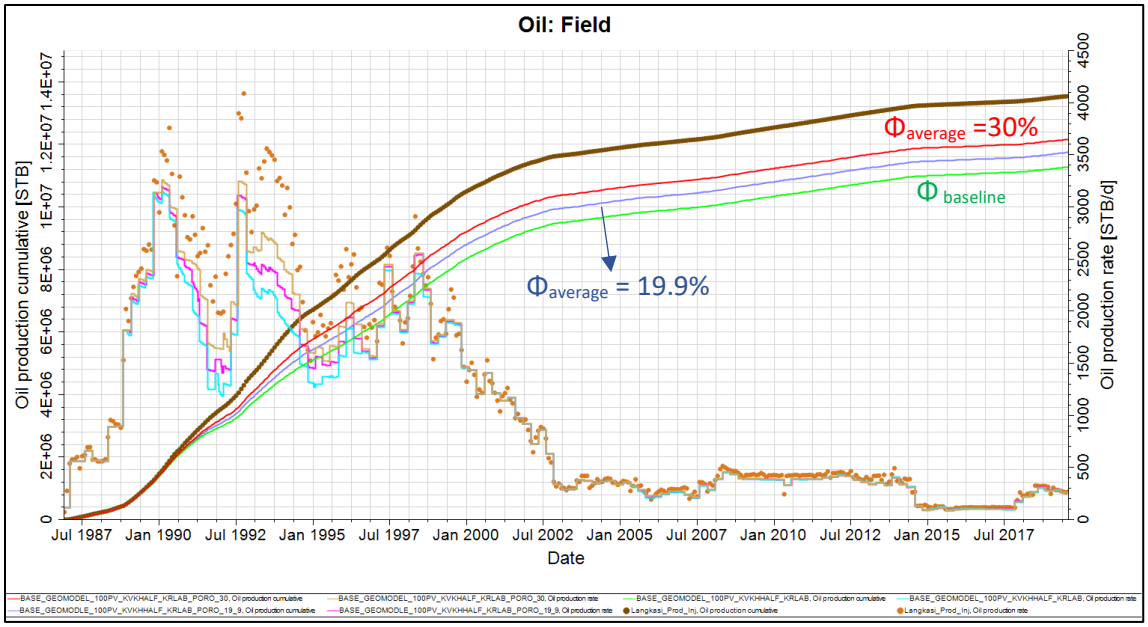

Figure IV-45. Oil production profiles with porosity variations.

Figure IV-46 and Figure IV-47 show water and gas production profiles, respectively. An inverse profile is observed for the water production plot. Therefore, even though more void space is available, most of it is filled with oil. The gas rate profile proportionally follows the trend of the oil production profile, as shown in Figure IV-47.

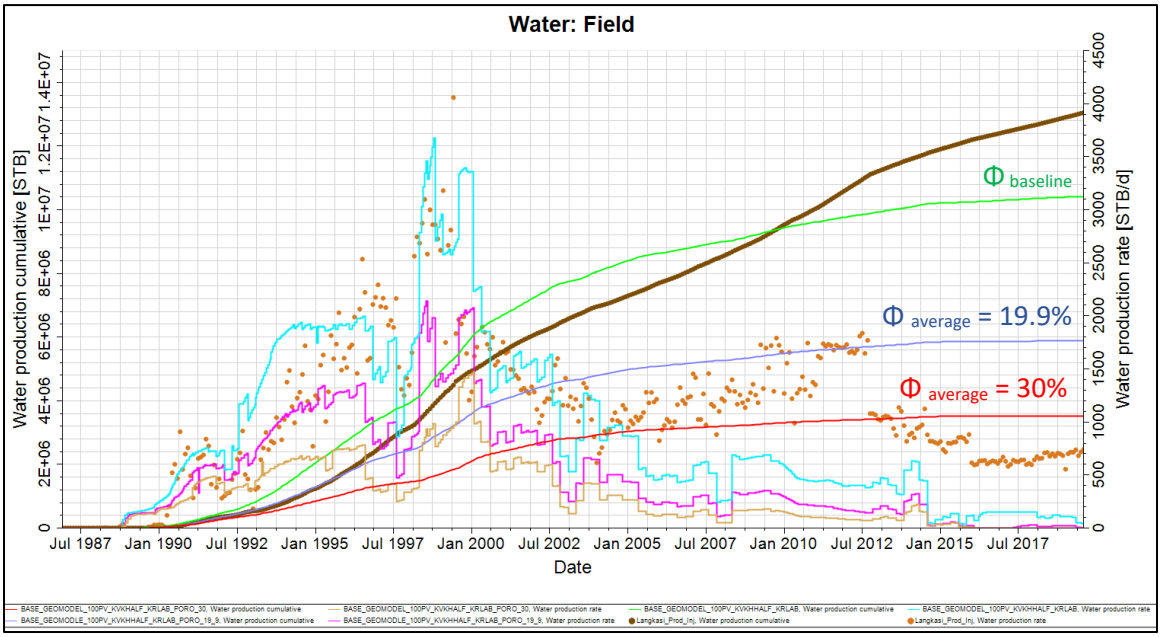

Figure IV-46. Water production profiles with porosity variations

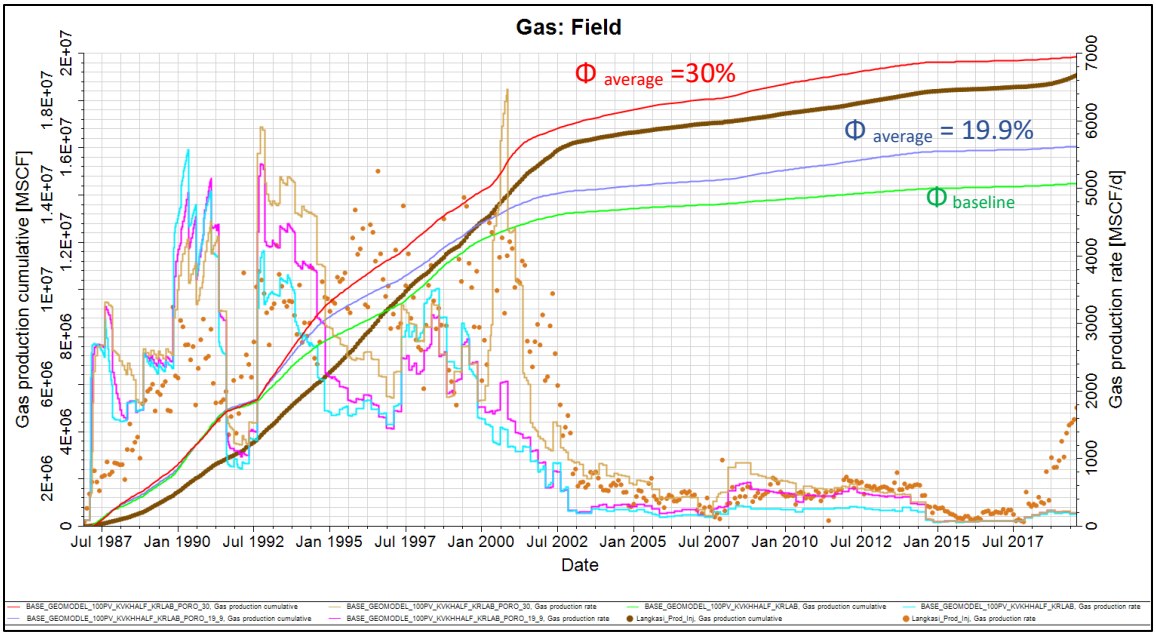

Figure IV-47. Gas production profiles with porosity variations

IV.8 Interim History Match Result

This result shows the best match between simulation and observed data by utilizing global changes only. For this result, the distribution in the geomodel was honored, as no regional or local changes were made to alter the populated properties. The permeabilities were multiplied globally by a factor of 3 and have average values of 147 mD and 73.9 mD in the horizontal and vertical directions, respectively. The porosity, in this case, was kept as per the geomodel value.

The regional variations were only applied to the vertical permeability in terms of varying k_v/k_h ratio in the reservoir. Bottom aquifer as the external support to the reservoir is required. In summary, regions around two wells were assigned a higher k_v/k_h ratio (0.9). The bottom PV multiplier around these two wells was much higher compared to the entire field (500). Using these combined PV multipliers, the aquifer volume ratios to OOIP ratio between these two are between 77.7 (with net oil) and 98.3 (with total oil). These ratios are very close with aquifer volume to the OOIP ratio from the MBAL study (113). Therefore,

these ratios are reasonably right and convincing. Figures IV-48 and IV-49 show these property modifications.

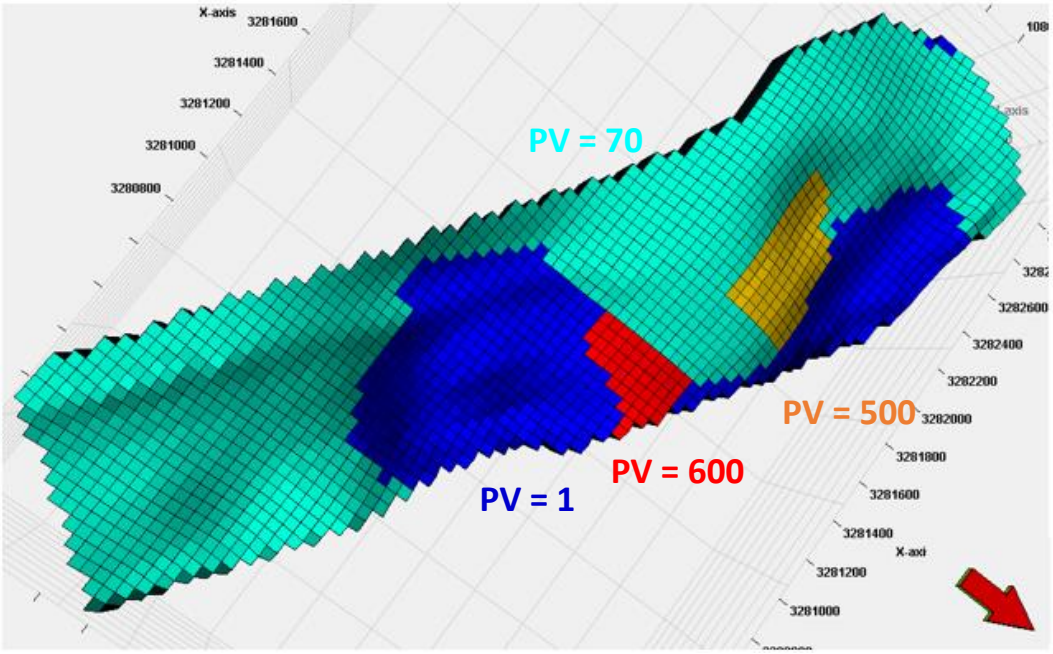

Figure IV-48. PV multipliers in different parts of the interim model

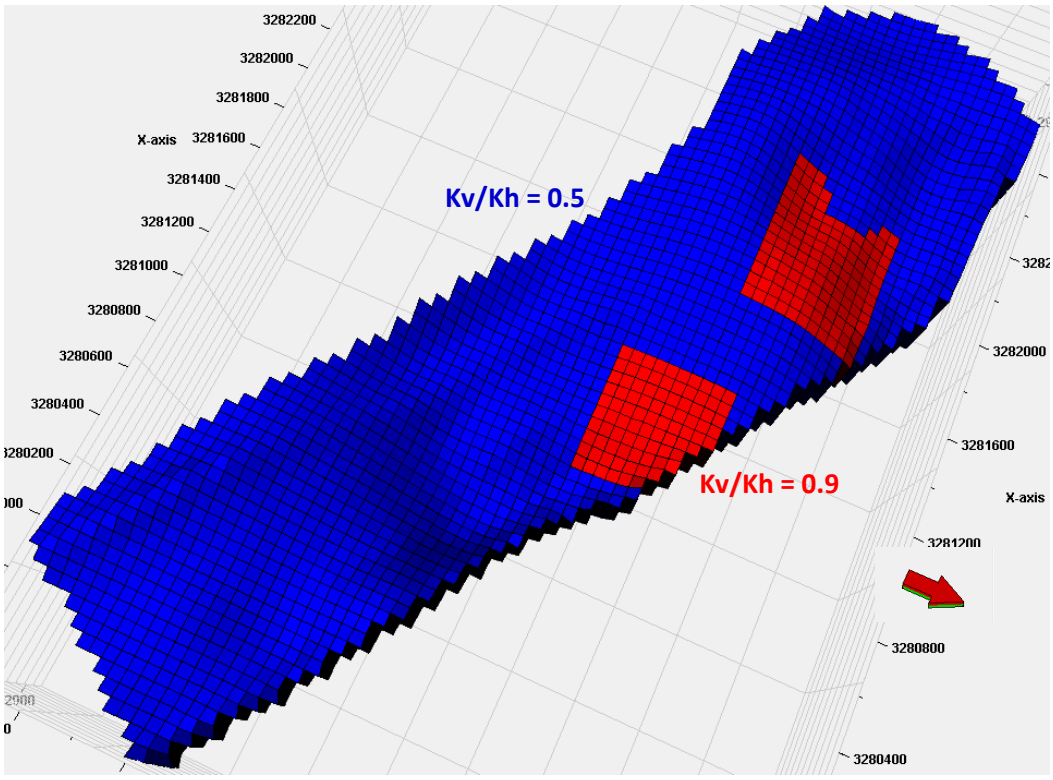

Figure IV-49. Kv/kh ratios in the interim model

Figure IV-50 and Table IV-4 show the results and comparison between the simulated value and measured data. Figure IV-51 shows the pressure profile obtained from this interim model. This interim model shows some improvement compare to the baseline history match model. However, to further improve the history match, more modifications were required. Some of the properties from this version can be carried forward to continue improving the history match.

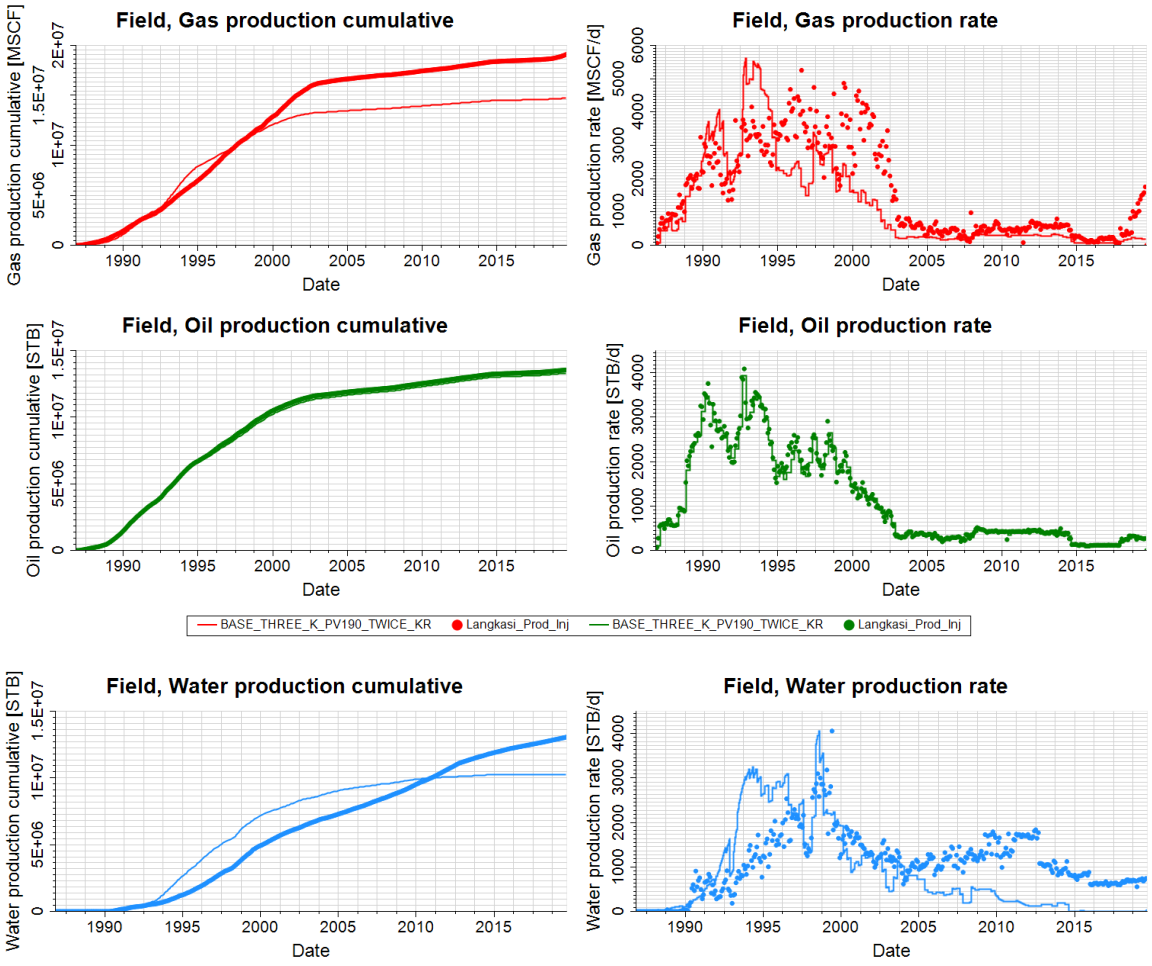

Figure IV-50. Interim history match results

Table IV-4. Comparison between simulation and field data (interim history match)

Property	Simulation	Field data	Error
Oil rate (BOPD)	268.87	272.33	1.2%
Water rate (BWPD)	10.7	742.14	~98.6%
Gas rate (MSCF/D)	206.77	1582.4	86.7%
Cumulative oil production (MMSTB)	13.365	13.546	1.5%
Cumulative water production (MMSTB)	10.3	13.502	23.7%
Cumulative gas production (MMSCF)	14.791	19.075	22.5%

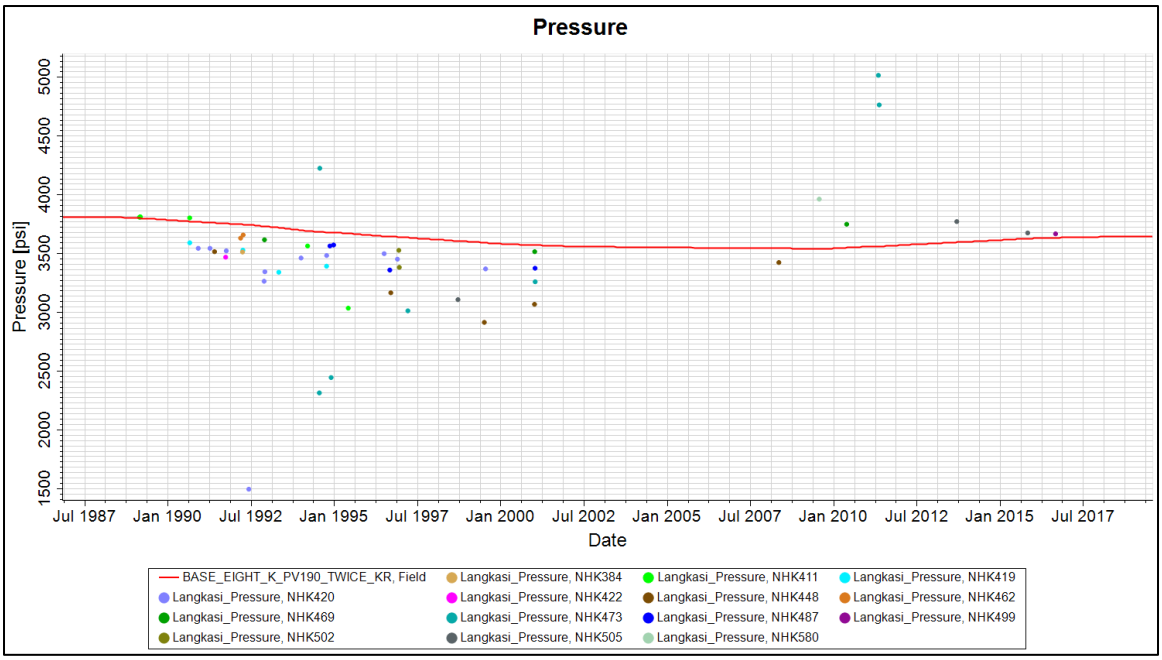

Figure IV-51. Pressure match in the interim history match model

IV.9 Final History Match Result

A history-matched reservoir model is non-unique because the same production history could be fit using a different combination of reservoir properties (*Tomomi, Y., 2010*). A numerical reservoir model must be calibrated against the dynamic behavior of the field so that it can be used as a reliable prediction tool. Even though several sophisticated methods such as assisted history matches are available, the common practice is to perform

forward history match simulations with trial and error. These iterations cease only when a satisfying history match is achieved. Therefore, the choice of parameters to be adjusted in the history matching procedure is a substantial matter. Nevertheless, the resulting model is non-unique.

At the end of the history match process, two models that could fit the historical data reasonably well were identified. In this manuscript, only the selected model is presented and further developed in the prediction scenario. Figures IV-52 to IV-57 show the PVT input used in the selected model.

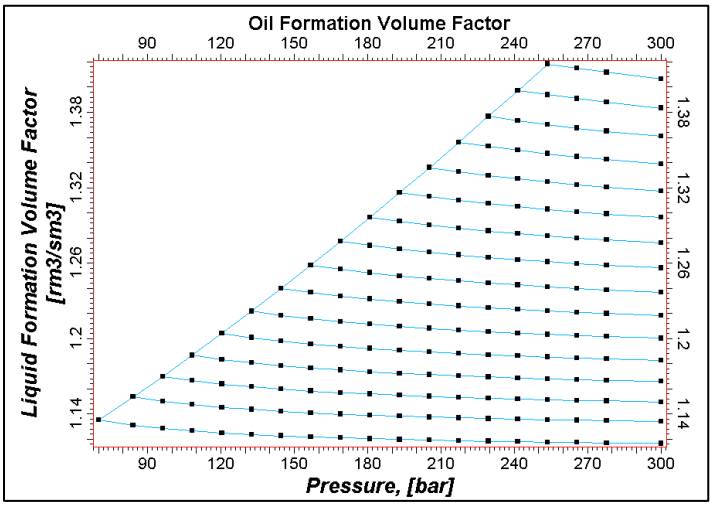

Figure IV-52 Pressure vs. oil formation volume factor

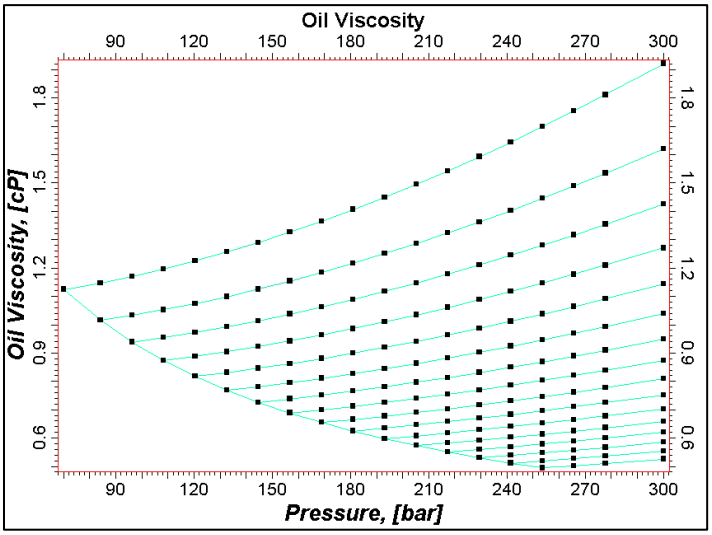

Figure IV-53 Pressure vs. oil viscosity

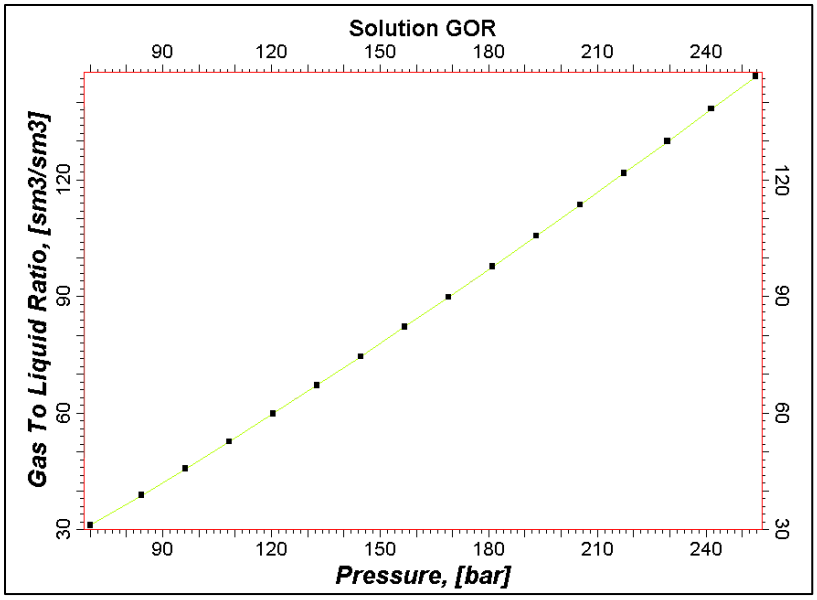

Figure IV-54. Solution Gas Oil Ratio

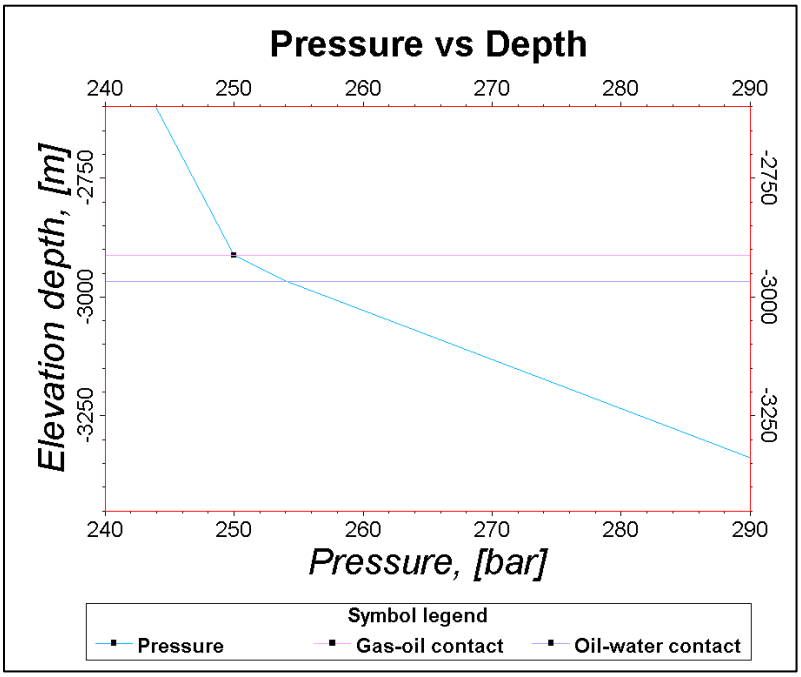

Figure IV-55. Pressure vs. depth profile

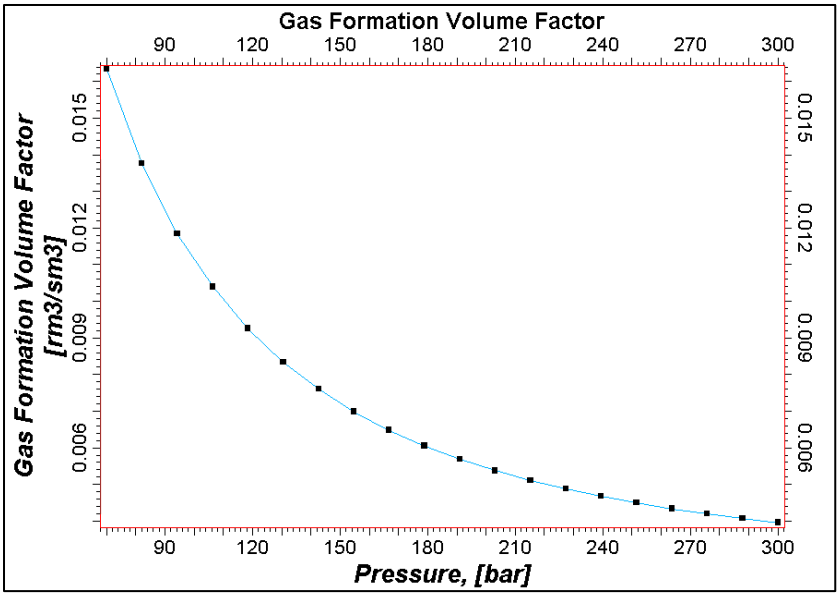

Figure IV-56. Gas formation volume factor

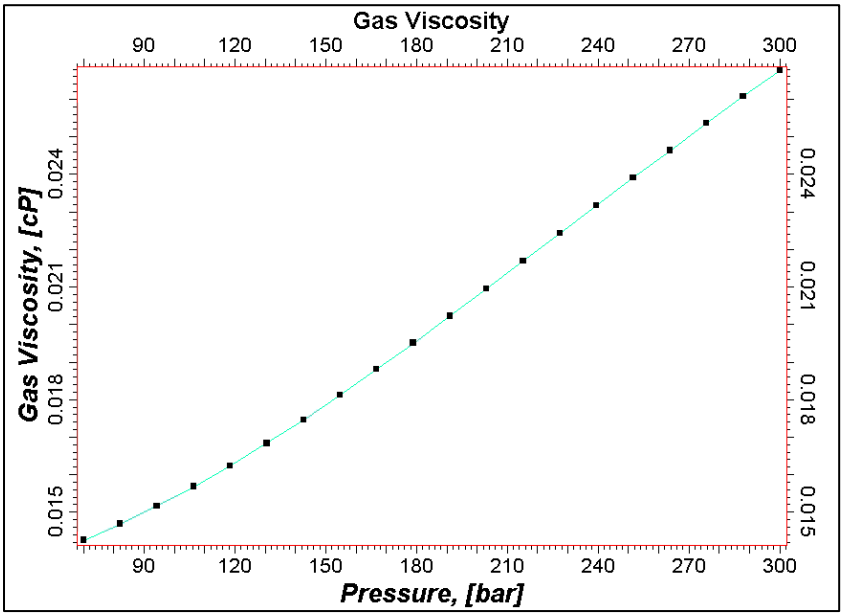

Figure IV-57. Gas viscosity

The final history match model in Petrel-Eclipse have the following input:

- PV multiplier = 70, except for the regions around NHK-505 and NHK-469 (PVs were 500 – 600).
- An edge aquifer that covers the area from central to the northern region.

- Average k_x and k_y = 243 mD, average k_z = 83 mD, with k_v/k_h variability at different locations.
- Average porosity= 13.9% and max porosity= 32.7%

Figures IV-58 and IV-59, show the final rock physics functions used to obtain this model.

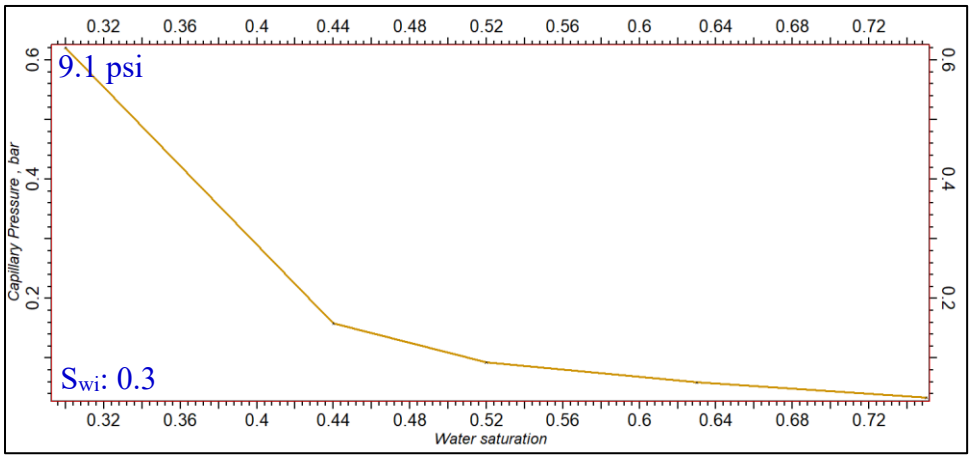

Figure IV-58. Capillary pressure for history match model

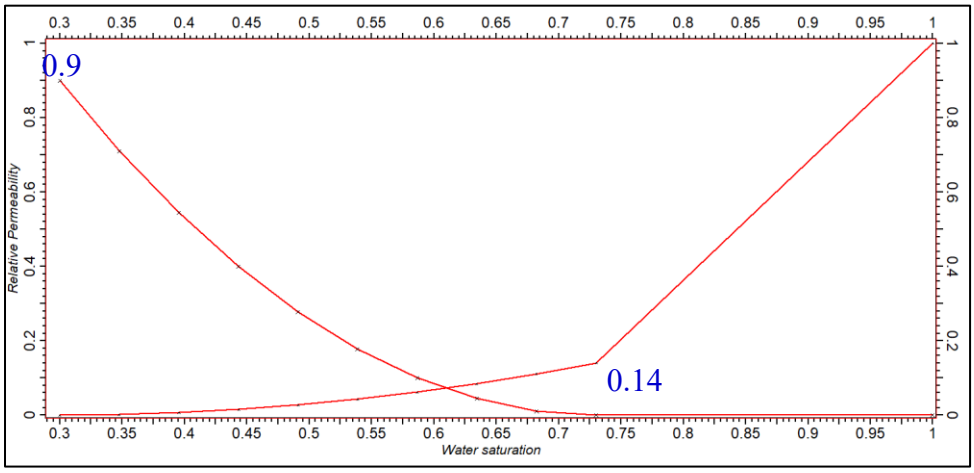

Figure IV-59. Relative permeability curve for history matched model

The pressure profile for this case is shown in Figure IV-60. This profile is the best pressure profile obtained in Petrel. Further improvements were made later when the Petrel model was loaded to CMG and processed for prediction runs.

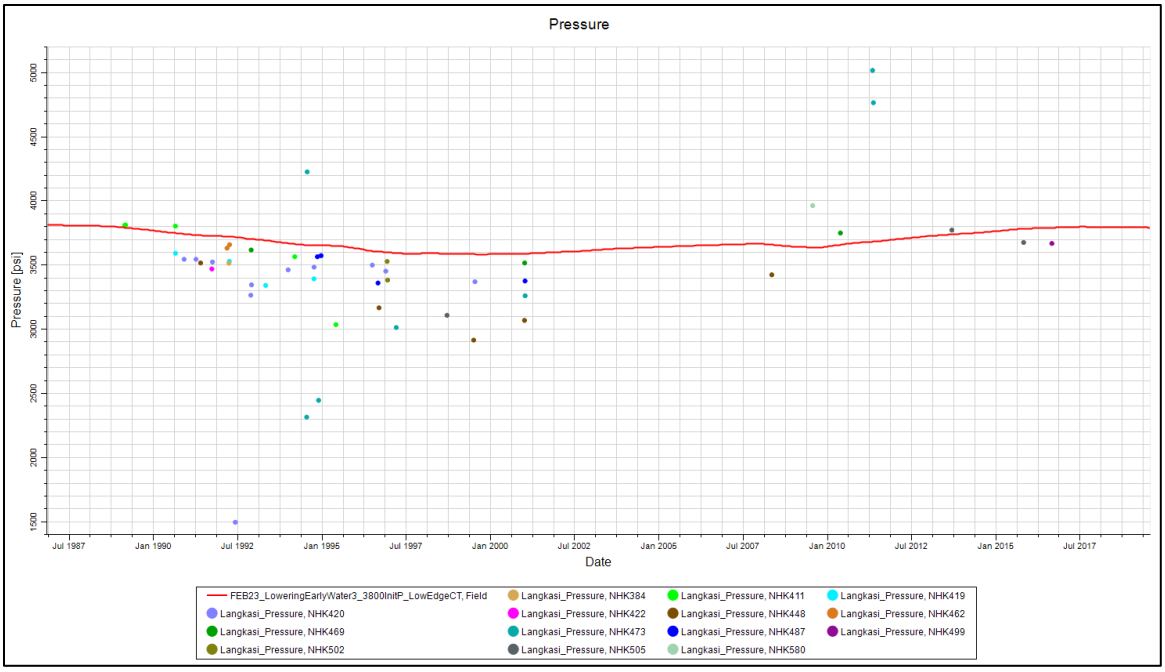

Figure IV-60. Fieldwide pressure profile for the history match model

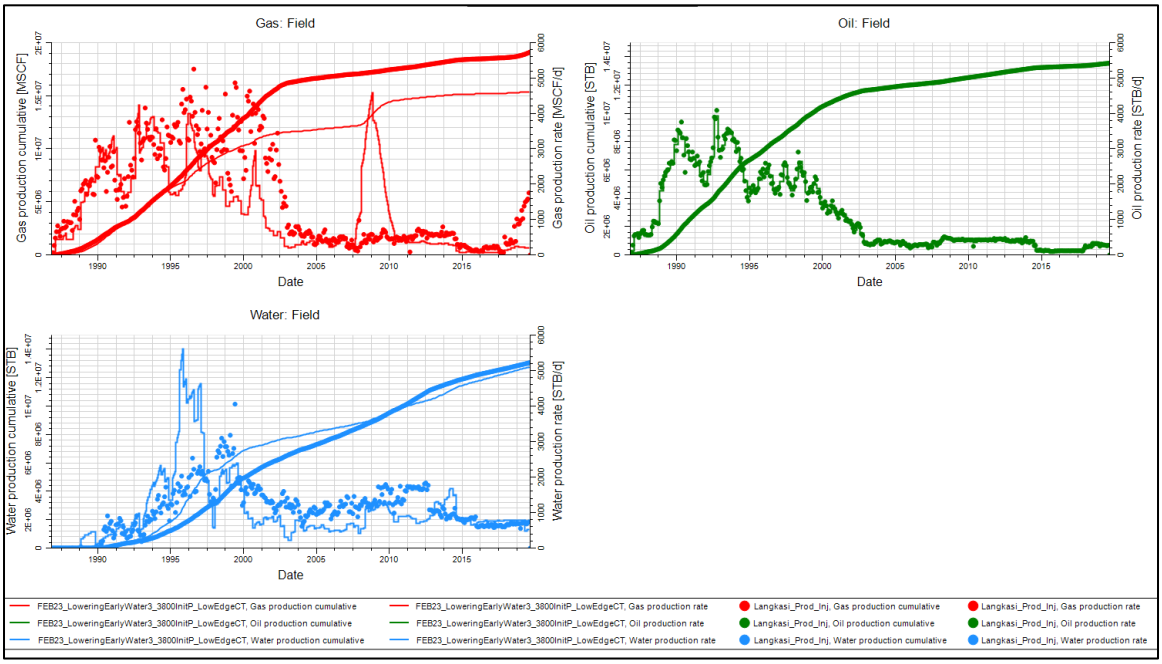

Figure IV-61.Fieldwide production matches for the history match model

Figure IV-61 and Table IV-5 show a comparison between the measured rate and the calculated rate from Petrel. The spike in the simulated gas rate was caused by one inactive well (NHK-391).

Table IV-5. Comparison of simulation and field data for history match model

Property	Simulation	Field data	Error
Oil rate (BOPD)	268.9	272.33	1.2%
Water rate (BWPD)	624.6	742.14	15.8%
Gas rate (MSCF/d) *	254.4	339	24.5%
Cumulative oil production (MMSTB)	13.532	13.546	0.1%
Cumulative water production (MMSTB)	12.809	13.502	5.1%
Cumulative gas production (MMSCF)	15.438	19.075	19%

For gas rate comparison, data points in July 2018 were used, as some inconsistencies in the measured gas rates were observed. Gas measurement match is acceptable because it is within 30% inaccuracy (as reported by the operator).

IV.5 Production Forecast

The objective of the history matching process was to calibrate reservoir properties to match the production data. Once this objective was achieved reasonably, this model was used to assess several future development options for the field. The calibrated reservoir model was used to identify and evaluate long-term development strategies to increase ultimate recovery.

A remaining oil map (HCPV oil) was created based on the oil saturation at the end of the time step, porosity for each grid cell, and grid cell volume. Based on this HCPV oil, I identified four prospects for future infill well locations. Therefore, four wells were proposed in the future prediction scenario. These wells were drilled one by one in a separate prediction case. The four wells are UH-1, UH-2, UH-3, and UH-3NE. UH-3 is located away from the current wells. Hence this well is considered a delineation well. UH-3NE is

a modification of the UH-3, where the target location is closer to the existing wells. Figure IV-62 shows the locations of the three infill wells and one delineation well.

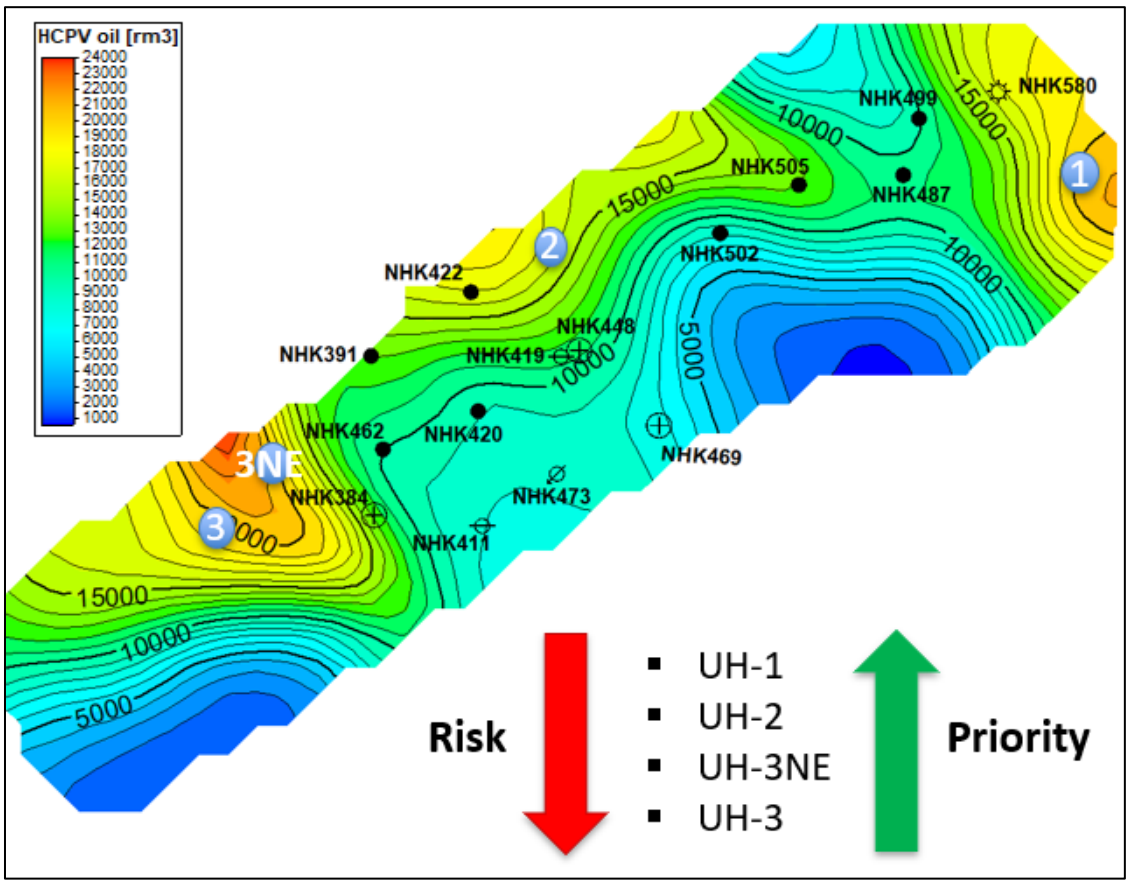

Figure IV-62. Remaining hydrocarbon pore volume at the end of history match

Table IV-6 summarizes the future development strategy that was tested/evaluated in the reservoir simulation study.

Table IV-6. Cases for prediction runs

No	Case	Description
1	Baseline (no investment)	Followed the last FBHP data and extended to 2040 (as is scenario)
2	Case 1 + workover case	Assumed acid stimulation job for active wells. Evaluation of reperforation indicated unattractive outcome.
3	Case 1 with varying injection rate	Injection rate increased in NHK-487 (evaluated range from 0 to 1250 STB/D). Increasing injection rate was not attractive
4	Case 1 with decreased FBHP operating mode	FBHP decreasing trend (evaluation ranged from 9 to 36 psi/yr)
5	Case 1 + 1 infill well in the north	Investment case with well UH-1
6	Case 1 + 1 infill well in the central	Investment case with well UH-2
7	Case 1 + 1 delineation well in the south	Investment case with well UH-3
8	Case 1 + 1 infill well in the south)	Investment case with well UH-3NE

Due to the unexpected challenge of Petrel's and Eclipse's license, we decided that the forecast carried out using Computer Modelling Group (CMG) software suites such as Builder, Imex, and Results.

IV.5.1 Case 1. Baseline Forecast

The first step was to obtain the output of the calibrated simulation model from Petrel via the rescue process and then upload that into CMG Builder. Using CMG Builder, the model was prepared, production and pressure data were formatted to suit the software input and then initialized. Unlike Petrel production data input, CMG does not have well

uptime as the input category. Therefore, the average monthly rate for producers and injectors was weighted average based on the total number of production days reported in GRPC database. After transferring the simulation model to CMG, one crucial step was to run the history match in CMG Imex and benchmark the results with a previous fieldwide match perform using Petrel Eclipse.

Figure IV-63 shows the pressure match between the fieldwide actual data and the model. Earlier time (before 2007) pressures match are reasonably good, and at a later time, pressures are matched perfectly. The most recent pressure data are more critical to match to ensure accurate production forecasts.

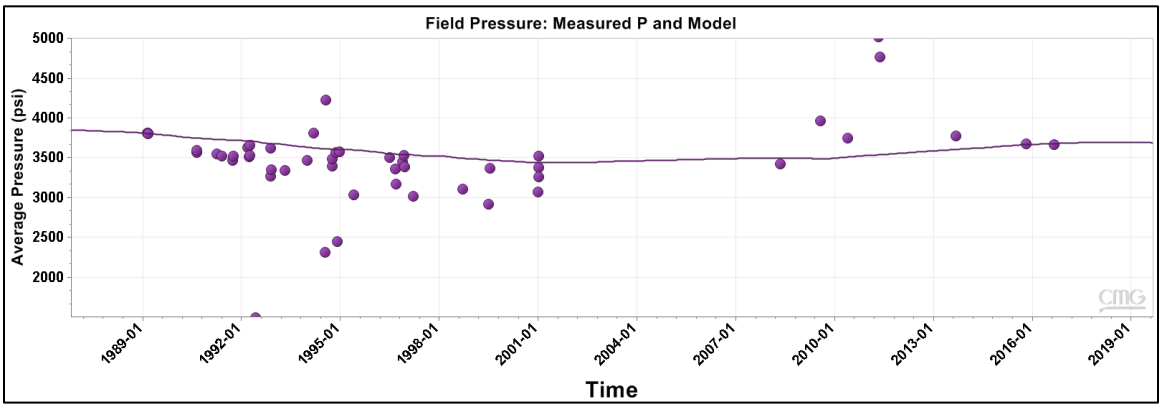

Figure IV-63. Fieldwide final pressure match in CMG

Using CMG, I could obtain a comparable fieldwide history match. Hence this model was right to use. Before proceeding to PI calibration, it is important to examine the water cut profiles in the four active producers. These four wells' water-cut matches were reasonably good, and match quite well with the most recent measured data point. This was important to avoid overly optimistic predictions. Figures IV-64 to IV-67 show the water cut match in the four active wells.

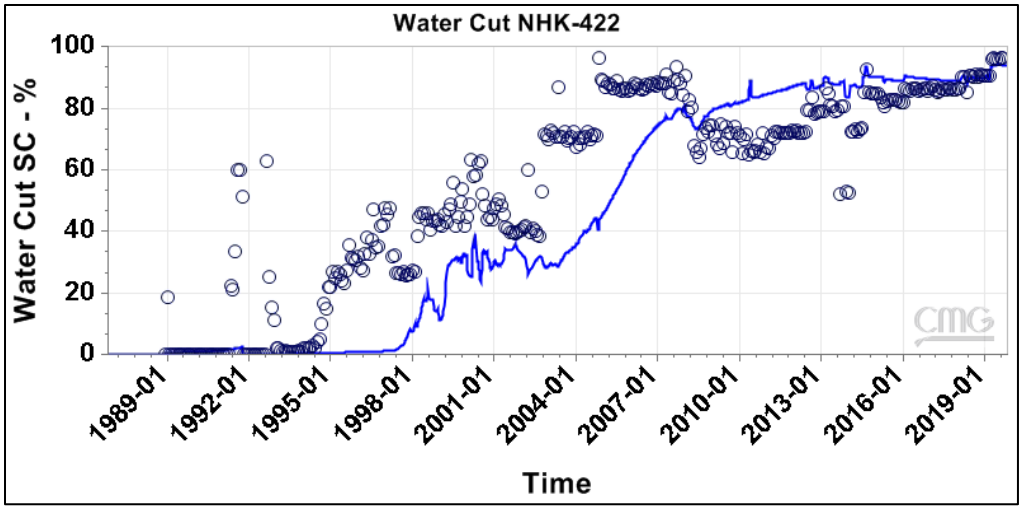

Figure IV-64. Water cut match for NHK-422

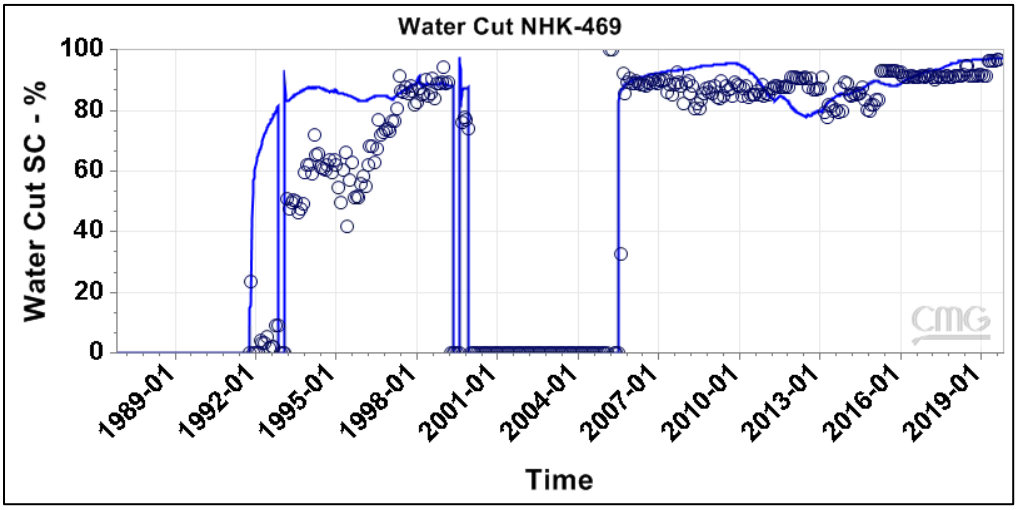

Figure IV-65. Water cut match for NHK-469

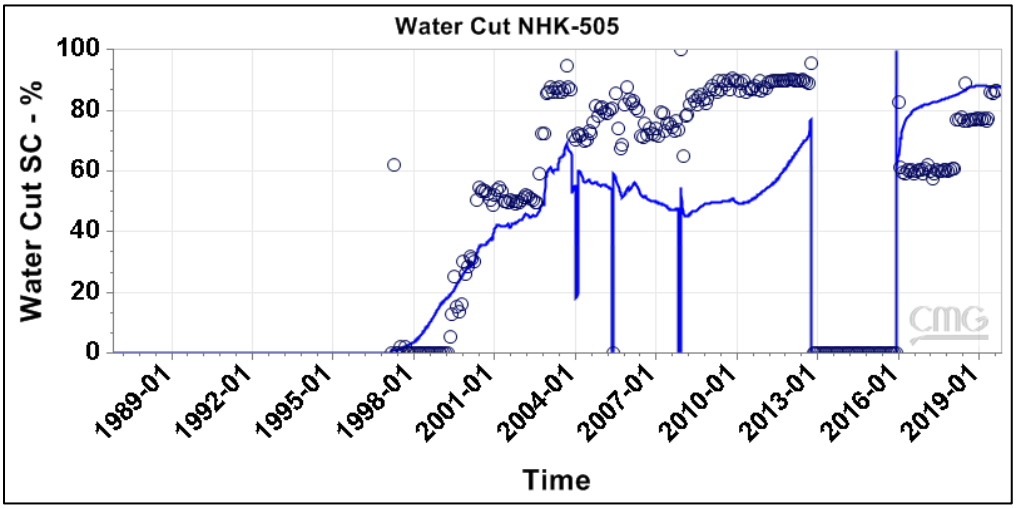

Figure IV-66. Water cut match for NHK-505

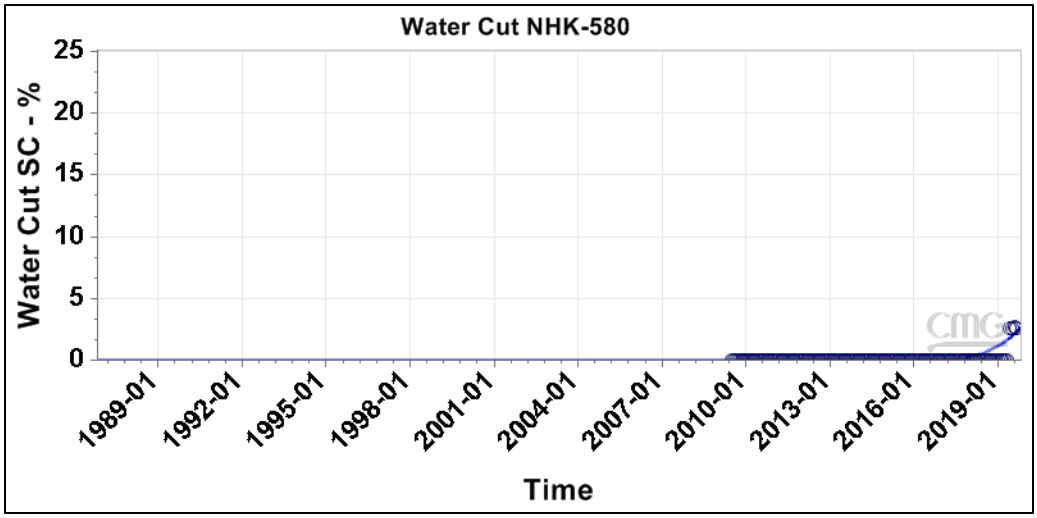

Figure IV-67. Water cut match for NHK-580

The next step was to perform the Production Index (PI) calibration. The objective was to ensure that the transition between production history match to the production forecast is smooth. PI calibration was performed by matching the flowing bottom-hole pressure (FBHP) from the model with the available FBHP data (by adjusting PI value using a multiplication factor). Table IV-7 summarizes the calibrated PI values for the four active producers in LK-4 at the end of the history match.

Table IV-7. Calibrated PI values

Well	**PI value (STB/day/psi)**
NHK-422	0.1
NHK-469	1.9
NHK-505	2.8
NHK-580	0.8

Figures IV-68 to IV-71 show the FBHP match for the four active producers (NHK-422, NHK-469, NHK-505, and NHK-580) and the forecasted FBHP until end of 2040. It is not a perfect match but is considered reasonable.

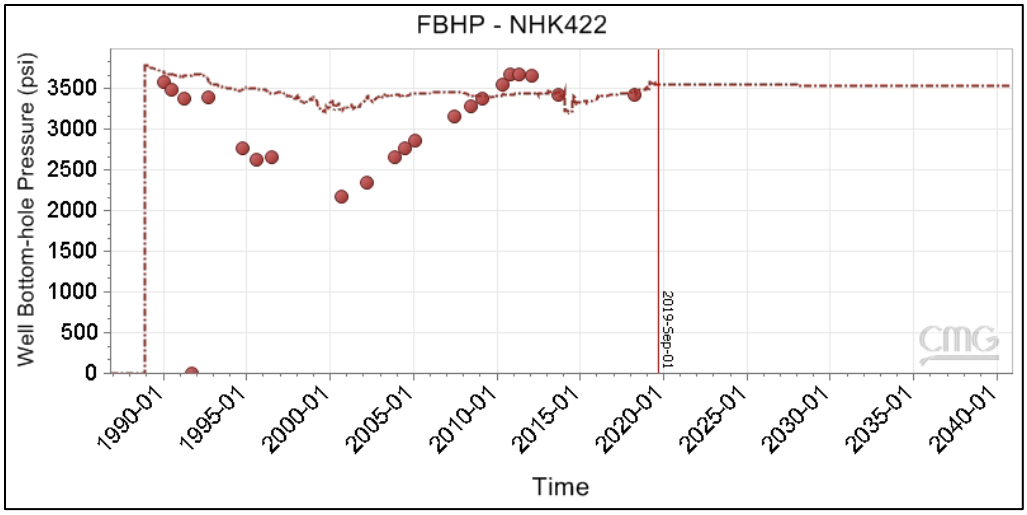

Figure IV-68. FBHP match for NHK-422

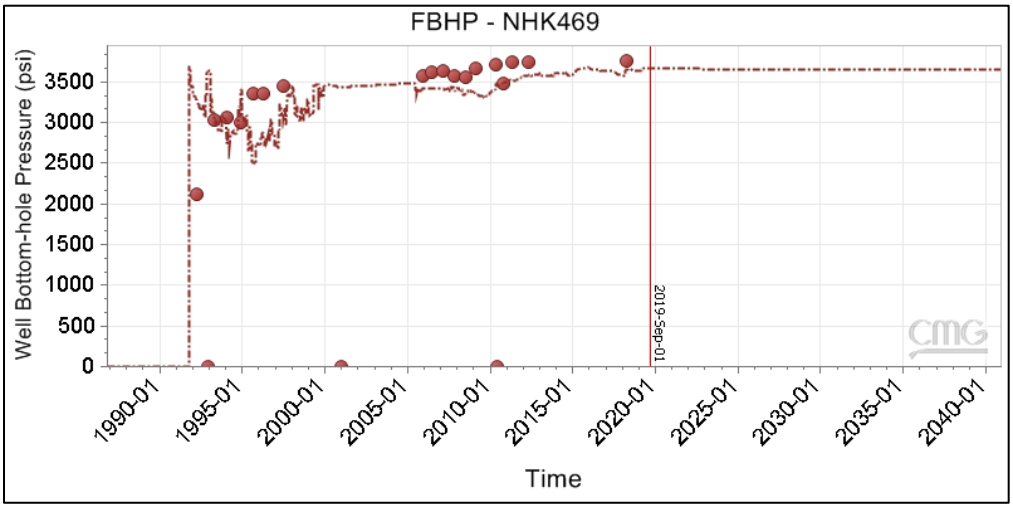

Figure IV-69. FBHP match for NHK-469

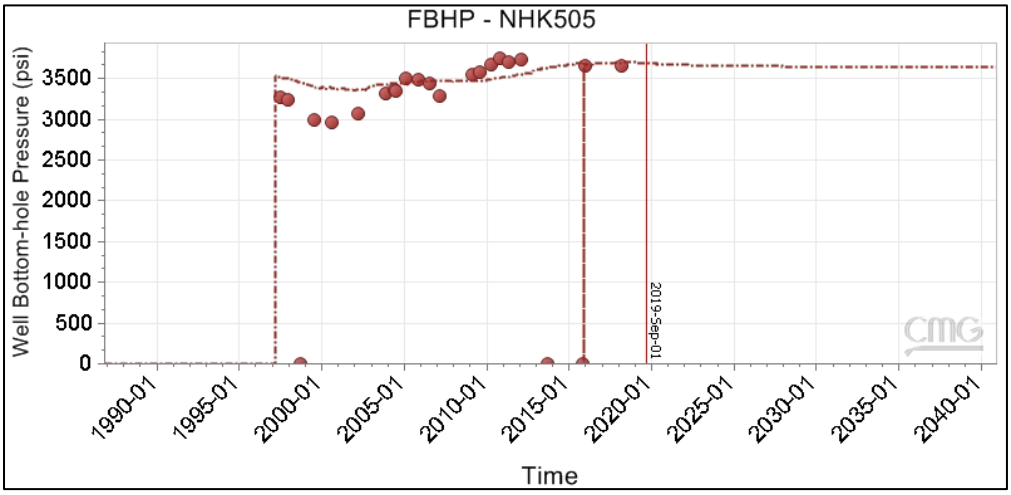

Figure IV-70. FBHP match for NHK-505

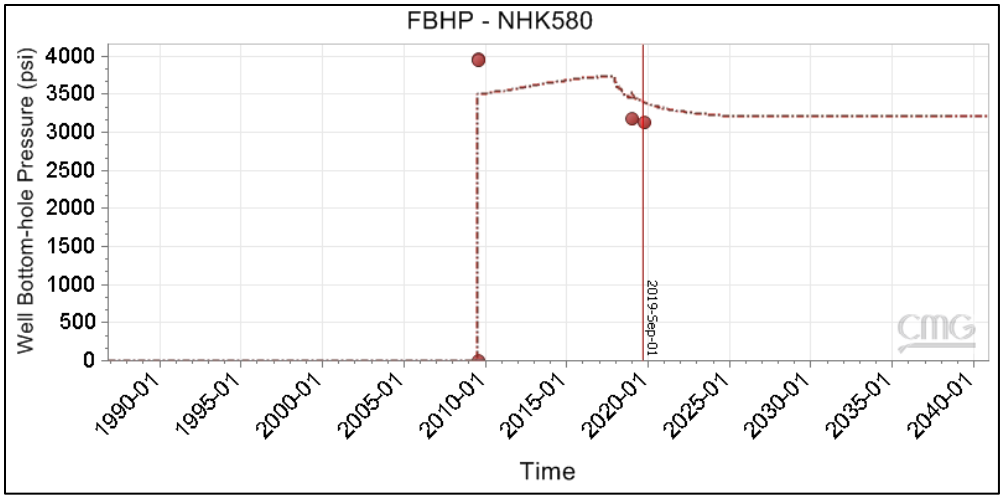

Figure IV-71. FBHP match for NHK-580

After completed the PI calibration process, the model was run while maintaining the total liquid as a constraint. The active well FBHPs were limited so that it will not decrease below each well's lowest historical FBHP. Figures IV-72 to IV-75 show the predicted oil rate for the four active producers.

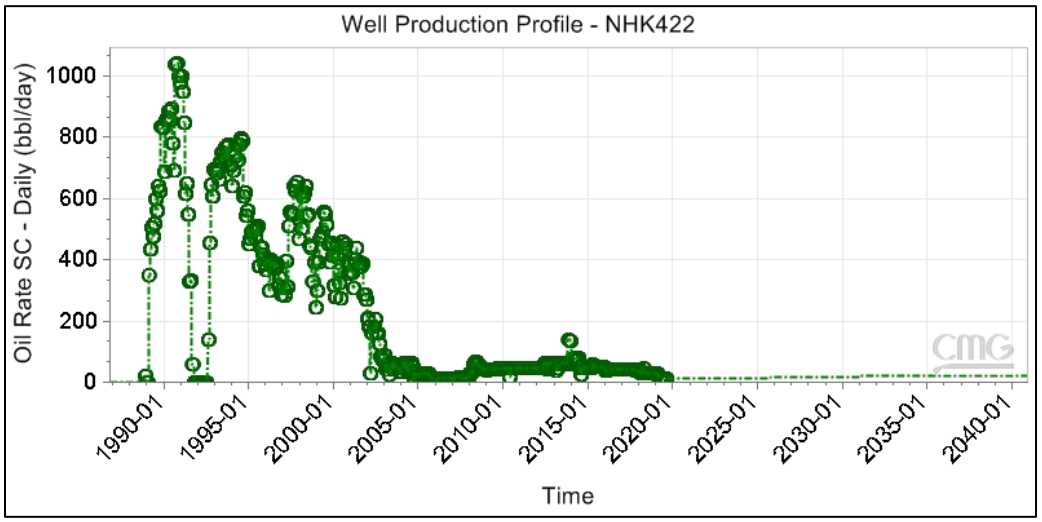

Figure IV-72.Oil production forecast for NHK-422

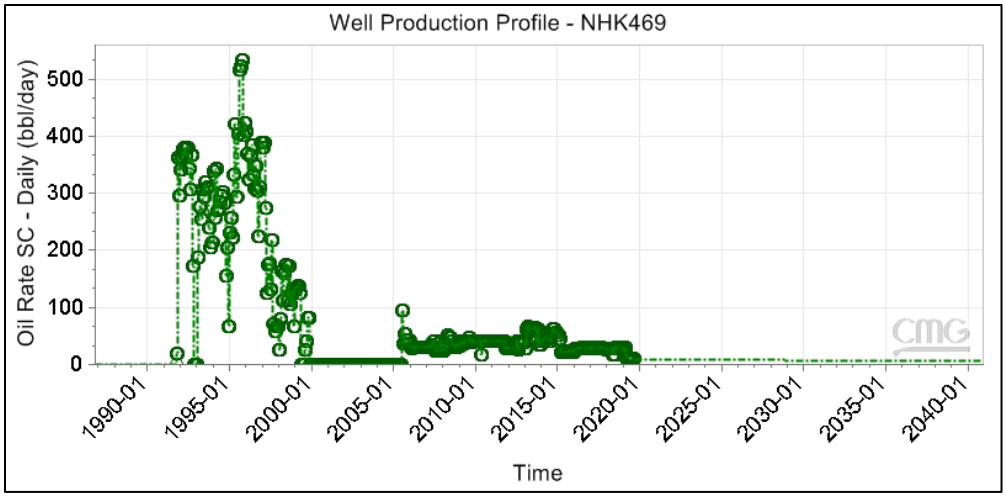

Figure IV-73.Oil production forecast for NHK-469

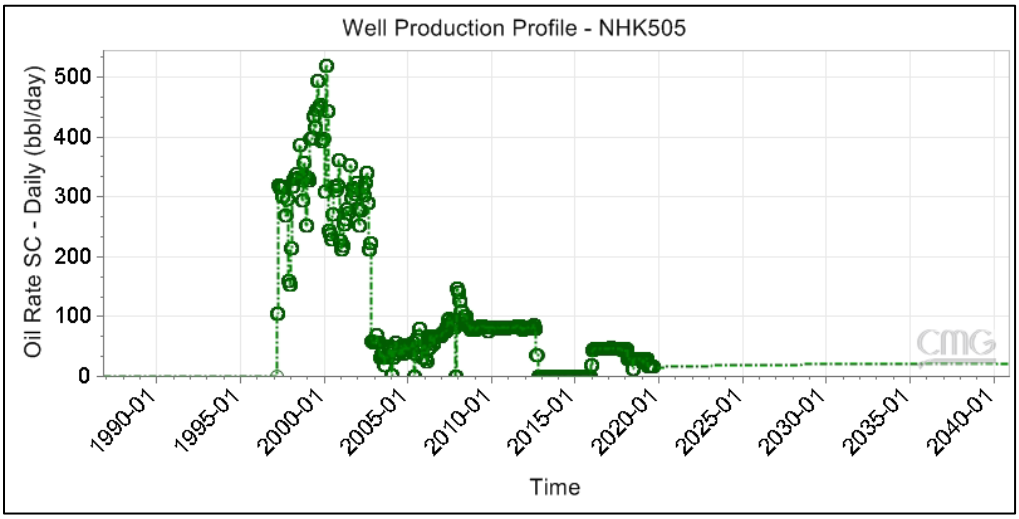

Figure IV-74.Oil production forecast for NHK-505

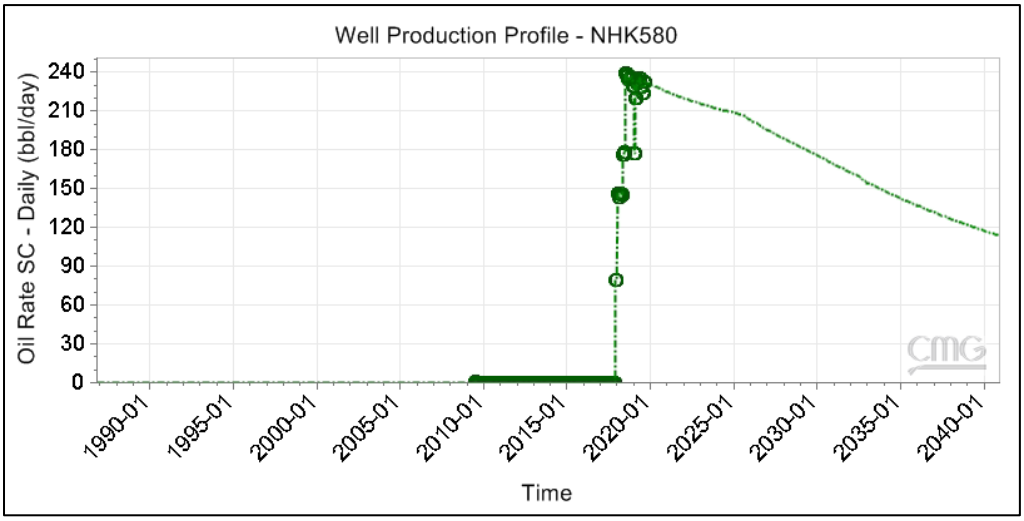

Figure IV-75. Oil production forecast for NHK-580

Figures IV-76 to IV-79 show the predicted water cut for the four active producers. It can be observed that there are not many changes in the predicted water cut from the end of history to the end of prediction. The exception is for NHK-580, as shown in Figure IV-79, where at the end of prediction (December 2040), its water cut was 38%.

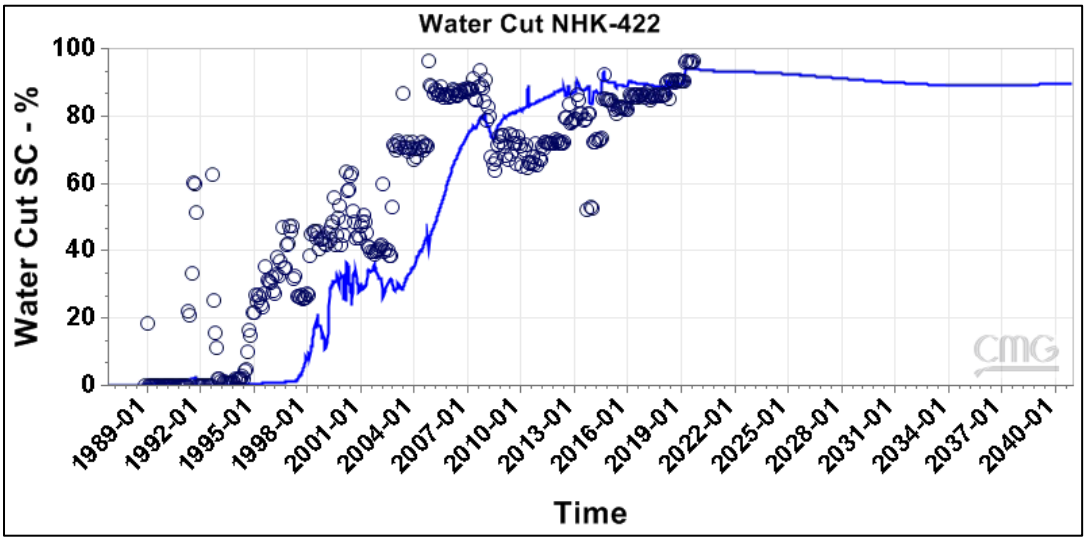

Figure IV-76. Historical and forecasted water cut profile for NHK-422

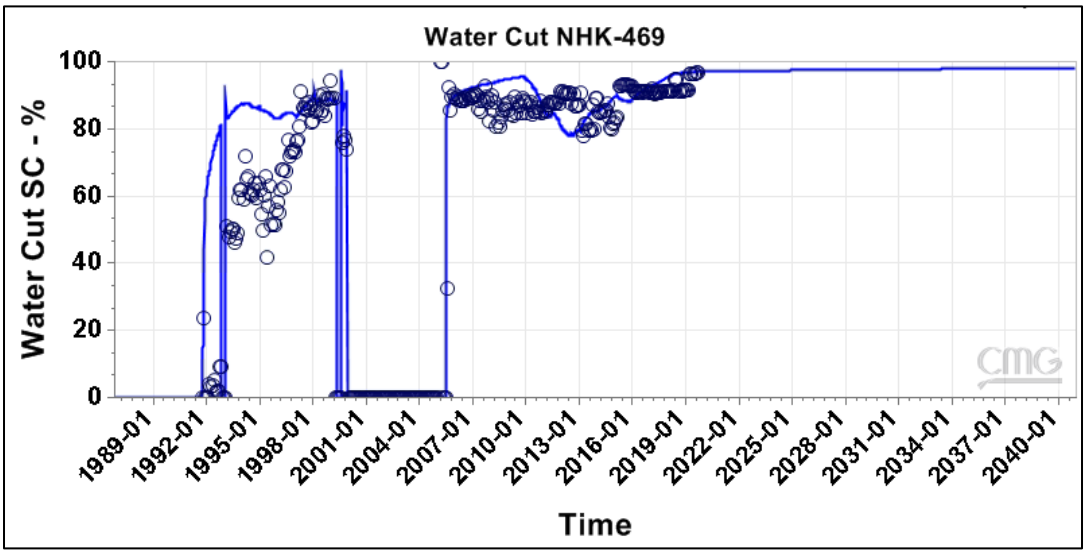

Figure IV-77. Historical and forecasted water cut profile for NHK-469

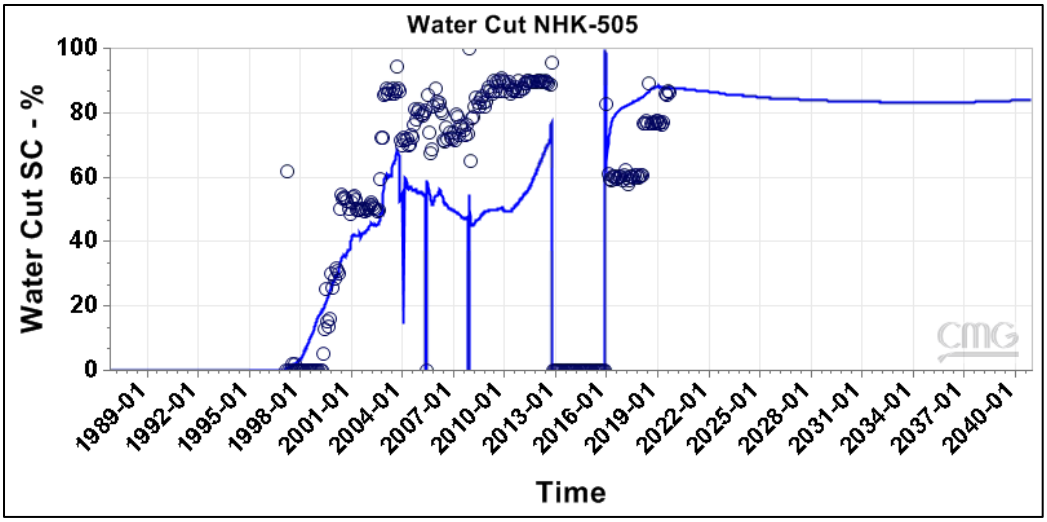

Figure IV-78. Historical and forecasted water cut profile for NHK-505

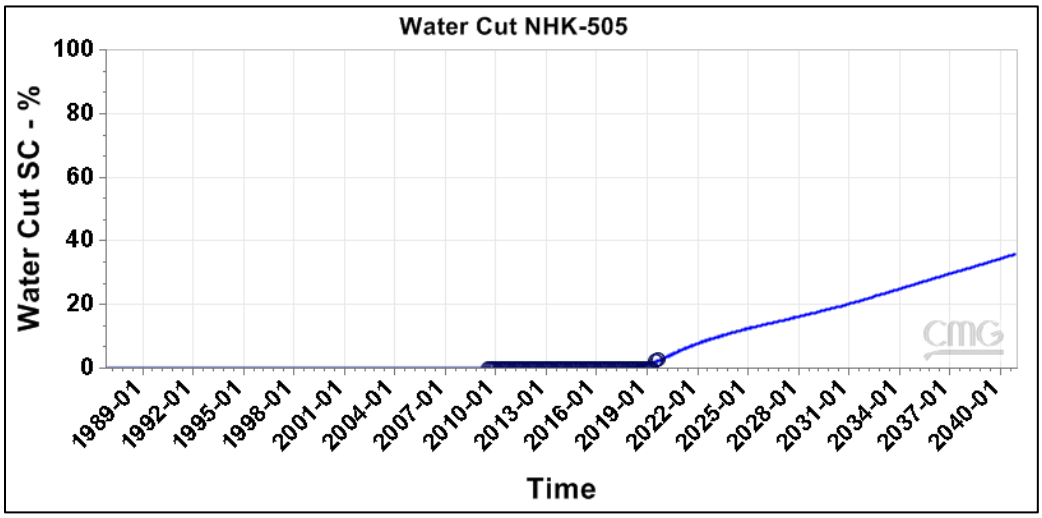

Figure IV-79. Historical and forecasted water cut profile for NHK-580

Figure IV-80 shows the pressure profile from history match to the end of prediction. At the end of the history match, the fieldwide average pressure was 3690 psi; at the end of prediction, it dropped to 3674 psi.

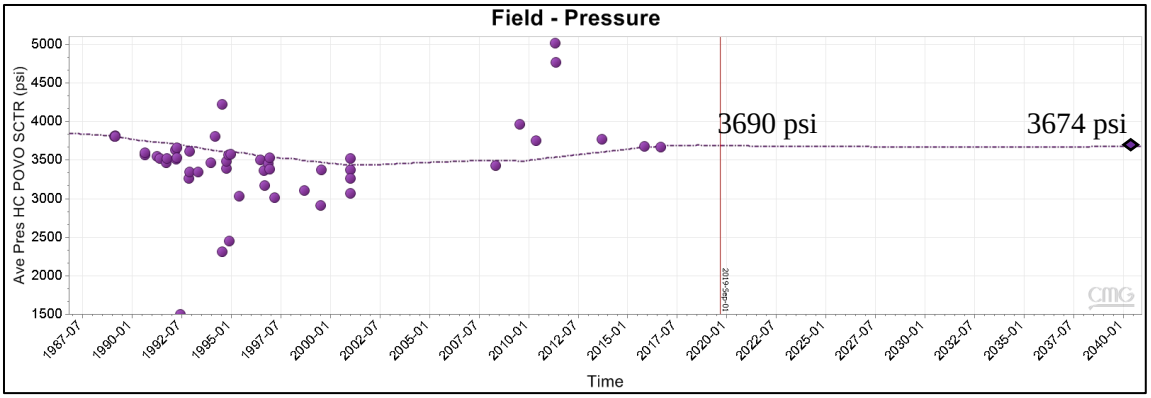

Figure IV-80. Fieldwide historical and forecasted pressure

Figures IV-81 to IV-83 show the production profiles for oil, water, and gas at a fieldwide level. At the end of the prediction run, the cumulative production and flow rate are presented inside the figures. Cumulative oil production for baseline forecast is 15.15 MMSTB; this is equivalent to a 38% ultimate recovery considering the OIL-reported OOIP (39.9 MMSTB).

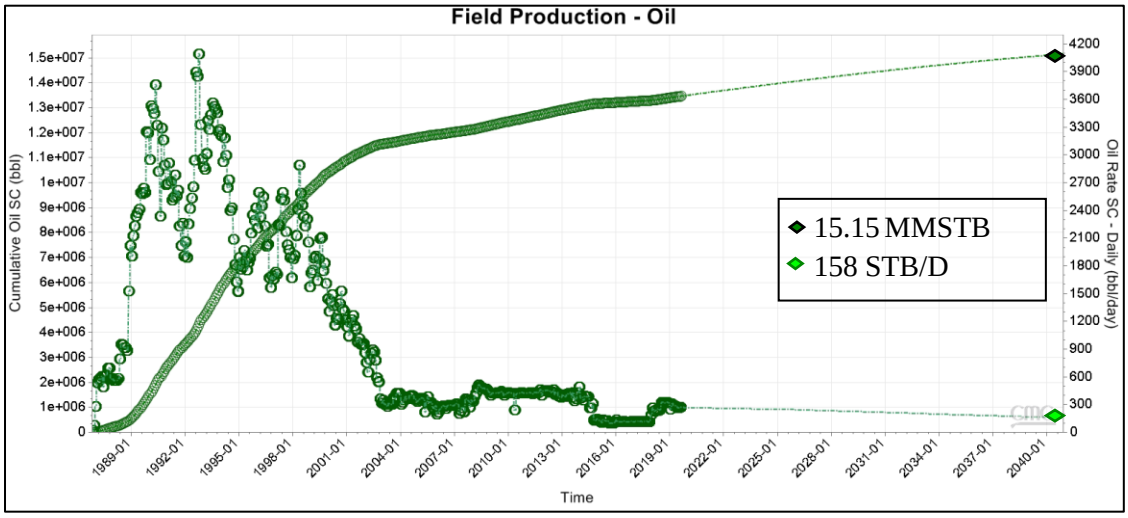

Figure IV-81. Fieldwide historical and forecasted oil production

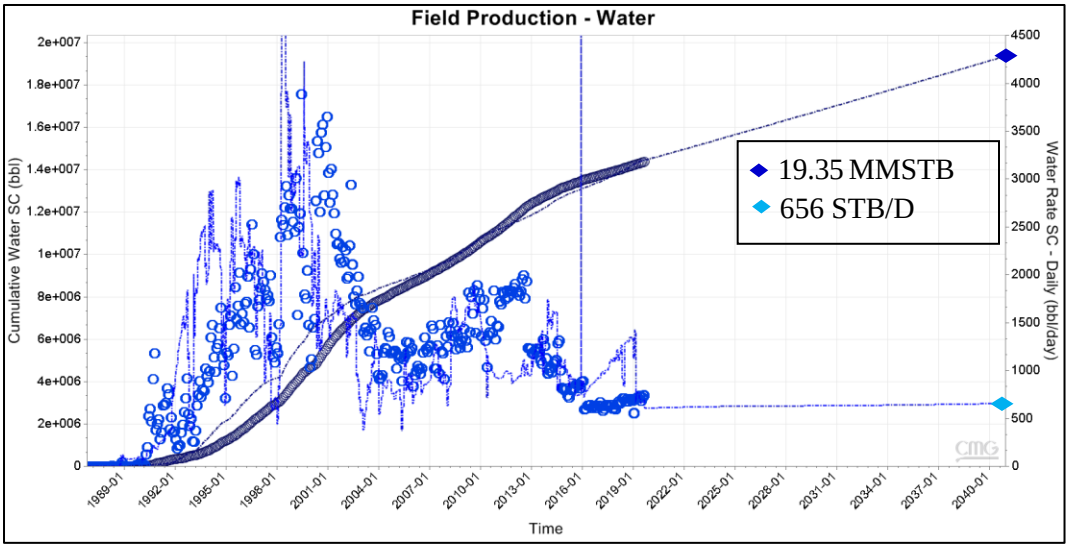

Figure IV-82. Fieldwide historical and forecasted water production

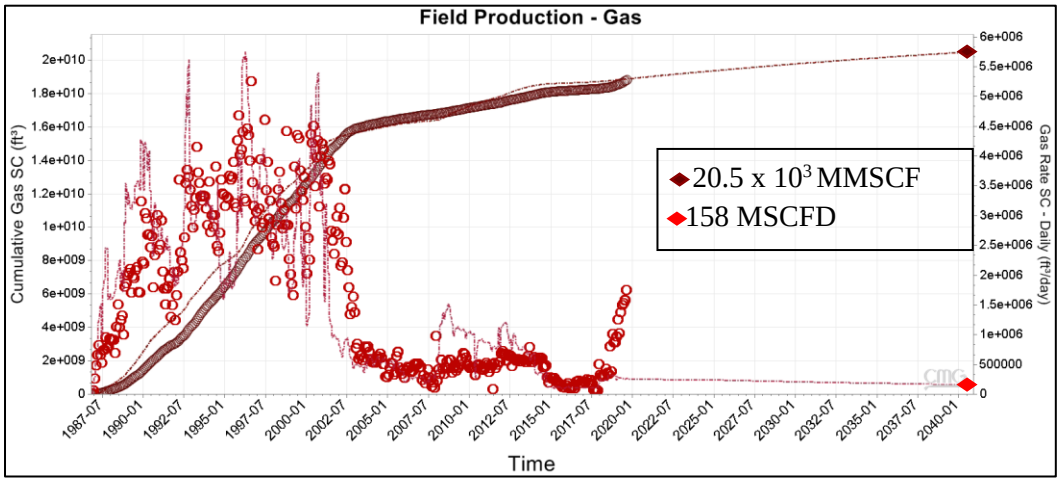

Figure IV-83. Fieldwide historical and forecasted gas production

IV.5.2 Case 2. Baseline + Workover

Case 2 is the evaluation of possible future workover in the four active wells. In the reservoir simulation study, I considered three options. These options are acid stimulation, reperforation, and a combination of both. Acid stimulations were modeled by applying a specific percentage PI increase to the treated intervals. These increases were also proportionally applied to increase the total liquid constraint. The evaluated scenarios include PI increases of 12.5%, 30%, and 50%.

I evaluated reperforations by examining oil saturation in the blocks near the well locations. These cases were created by closing the perforations adjacent to the high-water saturation blocks and opening new perforations around the blocks with high oil saturation. Unfortunately, there were not many opportunities to explore reperforation options. As a result, reperforations and combined reperforations-acid stimulation did not yield attractive product. Lower oil and higher water productions were observed, and these two scenarios, therefore, were not considered further.

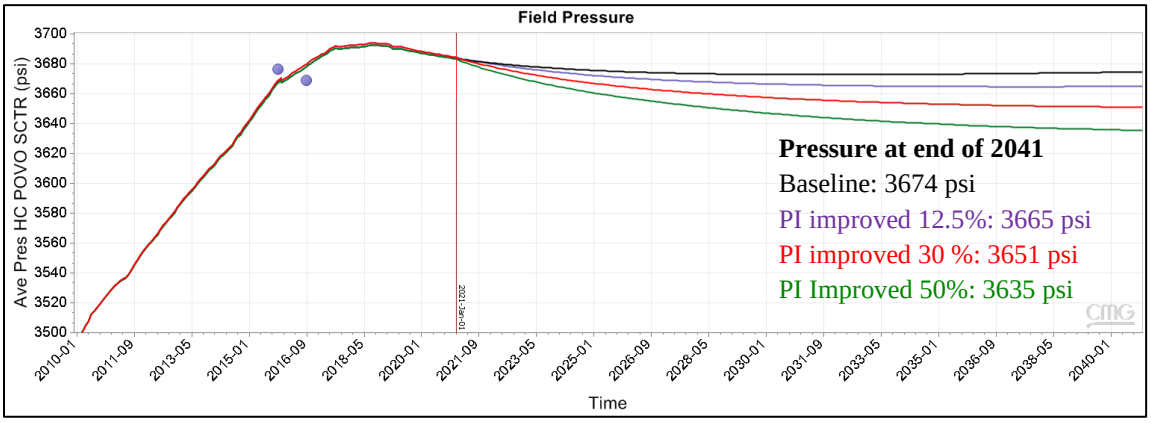

Figure IV-84. Predicted pressure profiles for three PIs scenarios

Figure IV-84 shows the variation of pressure and its value at the end of prediction. These profiles indicate model responses to the augmented PIs due to the acid stimulations. Figure IV-85 shows the oil production rate for a different PI case. The oil rate increase is directly proportional to the PI increase. The highest oil production observed with 'PI improved 50%', and as a result, this scenario yielded the highest-pressure decline. The black solid and dashed lines in both figures show the pressure and oil rate profiles for the baseline as a comparison to the acid stimulation cases.

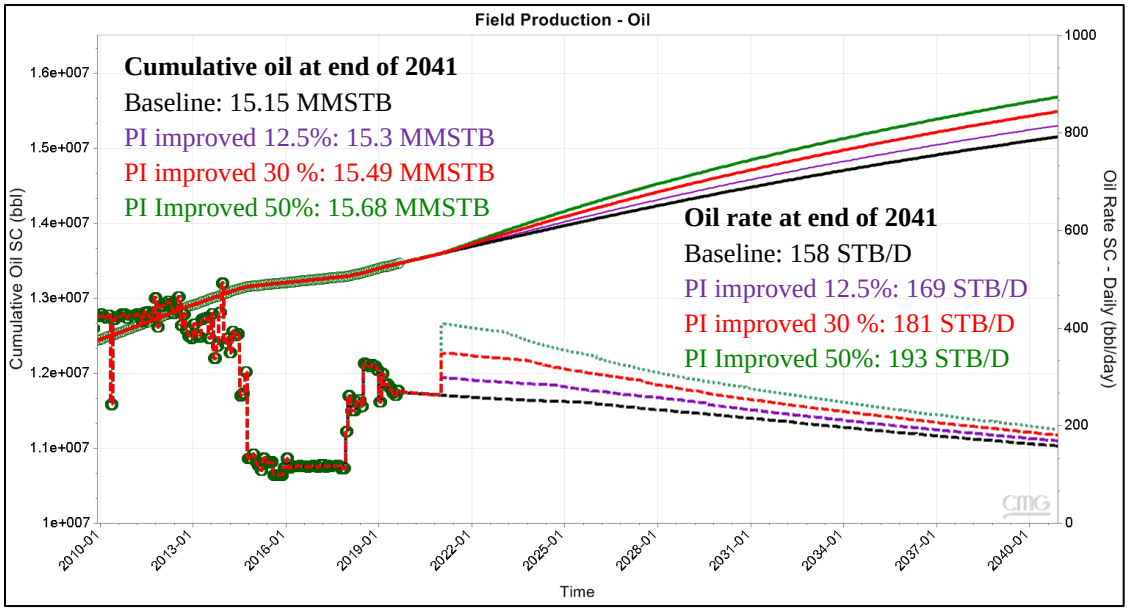

Figure IV-85. Predicted oil production for three different PIs scenario

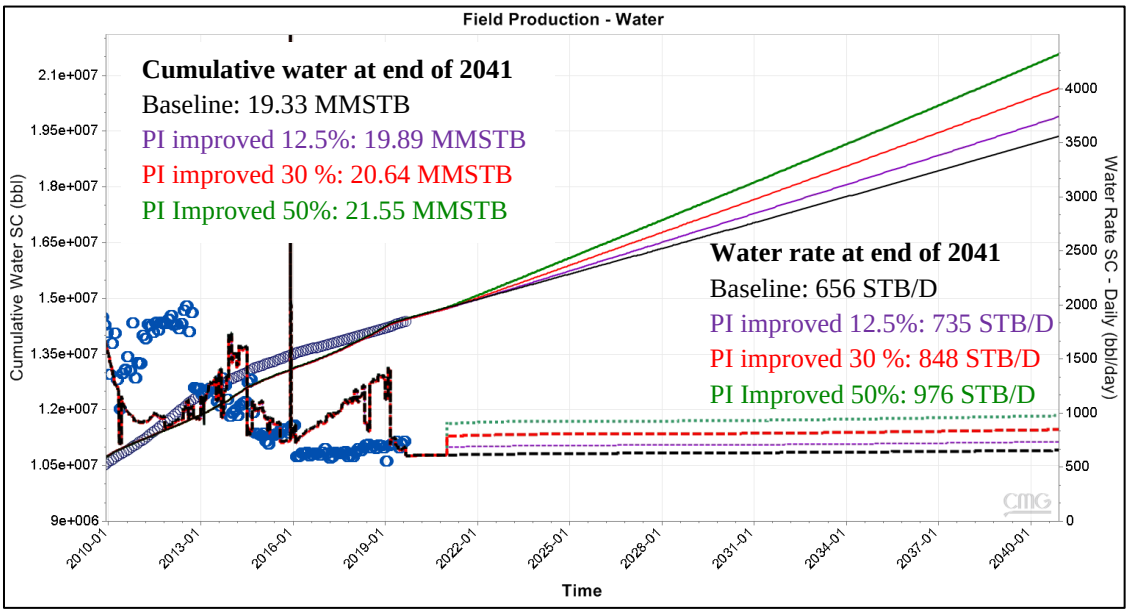

Figure IV-86. Predicted water production for three different PI scenarios

Figure IV-86 shows variations of predicted water production profile for the three different PI cases. Figure IV-87 shows variations in the predicted gas production profile for the three different PI cases. These values follow the profile trend observed for oil, where the highest rate case is ‘PI improved 50%’, and the lowest rate case is ‘PI improved 12.5%.

Solid and dashed black lines from the same figure indicates the baseline forecast that is provided as a comparison.

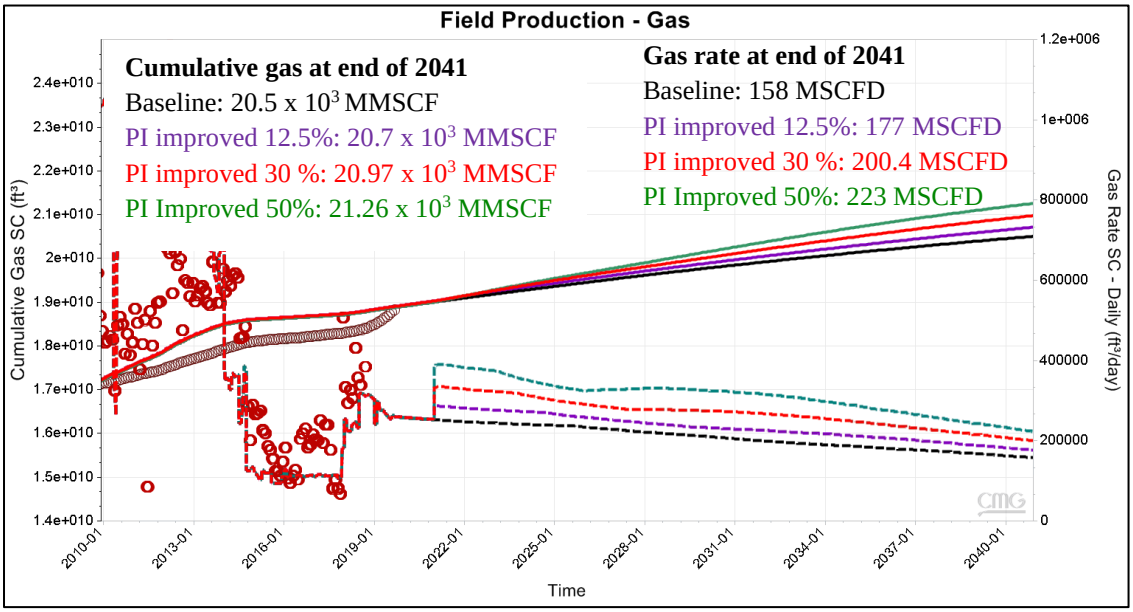

Figure IV-87. Variation of predicted gas production for three different PI scenarios

IV.5.3 Case 3. Baseline + Varying Injection Rate in NHK-487

Case 3 evaluates whether better production performance can be achieved by decreasing or increasing the current injection rate at NHK-487. I evaluated four different scenarios-no injection, and increased injection rates of 156 STB/D, 312 STB/D, and 1250 STB/D, respectively.

In the model, this condition was implemented in January 2021. This setting was kept until the end of prediction, as shown in Figure IV-88. In the increased injection rate scenarios, it is essential to set the injection pressure to values lower than formation fracturing pressure; this was achieved by setting a maximum pressure limit in the injection well.

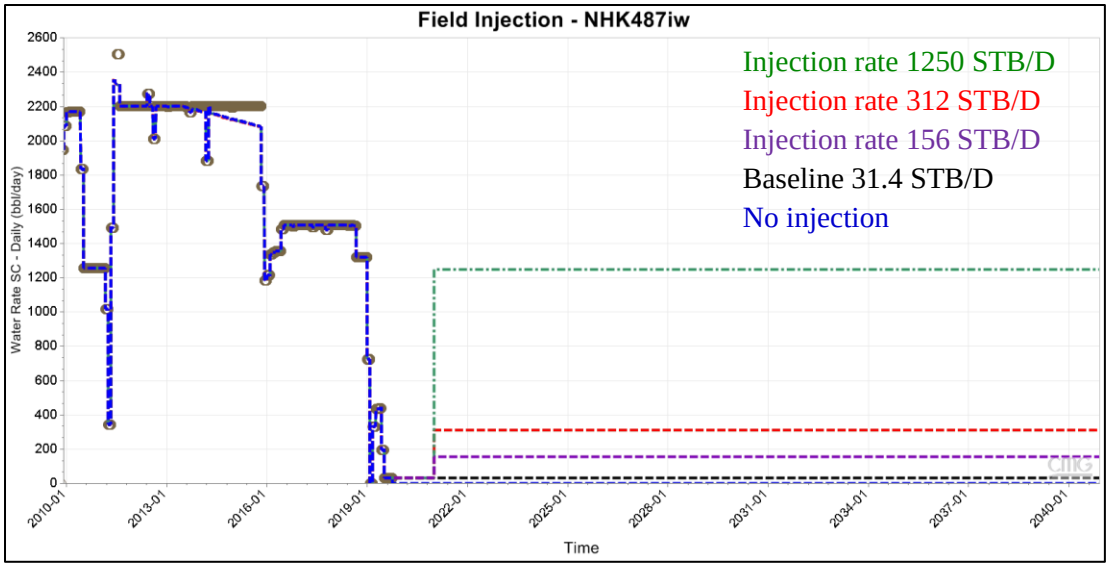

Figure IV-88. Different injection rate scenario

Figure IV-89 presents the pressure profiles to each scenario, and Table IV-8 shows the pressure at the end of 2040. The highest-pressure profile was observed in the highest injection rate scenario, and the lowest pressure was observed in the no injection scenario (0 STB/D). Figure IV-90 and Table IV-9 show oil production variations. Increasing the injection rate did not yield higher oil production as compared to the baseline case.

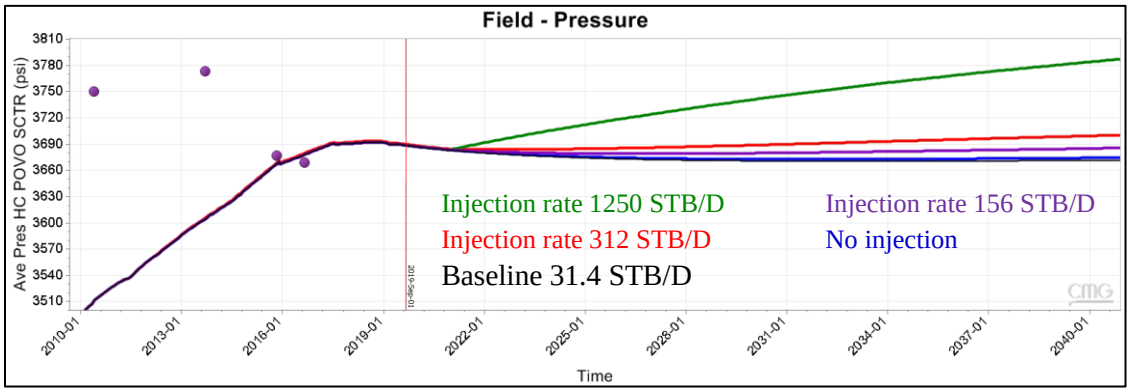

Figure IV-89. Predicted pressure profiles for different injection scenarios

Table IV-8. Pressure for different injection scenarios (end of 2040)

Case	Pressure (psi)
No Injection	3671
Baseline (31.4 STB/D)	3674
Injection 156 STB/D	3685
Injection 312 STB/D	3700
Injection 1250 STB/D	3787

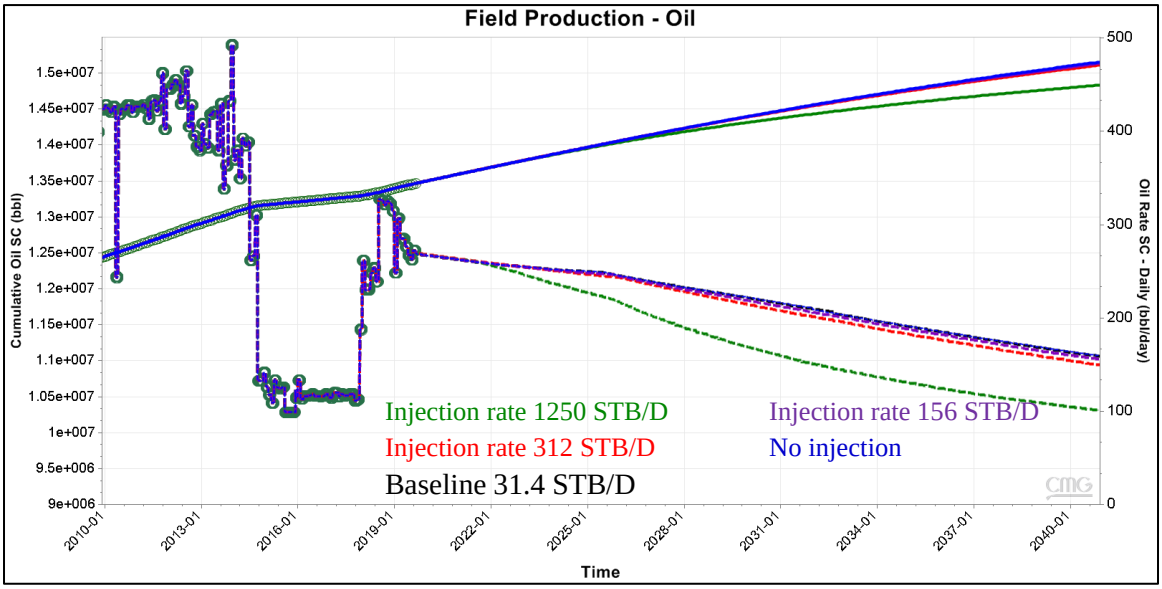

Figure IV-90. Predicted oil production for different injection scenarios

Figures IV-91 and IV-92 show water and gas production profiles for these different injection scenarios. Tables IV-9 and IV-10 summarize the result. Increasing the water injection rate did not benefit oil production. Less oil and more water are produced as the injection rate increased.

Table IV-9. Oil profiles with different injection rates (at the end of 2040)

Case	Oil rate (STB/D)	Oil cumulative (MMSTB)
No Injection	158	15.15
Baseline (31.4 STB/D)	158	15.15
Injection 156 STB/D	155	15.14
Injection 312 STB/D	149	15.1
Injection 1250 STB/D	101	14.83

Table IV-10. Water profile with different injection rates (at the end of 2040)

Case	Water rate (STB/D)	Water cumulative (MMSTB)
No Injection	654	19.36
Baseline (31.4 STB/D)	656	19.35
Injection 156 STB/D	665	19.4
Injection 312 STB/D	675	19.41
Injection 1250 STB/D	743	19.7

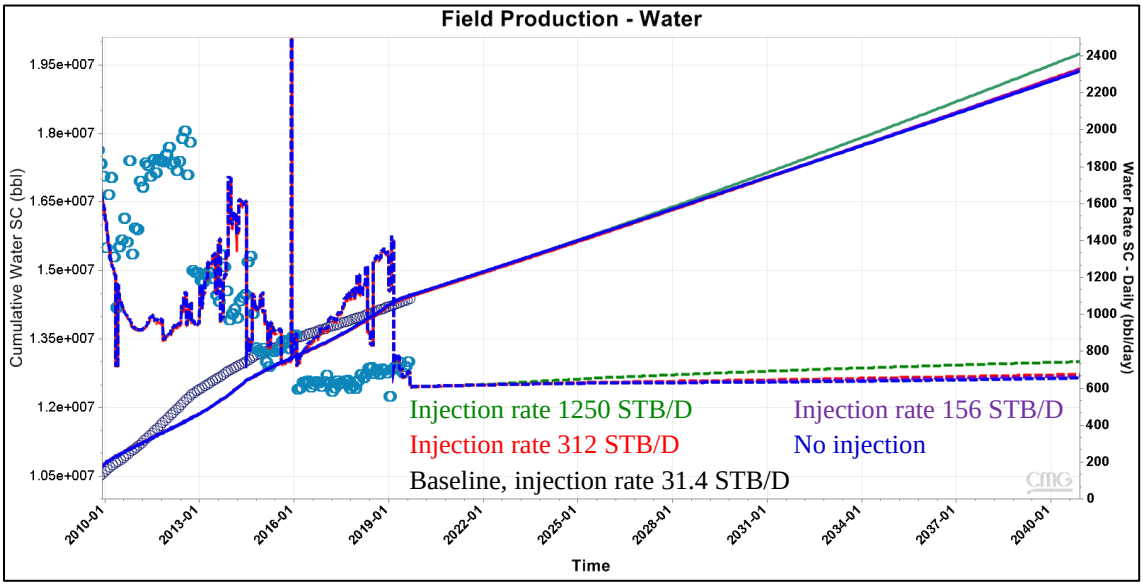

Figure IV-91. Predicted water production for the different injection scenarios

Table IV-11. Gas profile with different injection rates (at the end of 2040)

Case	Gas rate (MSCF/D)	Gas cumulative (MMSCF)
No Injection	161	20.51×10^3
Baseline (31.4 STB/D)	158	20.5×10^3
Injection 156 STB/D	149	20.48×10^3
Injection 312 STB/D	143.9	20.47×10^3
Injection 1250 STB/D	100.4	20.2×10^3

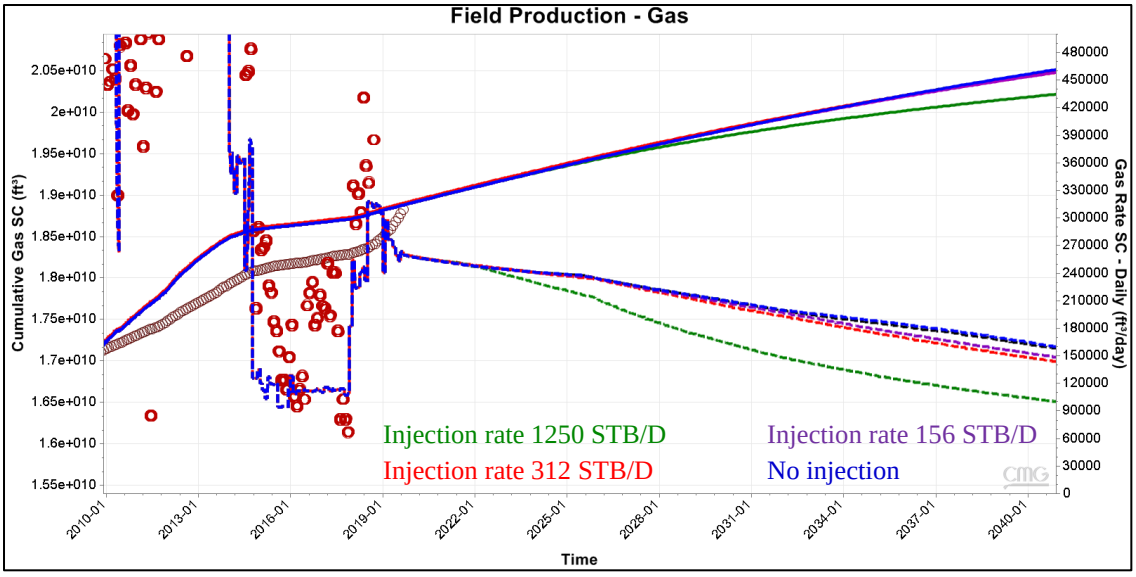

Figure IV-92. Predicted gas production for the different injection scenarios

IV.5.4 Case 4. Baseline + Decreasing FBHP

In this case, 37 psi is the highest possible decrease in FBHP, which is based on a 1% value of the last history match pressure point (3670 psi).

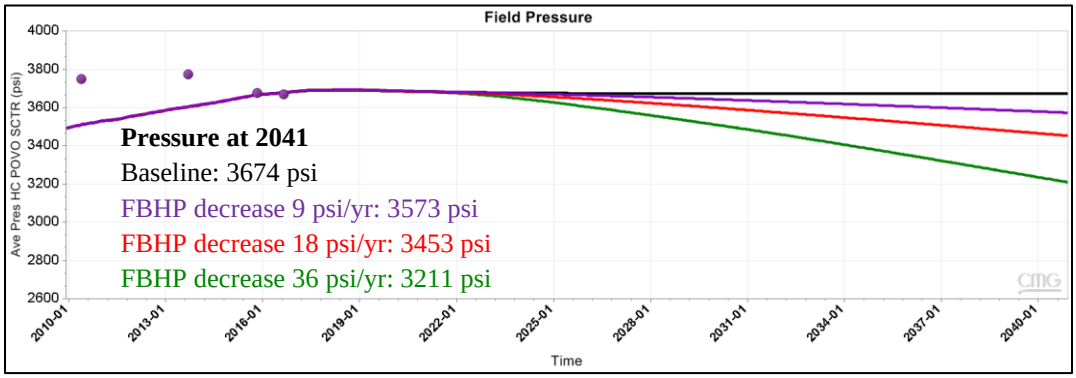

Figure IV-93. Predicted pressure profiles for the different FBHP scenarios

Table IV-12. Oil rate and cumulative production comparisons for varying FBHP (end of 2040)

Case	Oil rate (STB/D)	Oil cumulative (MMSTB)
Baseline	158	15.15
FBHP decrease 9 psi/yr	313	15.8
FBHP decrease 18 psi/yr	372	16.34
FBHP decrease 36 psi/yr	926	17.71

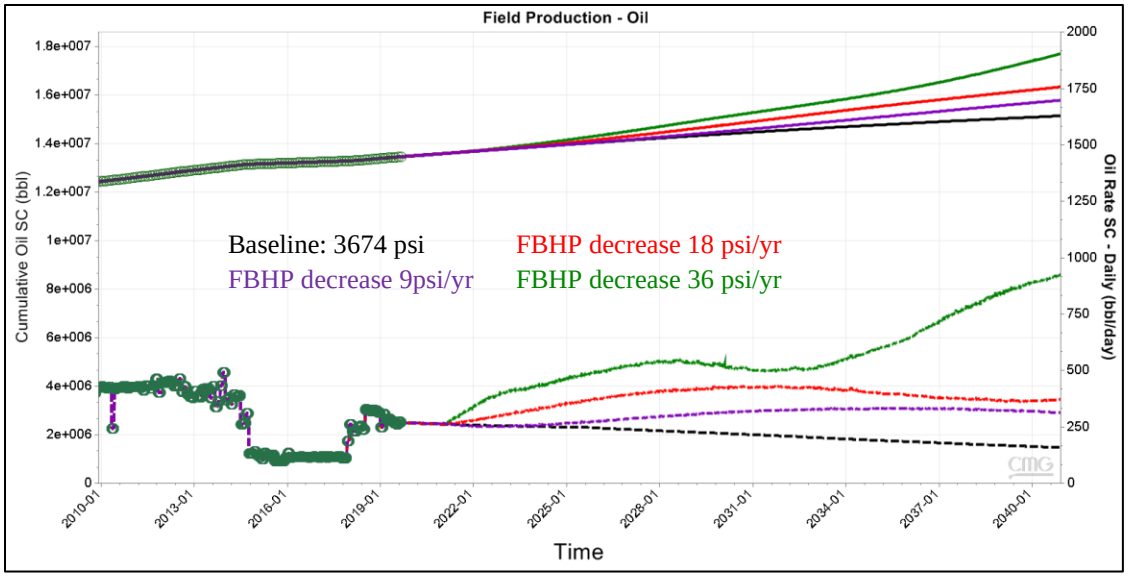

Figure IV-94. Predicted oil production for the different FBHP scenarios

Decreasing FBHP translates to modification of current operating conditions in the field. According to this model, even if the FBHP is lowered by only 9 psi per year, a substantial increase in oil production can be obtained. This approach is a promising way to boost oil production and should be proposed to the operator. Currently, only NHK-469 is using an artificial lift mechanism.

Table IV-13. Water rate cumulative production profile for different FBHP scenarios (end of 2040)

Case	Water rate (STB/D)	Water cumulative (MMSTB)
Baseline	656	19.36
FBHP decrease 9 psi/yr	2104	25.26
FBHP decrease 18 psi/yr	3728	32.29
FBHP decrease 36 psi/yr	6239	45.32

Figure IV-95 and Figure IV-96 show the water production profile for the different FBHP scenarios. The water and gas production rates follow the trend of the oil production rate, i.e., lowering FBHP could increase production for oil, water, and gas.

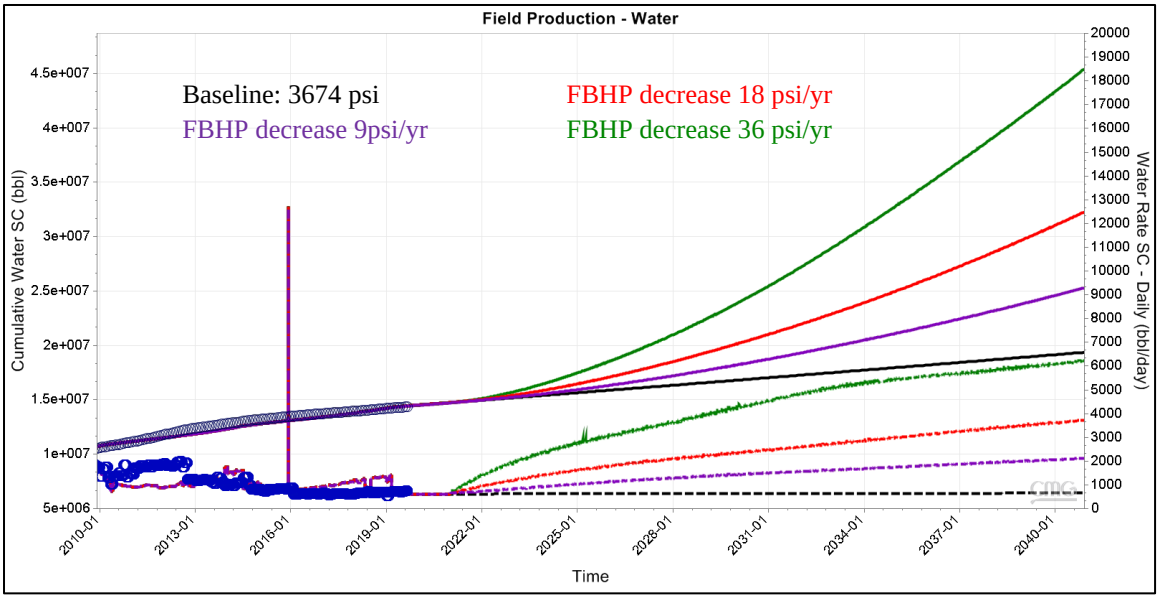

Figure IV-95. Predicted water production for the different FBHP scenarios

Table IV-14. Comparison of gas production for different FBHP scenario (end of 2040)

Case	Gas rate (MSCF/D)	Gas cumulative (MMSCF)
Baseline	158	20.5 x 10^3
FBHP decrease 9 psi/yr	318	21.1 x 10^3
FBHP decrease 18 psi/yr	647	22.5 x 10^3
FBHP decrease 36 psi/yr	1426	25.99 x 10^3

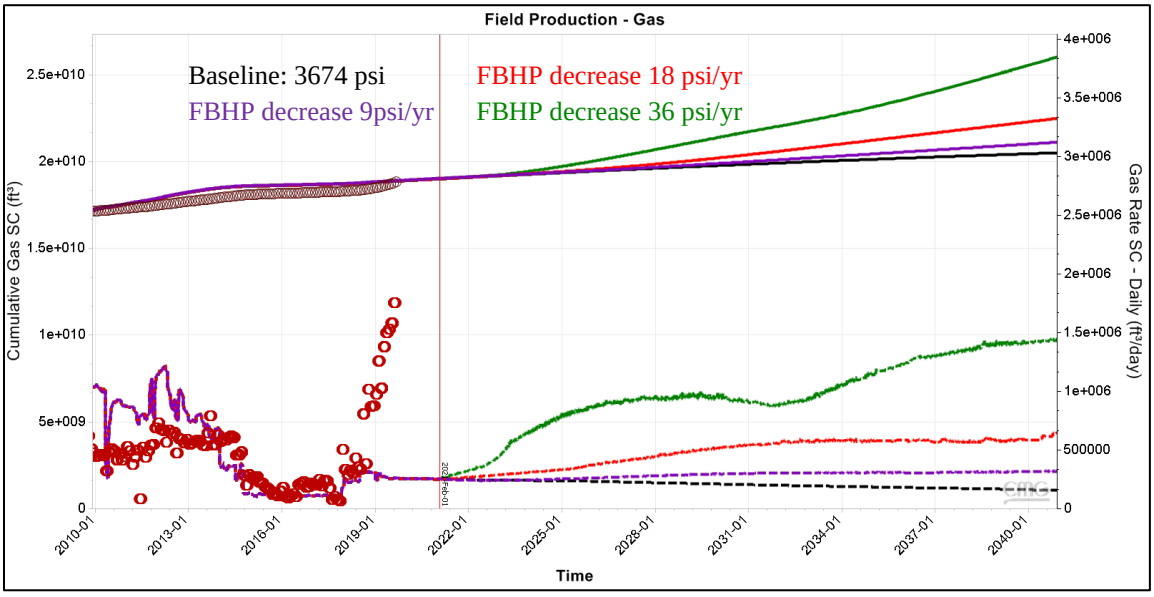

Figure IV-96. Predicted gas production for the different FBHP scenarios

IV.5.5 Baseline + Drilling New Wells (Case 5, Case 6, Case 7 and Case 8)

I identified the location of future new wells by using previously created remaining hydrocarbon pore volume map. The objective was to find the location with high oil potential. Four locations were identified and evaluated in these cases. Three wells (UH-1, UH-2, and UH-3 NE) were considered as infill wells due to their proximity with the current wells in LK-4, while one well (UH-3) was considered as a delineation well. The following sub-section will discuss the proposed well locations and their relative distance to the offset (neighboring) wells.

IV.5.5.1 Infill Well UH-1

The UH-1 is located in the northern part of the LK-4 field. It is surrounded by wells NHK-580, NHK-505, and NHK-499. Figure IV-97 illustrates the UH-1 position relative to NHK-505. It is located 18 blocks away (900 m or 2950 ft).

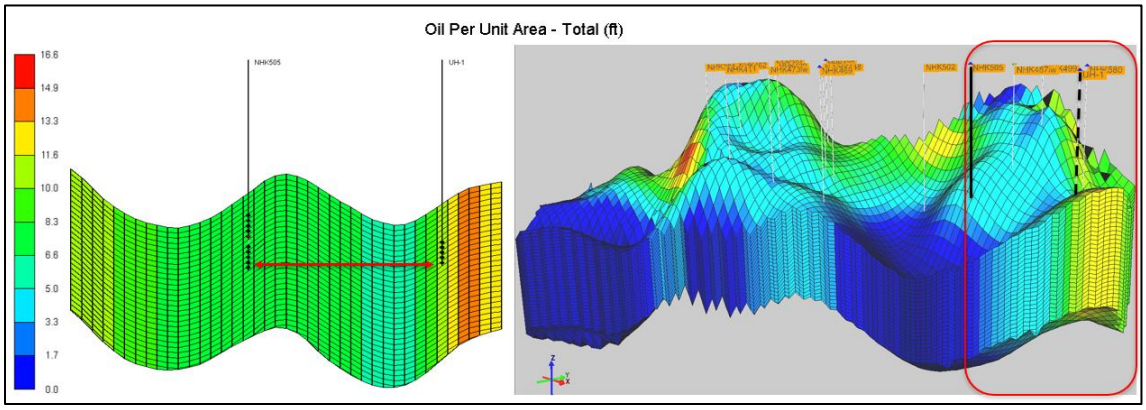

Figure IV-97. UH-1 and NHK-505 locations

Figure IV-98 shows the UH-1's relative position with respect to the other offset well NHK-580. UH-1 is located five blocks away from NHK-580 in the x-direction and seven blocks away from the same in the y-direction. This distance is equivalent to 250 m (820 ft) in the X-direction and 350 m (1148 ft) in the Y-direction. The length of the hypotenuse between UH-1 to NHK-580 is 430 m (1400 ft).

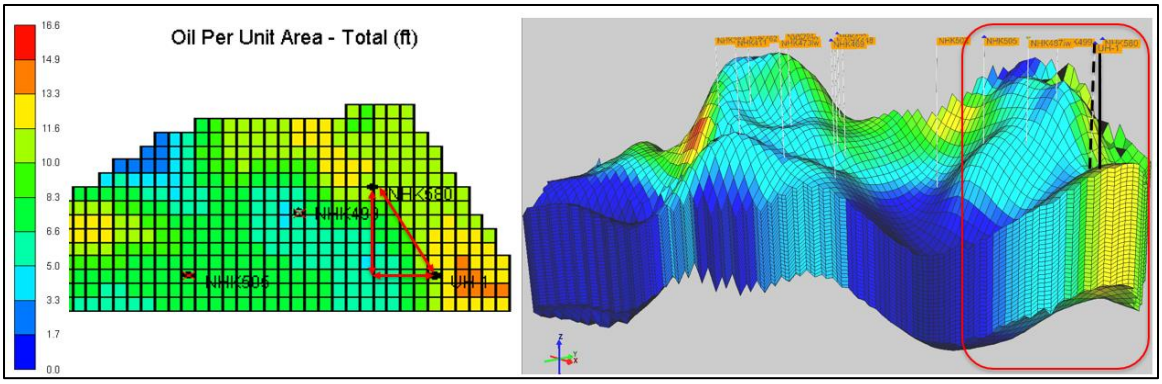

Figure IV-98. UH-1 and NHK-580 locations

Figure IV-99 shows the UH-1's relative position with respect to the other offset well NHK-499. UH-1 is located ten blocks away from NHK-580 in the X-direction and five blocks away from the same in the Y-direction. This distance is equivalent to 500 m (1640 ft) in the x-direction and 250 m (820 ft) in the y-direction. The length of the hypotenuse between UH-1 to NHK-499 is 560 m (1830 ft).

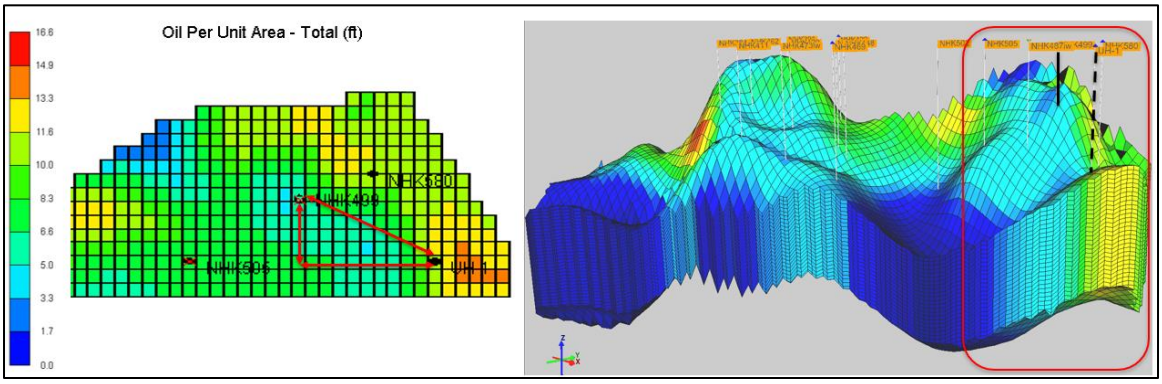

Figure IV-99. UH-1 and NHK-499 locations

IV.5.5.2 Infill Well UH-2

The UH-2 located in the central area of LK-4. It surrounded by wells NHK-505, NHK-502, NHK-448, NHK-422, NHK-419, and NHK-499. Figure IV-100 shows the UH-2's relative position with respect to the other offset NHK-505. UH-2 is located 11 blocks away from well NHK-505 in the X-direction and one block away from the same in the Y-direction. This distance is equivalent to 550 m (1804 ft) in the X-direction and 50 m

(164 ft) in the Y-direction. The length of the hypotenuse between UH-2 to NHK-505 is 552 m (1810 ft).

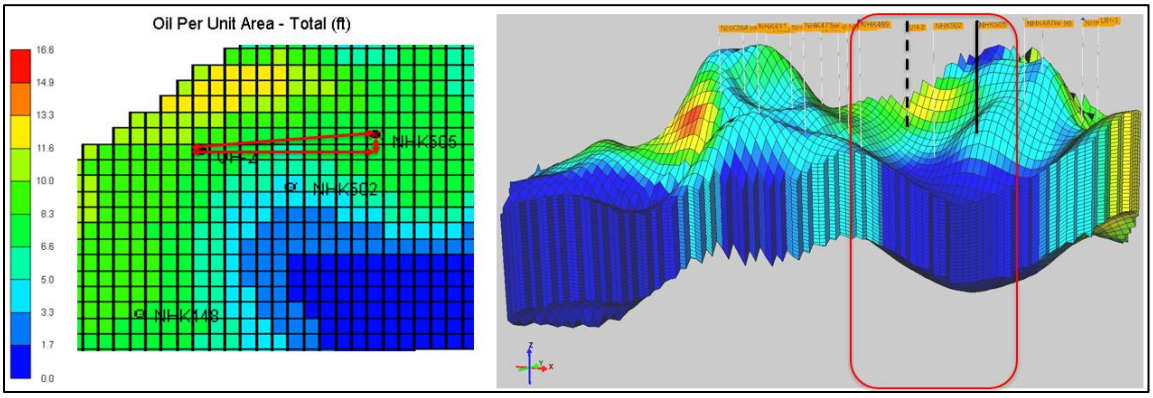

Figure IV-100. UH-2 and NHK-505 locations

Figure IV-101 shows the UH-2's relative position with respect to the other offset well NHK-502. UH-2 is located six blocks away from NHK-502 in the X-direction and two blocks away from the same in the Y-direction. This distance is equivalent to 300 m (984 ft) in the x-direction and 100 m (328 ft) in the y-direction. The length of the hypotenuse between UH-2 to NHK-502 is 316 m (1037 ft).

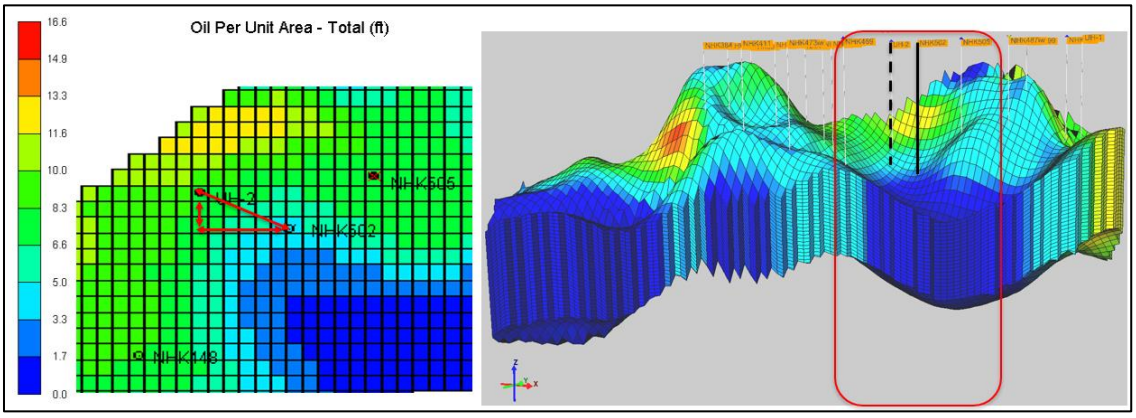

Figure IV-101. UH-2 and NHK-502 locations

Figure IV-102 shows the UH-2's relative position with respect to the other offset well NHK-448. UH-2 is located four blocks away from NHK-448 in the X-direction and ten blocks away from the same in the Y-direction. This distance is equivalent to 200 m

(654 ft) in the X-direction and 500 m (1640 ft) in the Y-direction. The length of the hypotenuse between UH-2 to NHK-448 is 538 m (1766 ft).

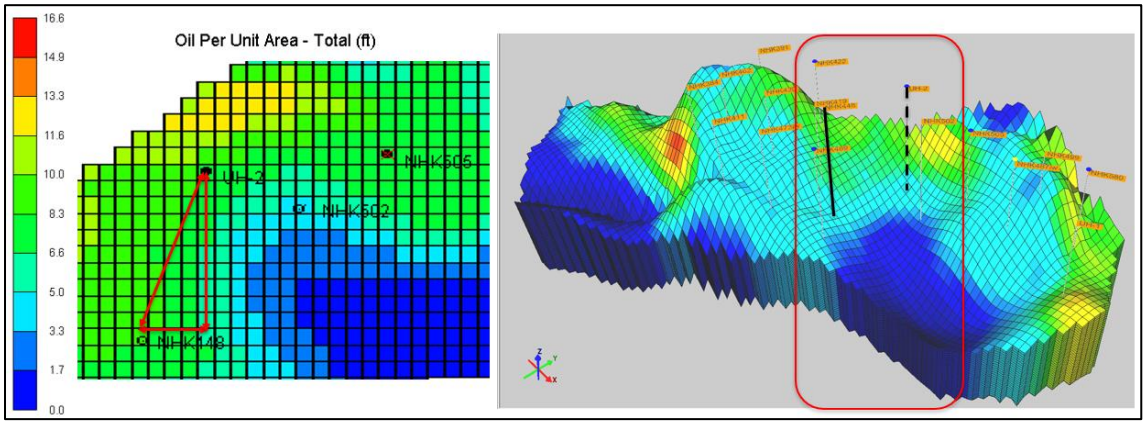

Figure IV-102. UH-2 and NHK-448 locations

Figure IV-103 shows the UH-2's relative position with respect to the other offset well NHK-422. UH-2 is located six blocks away from NHK-422 in the X-direction and 11 blocks away from the same in the Y-direction. This distance is equivalent to 300 m (984 ft) in the x-direction and 550 m (1804 ft) in the y-direction. The length of the hypotenuse between UH-2 to NHK-422 is 626 m (2053 ft).

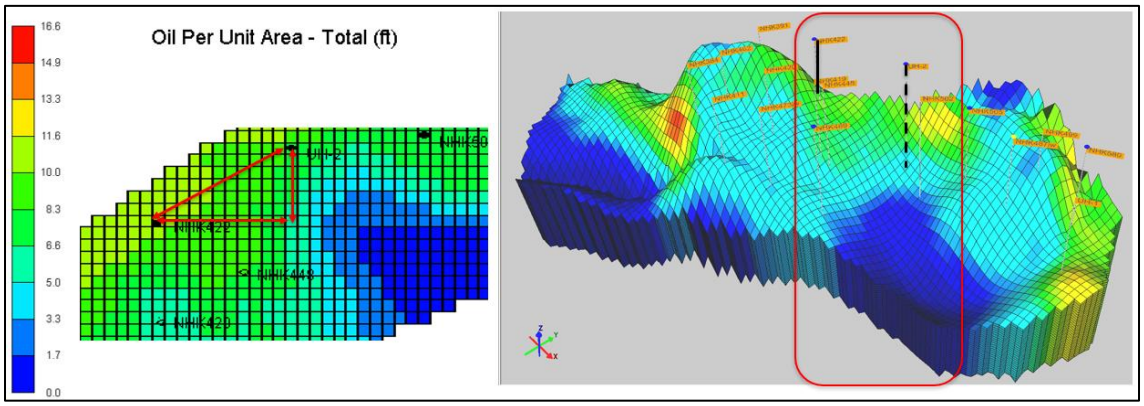

Figure IV-103. UH-2 and NHK-422 locations

Figure IV-104 shows the UH-2's relative position with respect to the other offset well NHK-419. UH-2 is located three blocks away from NHK-419 in the X-direction and nine blocks away from the same in the Y-direction. This distance is equivalent to 150 m

(492 ft) in the X-direction and 450 m (1476 ft) in the Y-direction. The length of the hypotenuse between UH-2 to NHK-419 is 474 m (1556 ft).

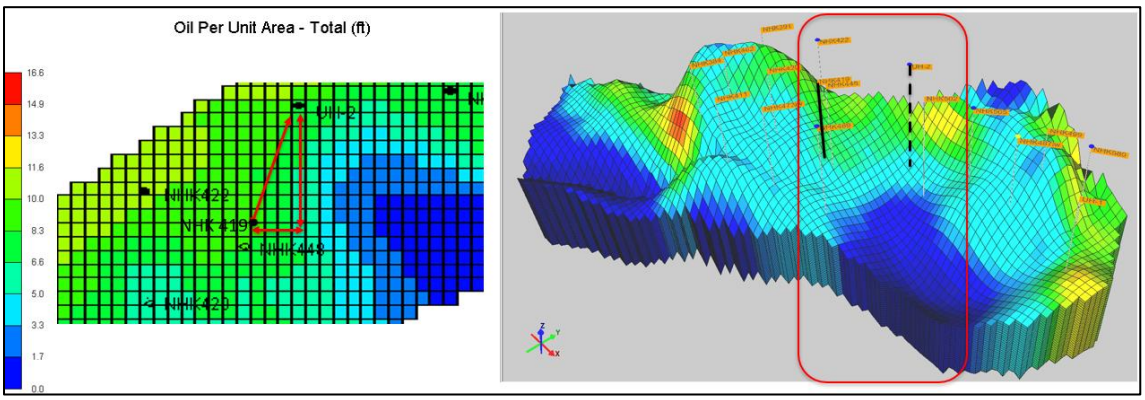

Figure IV-104. UH-2 and NHK-419 locations

IV.5.5.3 Delineation Well UH-3

UH-3 is a delineation well located in the southern sector of the LK-4 field. It is considered a delineation well because it penetrated an area that is far away from existing producers. UH-3 is surrounded by wells NHK-384, NHK-462, and NHK-391.

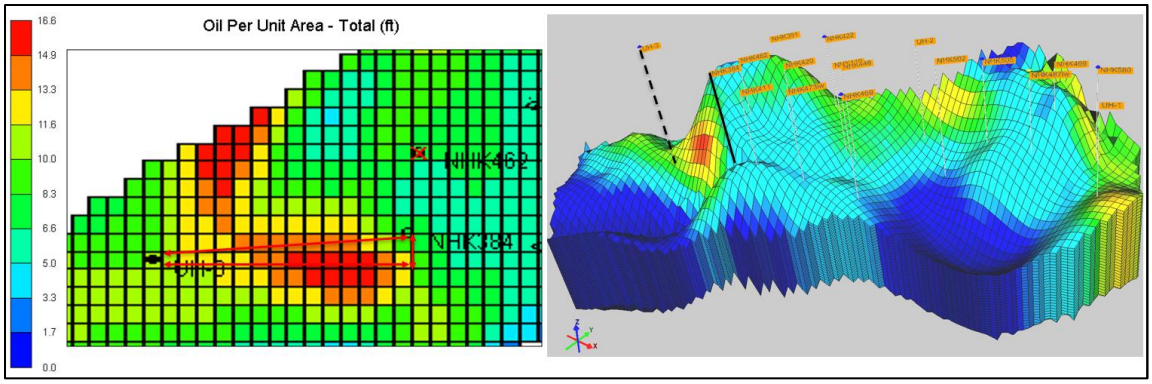

Figure IV-105. UH-3 and NHK-384 locations

Figure IV-105 shows the UH-3's relative position with respect to the other offset well NHK-384. UH-3 is located 14 blocks away from NHK-384 in the X-direction and two blocks away from the same in the Y-direction. This distance is equivalent to 700 m (2296

ft) in the X-direction and 100 m (368 ft) in the Y-direction. The length of the hypotenuse between UH-3 to NHK-384 is 707 m (2319 ft).

Figure IV-106 shows the UH-3's relative position with respect to the other offset well NHK-462. UH-3 is located 15 blocks away from NHK-462 in the X-direction and six blocks away from the same in the Y-direction. This distance is equivalent to 750 m (2460 ft) in the X-direction and 300 m (984 ft) in the Y-direction. The length of the hypotenuse between UH-3 to NHK-462 is 808 m (2650 ft).

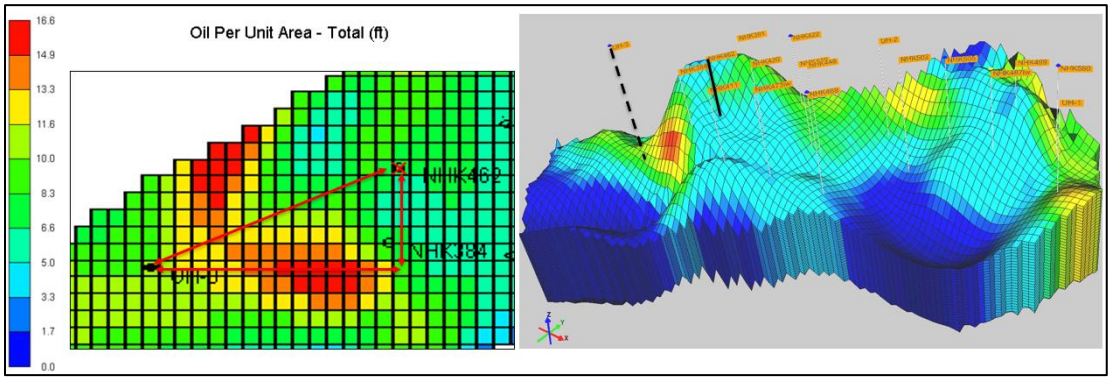

Figure IV-106. UH-3 and NHK-462 locations

Figure IV-107 shows the UH-3's relative position with respect to the other offset well NHK-391. UH-3 is located 13 blocks away from NHK-391 in the X-direction and 11 blocks away from the same in the Y-direction. This distance is equivalent to 650 m (2132 ft) in the X-direction and 550 m (1804 ft) in the Y-direction. The length of the hypotenuse between UH-3 to NHK-391 is 851 m (2793 ft).

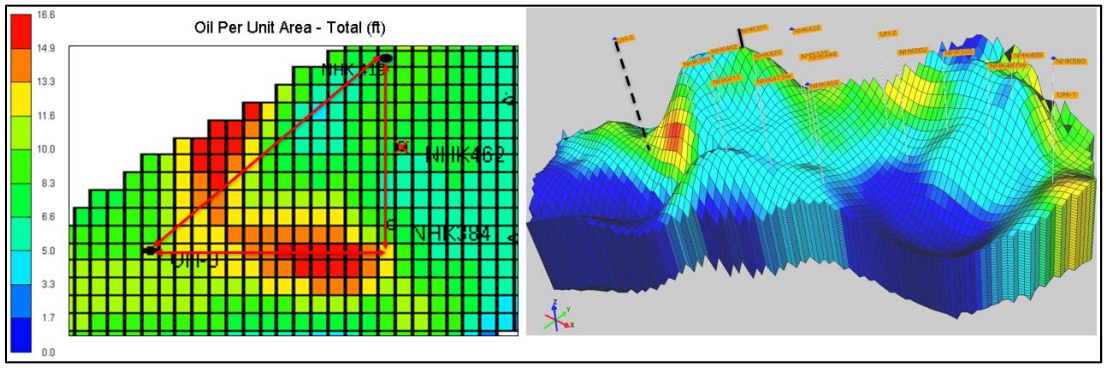

Figure IV-107. UH-3 and NHK-391 locations

IV.5.5.4 Infill Well UH-3NE

Well UH-3NE is also located in the southern part of the LK-4 field. This well is closer to the existing producer compared to UH-3. Therefore, it is considered as an infill well. This well is in the north-east direction of UH-3 well.

Figure IV-108 shows the UH-3NE's relative position with respect to the other offset well NHK-384. UH-3NE is located eight blocks away from NHK-384 in the X-direction and one block away from the same in the Y-direction. This distance is equivalent to 400 m (1312 ft) in the X-direction and 50 m (164 ft) in the Y-direction. The length of the hypotenuse between UH-3NE to NHK-384 is 403 m (1321 ft).

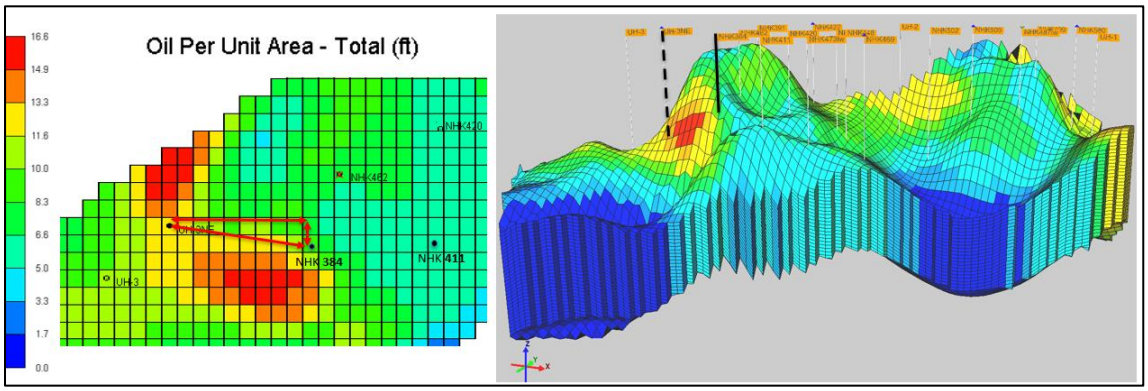

Figure IV-108. UH-3NE and NHK-384 locations

Figure IV-109 shows UH-3NE's relative position with respect to the other offset well NHK-462. UH-3NE is located ten blocks away from NHK-462 in the x-direction and three blocks away from the same in the y-direction. This distance is equivalent to 500 m (1640 ft) in the x-direction and 150 m (492 ft) in the y-direction. The length of the hypotenuse between UH-3NE to NHK-462 is 522 m (1712 ft).

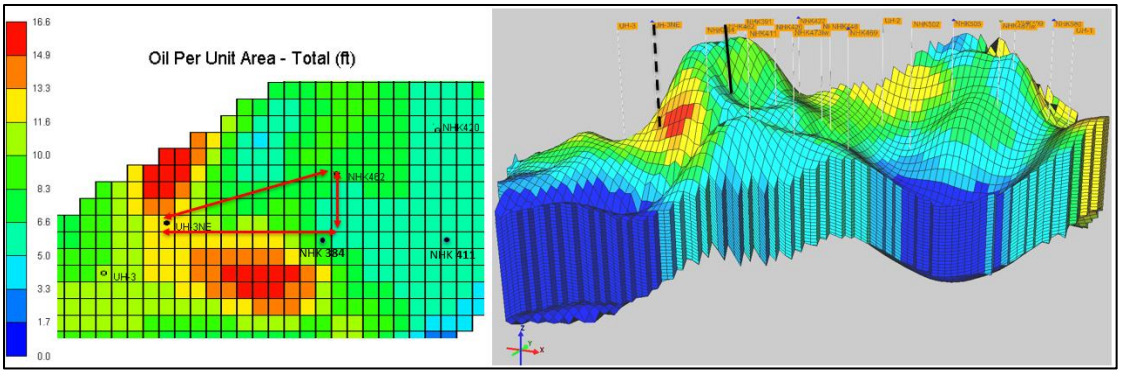

Figure IV-109. UH-3NE and NHK-462 locations

Figure IV-110 shows the UH-3NE's relative position with respect to the other offset well NHK-391. UH-3NE is located ten blocks away from NHK-391 in the X-direction and ten blocks away from the same in the Y-direction. This distance is equivalent to 500 m (1640 ft) in the X-direction and 500 m (1640 ft) in the Y-direction. The length of the hypotenuse between UH-3NE to NHK-391 is 707 m (2319 ft).

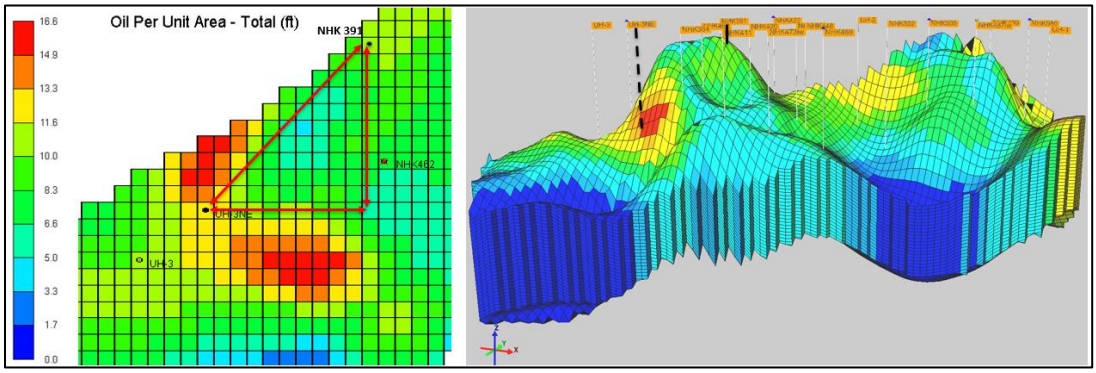

Figure IV-110. UH-3NE and NHK-391 locations

IV.5.6 Drilling New Wells: Constraints and Results

The previous processes were used to get an approximation of the distance of the new well relative to the existing wells. The processes described in that section qualitatively show how far the proposed wells are from the cluster of existing producers. These could also help to weigh the potential risks that may be associated with proposed targets. Figure IV-111 shows the locations of these four new wells in the model relative to the existing wells.

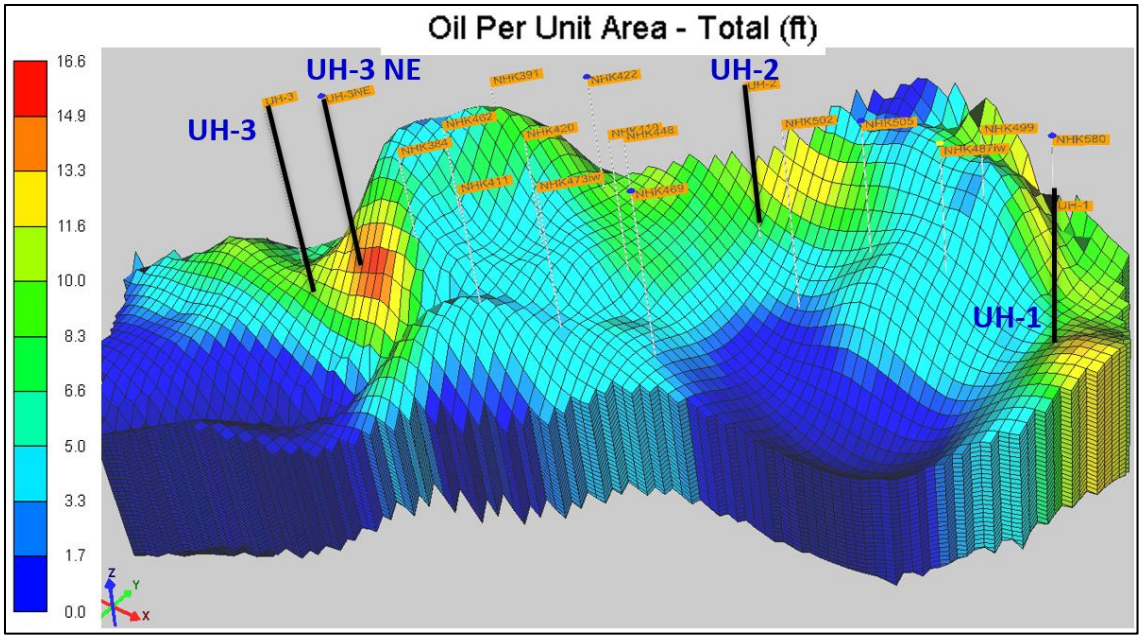

Figure IV-111. The locations of the four new wells in the model locations

These offset wells are used as information sources to set constraints for the future well predictions. This constraint is fundamental to ensure that the predicted flowrate from proposed wells is reasonable. Table IV-15 shows the approach to provide constraints for future wells. Offset well information such as FBHP, PI, and the total liquid were collected and grouped for the well candidates.

Table IV-15. Constraints for the newly drilled wells

Case	Well Name	FBHP (psi)	PI (STB/D/psi)	Average Total liquid, STB/D	Offset Wells
Case 5	UH-1 (north)	Minimum 3415	Average = 1.8	182.3	NHK-505, NHK-580 and NHK-499.
Case 6	UH-2 (central)	Minimum 3390	Average = 1.92	501.6	NHK-422, NHK-419, NHK-448, NHK-502, and NHK-505.
Case 7	UH-3 (south)	Minimum 3429	Average = 3.05	403	NHK 384, NHK-462, NHK-391.
Case 8	UH-3NE	Minimum 3429	Average = 3.05	403	NHK-384, NHK-462, NHK-391.

Figure IV-112 shows the variation of the pressure profile for each case with respect to the baseline. The lowest pressure profile was observed in Case 8 (drill UH-3NE). The primary reason for the rapid pressure declined in case 8 is the high fluid extraction rate.

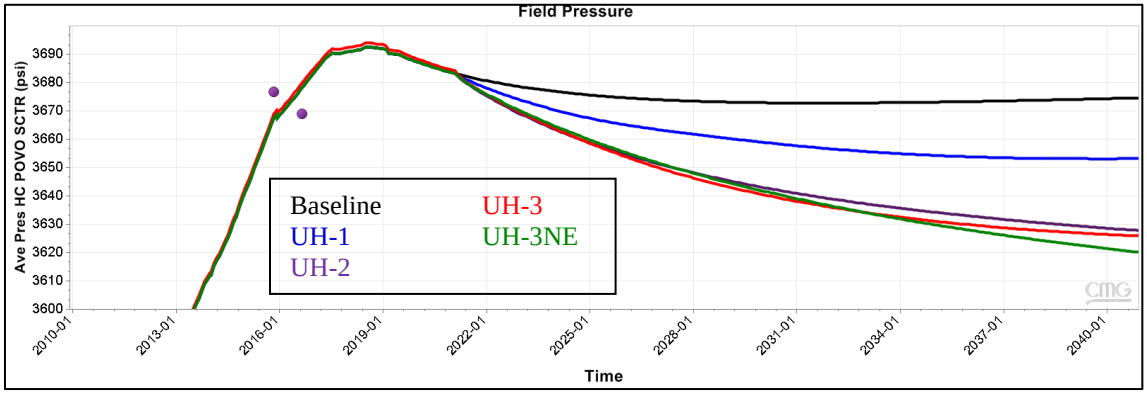

Figure IV-112. Predicted pressure profiles for the different well locations

Table IV-16. Pressure comparisons

Cases	Pressure at the end of 2040, psi
Baseline	3674
Infill well UH-1	3653
Infill well UH-2	3628
Delineation well UH-3	3626
Infill well UH-3NE	3620

Figure IV-113 shows the oil production profiles for the four new well cases and their comparison with the baseline case. UH-3NE yields the highest oil recovery, followed by UH-3, UH-2, and UH-1. Table IV-17 provides total production at the end of 2040.

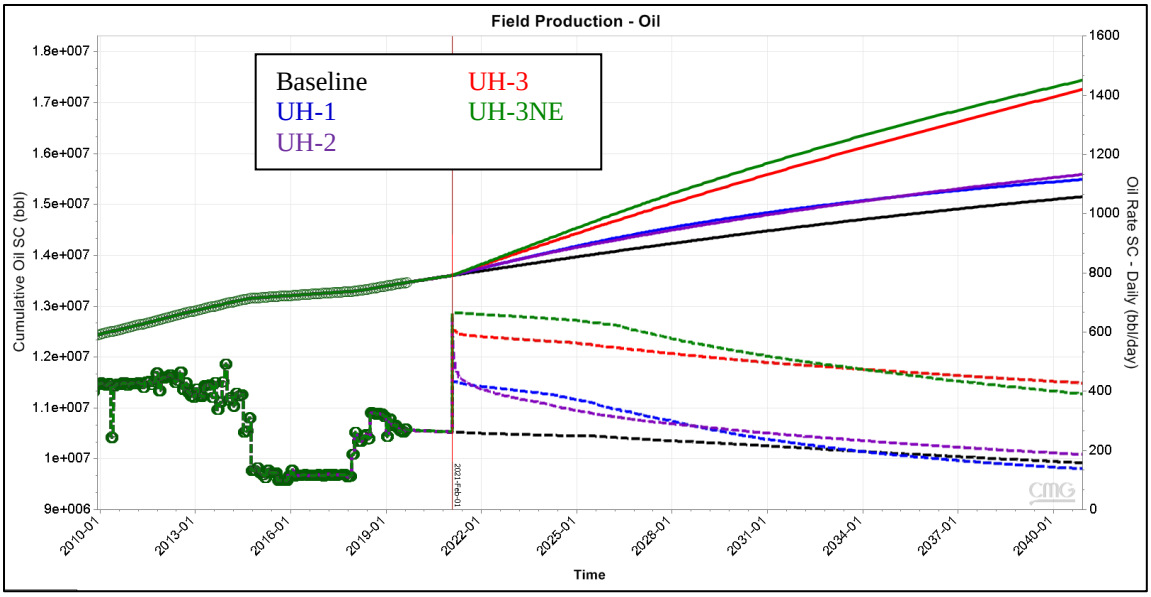

Figure IV-113. Predicted oil production profiles for the different well locations

Table IV-17. Comparison of oil production rate and cumulative production for different well locations (end of 2040)

Case	Oil rate (STB/D)	Oil cumulative (MMSTB)
Baseline	158	15.15
Infill well UH-1	139	15.49
Infill well UH-2	187	15.59
Delineation well UH-3	428	17.26
Infill well UH-3NE	391	17.44

Figure IV-114 and Figure IV-115 show water and gas production profiles for each case. Tables IV-18 to IV-19 show the respective value.

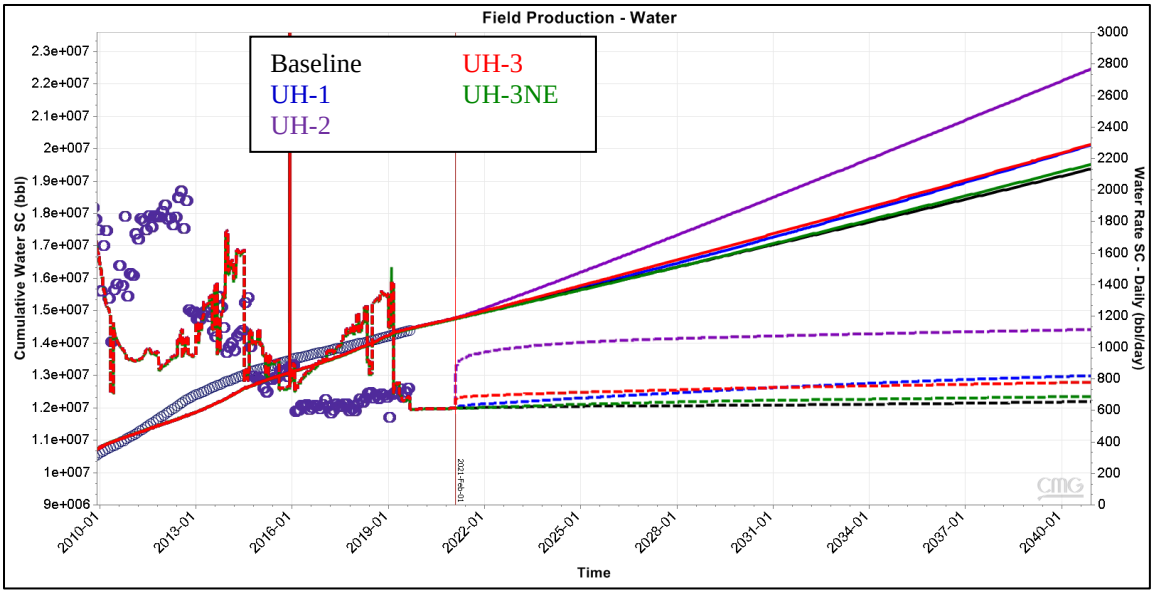

Figure IV-114. Predicted water production profiles for the different well locations

Table IV-18. Comparison of water production rate and cumulative production for different well locations (end of 2040)

Case	Water rate (STB/D)	Water cumulative (MMSTB)
Baseline	656	19.36
Infill well UH-1	820	20.09
Infill well UH-2	1113	22.45
Delineation well UH-3	780	20.12
Infill well UH-3NE	689	19.5

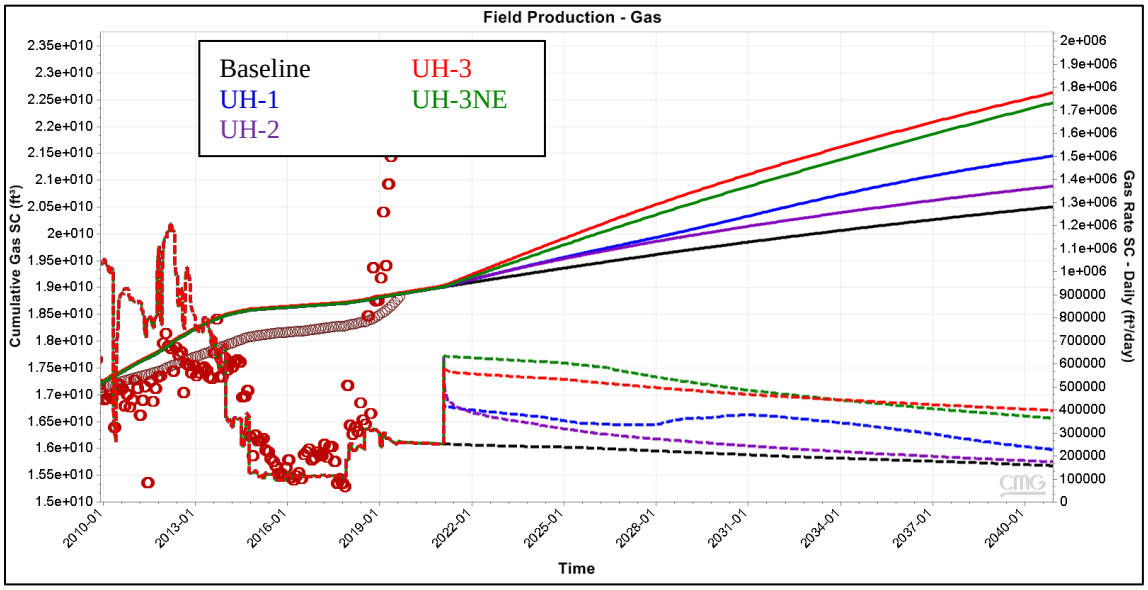

Figure IV-115. Predicted gas production profiles for the different well locations

Table IV-19. Comparison of gas production rate and cumulative production for different well locations (end of 2040)

Case	Gas rate (MSCF/D)	Gas cumulative (MMSCF)
Baseline	158	20.5×10^3
Infill well UH-1	228	21.5×10^3
Infill well UH-2	175	20.9×10^3
Delineation well UH-3	397	22.6×10^3
Infill well UH-3NE	364	22.4×10^4

IV.5.7 Combining/Multiple New Wells

These cases were run by combining several new wells. Three different combinations were made: drill UH-3NE and UH2, drill infill wells only, and drill top three highest wells. Table IV-20 and Figure IV-116 provide the pressure profiles and respective values.

Table IV-20. Pressure comparisons for multiple new wells (end of 2040)

Cases	Pressure, psi
Baseline	3674
Drill UH-3 NE and UH-2	3590
Drill infill wells (UH-1, UH-2, and UH-3)	3575
Drill three highest wells (UH-3NE, UH-3, and UH-2)	3566

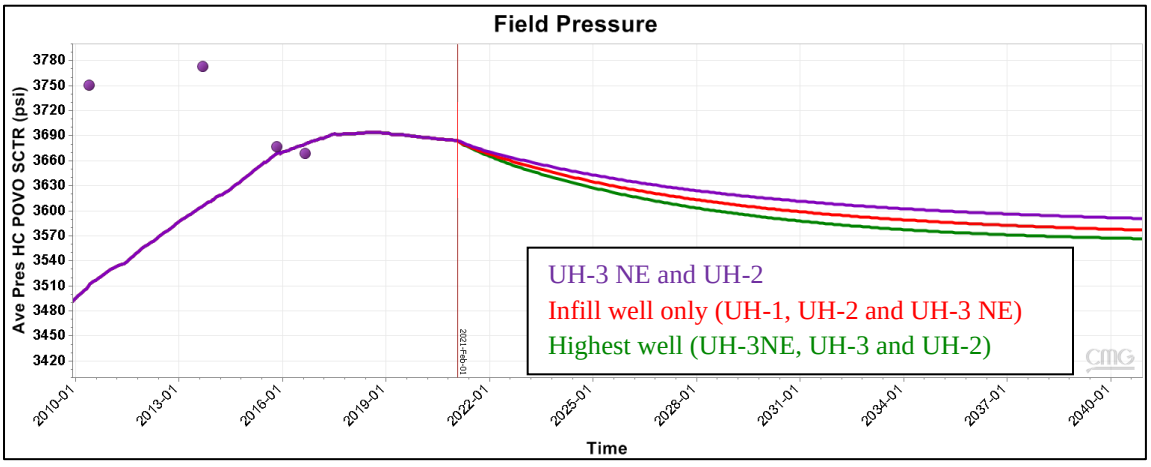

Figure IV-116. Predicted pressure profiles for the different well combinations

Figure IV-117 shows the oil production rates and oil production cumulative profiles. Table IV-21 summarizes the oil rate and the cumulative oil production at the end of 2040. As observed from Table IV-21, drilling the top three wells (UH-3NE, UH-3, and UH-2) yielded the highest oil recovery.

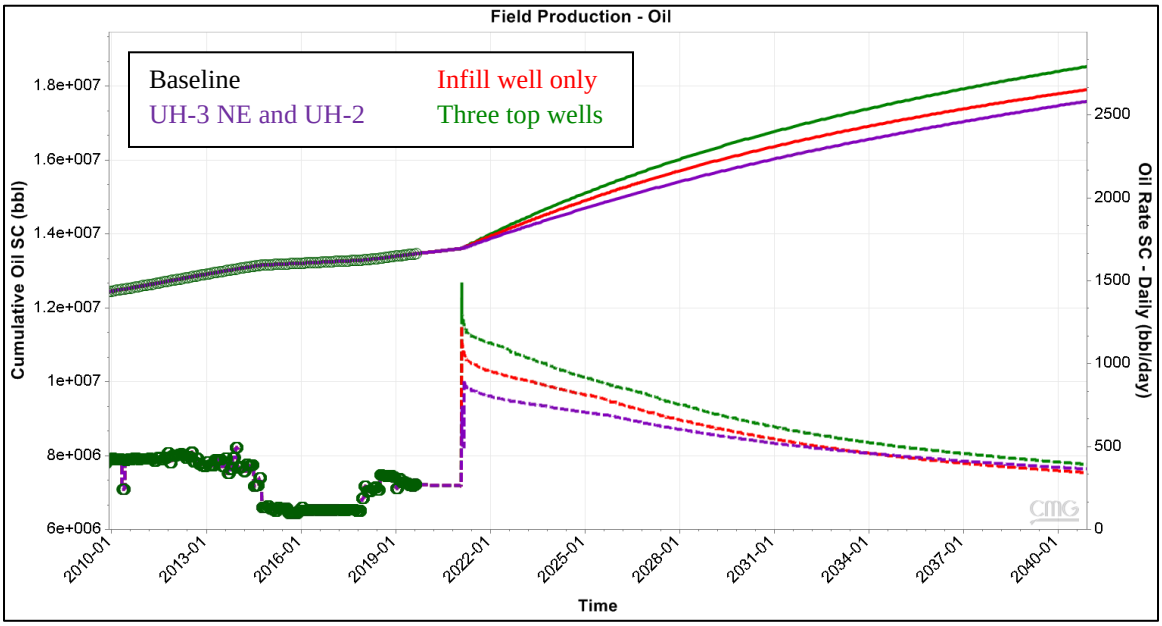

Figure IV-117. Predicted oil production profiles for the different well combinations

Table IV-21. Comparison of oil production for different well combinations (end of 2040)

Case	Oil rate (STB/D)	Oil cumulative (MMSTB)
Baseline	158	15.15
UH-3NE and UH-2	365	17.59
Infill wells only (UH-1, UH-2, and UH-3NE)	343	17.91
Three top wells (UH-3NE, UH-3 and UH-2)	393	18.53

Table IV-22. Comparison of water production for different well combinations (end of 2040)

Case	Water rate (STB/D)	Water cumulative (MMSTB)
Baseline	656	19.36
UH-3NE and UH-2	1062	22.2
Infill wells only (UH-1, UH-2, and UH-3NE)	1197	22.9
Three top wells (UH-3NE, UH-3 and UH-2)	1063	22.73

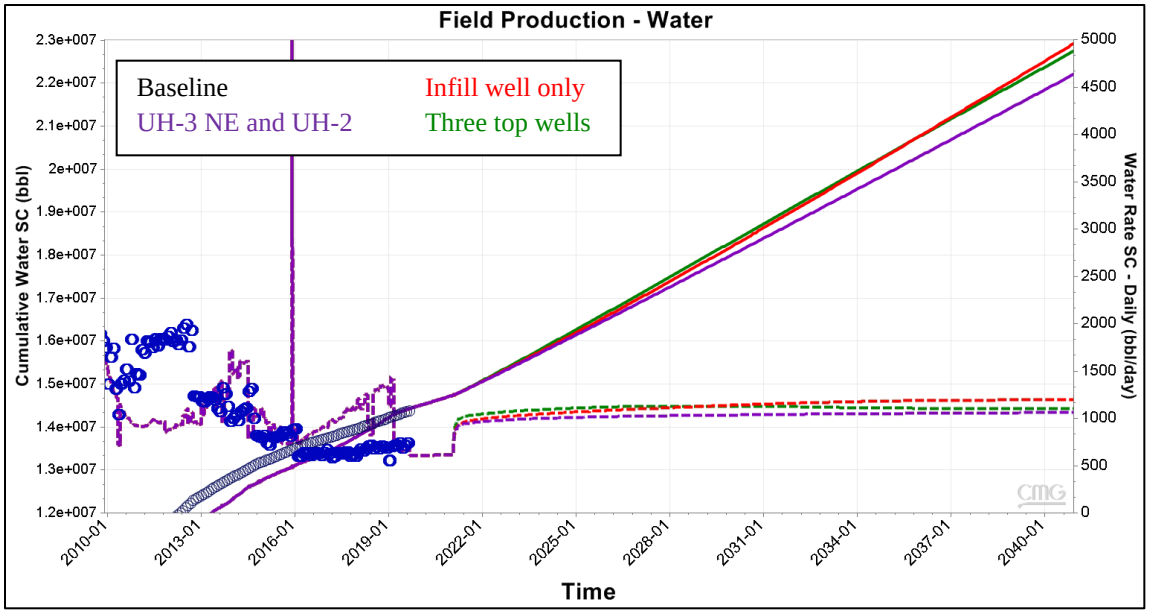

Figure IV-118. Predicted water production profiles for the different well combinations

Figures IV-118 and IV-119 show water and gas production profiles for the combined cases. Table IV-22 and Table IV-23 summarize the value of water and gas production for each case at the end of 2040. There is not much difference in terms of cumulative water production for all three cases. The gas production rate is similar to the oil production rate.

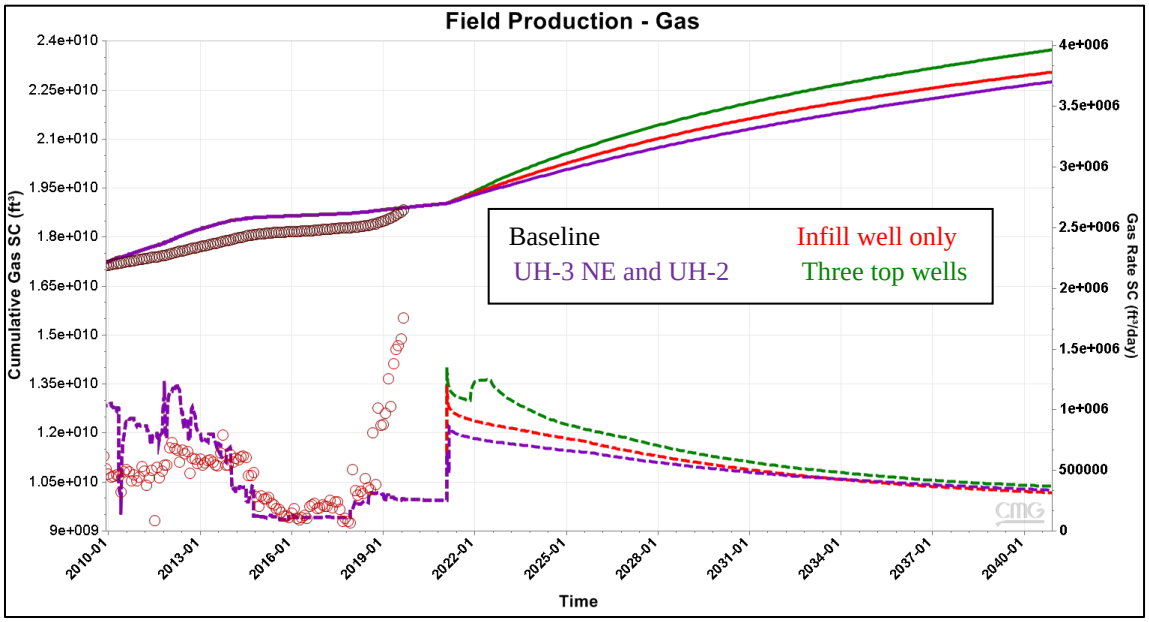

Figure IV-119. Predicted gas production profiles for the different well combinations

Table IV-23. Comparison of gas rate and cumulative production for different well combinations at the end of 2040

Case	Gas rate (MSCF/D)	Gas cumulative (MMSCF)
Baseline	158	20.5 x 10^3
UH-3NE and UH-2	337	22.8 x 10^3
Infill wells only (UH-1, UH-2, and UH-3NE)	316	23.1 x 10^3
Three top wells (UH-3NE, UH-3 and UH-2)	372	23.7x 10^3

IV.6 Production Forecast Comparison

This section provides the oil production comparison of all the eight cases that were discussed in the previous sub-section. The purpose is to get a comparable view of how much additional oil was produced in those cases. The comparison provided here does not include the three combined wells case as described in sub-section IV.5.6, because of the need for comparison of each case to the others. Figure IV-120 shows the variation in field pressures for all the cases mentioned.

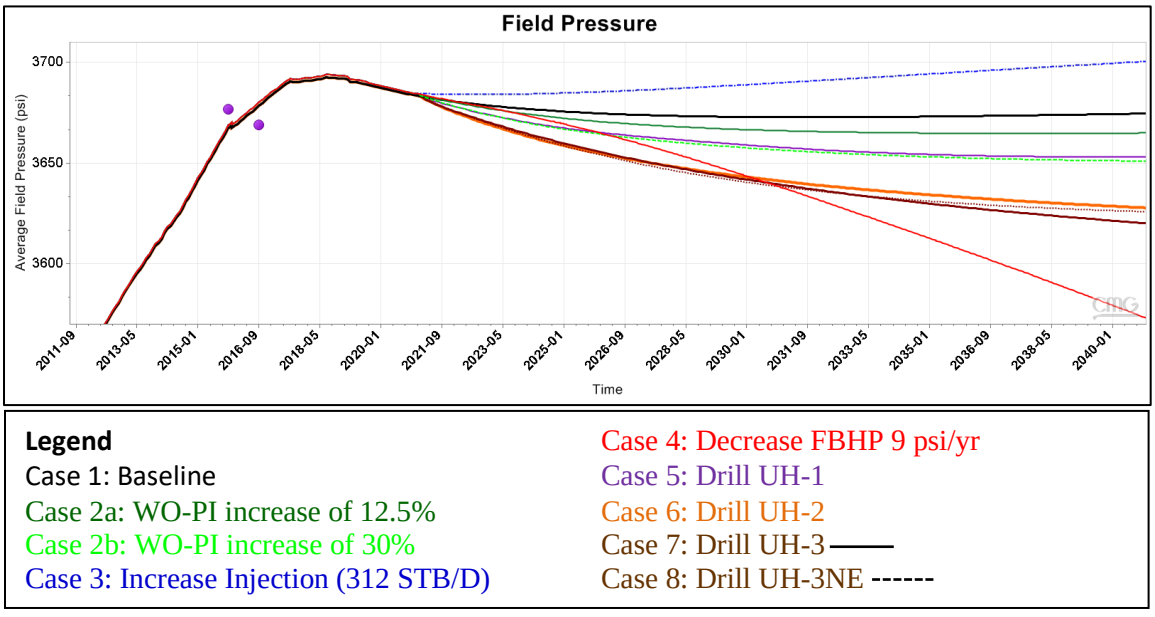

Figure IV-120. Predicted pressure profiles from each best scenario

Table IV-24. Pressure values for variety of cases (end of 2040)

Case	Pressure psi
Case 1. Baseline	3674
Case 2a. WO-PI increase 12.5%	3665
Case 2b. WO-PI increase 30%	3651
Case 3. Increase injection rate (312 STB/D)	3710
Case 4. Decrease FBHP 9 psi/yr	3573
Case 5. Drill UH-1	3653
Case 6. Drill UH-2	3628
Case 7. Drill UH-3	3626
Case 8. Drill UH-3NE	3620

Figure IV-121 and Figure IV-122 show variations in cumulative oil production and oil rate for each case. These comparison plots show that UH-3NE provides the highest oil recovery. The increasing injection rate yields the lower incremental oil recovery relative to other case forecasts. Among the future scenarios, the only ones that give a sizable increase are drilling new wells. If PI increases and FBHP reduction are not included, there is no change.

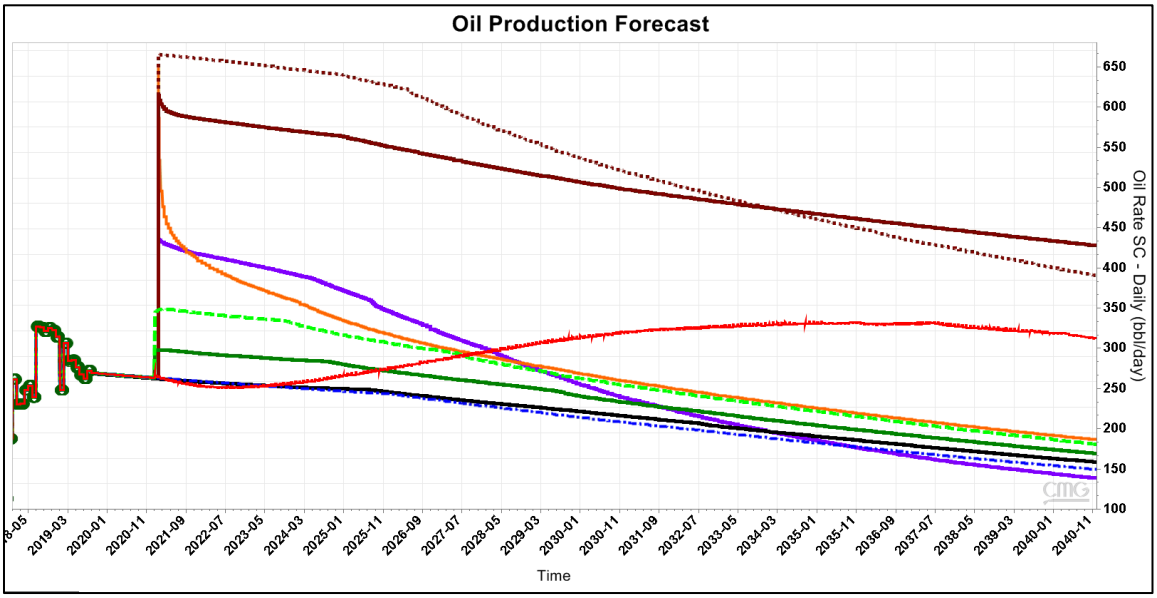

Figure IV-121.Predicted oil production rates from each best scenario

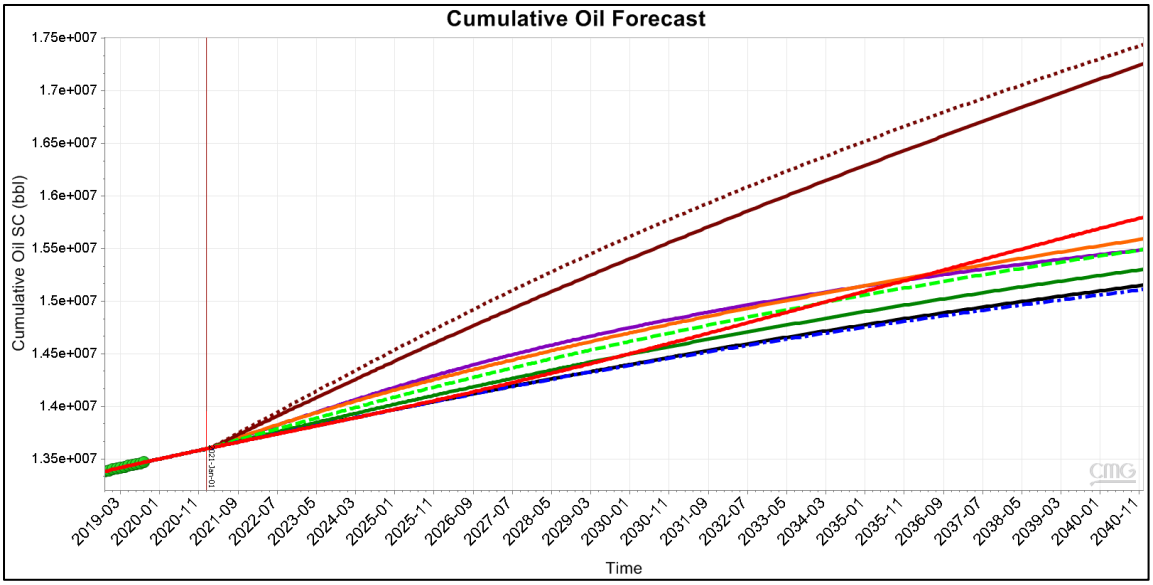

Figure IV-122. Predicted oil cumulative production profiles from each best scenario

Legend

Case 1: Baseline

Case 2a: WO-PI increase of 12.5%

Case 2b: WO-PI increase of 30%

Case 3: Increase Injection (312 STB/D)

Case 4: Decrease FBHP 9 psi/yr

Case 5: Drill UH-1

Case 6: Drill UH-2

Case 7: Drill UH-3 ——

Case 8: Drill UH-3NE ------

Figure IV-123. Legend for Figure IV-121 and IV-122

Table IV-25 shows a detailed comparison of oil production for the other eight cases. Drilling UH-3NE and UH-3 (higher risk) have the highest incremental oil potential. Increasing the injection rate did not give incremental oil cumulative production; it yielded lower cumulative oil compared to baseline. Evaluation of lowering FBHP is worth considering. Currently, only one (NHK-469) out of the four producers is operating with artificial lift mechanisms. Acid stimulation jobs will provide another means to increase oil production from the current active producer.

Table IV-25. Comparison of oil rate and cumulative production for the eight cases at the end of 2040

Case	Oil rate (STB/D)	Oil cumulative (MMSTB)
Baseline	158	15.15
Case 2a - Workover PI increase of 12.5%	169	15.3
Case 2b - Workover PI increase of 30%	181	15.49
Case 3 - Injection 312 STB/D	149	15.10
Case 4 - Decrease FBHP 9 psi/yr	313	15.8
Case 5 - Drill infill well (UH-1)	139	15.49
Case 6 - Drill infill well (UH-2)	187	15.59
Case 7 - Drill delineation well (UH-3)	428	17.26
Case 8 - Drill infill well (UH-3 NE)	391	17.44

Appendix 1 provide a comparison between the oil production forecast and the oil production rate until March 2020. Based on the new additional data (September 2019 to March 2020), this model can predict oil production with 98.2% accuracy.

CHAPTER V. CONTRIBUTION OF THIS STUDY

Original Oil In Place (OOIP) and Estimated Ultimate Recovery (EUR) are two of the multi-millions dollar questions that every operator is interested in answering at any stage of the field development. Thus, this research work revolves around these questions. For a given field, there is only one correct value of OOIP, which none of the operators will be able to quantify precisely. The uncertainty in OOIP is higher during the early stages of field development when less data is available. More accurate values of OOIP and EUR are usually obtained at the very end of the field life (abandonment time). At the current stage, the LK-4 reservoir's OOIP has a high uncertainty range. Therefore, two additional methods that were not used in the previous studies were utilized to minimize the estimated OOIP.

The first method is the Rate Transient Analysis (RTA). This method looks for empirical trends in the flowrate data. RTA is a methodology to analyze long term production data from individual well or group of wells. It allows for interpretation of a simple situation, where the production takes place at constant Bottom Hole Pressure (BHP) while the production rate keeps declining. It also allows for the interpretation of a more general situation, where production is declining, and BHP is adjusted by the operator. RTA is an analytical method that that has been used on many occasions in the industry.

RTA can be used to analyze and make a model based on rate only or based on rate and pressure if pressure data is available continuously. A history match is done with a simple homogenous model. In this study, well and reservoir parameters were quantified based on the RTA model. RTA provided an estimate of the reservoir properties such as permeability, skin factor, drainage radius, and in-place volume.

The second method is the Transient Productivity Index (*Medeiros, F., Kazemi, H., and Kurtoglu, B., 2010*). This method provides two types of equations that can be used for oil and gas reservoirs. This method was originally proposed for the tight oil and tight gas reservoir; however, the authors do not limit its usage to other types of reservoirs.

There are at least two publications that demonstrate the use of this method to estimate Original Gas In Place (OGIP) in a conventional gas reservoir. *Kabir, C. S., Ismadi, D., and Fountain, S., 2010*), and (*Ismadi, D., Kabir C. S., and Hasan, R., 2011*) had demonstrated successful application of the gas equation to be used in OGIP estimation for conventional gas reservoirs.

Kabir et al. (2010) mentioned that the application of the transient PI methods on a conventional gas reservoir was useful on two counts. First, the graph gives diagnostic clues about the nature of the porosity system (single or dual). Second, it yields a reasonable estimate of the connected pore volume by a trial and error solution. The transient PI method has attributes, such as diagnosis of reservoir heterogeneity, reservoir pore volume calculation, and pressure estimation. It also assists in the validation of RTA derived in-place volume.

Nevertheless, no publication demonstrates the use of the oil equation in this method to investigate OOIP in the conventional oil reservoirs. I propose that this method will work well for conventional oil reservoirs because, even though there are some differences in the reservoir properties, there are similarities as well. This method was developed to estimate the connected pore volume within the Stimulated Reservoir Volume (SRV). An analog to SRV in tight oil is the conventional reservoir itself, where the pore volumes are naturally connected through a higher permeability pathway. In addition, the equations themselves

suggest that this method will remain valid for conventional reservoirs. Therefore, this method was evaluated in this reservoir to test its capability in OOIP estimation.

V.1. Rate Transient Analysis

Houze, O., Viturat, D., and Fjaere, O., (2019) mentioned that RTA started purely empirically based on observations on the decline rate. In the beginning, attempts were made to establish a relation between the first-year production and the ultimate recovery. Later, evaluation of the production decline response was performed on a linear plot. In the 1940s, Arps published a formulation of constant pressure production, including exponential, hyperbolic and harmonic decline responses.

By the end of the 1970s, the methodology was equivalent to the standard procedure in Pressure Transient Analysis (PTA). During this time, the Arps plot was a counterpart of the Horner plot, and the constant pressure-type curves were the counterparts of the PTA constant rate type-curves. Unlike PTA, which is only for a short duration of time during a well test, RTA covers a much wider time range, considers a time-dependent skin, and also the well drainage area.

Kappa Topaze® software was used in the analysis. In Kappa Topaze, equations that are used for the oil case are as follows

$$q_d = \frac{141.2\ q\ B_o\ \mu}{k\ h\ (p_i - p_{wf})} \tag{5-1}$$

$$Q_{DA} = \frac{0.8936\ Q\ B_o}{\Phi\ h\ A\ c_t\ (p_i - p_{wf})}. \tag{5-2}$$

The dimensionless cumulative production (Q_{DA}) can be expressed in terms of the fluid in place

$$\mathrm{N} = \frac{\Phi\ \mathrm{h}\ \mathrm{A}}{5.615\ B}. \tag{5-3}$$

Therefore, dimensionless cumulative production (Q_{DA}) is expressed as

$$Q_{DA} = \frac{0.8936\ Q}{5.615\ \mathrm{N}\ c_t\left(p_i - p_{wf}\right)} = \frac{Q}{2\ \pi\ N\ c_t\left(p_i - p_{wf}\right)}. \quad (5\text{-}4)$$

The linear relationship between dimensionless rate (q_d) and cumulative then becomes

$$q_d = \frac{141.2\ q\ B\ \mu}{k\ h\left(p_i - p_{wf}\right)} = \frac{1}{2\ \pi} - \frac{0.8936\ Q}{5.615\ \mathrm{N}\ c_t\left(p_i - p_{wf}\right)} \quad (5\text{-}5)$$

From this equation, plot of $\frac{q}{(p_i - p_{wf})}$ vs. $\frac{Q}{c_t\left(p_i - p_{wf}\right)}$ at the boundary dominated flow will exhibit a straight line which interception will yield N (OOIP). Using these equations, the simplest analytical solution, homogeneous circular reservoir will be suitable to model the well drainage area and to estimate the OOIP.

Preliminary information obtained from the 3D seismic survey was utilized in this study. It was suggested that the LK-4 can be subdivided into two different regions/sectors, as illustrated by the blue and orange square boxes in Figure V-1.

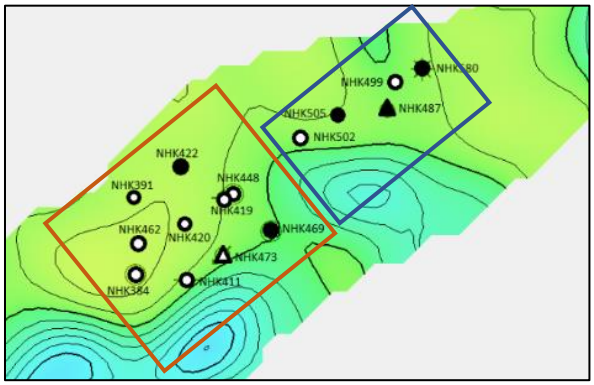

Figure V-1. The northern and southern wells in the LK-4 reservoir

V.1.1 The Northern Sector

The northern sector is comprised of five wells, as shown in Figure V-2. This sector consists of an active injector, i.e., NHK-487 (from November 2009 to present), and four producers, which are NHK-499, NHK-502, NHK-505, and NHK-580. Among these four

producers, two wells (NHK-505 and NHK-580) are currently active. Initially, NHK-487 was a production well that was converted to an injection well in November 2009.

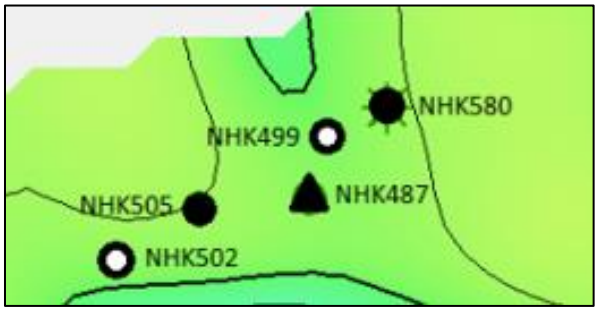

Figure V-2. The northern wells in the LK-4 reservoir

Figure V-3 below shows the results for this group of wells after a satisfactory production rate (q), and cumulative (Q) match was obtained. The OOIP for this group of wells is 17.1 MMSTB (2.72 MMSm^3), permeability is 90.2 mD, and the skin factor is 9.5.

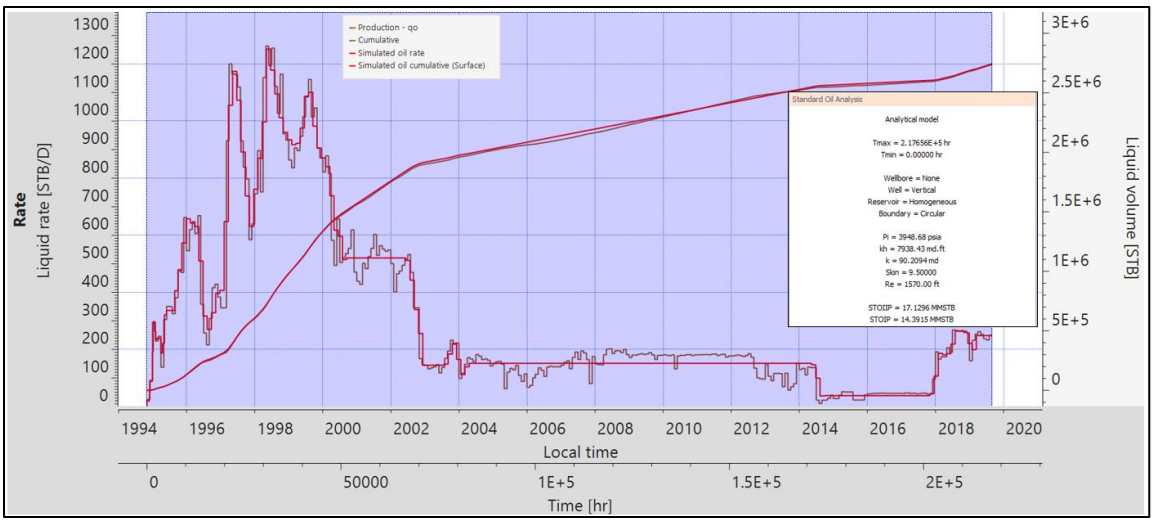

Figure V-3. Rate transient analysis results for the northern wells

V.1.2 The Southern Sector

The southern sector is comprised of 10 wells, as shown in Figure V-4. Initially, all of them were producing wells. Later, NHK-473 was converted to an injection well that was active from November 2009 to June 2017. The other nine wells are NHK-384, NHK-391,

NHK-411, NHK-419, NHK-420, NHK-422, NHK-448, NHK-462, and NHK-469. Among these producers, NHK-422 and NHK-469 are currently active.

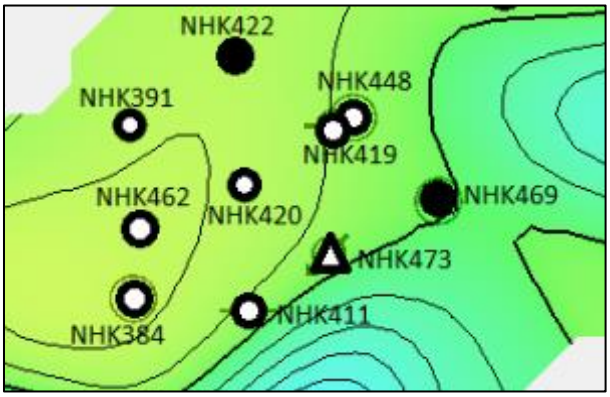

Figure V-4. The southern wells in the LK-4 reservoir

Figure V-5 shows the results obtained for this group of wells after a satisfactory production rate (q), and cumulative (Q) match was obtained. The OOIP for this group of wells is about 24.8 MMSTB (3.94 $MMSm^3$), permeability is 123 mD, and the skin factor is -3.4.

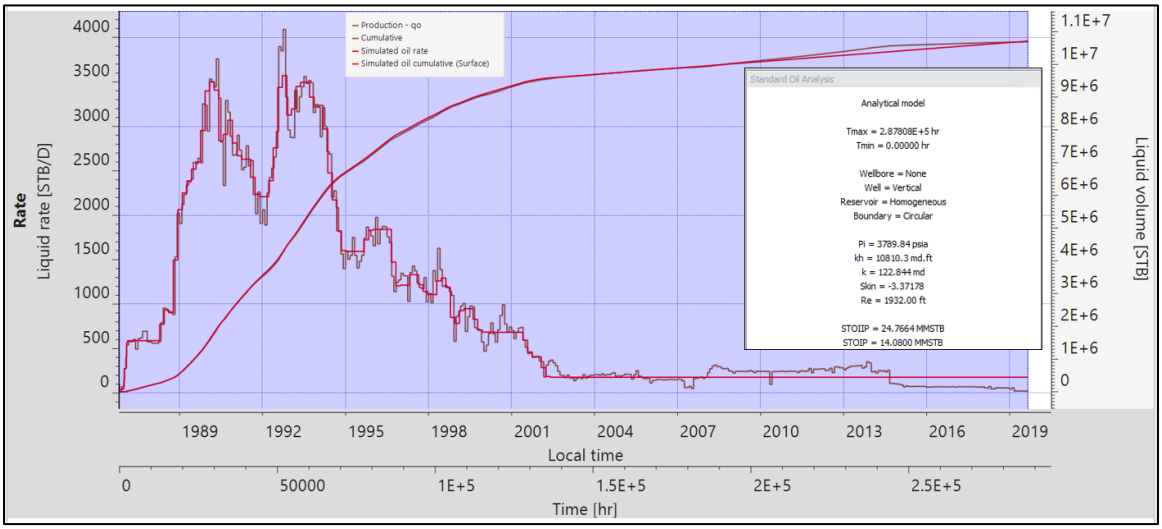

Figure V-5. Rate transient analysis result for the southern wells

V.2. Transient Productivity Indices

In this section, I explore the application of the Transient PI method (*Medeiros et al., 2010*) to confirm the OOIP solution obtained from RTA. The transient PI method is useful in providing diagnostic clues about the nature of the porosity system. It could potentially yield a reasonable estimate of the connected pore volume by trial and error solution. Following (*Araya, A., and Ozkan, E., 2002*), transient productivity index for liquid flow is defined using Equations 5-6 to 5-8

$$J(t_e) = \frac{q(t)}{\Delta p_{wf}(t) - \Delta \bar{p}(t)} \tag{5-6}$$

where

$$\Delta p_{wf}(t) = p_i - p_{wf}(t) \tag{5-7}$$

and

$$\Delta \bar{p}(t) = p_i - \bar{p}(t) = \frac{0.234 \cdot B_o \cdot Q(t)}{A \cdot h \cdot \phi \cdot c_t}. \tag{5-8}$$

Average reservoir pressure ($\bar{p}$) is estimated by decrementing p_i by the term associated with the corresponding cumulative production at a given timestep (Equation 5-8). The second equality, as given in the same equation, follows from the material balance for a constant compressibility fluid in a reservoir volume. The term t_e is the material balance time, as explained by *Raghavan et al. (1993)*, is shown in Equation 5-9

$$t_e = \frac{1}{q(t)} \int_0^t q(\tau)\, d\tau = \frac{Q\,(t)}{q\,(t)}. \tag{5-9}$$

Where:

A = drainage area (ft^2)

B_o = oil formation volume factor, RB/STB

c_t = total compressibility (psi^{-1})

h = reservoir thickness (ft)

J = transient productivity index (STB/D/psi)

q = production flow rate (STB/D)

Q = cumulative production (STB)

P_i = initial reservoir pressure (psi)

P_{wf} = flowing wellbore pressure (psi)

$\bar{p}$ = average reservoir pressure (psi)

t_e = material balance time (days or hour)

According to *Medeiros et al., (2010)*, the Equations 5-6 to 5-9 are useful in the computation of model (theoretical) and field transient productivity indices for oil reservoirs. They also provide the equivalent set of equations for gas reservoirs. Equations 5-6 to 5-9 were used in this study to analyze the LK-4 well data.

This procedure is iterative, where the connected pore volume was deduced from trial and error. At the end of the process, I can estimate reservoir pore volume. In this procedure, the correct estimate of reservoir pore volume yields a constant (flat line) transient productivity index at late time. The low and high estimates cause upward and downward bends, respectively. The transient productivity indices should be plotted against material balance time to eliminate the effect of variable rate production on field data. Figure V-6 presents the workflow for this method.

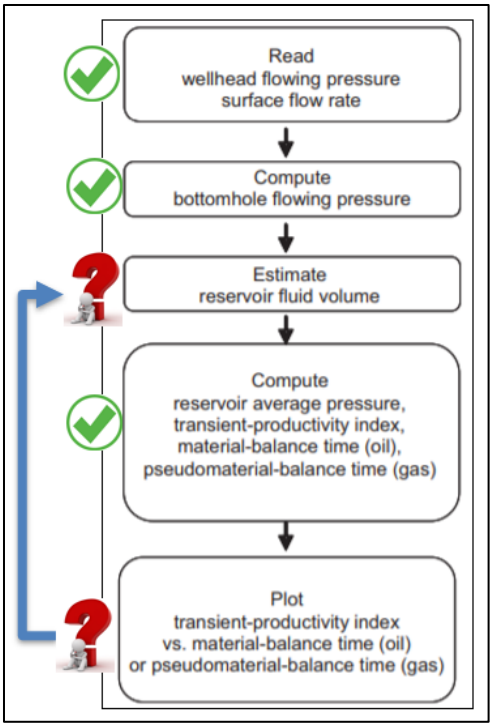

Figure V-6. Workflow to compute transient PI (*Medeiros et al., 2010*)

V.2.1 The Northern Sector

The process started with reviewing the available flowing bottom hole pressure (FBHP) data. These data were recorded from slightly different depths for all the wells. Therefore, it was necessary to normalize the data to the average depth. A trendline with the highest R^2 value was selected to obtain the pressure value at each time step.

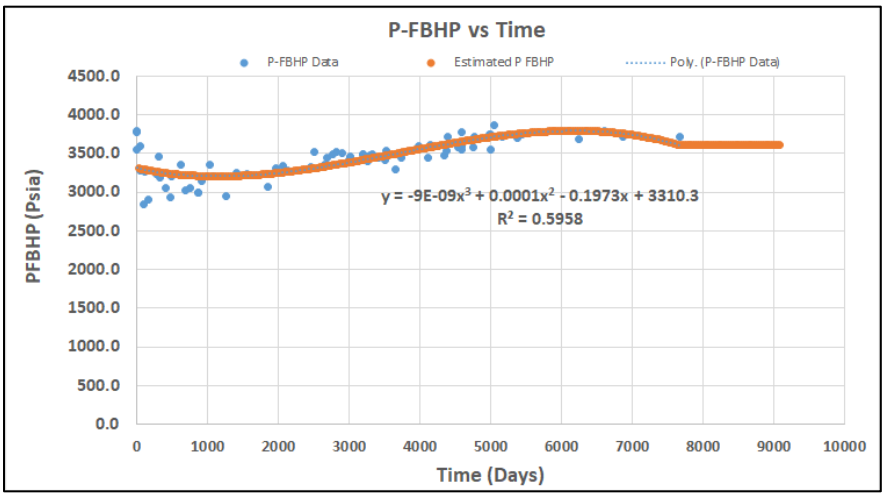

Figure V-7. Flowing Bottom Hole Pressure (FBHP) in the northern wells

The transient Productivity Index and material balance time were calculated using Equations 5-6 to 5-9. This result was then plotted on a log-log scale, and iteratively continued until the flat trend at the late time was obtained. Figures V-8 to V-10 illustrate the iterations to obtain the connected pore volumes.

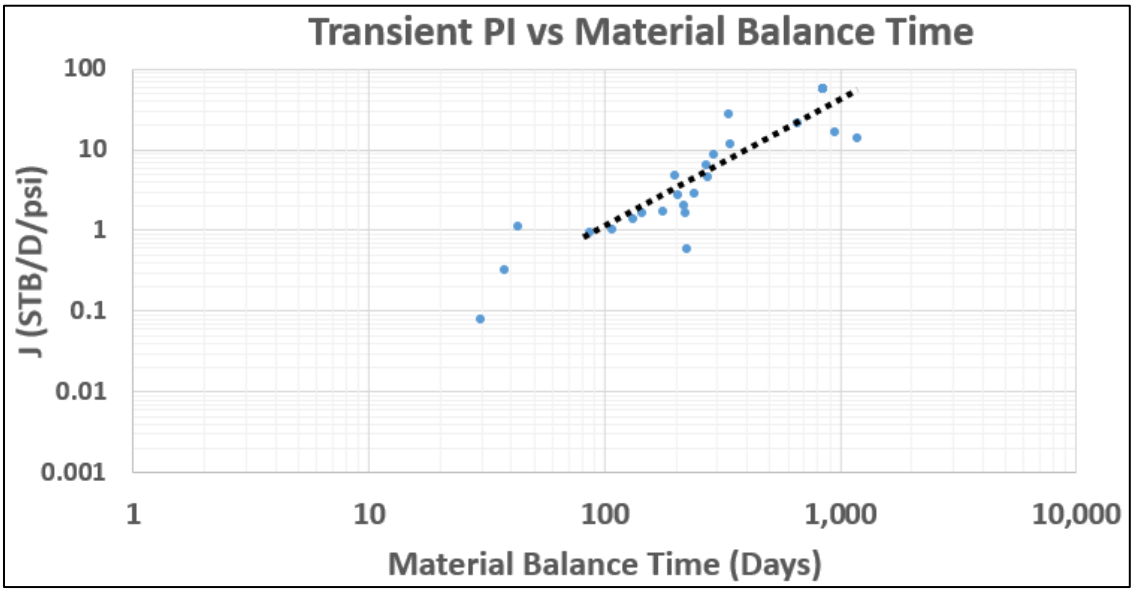

Figure V-8. J vs. MBT in the northern LK-4. Pore volume estimation is too low

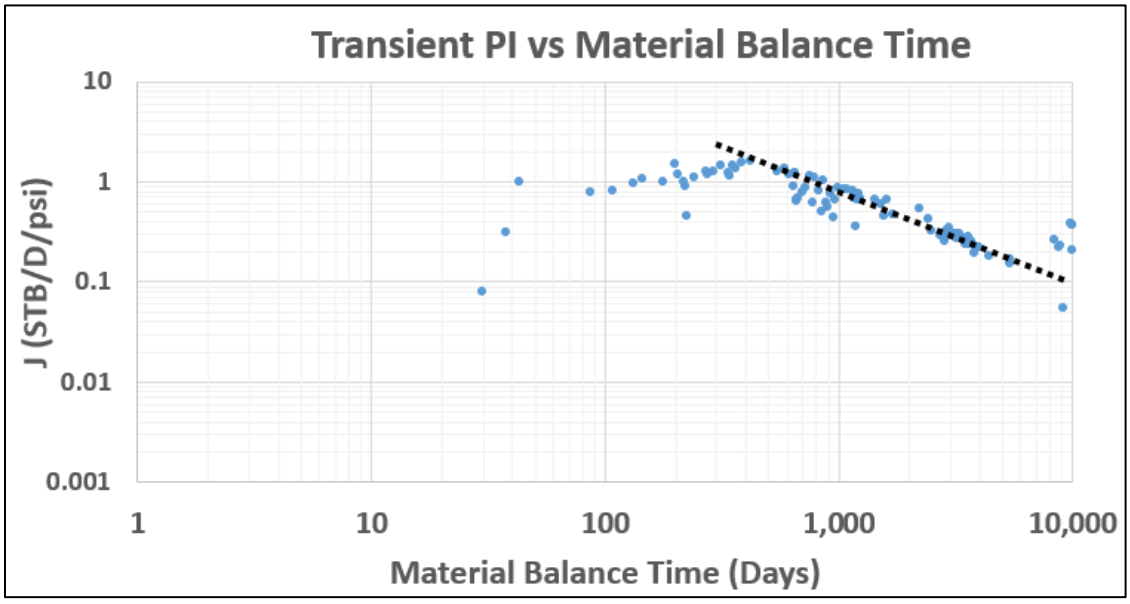

Figure V-9. J vs. MBT in the northern LK-4. Pore volume estimation is too high

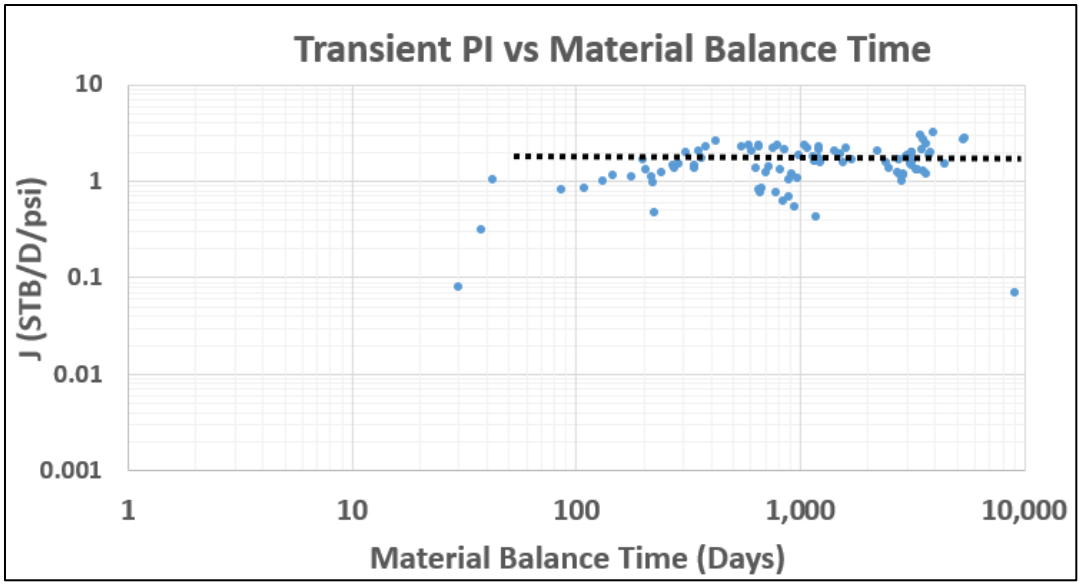

Figure V-10. J vs. MBT in the northern LK-4. Pore volume estimation is reasonable

Reasonable results were obtained with pore volume ≈ 34,572,169 RBbl. Initial oil saturation in this reservoir (S_{oi}) is 0.7, OOIP is ≈ 23.5 MMRBbl (16.6 MMSTB or 2.64 $MMSm^3$) in the northern sector.

V.2.2 The Southern Sector

Similar to the northern sector, in the southern sector, the process also started with reviewing the available FBHP data. The data points were quality checked, normalized, and curve fit to obtain the pressure value at every time step.

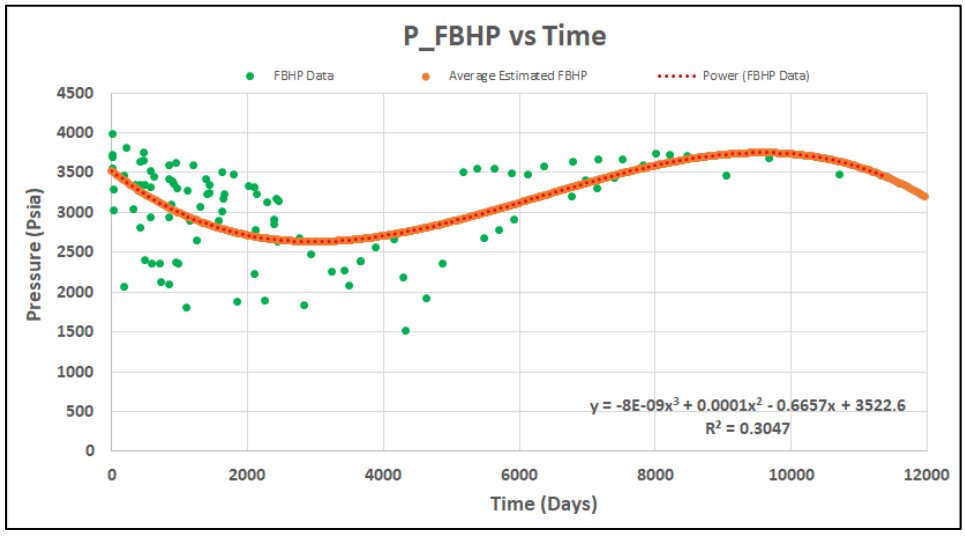

Figure V-11. Flowing Bottom Hole Pressure (FBHP) estimation in the southern sector

Next step was to plot the transient productivity index and material balance time and iterate until a flat trend was obtained at a later time.

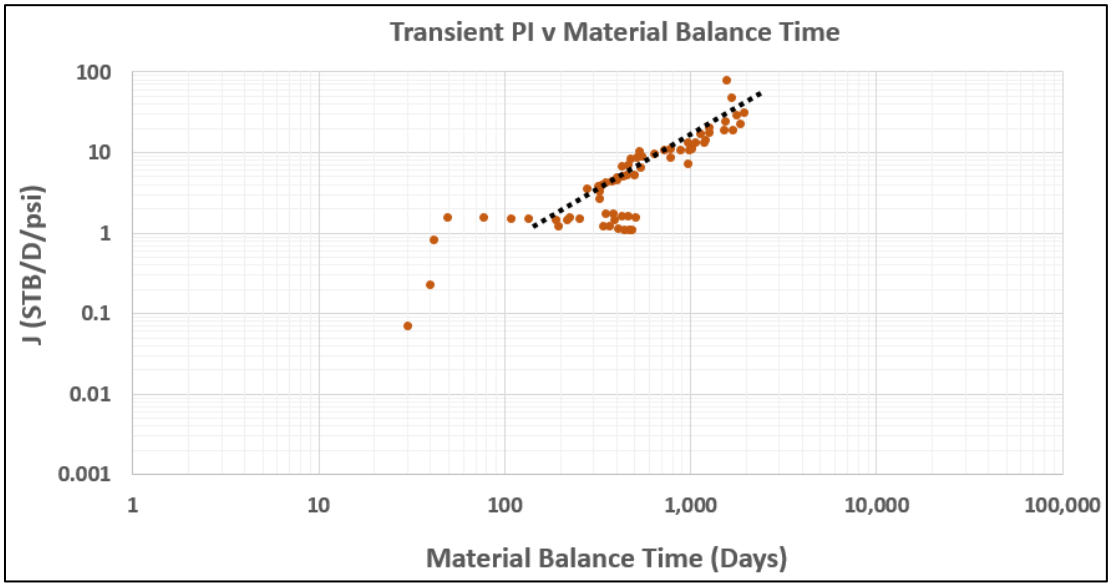

Figure V-12. J vs. MBT in the southern LK-4. Pore volume estimation is too low

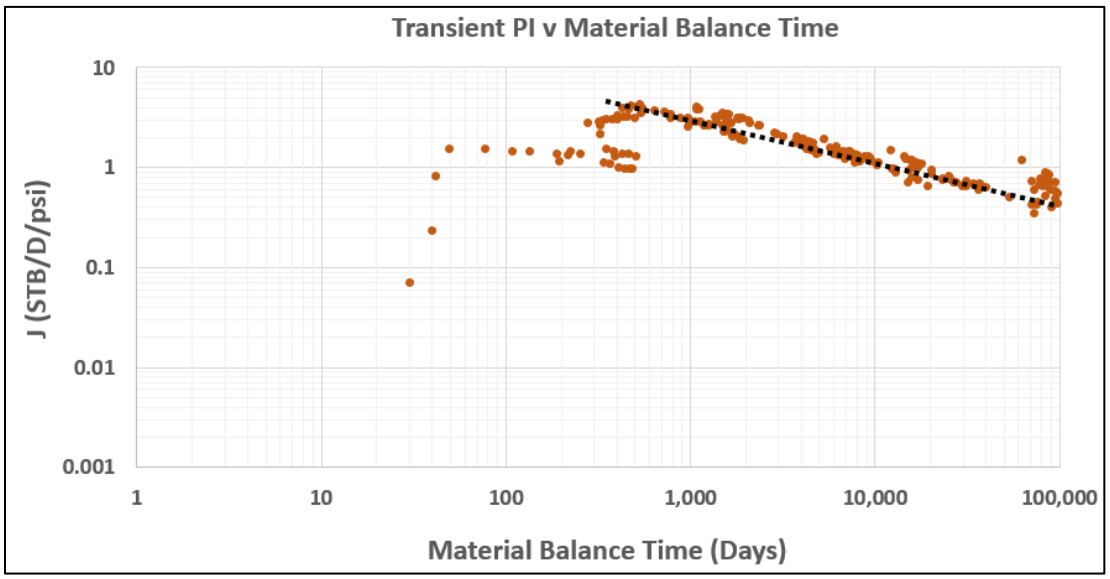

Figure V-13. J vs. MBT in the southern LK-4. Pore volume estimation is too high

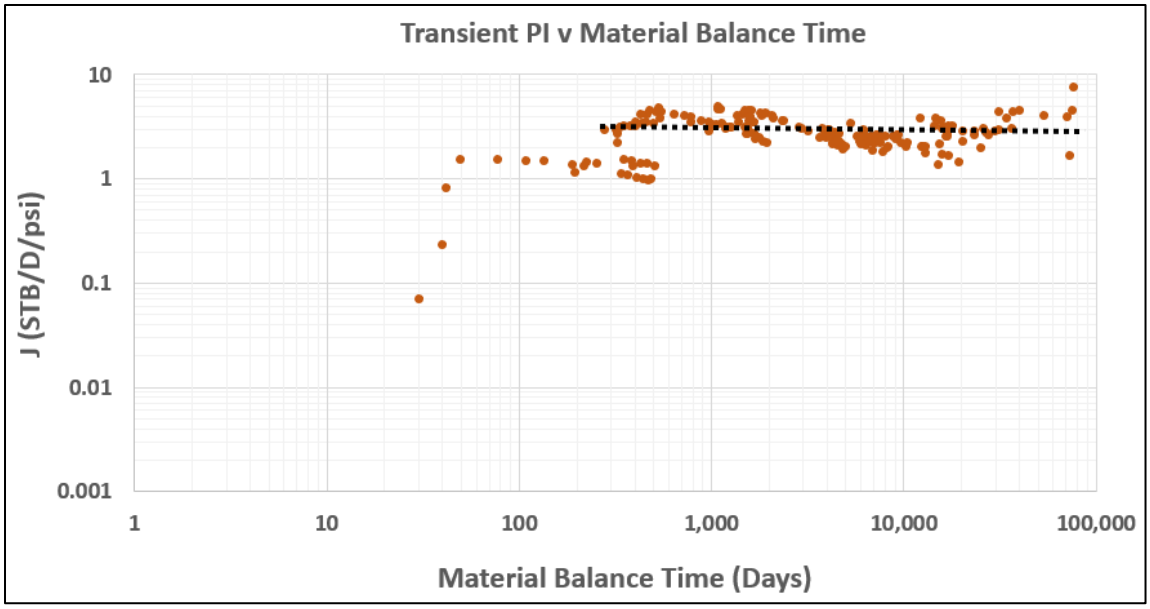

Figure V-14. J vs. MBT in the southern LK-4. Pore volume estimation is reasonable

Reasonable results were obtained with pore volume of about 47,536,733 RBbl. Initial oil saturation (S_{oi}) is 0.7, and OOIP is around 33.28 MMRBbl (23.59 MMSTB or 3.75 $MMSm^3$) in the southern sector.

CHAPTER VI. CONCLUSIONS AND RECOMMENDATIONS

The main objective of the research presented in this thesis was to minimize the uncertainty in Original Oil In Place (OOIP) estimation for the LK-4 reservoir. To achieve this target, the application of a variety of analytical, numerical, and reservoir simulation methods were required. This also includes theoretical discussions and incorporation of existing published theory into the analysis. Based on the application of a variety of techniques, the OOIP for this LK-4 reservoir can be summarized as follows:

- Volumetric calculation: 46.7 MMSTB (7.43 $MMSm^3$)
- Material balance analysis (MBAL): 43.1 – 43.2 MMSTB (6.9 $MMSm^3$)
- Reservoir simulation: 49.1 to 50.4 MMSTB (7.8 to 8.02 $MMSm^3$)
- Rate Transient Analysis: 41.9 MMSTB (6.7 $MMSm^3$)
- Transient Productivity Index: 40.2 MMSTB (6.4 $MMSm^3$)

The OOIP estimation based on production data converged around 40.2 – 43.2 MMSTB (6.4 – 6.9 $MMSm^3$). The OOIPs from the volumetric calculation and reservoir simulation are closer to each other, i.e., they fall between 46.7 and 50.4 MMSTB (7.43 to 8.02 $MMSm^3$). One possible cause of the observed discrepancy in the current lateral boundary of the LK-4 field in the south, which is possibly too large. This boundary is currently being reviewed by UH-EIP team using new information/data provided by the operator.

Another objective was to determine the range of Estimated Ultimate Recovery (EUR) for the LK-4 field. By applying a variety of methods, the base case EUR was obtained more accurately. The base case EUR ranges between 13.93 and 15.15 MMSTB

(2.21 to 2.41 $MMSm^3$). Depending on the methods and the future development scenarios, base case LK-4 EUR obtained from a variety of methods can be summarized as follows:

- Decline Curve Analysis: 13.93 to 14.14 MMSTB (2.21 – 2.25 $MMSm^3$)
- Water Oil Ratio (WOR) vs. Cumulative Oil (N_p) plot: 14.4 to 16 MMSTB (2.29 to 2.54 $MMSm^3$)
- Oil rate (q) vs. Cumulative Oil Plot (N_p): 14.1 MMSTB (2.24 $MMSm^3$)

The current calibrated history match model is significantly improved compared to the earlier model in December 2019. The current model is a better representative of the water cut in the four active producers. The OWC depth is more accurately pinpointed in this model. This OWC is consistent with the OWC depth identified by independent petrophysical analysis using well log data (± 3 m or 9.8 ft discrepancy).

The average key properties of the calibrated history matched model are I-permeability = 209 mD, J-permeability = 252 mD, and K-permeability = 113 mD. The model used an average porosity of 13.9%, and a bottom PV multiplier of 70 for most of the volume below OWC, except for regions around NHK-505 and NHK-469, where the PV multiplier ranges from 500 to 600. Improvement in water production match will be very difficult to achieve without using capillary pressure data, a lower k_v/k_h ratio for the region near NHK-580, and the addition of an edge-aquifer support from the central to the northern area of the reservoir.

Based on the calibrated reservoir simulation model, several future investment cases were evaluated. I suggest sharing cases that would yield incremental oil recovery to the operator.

Potentially attractive cases are mentioned below:

- Workover case: Lower PI improvement would yield 15.3 MMSTB, and greater PI improvement would yield 15.49 MMSTB incremental oil.
- Drilling case: There are four different proposed location for infill wells and the additional oil recoveries are as follow 15.49 MMSTB (UH-1), 15.59 MMSTB (UH-2), 17.26 MMSTB (UH-3 [delineation]), and 17.44 MMSTB (UH-3NE). The highest oil recovery may be obtained by drilling the top three future wells.
- Varying FBHP is also an attractive alternative to increase oil production. By modifying the operations to obtain a 9 psi/year decline, 15.78 MMSTB of oil will potentially be recovered. Currently, there is only one well (NHK-469) that is using an artificial lift mechanism. Implementing artificial lift methods to the other three active producers are recommended. These are potential low hanging fruit projects.

First time application of RTA, and Transient PI methods in the LK-4 reservoir has increased our confidence in the OOIP results. I suggest the application of RTA and Transient PI methods to other reservoirs that are understudied. Applying a variety of methods will increase confidence in the OOIP and EUR estimates.

In addition to the conclusions and recommendations presented above, scope exists for the following future research:

1. Test the calibration properties obtained in this history match model on the soon-to-be-released geomodel. Evaluate whether it yields a reasonable history match profile.
2. Conduct a production forecast using a probabilistic approach generated by creating three different geomodels (P-10, P-50, and P-90). The next step is to calibrate each

model using the production history match process. Finally, use each calibrated model to obtain a range of P-10, P-50, and P-90 production forecasts.

- This study would be particularly useful when the recommendation is shared with the operator. A probabilistic forecast would help decision-makers to make an investment decision with the full understanding of the low and high side of the possible outcomes.

3. Pattern flood evaluation: Conversion of existing high water cut wells into injectors. Even though increasing the injection rate in the currently active wells did not benefit the production, it is worth considering and studying proper waterflood patterns. Such a study would be particularly useful via a more robust geomodel.
4. Tertiary recovery evaluation (CO_2 flooding): The current recovery factor of this reservoir is high (≈ 34%). With infill wells and lower FBHP, it could reach recovery factor to as much as 37.8% (of simulation OOIP). The reservoir pressure is still high; therefore, it would be worthwhile to evaluate whether CO_2 flooding increases recovery in this reservoir any further. Based upon my discussions with the EIP-UH Team, this reservoir would also be a good candidate for CCUS (Carbon Capture, Utilization and Storage).

REFERENCES

Araya, A and Ozkan, E. 2002. *An Account of Decline-Type-Curve Analysis of Vertical, Fractured, and Horizontal Well Production Data*. SPE 77690. https://doi.org/DOI:10.2118/77690-MS.

Arps, J. J. 1945. *Analysis of Decline Curve*, Trans., AIME 160: 228 – 247.

Chatterjee, Sumantra. 2019. *Langkasi Geomodel*. Internal UH-EIP presentation. University of Houston, Houston, Texas (unpublished).

CMG. 2016. IMEX Black Oil and Unconventional Reservoir Simulator, Version 2016. User Guide. Calgary, Alberta: CMG.

CMG. 2016. IMEX Black Oil and Unconventional Reservoir Simulator Software, https://www.cmgl.ca/imex.

Crain, E. Ross. 2010. *Petrophysical E-handbook.* Chapter: Capillary Pressure.

Danu, Ismadi., Kabir, C. Shah., Hasan, A. R. 2011. *The Use of Combined Static and Dynamic Material Balance Methods in Gas Reservoir*. SPE 145798. https://doi.org/DOI:10.2118/145798-MS.

Dykstra, H., and Parsons, R. 1950. *The Prediction of Oil Recovery by Water Flooding, Secondary Recovery of Oil in the United States*, 2nd ed. American Petroleum Institute.

Essley, P. L. 1965. *What is Reservoir Engineering*, Journal of Petroleum Technology https://doi.org/DOI:10.2118/920-PA.

Fanchi R. J. 2010. *Integrated Reservoir Asset and Management Principle and Best Practices*. Page 49 to 69. ISBN 978-0-12-382088-4.

Houze, Olivier., Viturat, Didier., and Fjaere, Ole S. 2019. *Kappa-Dynamic Data Analysis Book*. Chapter 4 Page 127 - 164.

Jideofor, Odinukwe Celia de Amor Gomes Correia. 2010. *History Matching and Uncertainty Assessment of The Norne E-Segment Using PETREL*. Norwegian University of Science and Technology.

Kabir, C. Shah., Chien M.C.H., and Landa J. L. 2003. *Experiences with Automated History Matching* SPE. https://doi.org/DOI10.2118/79670-MS.

Kabir, C. Shah., Danu, Ismadi., and Sandra, Fountain. 2010. *Reservoir Management with Real Time and Periodic Surveillance Data*. SPE 132967. https://doi.org/DOI:10.2118/132967-MS.

Kantzas, Apostolos., Bryan, Jonathan., and Taheri, Saeed. 2018. *Fundamental of Fluid Flow in Porous Media, E-book.* Chapter 2 Porous Medium – Empirical Correlations of Relative Permeability.

Kappa Engineering. 2017. Topaze – Rate Transient Analysis Software, https://www.kappaeng.com/software/topaze.

Manrique, Eduardo., Thomas, Charles., Ravikiran, Ravi., Izadi, Mehdi., and Lantz, Michael. 2010. *EOR. Current Status and Opportunities*. SPE Improved Oil Recovery Symposium, Tulsa, Oklahoma, USA. https://doi.org/DOI:10.2118/130113-MS.

Medeiros, Flavio., Kurtoglu, Basak., Ozkan., Erdal and Kazemi, Hossein. 2010. *Analysis of Production Data from Hydraulically Fractured Horizontal Wells in Shale Reservoirs*. SPE 110848. https://doi.org/DOI:10.2118/110848-PA.

Petroleum Expert, 2010. MBAL - Reservoir Engineering Toolkit Material Balance Analysis Software, https://www.petex.com/products/ipm-suite/mbal.

Petroleum Expert, 2010. MBAL - Material Balance Analysis User Manual. Edinburgh, United Kingdom: Petroleum Expert.

Schlumberger GeoQuest. 1999. Eclipse 100 Black Oil Simulator User Manual. Houston, Texas: Schlumberger.

Schlumberger. 2017. Petrel Platform Eclipse-100 (E-100) Reservoir Engineering Software, https://www.software.slb.com/products/petrel.

Sharma Akash and Lee, W. John. 2016. *Improved Workflow for EUR Prediction in Unconventional Reservoirs.* https://doi.org/SPEDOI:10.15530-URTeC-2016-244280.

Surguchev, Leonid Manrique., Eduardo, Vladimir., Alvarado, Vladimir. 2005. *Improved Oil Recovery: Status and Opportunities*. The 18th World Petroleum Congress, Johannesburg, South Africa. WPC-18-0886.

Thakur, Ganesh C. 1990. *Reservoir Management: A Synergistic Approach.* SPE. https://doi.org/DOI:10.2118/20138-MS.

Thakur, Ganesh C. 1991. *Waterflood Surveillance Techniques - A Reservoir Management Approach*. SPE. https://doi.org/DOI:10.2118/23471-PA.

Thakur, Ganesh C., and Satter, Abdus. 1998. *Integrated Waterflood Asset Management. Houston: PennWell Publishing Co.*

Tomomi, Yamada. 2000. *Non-Uniqueness of History Matching*. https://doi.org/SPE-59434-MS.DOI:10.2118/59434-MS.

Watson, A.T. 1989. *Sensitivity Analysis of Two-Phase Reservoir History Matching*. SPE 17000-PA. https://doi.org/DOI:10.2118/17000-PA.

Zhu, Y. 2019. *Waterflooding Management and Identifying IOR/EOR Opportunities in A Mature Reservoir.* Master Thesis, University of Houston, Texas (December 2019).

APPENDIX

1. Evaluating Forecast Accuracy

OIL shared updated production data (from September 2019 to March 2020) on April 27th, 2020. It provided us an opportunity to compare our forecast with the actual values for the last 7 months of production data. Based on the Figure VII-1, Figure VII-2, and Figure VII-3, oil production forecast matches with 98.2% accuracy (average).

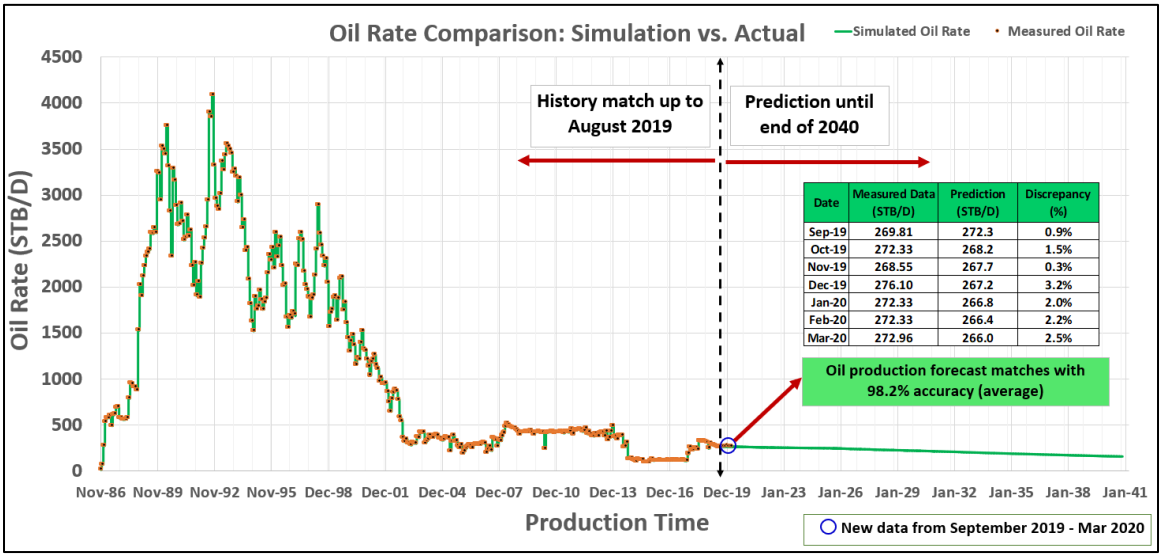

Date	Measured Data (STB/D)	Prediction (STB/D)	Discrepancy (%)
Sep-19	269.81	272.3	0.9%
Oct-19	272.33	268.2	1.5%
Nov-19	268.55	267.7	0.3%
Dec-19	276.10	267.2	3.2%
Jan-20	272.33	266.8	2.0%
Feb-20	272.33	266.4	2.2%
Mar-20	272.96	266.0	2.5%

Figure VII-1. Simulated vs. actual oil rate comparison

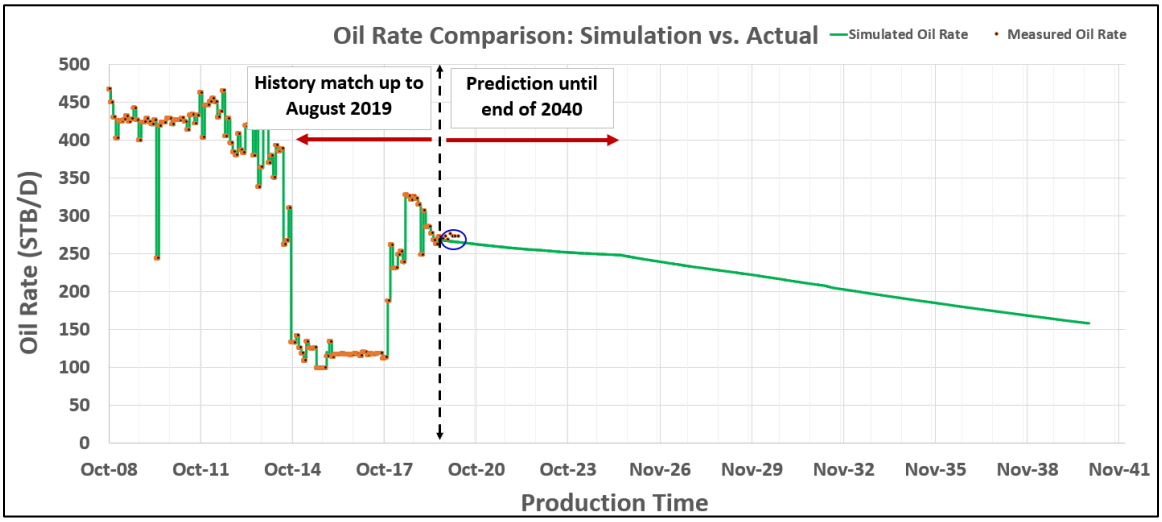

Figure VII-2. Simulated vs. actual oil rate comparison (zoom-in)

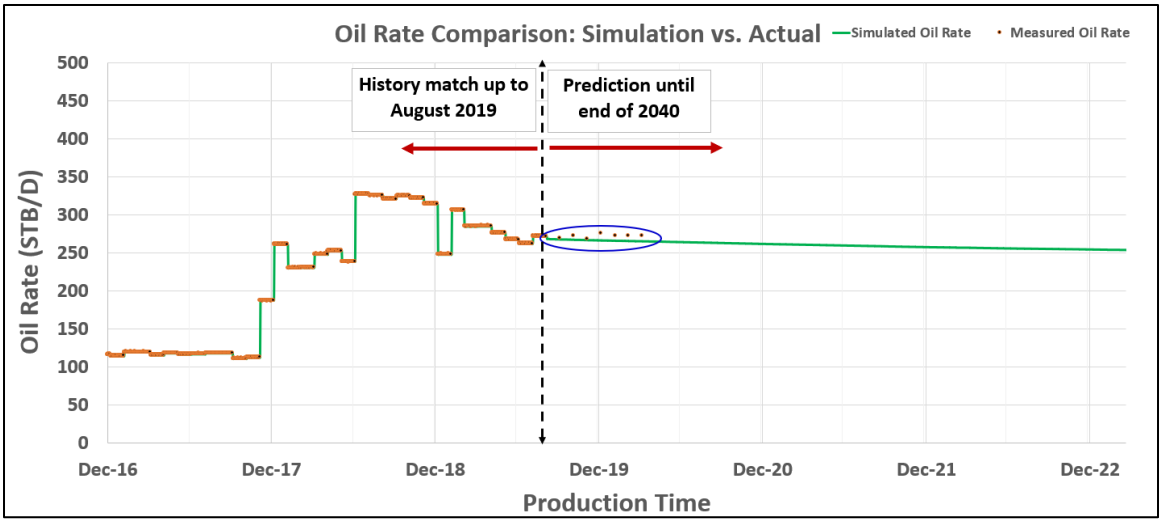

Figure VII-3. Simulated vs. actual oil rate comparison (last few years)